NUREG/CR–6160
NEA–CSNI–R(94)3
EGG–2721

Summary of Important Results and SCDAP/RELAP5 Analysis for OECD LOFT Experiment LP–FP–2

Prepared by
E. W. Coryell

EG&G Idaho, Inc.

Prepared for
U.S. Nuclear Regulatory Commission

9405310168 940430
PDR NUREG
CR-6160 R PDR

AVAILABILITY NOTICE

Availability of Reference Materials Cited in NRC Publications

Most documents cited in NRC publications will be available from one of the following sources:

1. The NRC Public Document Room, 2120 L Street, NW., Lower Level, Washington, DC 20555-0001

2. The Superintendent of Documents, U.S. Government Printing Office, Mail Stop SSOP, Washington, DC 20402-9328

3. The National Technical Information Service, Springfield, VA 22161

Although the listing that follows represents the majority of documents cited in NRC publications, it is not intended to be exhaustive.

Referenced documents available for inspection and copying for a fee from the NRC Public Document Room include NRC correspondence and internal NRC memoranda; NRC bulletins, circulars, information notices, inspection and investigation notices; licensee event reports; vendor reports and correspondence; Commission papers; and applicant and licensee documents and correspondence.

The following documents in the NUREG series are available for purchase from the GPO Sales Program: formal NRC staff and contractor reports, NRC-sponsored conference proceedings, international agreement reports, grant publications, and NRC booklets and brochures. Also available are regulatory guides, NRC regulations in the *Code of Federal Regulations*, and *Nuclear Regulatory Commission Issuances*.

Documents available from the National Technical Information Service include NUREG-series reports and technical reports prepared by other Federal agencies and reports prepared by the Atomic Energy Commission, forerunner agency to the Nuclear Regulatory Commission.

Documents available from public and special technical libraries include all open literature items, such as books, journal articles, and transactions. *Federal Register* notices, Federal and State legislation, and congressional reports can usually be obtained from these libraries.

Documents such as theses, dissertations, foreign reports and translations, and non-NRC conference proceedings are available for purchase from the organization sponsoring the publication cited.

Single copies of NRC draft reports are available free, to the extent of supply, upon written request to the Office of Administration, Distribution and Mail Services Section, U.S. Nuclear Regulatory Commission, Washington, DC 20555-0001.

Copies of industry codes and standards used in a substantive manner in the NRC regulatory process are maintained at the NRC Library, 7920 Norfolk Avenue, Bethesda, Maryland, for use by the public. Codes and standards are usually copyrighted and may be purchased from the originating organization or, if they are American National Standards, from the American National Standards Institute, 1430 Broadway, New York, NY 10018.

DISCLAIMER NOTICE

This report was prepared as an account of work sponsored by an agency of the United States Government. Neither the United States Government nor any agency thereof, or any of their employees, makes any warranty, expressed or implied, or assumes any legal liability of responsibility for any third party's use, or the results of such use, of any information, apparatus, product or process disclosed in this report, or represents that its use by such third party would not infringe privately owned rights.

NUREG/CR-6160
NEA-CSNI-R(94)3
EGG-2721

Summary of Important Results and SCDAP/RELAP5 Analysis for OECD LOFT Experiment LP-FP-2

Manuscript Completed: February 1994
Date Published: April 1994

Prepared by
E. W. Coryell

Contributing Authors
D. W. Akers, C. M. Allison, M. L. Carboneau, R. R. Hobbins,
J. K. Hohorst, S. M. Jensen, S. M. Modro

EG&G Idaho, Inc.
Idaho Falls, ID 83415

Prepared for
Division of Systems Research
Office of Nuclear Regulatory Research
U.S. Nuclear Regulatory Commission
Washington, DC 20555-0001
NRC FIN L1367

ABSTRACT

This report summarizes significant technical findings from the LP-FP-2 Experiment sponsored by the Organization of Economic Cooperation and Development (OECD). It was the second, and final, fission product experiment conducted in the Loss-of-Fluid Test (LOFT) facility at the Idaho National Engineering Laboratory. The overall technical objective of the test was to contribute to the understanding of fuel rod behavior, hydrogen generation, and fission product release, transport, and deposition during a V-sequence accident scenario that resulted in severe core damage.

An 11 by 11 test bundle, comprised of 100 prepressurized fuel rods, 11 control rods, and 10 instrumented guide tubes, was surrounded by an insulating shroud and contained in a specially designed central fuel module, that was inserted into the LOFT reactor. The simulated transient was a V-sequence loss-of-coolant accident scenario featuring a pipe break in the low pressure injection system line attached to the hot leg of the LOFT broken loop piping. The transient was terminated by reflood of the reactor vessel when the outer wall shroud temperature reached 1517 K. With sustained fission power and heat from oxidation and metal-water reactions, elevated temperatures resulted in zircaloy melting, fuel liquefaction, material relocation, and the release of hydrogen, aerosols, and fission products.

A description and evaluation of the major phenomena, based upon the response of on line instrumentation, analysis of fission product data, postirradiation examination of the fuel bundle, and calculations using the SCDAP/RELAP5 computer code, are presented.

CONTENTS

List of Figures

List of Tables

EXECUTIVE SUMMARY

Experiment LP-FP-2 was the second fission product (FP) release and transport test performed in the Loss-of-Fluid Test (LOFT) facility. This experiment was initiated on July 9, 1985, and was the eighth and final experiment performed under the sponsorship of the Organization for Economic Cooperation and Development (OECD). Experiment LP-FP-2 provided information on the release, transport, and deposition of fission products and aerosols during a V-sequence accident scenario that resulted in severe core damage. The specific V-sequence loss-of-coolant accident (LOCA) scenario was a simulated pipe break in the low pressure injection system (LPIS) line, attached to the hot leg of the LOFT broken loop piping. The intact loop cold leg (ILCL) break line served as the primary blowdown pathway prior to fission product release. During fission product release, only the LPIS line was open; therefore, fission products released from the center fuel module (CFM) were transported and deposited in the reactor vessel (RV) upper plenum, the LPIS line, and the blowdown suppression tank (BST).

Experiment Overview

The LP-FP-2 core consisted of four square (15 by 15 design) and four triangular-shaped peripheral fuel modules, and a centrally located fuel module. The CFM consisted of 11 control rods, 100 prepressurized (2.41 MPa) fuel rods enriched to 9.744 weight% ^{235}U, and 10 instrumented guide tubes. The CFM was separated from the peripheral fuel assemblies by a 0.025-m-thick, zircaloy clad, zirconium-oxide insulated thermal shroud. The center bundle design enabled the CFM fuel rods to heat up to temperatures above 2100 K while maintaining the peripheral bundle fuel rods below 1390 K.

The LP-FP-2 Experiment consisted of four distinct phases: (a) fuel preconditioning, (b) pretransient, (c) transient, and (d) posttransient (or postreflood).

- The purpose of the fuel preconditioning phase was to subject the CFM fuel rods to a minimum burnup, generate the long-lived fission product inventory, and establish sufficient decay heat to ensure that there would be enough energy to heat the CFM above 1400 K following reflood.
- The pretransient phase finished the planned irradiation, generated the short-lived fission product inventory, and established the initial thermal-hydraulic boundary conditions for the experiment.
- The transient phase of the experiment started with reactor scram and ended with closure of the LPIS line 1778 s later. The transient was terminated when the external temperature on the CFM shroud reached 1517 K, at which time reflood of the reactor was initiated.
- The posttransient phase of the experiment began with closure of the LPIS line and included reflood (> 1783 s). The posttransient phase continued for 44 days, during which time the concentration of fission products in the BST and primary coolant system (PCS) were measured.

The actual pretransient irradiation history produced a total burnup for the CFM, of 448 ± 25 MWd/tU, a cesium-to-iodine (Cs/I) ratio of 4.2, and total core decay heat of 684.5 kW at 200 seconds into the transient.

One of the principal objectives of Experiment LP-FP-2 was to provide on-line and postexperiment data concerning airborne and deposited fission products and aerosol concentrations. These measurements were obtained from several instruments that encompassed the fission product measurement system. The fission product measurement system (FPMS) consisted of three basic subsystems: (a) four gamma spectrometers and one gross gamma

detector (b) a deposition sampling system; and (c) steam/aerosol sampling lines.

The four on-line gamma spectrometers (G1, G2, G3, and G5) and the gross gamma detector (G6) were strategically located at five different sampling locations. Each of the gamma detectors was designed to be operated remotely and could be calibrated using a ^{238}Th source mounted on a collimator wheel.

The deposition sampling system consisted of six stainless steel coupons in the upper plenum, located in pairs at three separate elevations, and two deposition spool pieces in the LPIS line. At each of the three elevations, both coupons were exposed to the fluid stream flow during the preconditioning and transient phases of the experiment. Before reflood, one coupon at each elevation was to be isolated from the primary coolant system (PCS), to protect it from posttransient deposition or removal of fission products. The two deposition spools, located near the inlet and outlet of the LPIS line, were designed to provide a measurement of the PCS deposition of fission products during the preconditioning and transient phases of the experiment. Since the LPIS line was isolated before reflood, these spool pieces were protected from reflood water.

The remaining instrumentation in the FPMS consisted of two aerosol/steam sampling lines and an aerosol filter on the LPIS outlet, upstream of the BST. The aerosol/steam sampling instrumentation was designed to provide a continuous sampling of vapor and aerosols during the transient phase of the experiment. The F1 sample line, situated 180 cm above the lower tie plate and directly above the CFM, and the F2 sample line, situated outside the upper plenum, joined before the BST to form a single line (designated F1+F2), which passed the G2 gamma spectrometer. The LPIS filter, designated F3, collected aerosol material (~0.4 μm or larger) at the end of the LPIS and immediately upstream of the BST.

The LP-FP-2 transient was initiated by scramming the reactor with the peripheral control rods (defining t = 0.0). The primary coolant pumps (PCPs) were then turned off at ~10 seconds. After the PCS flow had decreased to 190 kg/s (22 seconds), the CFM control rods were unlocked and allowed to fall into the CFM. At 24 seconds, the control rods were fully inserted into the core. The ILCL break line was opened at 33 seconds, and the LPIS line was opened at 222 seconds. The core started heating up at 662 seconds, when the liquid level decreased in the peripheral bundles. The CFM began heating up at 689 seconds. The ILCL break was closed at 736 seconds; however, it was reopened at 878 seconds, to accelerate the PCS depressurization rate.

Besides reopening the ILCL break, the power-operated relief valve (PORV) was opened at 882 seconds. After system pressure dropped below 1.38 MPa, the ILCL and PORV lines were closed, at 1022 and 1162 seconds, respectively. Fission products were first detected in the F1 and F2 lines at about 1200 seconds. Metal-water reaction began at about 1450 seconds, and control rod rupture occurred at ~1500 seconds. The hottest measured cladding temperature reached 2100 K by 1504 seconds. The transient continued until the outer shroud wall temperature limitation of 1517 K was reached at 1766 seconds. At this time, the transient was terminated by closing the LPIS line break and initiating emergency core cooling system (ECCS) injection (reflood).

Liquid water entered the core at about 1790 seconds, and the peripheral fuel modules quenched soon afterward. However, the CFM did not quench quickly. In fact, evidence indicates that a rapid temperature excursion occurred within the CFM during reflood, caused by enhanced metal-water reactions. The plant was maintained in a quiescent state for 14 days while data were taken, using the on-line FPMS and thermal-hydraulic measurement systems. Also, several grab samples (both liquid and vapor) were taken from the BST and PCS. During the early part of the posttransient period, the PORV was cycled twice to prevent PCS overpressurization, and a feed-and-bleed operation on the steam generator was initiated.

Significant Thermal-Hydraulic and Fission Product Results

Thermocouple responses in the CFM and at the upper tie plate indicate that the highest temperatures were reached during reflood and that temperatures in the region of ceramic blockage in the bundle remained hot for several hundred seconds following reflood. Additionally, posttest measurements and analyses of the locations of noble gases, volatile fission products, and hydrogen suggests that approximately 70% of noble gases and volatile fission products released during the experiment were released during reflood and 80% of the hydrogen generated during the experiment was produced during reflood.

The stainless steel upper tie plate at the top of the CFM sustained severe damage due to melting and foaming oxidation. The damage to the upper tie plate indicates that much of the energy produced during reflood was deposited in a narrow axial zone at the top of the fueled region.

Of the highly volatile fission products iodine (I) and cesium (Cs), 3.0% and 0.80%, respectively, of the bundle inventories were released during the transient; and approximately 60% of these releases were deposited on the upper plenum surfaces. Of the lower-volatility fission products barium (Ba) and tellurium (Te), 0.84% and 0.54%, respectively, of the bundle inventories were released; 93% of the Ba and 76% of the Te were deposited on upper plenum surfaces. During the transport of these fission products to the collection tank, the fractions deposited in the long, small-diameter, simulated LPIS line (the fission product release pathway in a V-sequence) leading to the tank were, for I, 0.10; for Cs, 0.27; for Ba, 0.10; and for Te, 0.20. Measurements of aerosol size and composition indicated that these fission products were transported through this pipe on aerosols (approximately 0.3-μm in diameter) composed mainly of tin (Sn) from the zircaloy cladding.

Measurements of deposition on coupons placed in the upper plenum and protected from washing during reflood showed that much larger quantities of silver (Ag) and I were present than Cs. Based on these observations and thermodynamic calculations of the stability of I species under the LP-FP-2 conditions, it is postulated that the primary chemical form of I being transported from the CFM was AgI. Thermodynamic calculations show that AgI is favored at temperatures below 1800 K when there is a large excess of Ag in the vapor state relative to I (Hahn and Ache 1984). These conditions were met in the LP-FP-2 Experiment because of the dispersion of Ag due to the burst failure mode of the silver-indium-cadmium (Ag-In-Cd) control rods at the low system pressure in this experiment.

Although research has shown that H_3BO_3 can react with CsOH to produce $CsBO_2$, the deposition pattern of Cs in the upper plenum is more compatible with calculations of the chemisorption of CsOH than for condensation of $CsBO_2$. In addition, boron (B) was not detected on the protected coupons that contained Cs.

The oxidic fission products cerium (Ce) and strontium (Sr) were strongly retained (57% and 88%, respectively) in samples of ceramic melts. The volatile fission products I and Cs were retained at about 15% of inventory in these samples. The medium volatility metal antimony (Sb) was retained at about 24%, and the relatively low volatility metal ruthenium (Ru) was retained only to about 10%. There is evidence of the accumulation of Sb in metallic melts.

Summary of Severe Core Damage Results

The LP-FP-2 Experiment simulated the early stages of a V-sequence (an interfacing systems LOCA) and was initiated by reactor scram and a PCS blowdown that reduced the system pressure to the neighborhood of 1.1 MPa. Decay heat in the core caused the CFM to heat up and, in conjunction with continued slow

depressurization, caused steaming from the pool of coolant remaining in the lower head beneath the core. The heatup in the central bundle caused melting of core components and relocation and freezing of melts into partial flow blockages in the core. (This scenario was carefully avoided in the remainder of the core by preferential enrichment of the test bundle fuel, causing the CFM to run at a higher power rating and hence at a higher decay heat rate than the peripheral fuel.)

The lower blockage in the LP-FP-2 test is made up primarily of molten metals that relocated downward and froze at the location of the lower spacer grid. The metals are zirconium (Zr), from control rod guide tubes and fuel rod cladding; iron (Fe), nickel (Ni), and chromium (Cr), from control rod cladding and spacer grids; and Ag, In, and Cd, from the control rod alloy. The Ag, In, and Cd were sometimes found alloyed with Zr and other times were found in ingots having a composition essentially unchanged from the as-fabricated control rod alloy. In addition to metals in the lower blockage, some fuel fragments were also present. The lower blockage caused a 78% reduction in the as-fabricated flow area.

An upper blockage occurred at the location of the second spacer grid, causing a 63% reduction in flow area. This blockage consisted of metallic alloys and a small amount of previously molten ceramic debris at the lowest elevation, with increasing ceramic content (becoming the dominant phase) at higher elevations within the blockage. The metallic alloys were the same as those found in the lower blockage at the first spacer grid. The ceramic debris is primarily $(U,Zr)O_2$, which resulted from the dissolution of UO_2 in molten zircaloy, steam oxidation of this metallic-ceramic melt, and melting of UO_2 and ZrO_2.

Above the ceramic blockage is a region in which rod-like geometry is present. The cladding of the fuel rods has ballooned and has been fully oxidized. Melts, mainly ceramic, fill the space between the fuel and the ballooned cladding and also, to some degree, are present in flow channels. Some fuel fragments have been lost through openings in the ballooned cladding. The $(U,Zr)O_2$ ceramic melts generally originated locally from the dissolution of UO_2 by molten zircaloy. However, some of this melt containing dissolved UO_2 may have relocated downward, and some may have relocated to this region from above. Steam access to this region converted the metallic melts to ceramics. Restraint from oxidized cladding shells and ceramic melts within the ballooned rods and in the flow channels between rods was apparently adequate to prevent large-scale fragmentation of the fuel stacks in this region upon reflood.

At the top of the LP-FP-2 center fuel bundle is a rubble bed of fuel fragments containing no cladding remnants and only small amounts of previously molten materials, mainly ceramic. The absence of cladding remnants suggests that zircaloy melted and relocated downward in the bundle. Without restraint from cladding and surface tension from wetting of melts, fuel fragments were free to crumble from pellet stacks to form a rubble bed, especially upon reflood.

Both blockages occurred at spacer grids in the LP-FP-2 CFM. The spacer grids apparently provide an impediment to the flow of melt and additional surface area for heat transfer, thereby enhancing the probability of melt solidification and debris accumulation in regions where the temperature is below the freezing temperature of the debris.

ACKNOWLEDGMENTS

The authors acknowledge the significant foundation for this work that was built by the Nuclear Energy Agency (NEA) of the OECD. The material presented in this document has been made possible because of the efforts of many people within the NEA as well as those from the OECD LOFT sponsors. Without the OECD support, there would have been no LOFT severe accident data with which to compare analytic results. Hundreds of personnel have contributed to the successful completion of the experimental program, both within the INEL and at other institutes around the world. It would be unwise to try to list all who have contributed to this effort. A heartfelt thanks is extended to all who have contributed to any of the many efforts involved in arriving at a state-of-the-art which permits the presentation of these comparisons of code calculations with the OECD LOFT LP-FP-2 data. The authors especially acknowledge the financial and technical support provided by the U. S. Nuclear Regulatory Commission, which allowed this report to be added to the world's severe accident data base.

ACRONYMS

BST	Blowdown Suppresion Tank
CFM	Center Fuel Module
ECCS	Emergency Core Cooling System
FPMS	Fission Product Measurement System
HPIS	High Pressure Injection System
ILCL	Intact Loop Cold Leg
INEL	Idaho National Engineering Laboratory
LOCA	Loss Of Coolant Accident
LOFT	Loss of Fluid Test
LPIS	Low Pressure Injection System
OECD	Organization for Economic Cooperation and Development
PBF	Power Burst Facility
PCS	Primary Coolant System
PCP	Primary Coolant Pump
PIE	Post Irradiation Examination
PORV	Power Operated Relief Valve
SFD	Severe Fuel Damage Experiments
SEM	Scanning Electron Microscope
TAN	Test Area North
TMI-2	Three Mile Island Facility, Unit 2.
WDS	Wavelength Dispersive X-ray Spectroscopy

Summary of Important Results and SCDAP/RELAP5 Analysis for OECD LOFT Experiment LP-FP-2

1. INTRODUCTION

This report summarizes significant technical findings from the LP-FP-2 Experiment sponsored by the Organization of Economic Cooperation and Development (OECD). It was the second, and final, fission product experiment conducted in the Loss-of-Fluid Test (LOFT) facility at the Idaho National Engineering Laboratory (INEL).

1.1 Background

The LOFT facility at the INEL simulated a typical commercial 4-loop pressurized water reactor (PWR) core, primary coolant system (PCS), and emergency core cooling system (ECCS). Details of the facility are provided in Appendix A. The original purpose of LOFT was to identify the physical phenomena and the course of events of a large-break loss-of-coolant accident (LOCA) in a nuclear plant not provided with designed safety systems and with no operational mitigation of the consequences. However, as a direct consequence of the small-break LOCA that occurred at the Three Mile Island Unit 2 (TMI-2) nuclear power plant in 1979, the mission for LOFT was changed to the investigation of small-break LOCAs with operational safety systems and operator intervention to minimize the consequences. The experimental program, sponsored by the U.S. Nuclear Regulatory Commission (NRC) and conducted from 1976 to 1982, included a number of large- and small-break LOCAs and anticipated transients and contributed significantly to the existing data base for these types of accidents.

The OECD LOFT Project was sponsored by an international consortium, which collaborated on a program to use the LOFT facility for a program of safety experiments of interest to the international community. The OECD countries participating in the Project were Austria, Finland, Federal Republic of Germany, Italy, Japan, Sweden, Switzerland, the United Kingdom, and the United States [U.S. Department of Energy (DOE), NRC, and the Electric Power Research Institute (EPRI)]. The experimental program of the OECD LOFT Project, conducted from February 1983 to July 1985 at the INEL, comprised eight experiments: six thermal-hydraulic experiments (three small-break LOCA, two large-break LOCAs, and one loss-of-feedwater experiment); and two fission product experiments. The detailed results from these experiments provided valuable new evidence on thermal-hydraulic issues and an important national data base for computer code verification. Following the completion of the OECD LOFT Project, the LOFT facility was decommissioned.

1.2 Experiment LP-FP-2

OECD LOFT Experiment LP-FP-2 was the second fission product release and transport test performed in LOFT and was initiated on July 9, 1985. Experiment LP-FP-2 provided information on the release, transport, and deposition of fission products and aerosols during a V-sequence accident scenario that resulted in severe core damage. The specific V-sequence LOCA scenario was a simulated pipe break in the Low Pressure Injection System (LPIS) line, attached to the hot leg of the LOFT broken loop piping. Experiment LP-FP-2 is a major data source for fission product release and transport from failed fuel and severe core damage phenomena in a large fuel bundle.

The experimental results, fission product data, postirradiation examination (PIE), and code verification efforts for the LP-FP-2 Experiment

have been documented in great detail in a number of reports and papers. This report summarizes the most significant results and conclusions contained in these documents, which are listed bibliographically at the end of the report. First, brief descriptions of the LOFT LP-FP-2 system configuration and test conduct are presented. This is followed by highlights of the measured data and PIE and SCDAP/RELAP5 code verification and experiment analysis. Finally, significant results are interpreted and related to other severe core damage progression events and conclusions are presented.

2. SYSTEM DESCRIPTION

The LOFT facility and the LOFT LP-FP-2 Experiment test train, fuel bundle, and fission product monitoring devices are described briefly in the following sections. A more detailed description of the LOFT facility and nominal design characteristics of Experiment LP-FP-2 are provided in Appendices A (Fell and Modro 1990) and B (Carboneau et al. 1989).

2.1 Facility Description

The LOFT test facility was designed to represent the major components and system response of a commercial PWR. The facility was large-scale (1/50th volume of a full-sized PWR), with a reduced-length core (1.67 m) prototypical of full-size PWR bundles. The experimental system consisted of five major subsystems, which were instrumented so that variations in the system could be measured and recorded during the course of a simulated LOCA. These subsystems included: (a) the reactor vessel, (b) the intact loop (representing three loops of a Westinghouse 4-loop PWR), (c) the broken loop (representing the fourth loop) and blowdown suppression system (BST), used to collect effluent from the PCS, (c) and the ECCS. To simulate the thermal-hydraulic phenomena as accurately as possible, volume scaling (1/50 scale) was used to best duplicate in real time the flow regimes for the saturated blowdown and refill/reflood that occur during a large-break LOCA.

Important changes were made to the LOFT facility in order to conduct the LP-FP-2 Experiment. These changes included removal of the broken loop cold leg piping and the simulated steam generator, removal of the blowdown valves and header, installation of a simulated LPIS line at the broken loop hot leg, installation of a special central fuel module (CFM), and addition of the fission product measurement system (FPMS). The configuration of the LOFT facility for Experiment LP-FP-2 is shown in Figure 1.

2.2 Fuel Bundle and Test Train Design

The nuclear core of the LOFT PWR contained nine fuel assemblies identical to commercial fuel assemblies except that the fuel rods were half length. The fuel rods used in these assemblies were 10.7 mm in diameter and contained 4.05 wt% enriched UO_2 fuel. Four of the peripheral or outer assemblies were typical 15 by 15 PWR fuel assemblies, while the four corner assemblies were truncated to triangular shape (see Appendix A).

As noted above, a specially designed CFM, shown in Figure 2, was installed in place of the central fuel bundle for Experiment LP-FP-2. This module (an 11 by 11 fuel assembly) consisted of 11 control rods, 100 prepressurized (2.41 MPa) fuel rods enriched to 9.744 wt% ^{235}U, and 10 instrumented guide tubes. The fuel rods were separated from the outer fuel assemblies by a 0.025-m-thick, zircaloy-clad, zirconium-oxide insulated thermal shroud, that replaced the outer two rows of fuel rods in a typical fuel assembly. The center bundle design enabled the CFM fuel rods to heat up to temperatures above 2100 K, while maintaining the peripheral bundle fuel rods below 1390 K, thus restricting core damage to within the CFM. It also assured that fission products released during the experiment flowed only into the upper plenum of the test facility and facilitated removal of the damaged core from the reactor vessel, decontamination, and recovery of fuel.

The nuclear core was inserted into a reactor vessel that contained an annular downcomer, a lower plenum, lower core support plates, and an upper plenum (see Appendix A). The downcomer was connected to the cold legs of the intact and broken loops, and the upper plenum was connected to the hot legs. For the LP-FP-2 Experiment, the broken loop was a passive system that simulated a pipe break. The ECCS in the experiment, arranged as in a power plant, consisted of a high-pressure injection system

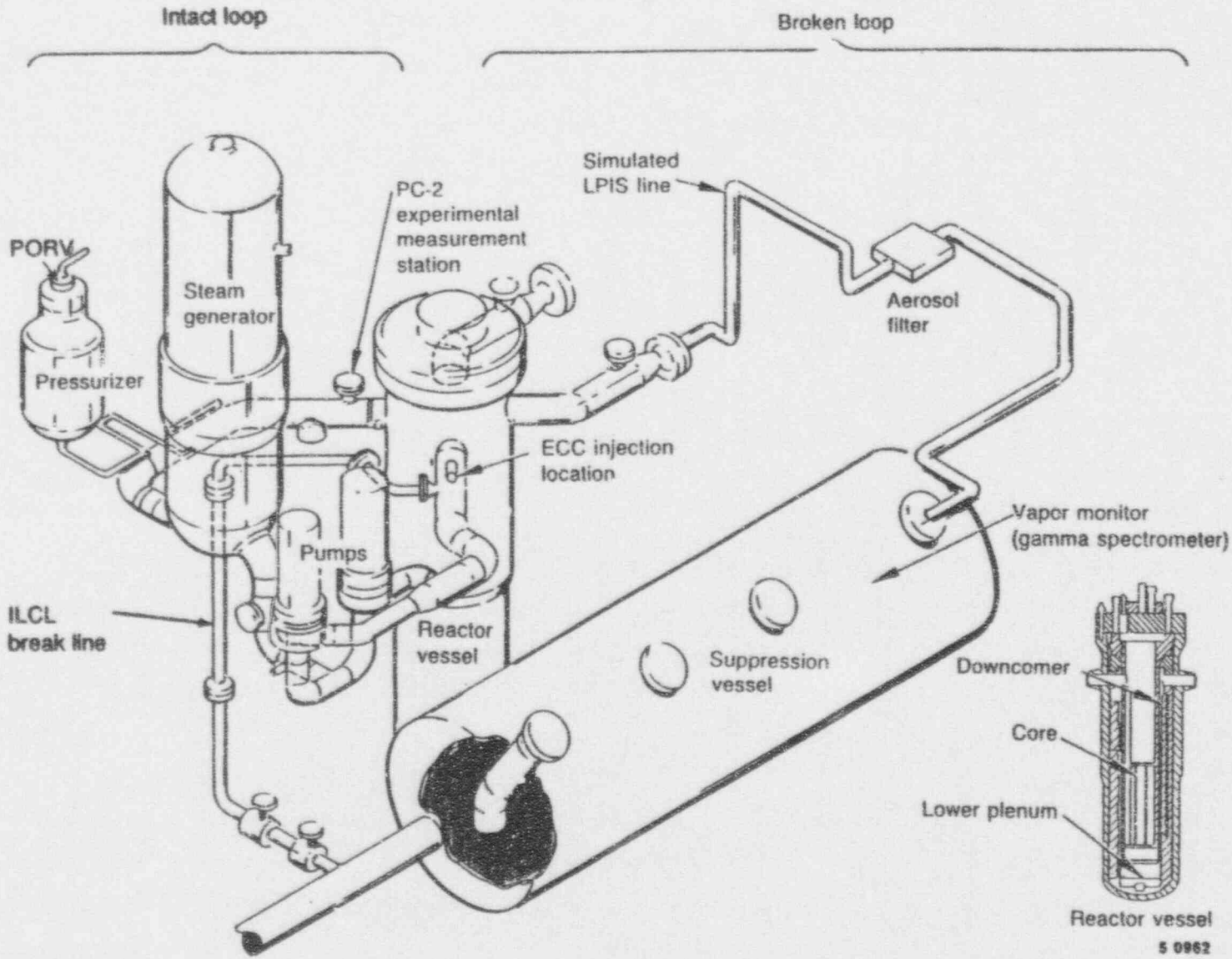

Figure 1. Axonometric view of the LOFT primary coolant system.

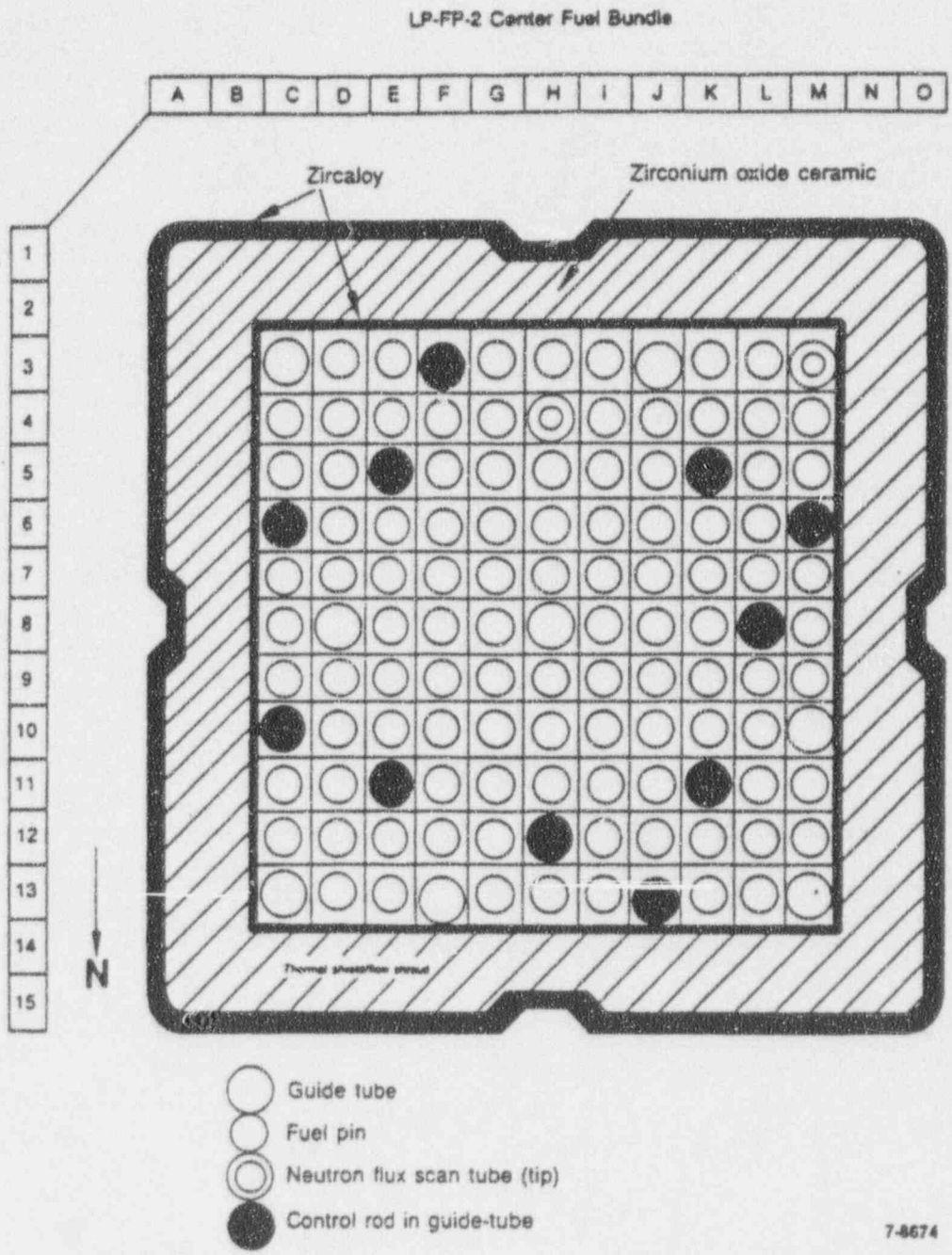

Figure 2. LOFT center fuel module design.

(HPIS), accumulator system, and an LPIS. The simulated LPIS pipe was connected to the end of the broken loop hot leg and provided a path for fission products to enter the BST. The characteristics of the LPIS could be varied during the experiment to attain desired conditions. No attempt was made to scale the ECCS operation for this experiment to represent commercial PWR operations; full accumulators with sufficient volume to bring the primary coolant system to a fully recovered state, were directed to the downcomer and lower plenum as well as the cold leg. This ECC injection, caused the system to reflood significantly faster than would be possible in a commercial PWR.

2.3 Instrumentation

Instrumentation used in the OECD LOFT Facility had been developed over a period of three decades using expertise from around the world. To be sure that all measurements taken during the test were accurate and of the best quality, only state-of-the-art instrumentation was used. This high-quality thermal-hydraulic instrumentation consisted of:

- Thermocouples surface-mounted on 79 fuel rods at either two, three, or four elevations
- Thermocouples mounted on guide tubes, upper and lower tie plates, and structural components
- Self-powered neutron detectors, which also provided a valuable indication of local core voidage
- Conductivity probes to detect liquid level
- Pressure and differential pressure transducers
- Gamma densitometers, coolant flow transducers, momentum flux transducers, and flow rate transducers.

The FPMS was designed and fabricated for use in detecting, identifying, and collecting radioisotopes in the PCS, the LPIS, and the BST. Figure 3 shows a schematic of the FPMS instrumentation location and sample lines. The FPMS consisted of three basis subsystems: (a)

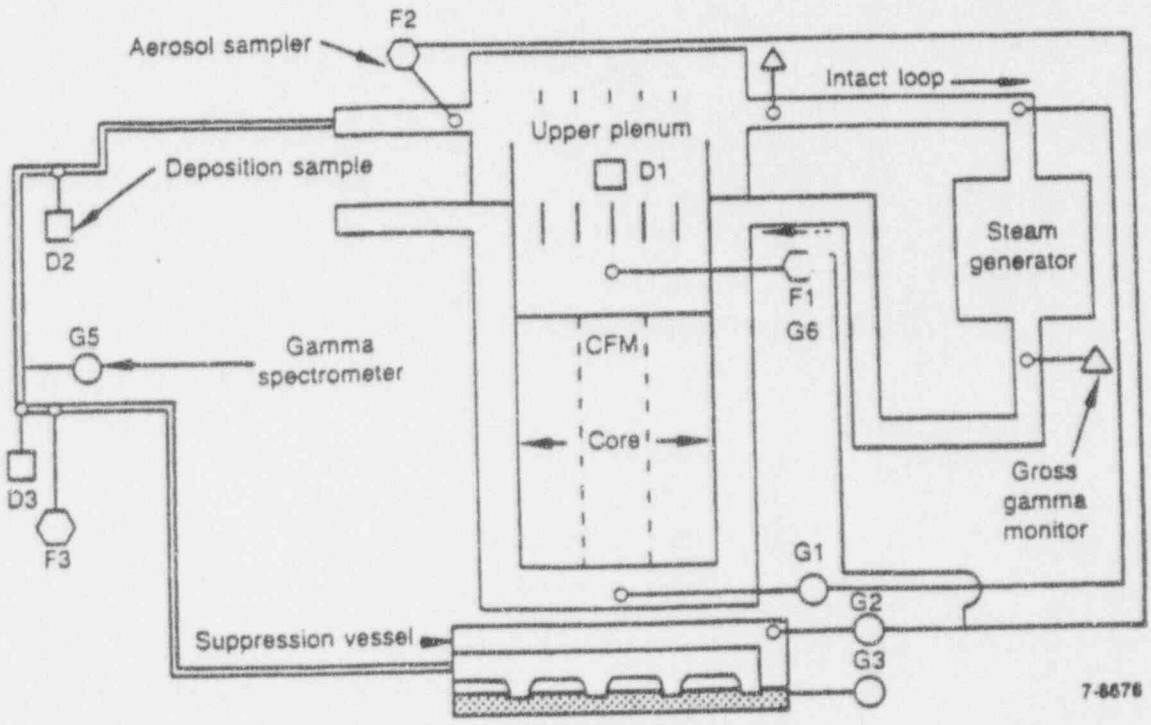

Figure 3. FPMS schematic

four gamma spectrometers and one gross gamma detector; (b) a deposition sampling system, and (c) steam/aerosol sampling lines. These subsystems are described briefly in this section and more completely in Appendix A.

The four on-line gamma spectrometers (G1, G2, G3, and G5) and the gross gamma detector (G6) were located at five different sampling locations, as was shown in Figure 3. The gamma spectrometers sampled from four locations in the system. G1 sampled liquid from the reactor vessel lower plenum during the transient phase or, alternately, from the intact loop hot leg during the posttransient phase. G2 sampled gas from the combined F1 and F2 sample line (i.e., F1 + F2) during the transient phase and from the BST vapor space during the posttransient phase. G3 sampled liquid from the BST liquid space during the posttransient phase. G5 sampled a vertical section of the LPIS line during the transient and posttransient phases. Gross gamma monitor G6 was placed near the F1 line at the top of the reactor vessel. Each of the gamma detectors was designed to be operated remotely and could be calibrated using a ^{238}Th source mounted on a collimator wheel.

The deposition sampling system consisted of six stainless steel coupons in the upper plenum and two deposition spool pieces in the LPIS. Two upper plenum coupons were located at each of three separate elevations above the CFM (for a total of six coupons, collectively designated as D1). At each of the three elevations, both coupons were exposed to the fluid stream flow during the preconditioning and transient phases of the experiment. Before reflood, one coupon at each elevation was to be isolated from the PCS, to protect it from posttransient deposition or removal of fission products. However the protective covering did not seal around the lowest-level coupon (194P), thus exposing it to reflood water. The coupons at higher elevations functioned as planned. The two deposition spools, located near the inlet and outlet of the LPIS line, were designated D2 and D3, respectively. These spool pieces were designed to provide a measurement of the PCS deposition of fission products during the preconditioning and transient phases of the experiment. Since the LPIS line was isolated before reflood, these spool pieces were protected from reflood water.

The remaining instrumentation in the FPMS consisted of two aerosol/steam sampling lines and an aerosol filter on the LPIS outlet, upstream of the BST. This instrumentation was designed to provide a continuous sampling of vapor and aerosols during the preconditioning and transient phases of the experiment. The F1 sample line, situated 180 cm above the lower tie plate and directly above the CFM, consisted of the following major components: (a) a sample line probe placed above the CFM, (b) an argon dilution gas supply, (c) dual cyclone separator and isolation valves, (d) a dilution filter, (e) a virtual impactor, (f) collection filters, (g) infrared moisture detectors, and (h) a hydrogen recombiner. The F2 sample line, situated outside the upper plenum, was similar but had no dilution gas supply or infrared moisture detectors. The F1 and F2 sample lines joined before the BST to form a single line (designated F1 + F2), which passed the G2 gamma spectrometer. The LPIS filter, designated F3, consisted of seven filter canisters and was constructed of a porous metal material that collected aerosol material (approximately 0.4 μm or larger) at the end of the LPIS and immediately upstream of the BST.

3. TEST CONDUCT

This section briefly describes the sequence of events and initial boundary conditions used for the LOFT LP-FP-2 Experiment. A more detailed description of preparation and each phase of the experiment sequence is provided in Appendix B (Carboneau et al. 1989).

3.1 Fuel Preconditioning Phase

The purpose of the fuel preconditioning phase of the experiment was to subject the CFM fuel rods to a minimum burnup and generate the long-lived fission product inventory. This phase of the experiment started when the plant was heated up just prior to power operation and ended when the required minimum burnup, 325 MWd/tU, was attained.

Figure 4 shows the power history used during the fuel preconditioning and pretransient phases to attain the desired initial conditions for the transient. To reach the desired burnup, the CFM fuel rods were irradiated at a reactor power of 32 MWt for approximately 84 hours. The reactor was then shut down, and the rods were allowed to cool for approximately 75 hours. Then, the CFM fuel rods were again irradiated, this time at a reactor power of 26.5 MWt. After approximately 80 hours, the CFM fuel rods reached the required minimum burnup and the reactor was shut down.

3.2 Pretransient Phase

The purpose of the pretransient phase of the experiment, which began at the termination of the preconditioning phase and ended upon the initiation of the transient, was to finish the

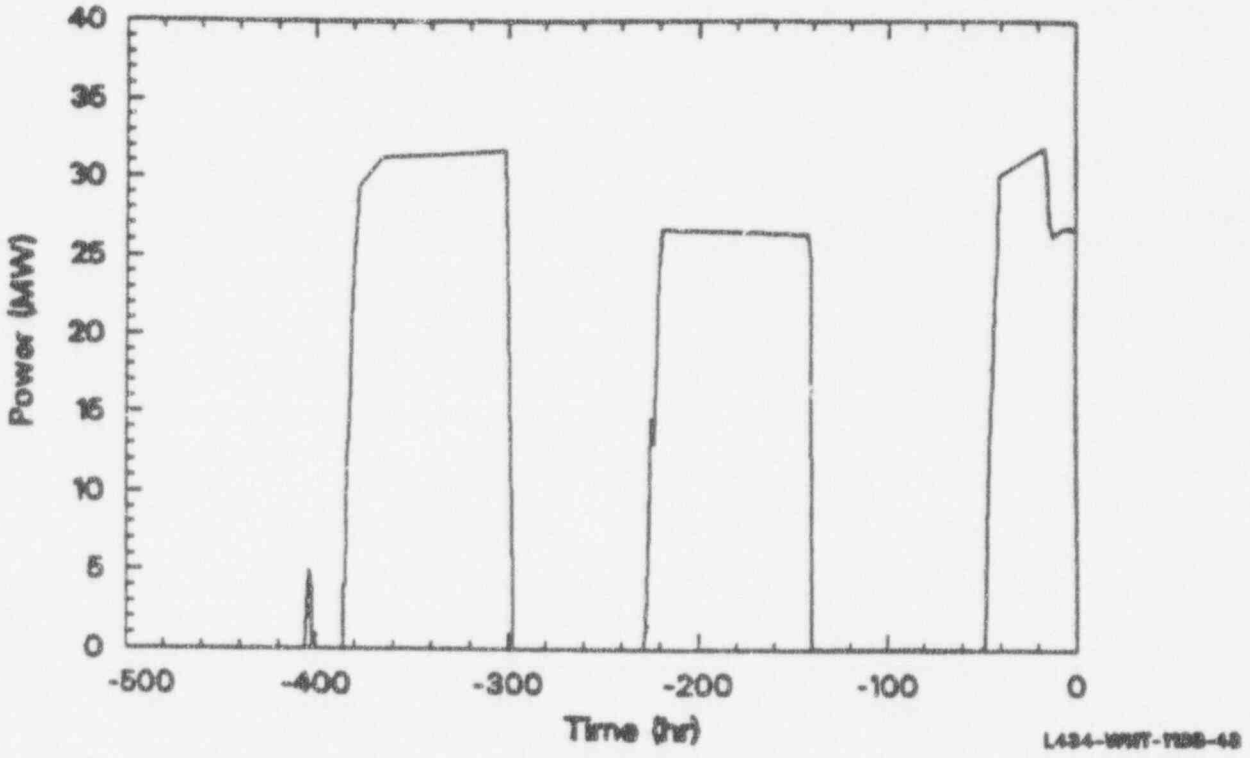

Figure 4. LOFT core power operation prior to initiation of Experiment LP-FP-2.

planned irradiation, generate the short-lived fission product inventory, and establish the initial thermal-hydraulic conditions of the experiment. The required initial conditions for Experiment LP-FP-2 included short-lived decay heat buildup (core decay heat of from 675 to 695 kW at 200 s after reactor scram), a cesium-to-iodine (Cs/I) fission product ratio of at least 2.9, and typical temperature, pressure, and coolant flow rates (see Appendix B). At the beginning of the pretransient phase, the reactor remained shut down so that the fission product measurement equipment could be initialized. The reactor was then brought to power (see Figure 4). The actual preirradiation history produced a burnup of 448 MWd/tU for the CFM fuel rods, a Cs/I ratio of 4.2, and a total core decay heat of 684.5 kW at 200 s into the transient. Thus, compared to the specified initial boundary conditions, the actual conditions for LP-FP-2 met or exceeded the desired experiment goals.

3.3 Transient Phase

The purpose of the transient phase, which began with reactor scram and ended with reflood, was to simulate a V-sequence accident with fission product release and transport phenomena. The specific V-sequence LOCA scenario was a simulated pipe break in the LPIS line, attached to the hot leg of the LOFT broken loop piping (see Figure 1). The intact loop cold leg (ILCL) break line served as the primary blowdown pathway prior to fission product release. During fission product release, only the LPIS line was open; therefore, fission products released from the CFM were transported and deposited in the reactor vessel upper plenum, the LPIS line, and the BST.

The LP-FP-2 transient was initiated by scramming the reactor with the peripheral control rods (defining t = 0.0). The primary coolant pumps (PCP) were then turned off at approximately 10 seconds. After the PCS flow had decreased to 190 kg/s (about 22 seconds), the CFM control rods were unlocked and allowed to fall into the CFM. At 24 seconds, the control rods were fully inserted into the core. The ILCL break line was opened at 33 seconds, and the LPIS line was opened at 222 seconds. The core started heating up at 662 seconds, when the liquid level decreased in the peripheral bundles. The CFM began heating up at 689 seconds. The ILCL break was closed at 736 seconds; however, it was reopened at 878 seconds, to accelerate the PCS depressurization rate.

Besides reopening the ILCL break, the power-operated relief valve (PORV) was opened at 882 seconds. After system pressure dropped below 1.38 MPa, the ILCL and PORV lines were closed, at 1022 and 1162 seconds, respectively. Fission products were first detected in the F1 and F2 lines at about 1200 seconds. Metal-water reaction began at about 1450 seconds, and control rod rupture occurred at approximately 1500 seconds. The hottest measured cladding temperature reached 2100 K by 1504 seconds. The transient continued until the outer shroud wall temperature limitation of 1517 K was reached at 1766 seconds. At this time, the transient was terminated by closing the LPIS line break and initiating ECCS injection.

3.4 Posttransient Phase

The purpose of the posttransient phase of the experiment was to recover the plant to a controlled steady-state shutdown and to obtain posttransient information on fission product and aerosol release, transport, and deposition. Plant recovery was initiated with the closing of the LPIS line and subsequent reflood of the reactor vessel and ended at approximately 3700 seconds following initiation of the transient. Measurement of fission product redistribution in the gas and liquid volumes of the BST and fission product leaching from the damaged CFM fuel rods continued for 44 days following initiation of the transient.

The LPIS line break was closed and FPMS lines were isolated at 1777 and 1778 seconds, respectively; ECCS injection was initiated at 1783 seconds. Liquid water entered the core at approximately 1790 seconds, and the peripheral fuel modules quenched soon afterward. However, observed phenomena indicate that the CFM did not quench quickly, in fact, a rapid

temperature excursion probably occurred within the CFM during reflood, due to enhanced metal-water reactions. This hypothesis is discussed in more detail in the Section 6 of this report.

During the early part of the posttransient phase, the PORV was cycled twice to prevent the PCS from overpressurizing, and a feed-and-bleed operation was performed on the steam generator. The plant was maintained in a quiescent state for 14 days while data were taken, using the on-line FPMS and thermal-hydraulic measurement systems. Also, several grab samples were taken from the BST and PCS. BST liquid samples were taken at 21 days, BST vapor samples were taken at 28 days, and PCS liquid samples were taken at 44 days.

The significant events for the transient and early posttransient phases of Experiment LP-FP-2 are listed in Table 1. The intact loop pressure history is shown in Figure 5, along with the identification of important events during the transient.

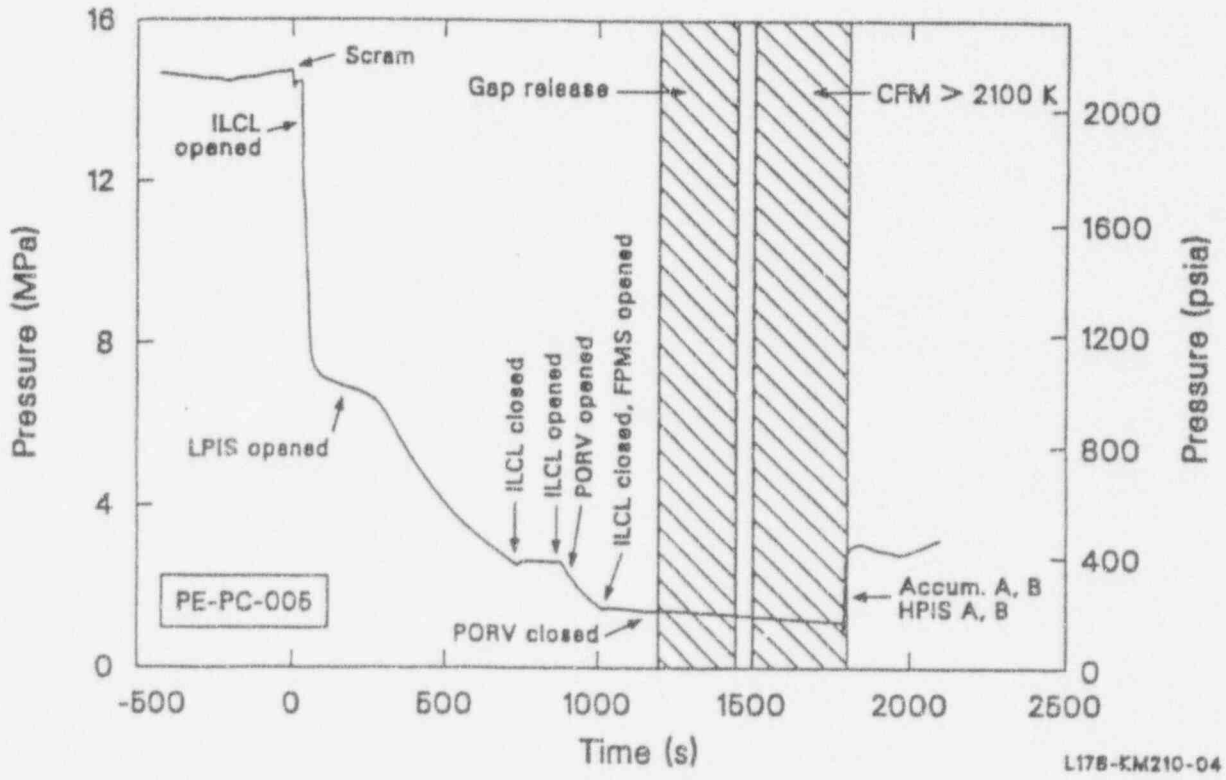

Figure 5. Primary system pressure history, showing significant events.

Table 1. Sequence of events for Experiment LP-FP-2.

Event	Time after Transient Initiation (s)
Scram (initiation of experiment)	0.0
Peripheral bundle control rod fully inserted	2.4 ± 0.1
Primary coolant pump coastdown initiated	9.7 ± 0.1
Begin dropping CFM control rods	22.4 ± 0.1
CFM control rods fully inserted	23.4 ± 0.5
Primary coolant pump coastdown completed	25.1 ± 0.1
ILCL break initiated	32.9 ± 0.1
End of subcooled blowdown	53.0 ± 1.0
Secondary relief valve cycle	56.0 ± 1.0
Pressurizer empty	60.0 ± 5.0
LPIS line break opened	221.6 ± 0.1
Secondary pressure exceeded primary system pressure	260.0 ± 10
Gamma densitometer sources isolated	262.0 ± 2
First coolant thermocouple deviation from saturation	
Upper plenum	300.0 ± 10
Hot leg pipe	390.0 ± 10
Fuel rod cladding heatup started in peripheral fuel modules	662.0 ± 2
Fuel rod cladding heatup started in CFM	689.0 ± 2
ILCL break closed	735.5 ± 0.1
ILCL break reopened	877.6 ± 0.1
PORV opened	882.0 ± 0.1
F3 filter on line	950.8 ± 0.1
LPIS bypass closed	951.9 ± 0.1
FPMS lines opened	1013.1 ± 0.1
ILCL closed	1021.5 ± 0.1
PORV closed	1162.0 ± 0.1
First indication of fission products at F1 (gap)	1200.0 ± 20
Initiation of metal-water reaction	1450.0 ± 30
Control rod rupture	1500.0 ± 100
First indication of fission products at F1, F2, and F3 (fuel)	1500.0 ± 10
Cladding temperatures reach 2100 K	1500.0 ± 1
Shroud temperature reached trip set point	
First thermocouple	1743.0 ± 1
Second thermocouple	1766.0 ± 1
LPIS line break closed	1777.6 ± 0.1
FPMS lines closed	1778.1 ± 0.1
Deposition coupons isolated	1780.6 ± 0.1
Reflood initiated	1782.6 ± 0.1
Accumulator flow stopped	1795.0 ± 6
Maximum LPIS line coolant temperature reached	1800.0 ± 5
Steam generator feed-and-bleed started	2600.0 ± 10
PORV opened	3350.0 ± 10
PORV closed	3380.0 ± 10
PORV opened	3680.0 ± 10
PORV closed	3690.0 ± 10

4. HIGHLIGHTS OF THE MEASURED DATA

4.1 Thermal-Hydraulic Data

The LP-FP-2 Experiment was designed to simulate a V-sequence accident scenario with fission product release. From a thermal-hydraulic point of view, a V-sequence accident is a small-break LOCA. However, the LP-FP-2 Experiment represented an unusual LOCA, consisting of two simultaneous breaks and discharge through the PORV. Although LP-FP-2 was not a true V-sequence type experiment, the multiple breaks did achieve the desired V-sequence thermal-hydraulic conditions at the time of fission product release and maximized the decay heat for core heat-up.

The primary core temperature objective for LP-FP-2 was to obtain peak CFM temperatures above 2100 K for at least three minutes while maintaining peripheral bundle fuel rods below 1390 K and the outside shroud temperature below 1517 K. Figure 6 shows an overlay of several core thermocouples (TCs), including the TC-5IO8-27 fuel centerline thermocouple that recorded the highest measured fuel temperature (2313 K) before reflood. The LP-FP-2 centerline TCs were located at the 0.686-m, or peak power, elevation. These thermocouples were constructed of tungsten-rhenium wires and were insulated with hafnia (HfO_2). The centerline thermocouples were tested (prior to LP-FP-2) up to 2700 K. These tests showed that the thermocouples remained within 112% of the reference temperature up to 2573 K, with some signs of shunting and calibration shifts beginning at 2673 K. The measured temperature data during LP-FP-2 indicate that the centerline TCs provided valid data well into the high-

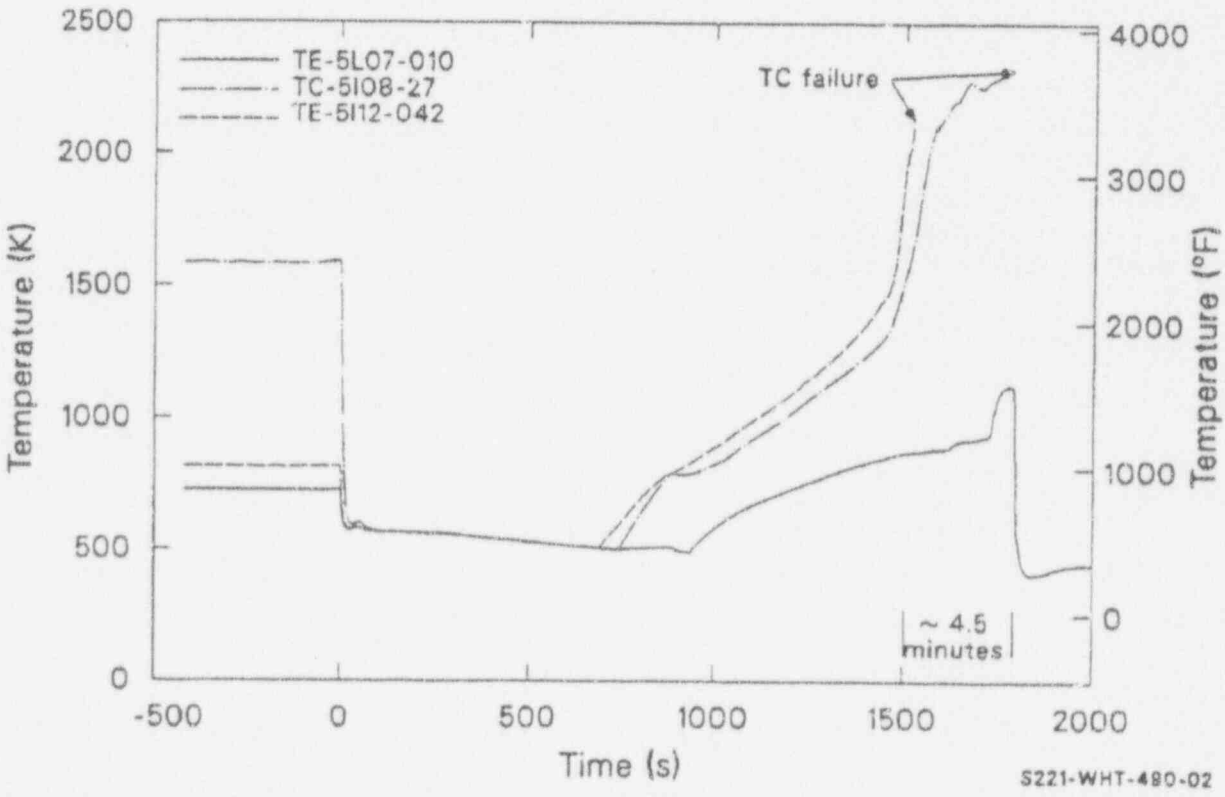

Figure 6. CFM thermocouple data at 0.25-, 0.68-, and 1.07-m elevations.

temperature transient. Since shunting effects are not evident in the centerline TC data during the transient, and since the centerline TCs were routed up through the CFM, peak fuel temperatures (above the 0.686-m elevation) must have been less than 2700 K. Detailed thermal-hydraulic computer code calculations reported in Carboneau et al. (1989) and confirmed by subsequent code analyses (see Section 6) predict that most of the CFM fuel was at temperatures less than 2700 K, with one section reaching 2800 K for a short time. Based on the measured data, it is concluded that peak transient fuel temperatures for LP-FP-2 ranged between 2300 K and 2700 K. The measured transient fuel temperatures do not indicate that fuel melting could have occurred in the CFM. Nevertheless, the PIE data (Jensen et al. 1989) show that the highest temperature region was located between the 0.686 and 0.864 m elevations. In this region, some fuel melting did occur, with peak fuel temperatures reaching 3120 K. Therefore, the transient centerline TC data are not consistent with the PIE observations unless it is assumed that the maximum fuel temperatures (i.e., fuel melting) occurred after reflood. In fact, review of the centerline TC data into the reflood period shows that a rapid temperature excursion of up to 3000 K probably occurred before TC failure (Modro and Carboneau 1990).

The measured upper plenum fluid temperatures above the CFM generally ranged from 500 K to 900 K, with an average temperature of about 730 K (calculated between 1500 and 1778 seconds). The upper plenum surface temperatures averaged about 8% cooler than the surrounding fluid. These temperatures indicate that the upper plenum conditions were relatively cool during the experiment and that most fission product chemical species in the upper plenum would exist in either a liquid or solid state.

The steam mass flow rate for the CFM was not a measured parameter. However, the steam mass flow rate for the F1 sample line, which sampled the effluent exiting the CFM, was calculated based on measured critical flow conditions in the F1 sample line (Carboneau et al. 1987; Carboneau et al. 1989). The calculated steam mass flow rate for the F1 line was checked against the mass of water collected in the F1 condenser by integrating the time-dependent mass flow rate over the time period the line was open. The two results agreed to within 6% (or 6 g). Since the averaged sampling fraction for the F1 probe (i.e., the ratio of F1 to CFM flow rates) could be estimated from other measured data, the steam mass flow rate exiting the center fuel bundle could also be determined. Figure 7 shows the best-estimate steam mass flow rate exiting the CFM based on the Experiment Analysis Summary Report (EASR) analysis (Carboneau et al. 1989). The uncertainty in the calculated CFM steam mass flow rate is about ± 50% and is mainly attributable to the uncertainty in the calculated F1 sampling fraction.

Unlike the CFM mass flow rate calculation, the steam mass flow rate for the LPIS line could be directly calculated from measured critical flow conditions for the LPIS venturi. The result of the analysis is shown in Figure 8.

4.2 Fission Product Data from the LPIS Line and BST

The on-line gamma spectrometer data consist of two data sets: (a) the G5 data from the LPIS line, and (b) the G2 data from the combined F1+F2 sample line. The xenon (Xe) gas data from G5 are shown in Figure 9, along with a curve representing the calculated limit of detectability. The measured krypton (Kr) data are similar to the Xe data in that very few Kr isotopes were detected at G5. The reason for the high limit of detectability for the noble gases at G5 is due to the high activities of deposited iodine (I) and cesium (Cs) isotopes in the G5 spool piece. Figure 10 shows the measured activity concentrations of I, Cs, and rubidium (Rb) isotopes as a function of time at the G5 spool piece. These data are reported in terms of an activity density (Ci/m^3); however, the measurement represents a combination of suspended and surface-deposited concentrations. For the G5 spool piece, the

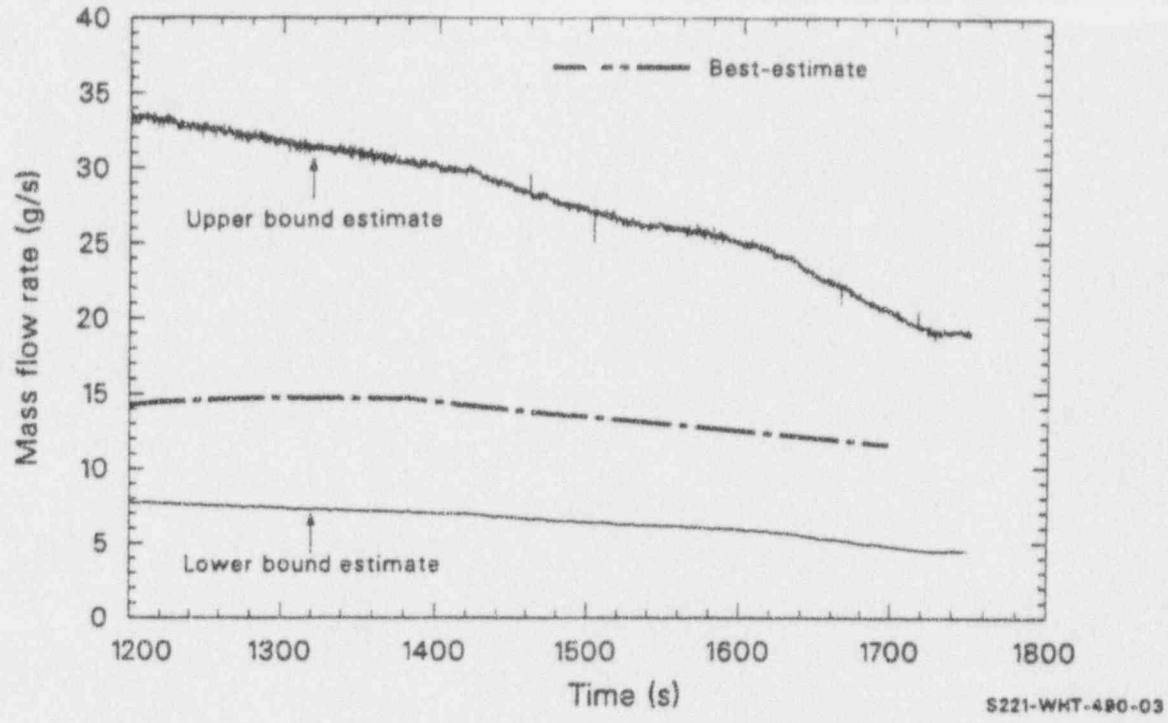

Figure 7. The best-estimate CFM steam mass flow rate.

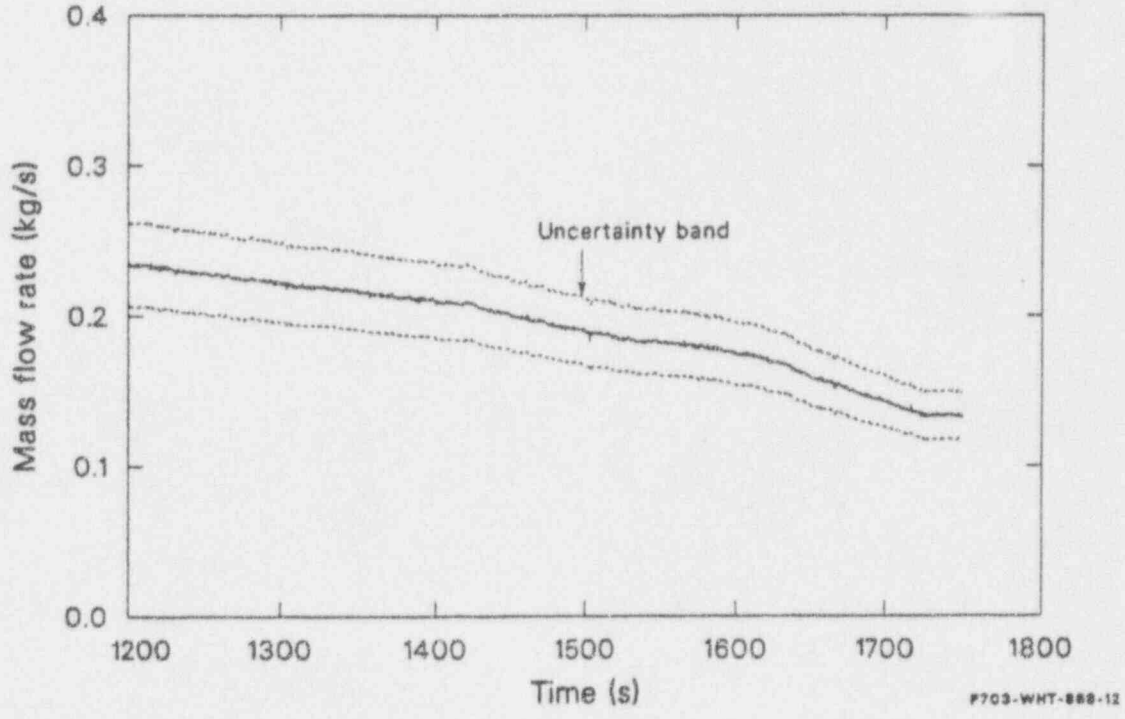

Figure 8. The best-estimate LPIS mass flow rate.

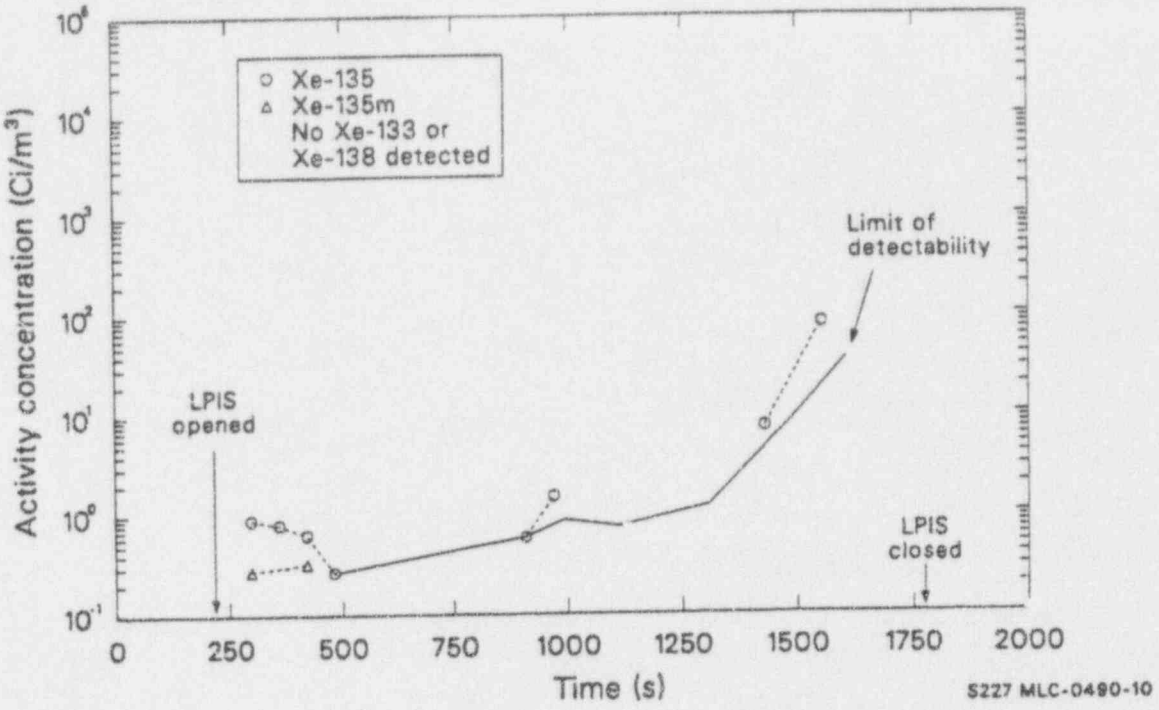

Figure 9. Measured concentrations of Xe with the theoretical limit of detectability at G5.

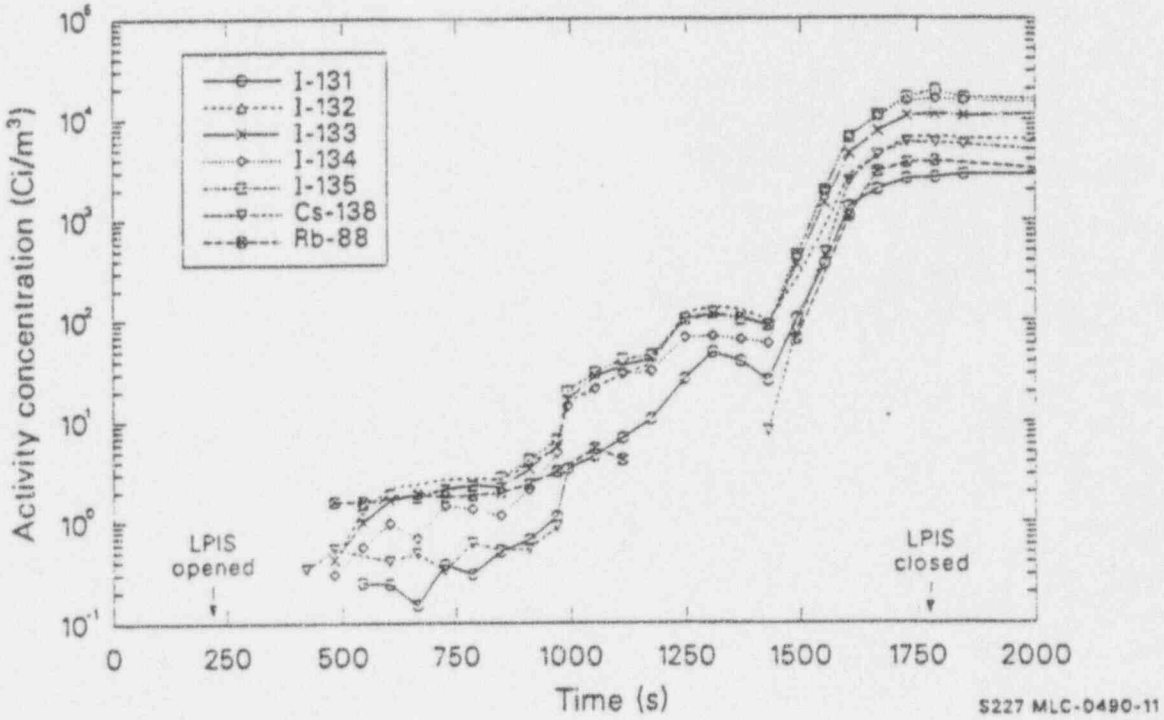

Figure 10. Measured activity concentrations of I, Cs, and Rb isotopes at G5.

deposited surface activity probably exceeded the suspended activity concentration.

The high deposition of radionuclides in front of the G5 gamma spectrometer influenced the noble gas detectability in the LPIS line. Corresponding to the measured activity concentrations shown in Figure 10, the elemental mass concentrations of Cs, I, and Rb were determined and are displayed in Figure 11(Results are decay corrected for times greater than 1778 s). Notice that the average I mass concentration can be determined from the five individually measured isotopes, while the elemental Cs and Rb mass concentrations are based on only one radionuclide. From Figure 11, the elemental I mass concentration at G5 was 0.055 ± 0.02 $\mu g/cm^3$, (or an equivalent surface concentration of 0.041 ± 0.02 $\mu g/cm^2$). Also based on this figure, the Cs mass concentration at G5 (suspended plus deposited material) following closure of the LPIS line (>1778 s) was about 0.10 $\mu g/cm^3$, (or, equivalently, 0.074 $\mu g/cm^2$). Therefore, the Cs/I mass ratio at G5 was 1.8. This can be compared with the Cs/I mass ratio of 4.2 for the CFM. The postexperiment examination of the D2 spool piece upstream of G5 showed a higher surface concentration of Cs (0.236 $\mu g/cm^3$) than at G5; and, at D3, downstream of G5, the Cs surface concentration was 0.067 g/cm^2. Also, data taken from the BST indicate that about 1% of the CFM inventory of I reached the BST, while only 0.23% of the Cs inventory was present. This implies a Cs/I mass ratio of only 1.1 for the BST. All data from the LPIS and BST indicate that Cs deposited in the LPIS line more readily than I indicating that Cs and I were traveling as different chemical species, and that the Cs specie deposited quickly. As shown in the following section, the reverse situation occurred in the reactor vessel upper plenum.

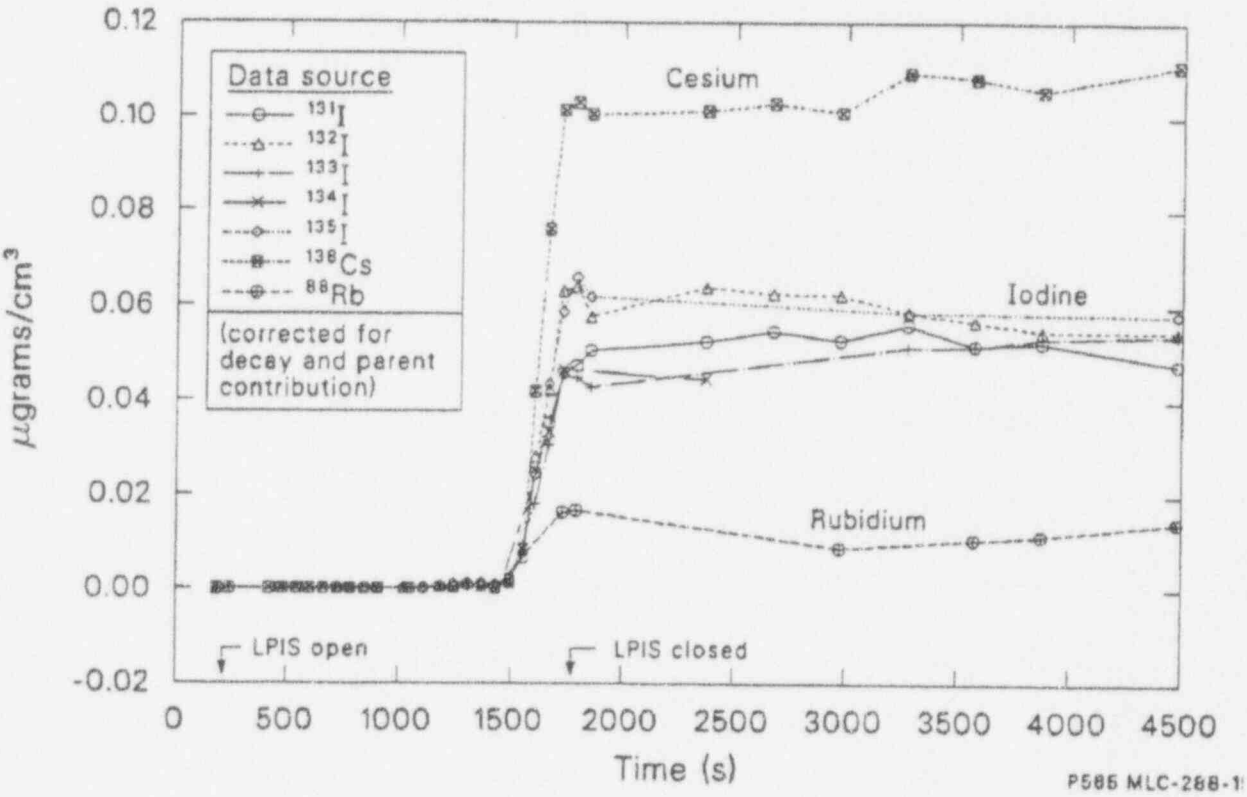

Figure 11. Elemental mass concentrations of Cs, I, and Rb at G5.

4.3 Upper Plenum Coupon Data and Possible Forms of Cs and I

The upper plenum deposition device (D1) was a long slender tube that contained six deposition coupons made of Type 304 stainless steel. Two coupons were placed at each of three axial locations. The three locations were situated at three different axial elevations-stations 194, 212, and 253, corresponding to 0.15, 0.61, and 1.65 m above the CFM upper tie plate (station 188). All coupons were exposed to the pretest reactor environment and the transient portion of the experiment. Immediately before reflood, one coupon at each elevation was to be isolated (covered). The coverable, or protected, coupons were identified as 194P, 212P, and 253P. The unprotected coupons (194U, 212U, and 253U) were exposed to the transient and reflood portions of the experiment and, therefore, provided information on the irreversible plateout of fission products. Protected coupons were designed to provide information on the total deposition of fission products and control rod aerosol material prior to reflood. The protected coupons were 2.2 cm^2 in surface area while the unprotected coupons were 1.6 cm^2

Inspection of the D1 device after the experiment showed that the lower section of the D1 tube did not seal properly around coupon 194P. As a result, this coupon was washed during reflood; and the data from coupon 194P do not represent a protected sample. Examination of coupons 212P and 253P showed that they were properly sealed.

Besides the protected coupon data, three protected coupon spacers (194S, 212S, and 253S) were also examined. Again, only the upper two coupon spacers were properly sealed before reflood. The effective deposition surface area for the coupon spacers was approximately 0.81 cm^2. Table 2 summarizes the most important data obtained from the two protected coupons, 212P and 253P, and the two protected coupon spacers, 212S and 253S. This table shows the measured data, the equivalent activity concentration of the measured nuclides, and the elemental mass concentrations. Based on the Cs mass concentration for the protected coupons and spacers, it is apparent that very little Cs was present on these samples. In fact, the Cs/I ratio for these samples varied from 0.0004 to 0.074. This result is very low compared to the Cs/I ratio for the CFM of 4.2. Furthermore, the average surface mass concentration of I on the four protected upper plenum samples was 0.060 $\mu g/cm^2$, which compares well with the I surface mass concentration of 0.041 $\mu g/cm^2$ at G5. However, the average Cs mass concentration on the four protected upper plenum samples was 0.0005 $\mu g/cm^2$, and the corresponding concentration on the D2 spool piece was 0.24 $\mu g/cm^2$.

The upper plenum coupon data indicate that I deposited on stainless steel surfaces in concentrations similar to that observed in the initial sections of the LPIS line. These data also show that Cs did not deposit in the upper plenum in any reasonable concentrations. In other words, in the LPIS line, both Cs and I behaved like a condensable species; whereas, in the upper plenum, I behaved like a condensable species and Cs did not. Collectively, this indicates that the primary I species was not cesium iodide (CsI). If CsI were the primary chemical form of I, then Cs should have been present in concentrations that would have produced a Cs/I ratio of at least 1.0. Since the measured Cs/I ratio was < 0.074 and not > 1.0, it is clear that the primary chemical species of I was not CsI.

Figure 12 shows the vapor pressure of several important compounds associated with reactor accident studies. Note that the vapor pressure of these compounds can be arranged as follows:

$$CsOH > CdI_2 > CsI > AgI > CsBO_2.$$

Due to the high concentrations of I on the upper plenum protected coupons and in the LPIS line at G5, it appears that I behaved like a condensable species during the experiment. Consequently, it is not likely that large concentrations of I appeared as either I_2 or HI. Also, the primary chemical form of I was

Table 2. Upper plenum coupon and coupon spacer data for 212P, 253P, 212S, and 253S.

	Measured sample activity (μCi/sample)			
Isotope	Coupon 212P[a]	Coupon 253P[a]	Spacer 212S[b]	Spacer 253S[b]
^{131}I	14000	1250	4300	740
^{137}Cs	0.062	0.069	0.0011	0.0135
^{140}Ba	30000	72	8300	29
^{129m}Te	52	24	13	6.8
	Activity concentrations (Ci/cm^2)			
Isotope	Coupon 212P[a]	Coupon 253P[a]	Spacer 212S[b]	Spacer 253S[b]
^{131}I	6364.	568	5292	911
^{137}Cs	0.028	0.031	0.0014	0.017
^{140}Ba	13640	32.7	10220	31.8
^{129m}Te	23.6	10.9	16	8.4
	Calculated elemental mass concentrations ($\mu g/cm^2$)			
Element	Coupon 212P[c]	Coupon 253P[c]	Spacer 212S[c]	Spacer 253S[c]
Iodine	0.116	0.0103	0.0957	0.0165
Cesium	0.00069	0.00076	0.000035	0.00042
Barium	0.504	0.00121	0.378	0.00117
Tellurium	0.039	0.014	0.021	0.011
Silver	201	104	ND[d]	ND[d]
Cadmium	30.9	21.4	ND[d]	ND[d]

a. The protected coupons have a surface area of 2.2 cm^2.

b. The protected coupon spacers have a surface area of 0.8125 cm^2.

c. Elemental results for iodine, cesium, barium, and tellurium were computed based on the isotopic mass concentration ($\mu Ci/cm^2$) and the ORIGEN2-calculated CFM inventory results presented in Carboneau et al., 1989. The elemental mass concentrations for Ag and Cd were measured. To convert from an isotopic activity to an elemental mass, the following ORIGEN2-calculated ratios for the CFM fuel were used: 54952 Ci ^{131}I/g I; 40.514 Ci ^{137}Cs/g Cs; 27070 Ci ^{140}Ba/g Ba; 757.4 Ci ^{129m}Te/g Te.

d. No data.

probably not CdI_2, because cadmium (Cd) has a high vapor pressure and most of the Cd was probably released from the control rods before significant concentrations of I were released from the fuel. Furthermore, leach data from the LPIS line and deposition data from the unprotected coupons suggest that I was deposited as a highly insoluble species. By a process of elimination, the only likely I compound that fits all observations is silver iodide (AgI). Note that from Figure 12, AgI and CsI have similar vapor pressure curves and, therefore, AgI would have behaved like CsI and condensed on surfaces in the upper plenum. Based on the data shown in Table 2, the upper coupon analysis indicates that I was not associated with Cs and the most likely I species was AgI. In addition, at every location for which I was detected, Ag was measured in quantities sufficient to support the presence of AgI.

The upper plenum coupon data can also be used to infer the probable chemical form of Cs. Based on the vapor pressure data shown in Figure 12 and the average upper plenum temperature of ~730 K, it is clear that for Cs not to deposit on the upper plenum coupons, the chemical form of Cs would have to support a relatively high vapor pressure. The most obvious candidate is cesium hydroxide (CsOH). Under the right temperature and concentration conditions, CsOH could pass through the upper plenum and not condense; but, upon reaching the colder LPIS line, would condense readily. Also from Figure 12, it is clear that Cs was not present as cesium metaborate ($CsBO_2$). Since $CsBO_2$ has a very low vapor pressure, any reasonable concentration of $CsBO_2$ would have produced significant concentrations of Cs on the upper plenum coupons or on deposited aerosols. Consequently, the observed upper plenum data imply that the preferred chemical form for cesium was CsOH.

In summary, the upper plenum protected coupon data indicates that the primary chemical species of Cs and I were CsOH and AgI. These chemical compounds are consistent with the LPIS line data.

4.4 On-line Fission Product Data from G2

The F1 and F2 sample lines joined to form a single line (identified as F1+F2) that passed near the G2 gamma spectrometer. During the transient, the G2 gamma spectrometer system recorded the activity concentrations of seven radioactive noble gases that passed through this sample system. Although the G2 data do not indicate which sample line the detected radionuclides entered, the sample line mass flow rate information and postexperiment deposition data from these lines show that 89% of the noble gases detected at G2 entered the F1 sample line from the CFM, and about 11% entered the F2 line from the broken loop hot leg (BLHL), upstream of the LPIS line. The measured Xe gas data, as collected at G2, are shown in Figure 13. Based on these data, the average elemental mass concentration for Xe was calculated and is shown in Figure 14, along with the average Kr mass concentration. Notice that the Xe and Kr releases peak at 1668 seconds (about 2 minutes before the end of the transient) and then decrease after the F1 and F2 lines were isolated from the PCS at 1778 seconds. The drop in the noble gas concentrations at 1668 seconds may have resulted from a partial blockage within the CFM that affected the fission product release or transport to the F1 probe. Note that the decrease in fission product concentrations at G2 was probably not due to a blockage in the F1 sample line because no sudden decrease in the steam mass flow rate entering F1 was observed. Other thermal-hydraulic observations (e.g., enhanced cooling of the peripheral bundles) also suggest that a partial blockage or flow diversion occurred within the CFM between 1500 and 1700 s. Code analysis has confirmed this hypothesis (see Section 6).

Using the average Xe (or Kr) mass concentrations from Figure 14, the time-dependent volumetric gas flow rate in the F1+F2 sample line at G2 (Carboneau et al. 1989), and the average flow fraction (89%) for the F1 line, the mass rate of Xe entering the F1 sample line from the CFM was computed. By dividing this

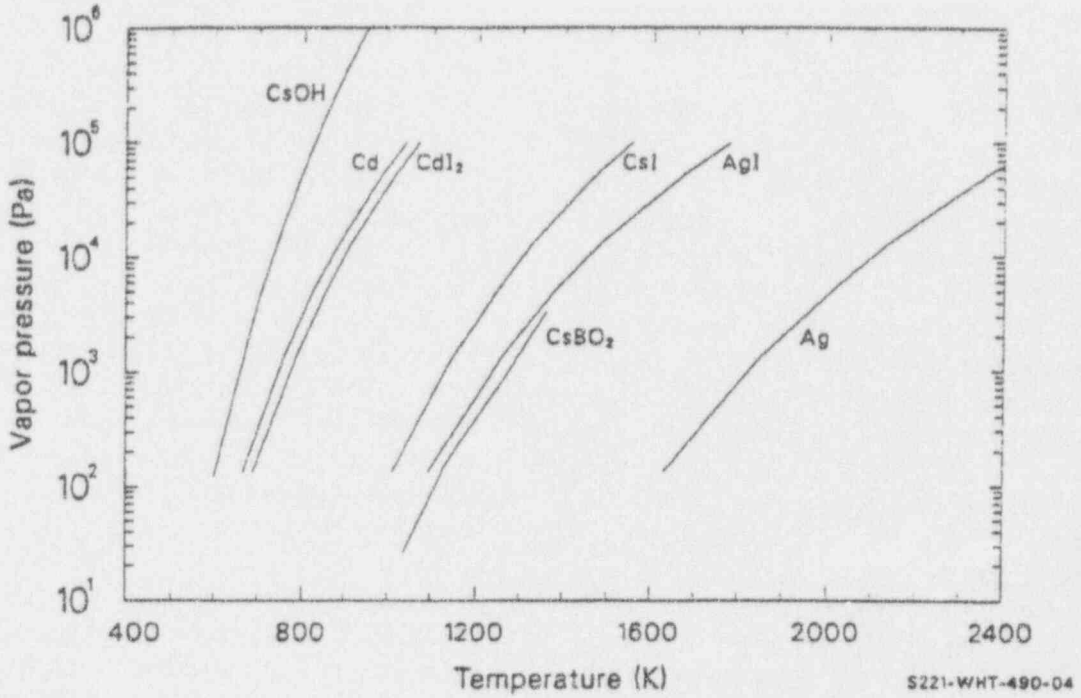

Figure 12. Vapor pressures of Cs, I, and Ag compounds as a function of temperature.

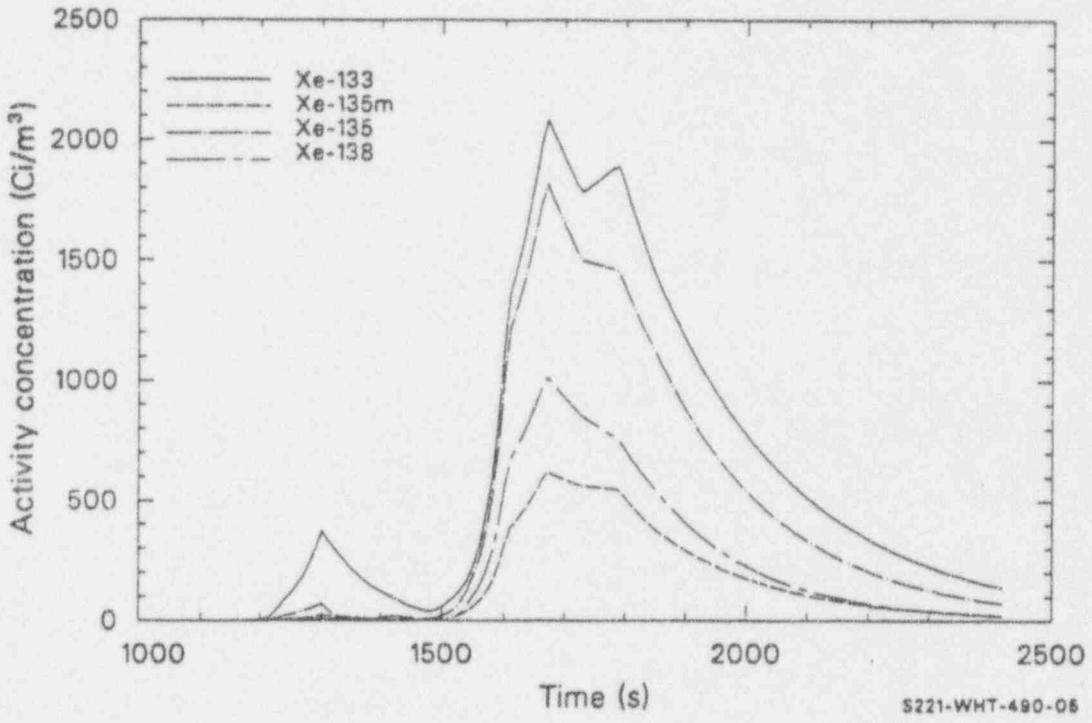

Figure 13. Measured Xe activity concentrations at G2.

result by the average sampling fraction for the F1 line (0.00763) and the initial Xe mass for the CFM, the transient noble gas release fraction for the CFM was determined. This result and the corresponding cumulative noble gas release fraction for the CFM are shown in Figure 15.

According to the data presented in Figure 15, the cumulative transient release fraction for the noble gases was about 2.3%. This compares well with the measured quantity of 1.7% Xe and 2.0% Kr gases collected in the BST. Computer code analyses reported by Carboneau et al. (1989) and subsequently confirmed (see Section 6) suggest two reasons for the small transient fission gas release: (a) the initially large grain structure of the fuel (approximately 14 μm) and (b) the limited fuel temperatures (< 2700 K) during the transient. Both factors probably contributed to limiting the release of fission products during the transient. However, analyses of the PCS water showed that at least 9% of the initial CFM inventory of Kr was trapped in the PCS following reflood. Therefore, the total Kr release for the LP-FP-2 Experiment was > 11%, with most of the Kr appearing in the PCS following reflood. The best-estimate transient and posttransient release fractions for Xe, Kr, Cs, and I are shown in Table 3. These data show that most released fission products were detected in the PCS (shortly after reflood), suggesting that these fission products were probably released because of reflood.

4.5 Hydrogen Generation and Distribution

The quantity of hydrogen gas in the BST vapor space was measured at 203 ± 11 g. An additional small amount of hydrogen dissolved in the BST water was calculated to be 2.4 ± 0.3 g, using Henry's Law. Therefore, the total amount of hydrogen that was transported to the BST was 205 ± 11 g. This hydrogen mass is equivalent to the oxidation of 11.6% of the zircaloy in the CFM; however, this result is too small to account for the observed oxidation of the CFM (58%) based on the PIE. Clearly, a large amount of hydrogen must have been generated during the experiment that was not transported to the BST. Since the PCS was vented to the BST via the LPIS line, it was not clear how hydrogen gas (or the fission products) could have been held up in the PCS. In order to investigate this matter, a detailed review of the PCS pressure and thermocouple data was undertaken. This investigation showed that three large gas bubbles had formed within the PCS a few hours following reflood. These bubbles existed in the reactor vessel upper plenum head, the pressurizer, and the steam generator tubes. The total volume of all three bubbles was approximately 28 m^3 (calculated at STP conditions). After the water vapor volume was subtracted from the total gas volume, the remaining dry, or noncondensable, gas volume was determined to be 12.3 m^3. Next, by subtracting the known volumes of noncondensable gases injected into the PCS [nitrogen (N) from the D1 coupon device and the accumulator water and argon (Ar) from the F1 sample line, with helium (He) and fission product gases estimated to produce negligible contributions], a residual gas volume of 7.0 m^3 was determined. This residual gas bubble was assumed to consist of only hydrogen. As a result of this analysis (see Carboneau et al. 1989 for details), it was determined that 819 ± 364 g of hydrogen was in the PCS following reflood (625 g in the noncondensable gas bubbles and 194 g dissolved in the PCS water). Summing the BST and PCS inventories of hydrogen, the total amount of hydrogen that was generated during the LP-FP-2 Experiment was 1024 ± 364 g. This result is equivalent to an oxidation of 58% of the zircaloy in the CFM, which agrees with the PIE estimate.

An obvious conclusion of the hydrogen analysis is that only a small amount of the hydrogen generated during the LP-FP-2 Experiment was transported to the BST. Either the hydrogen was generated during the transient and was held up in the PCS, or the hydrogen was generated after the BST was isolated from the PCS (i.e., following reflood). In order to decide which of the two alternatives represents the best-estimate scenario, the following observation needs to be made.

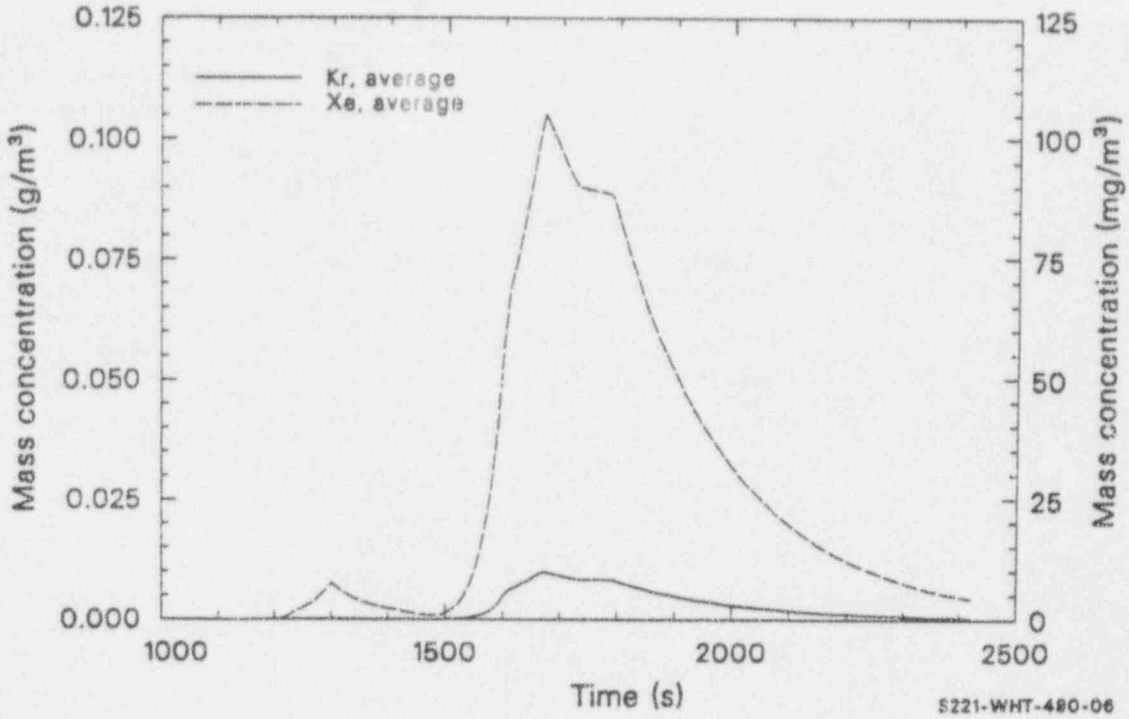

Figure 14. Total Xe and Kr mass concentrations at G2.

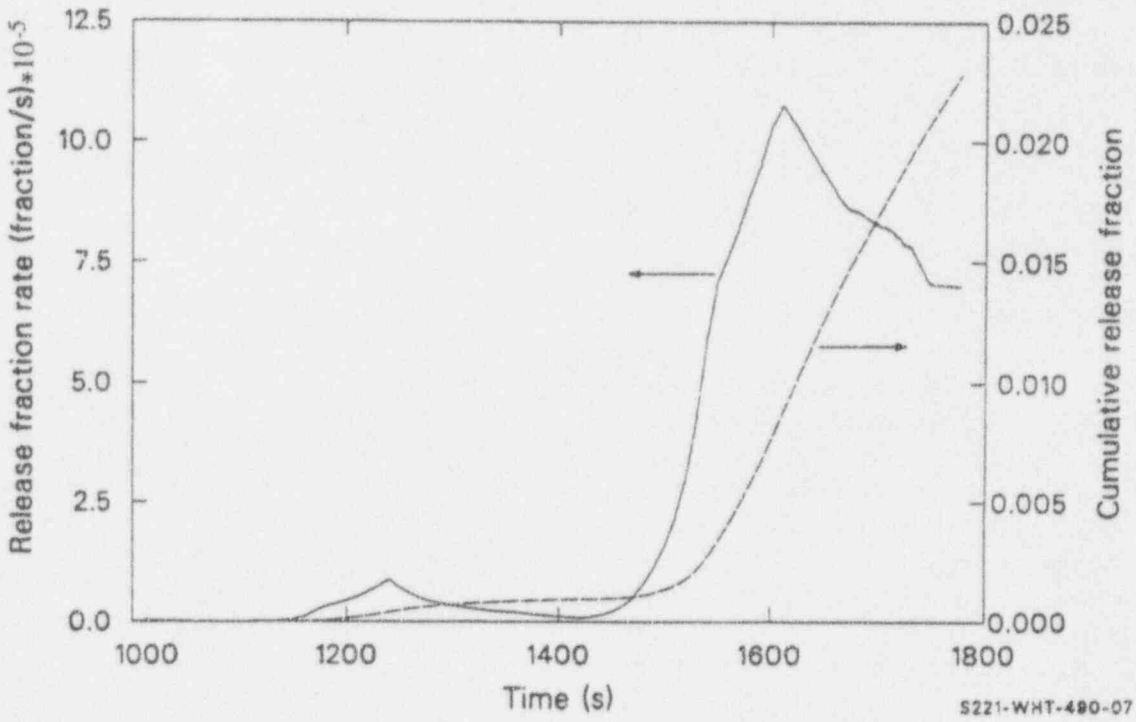

Figure 15. Noble gas release fraction rate and cumulative release fraction from G2 data.

Table 3. Measured and calculated transient and posttransient release fractions.

Species	Transient data		Posttransient data
	Estimated transient release fractions based on deposition or BST data	Calculated transient release fractions based on the F1 sample line	Measured release fractions computed for the PCS
Xenon	≥ 0.017	≤ 0.054	Not measured
Krypton	≥ 0.020	≤ 0.047	> 0.09
Iodine	0.030	0.052	0.123 to 0.135
Cesium	0.0080	0.029	0.156
Barium	0.0084	0.0022	0.082
Tellurium	0.0054	0.00025	0.029

Based on the F1 steam mass flow rate data and PIE of the bundle, steam exited the CFM during the entire transient and there was no indication of a steam flow path through the insulating shroud; therefore, steam-starved conditions did not occur for the entire CFM. However, due to the partial blockage that formed within the CFM, the steam flow distribution probably resulted in some regions of the bundle being steam-starved, thereby, limiting the metal-water reaction during the transient. This conclusion is also supported by PIE observations of the oxidation pattern within the CFM. As a result of the steam flow distribution within the CFM, not all the CFM steam was converted to hydrogen. Based on Figure 7, the average steam mass flow rate exiting the CFM during the high-temperature portion of the transient (from 1500 to 1778 s) was about 13 g/s. If all 1024 g of hydrogen were produced during the transient, then the average inlet steam mass flow rate for the CFM should have been 46 g/s (33 g/s of water converted to hydrogen plus 13 g/s exiting the CFM). This would have meant that the average steam mass exiting the core would have been 464 g/s (9.8x46 + 13, where 9.8 = PFM/CFM flow area ratio). This implies that the flow rate entering the LPIS line should have been 479 g/s (464 g/s core flow plus 15 g/s in-leakage from the reflood assist bypass system). However, the calculated LPIS flow rate of 479 g/s is not consistent with the average measured LPIS mass flow rate of 164 g/s determined from Figure 8 (between 1500 and 1778 s).

From the above analysis, it appears that most of the hydrogen gas generated during the LP-FP-2 Experiment was not produced during the transient, but rather was generated after the BST was isolated from the PCS (i.e., following reflood). In other words, most of the CFM oxidation probably occurred during reflood. If this did happen, then a thermal excursion within the CFM must have also occurred. Evidence of a rapid temperature excursion during reflood is discussed in the Experiment Analysis Report (Carboneau 1989).

4.6 Conclusions

Review of the centerline thermocouple data indicates that peak transient fuel temperatures ranged from 2300 to 2700 K. At these estimated temperatures, fuel melting should not have occurred within the CFM. However, examination of the CFM does show that fuel melting did occur at the 0.77-m elevation, with peak temperatures of about 3120 K. These two observations suggest that peak bundle temperatures did not occur during the transient.

Based on the F1 sample line mass flow rate data, steam exited the CFM during the entire transient. Therefore, the CFM was not steam-starved. However, due to the partial blockage that formed during the high-temperature portion of the transient (1500 to 1778 s), flow conditions within the CFM were not uniform and some regions above the blockage were probably steam-starved, thereby limiting the metal-water reaction during the transient. During this time period, the best-estimate average steam mass flow rate exiting the CFM was approximately13 g/s, and the average steam mass flow rate for the LPIS line was 164 g/s. The amount of hydrogen gas measured in the BS 05 ± 11 g, and the calculated amount of hydrogen in the PCS was 819 ± 364 g. Therefore, the total amount of hydrogen produced during the LP-FP-2 Experiment was 1024 ± 364 g, which is equivalent to the oxidation of approximately 58% of the CFM zircaloy. This result agrees with the PIE estimate of 58% total oxidation. Based on the average LPIS and CFM steam mass flow rate data, it appears that there was not sufficient steam passing through the CFM during the transient to account for all of the 1024 g of hydrogen calculated to have been produced. Due to the limited steam mass flow rate through the CFM during the transient and the eventual hydrogen distribution (20% BST and 80% PCS), it appears that most of the hydrogen gas produced during the experiment was generated after the BST was isolated from the PCS (e.g., during reflood).

The primary fission product chemical forms transported through the LOFT system during the LP-FP-2 transient were AgI and CsOH. CsI was not present in significant concentrations. These conclusions are based on observations from the upper plenum coupon and LPIS line data. The observation that CsI was not present during the experiment is based primarily on the upper plenum coupon data, which show large concentrations of silver and iodine but almost no cesium.

The transient releases of volatile fission products ranged from 2 to 5% of the initial CFM inventory. The primary reason for the small transient releases appears to be associated with the initially large grain structure of the fuel (approximately 14 μm) and the smaller-than-expected peak fuel temperatures (< 2700 K). The major release of volatile fission products (9% to 14% of the CFM inventory) appears in the PCS shortly after reflood.

5. POSTIRRADIATION EXAMINATION

Following the successful completion of the LP-FP-2 Experiment, it was decided to perform a PIE (postirradiation examination) of the fuel bundle to provide additional information to assist in determining the factors that may have influenced the thermal-hydraulic and fission product behavior. The PIE also expanded the scope of this experiment to include material behavior and interactions occurring within a fuel bundle during a severe core accident. Due to the size of the LP-FP-2 fuel assembly, the results from these examinations provided an important link between smaller scale severe fuel damage experiments (Knipe et al. 1986; Martinson et al. 1986; Martinson et al. 1989; Petti et al. 1989) and the Three Mile Island accident (Broughton et al. 1989).

The objectives of the PIEs were to provide data on (a) the final distribution of fuel and control rod materials; (b) the posttest metallurgical and chemical form of materials; (c) the maximum temperatures achieved as a function of position in the fuel bundle; and (d) fission product distribution in both fueled and nonfueled materials. This section summarizes the data that were obtained to successfully meet all these objectives.

A schematic cross-section through the LP-FP-2 fuel bundle is shown in Figure 16. The fuel assembly consisted of 100 UO_2 fuel rods with zircaloy cladding, eleven silver-indium-cadmium (Ag-In-Cd) control rods with stainless steel cladding surrounded by zircaloy guide tubes, six empty zircaloy guide tubes, and various instrumentation tubes. ZrO_2

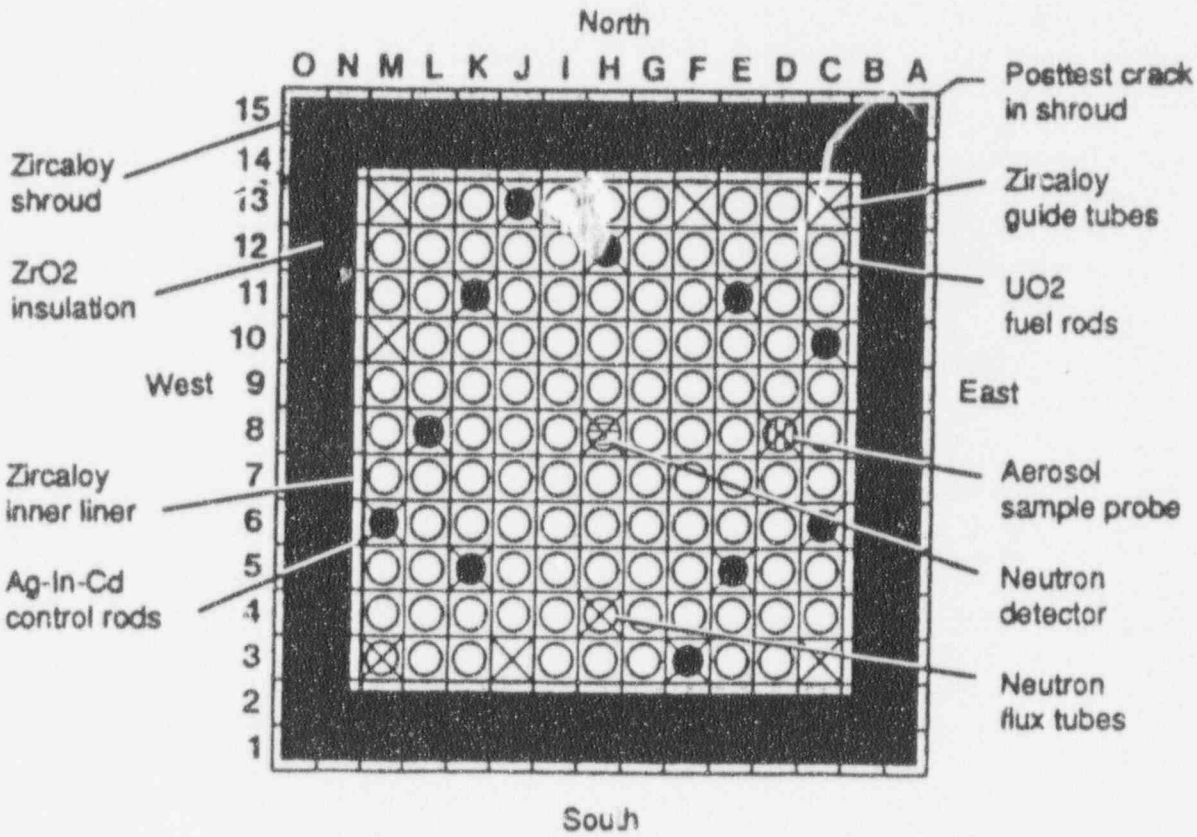

Figure 16. Cross section through the LP-FP-2 bundle.

insulation was sandwiched between a zircaloy inner liner and the zircaloy outer shroud. The fuel was 9.744 wt.% enriched and 94.7% of theoretical density. Additional fabrication details are provided elsewhere (Jensen et al. 1989).

Both nondestructive and destructive examinations of the center fuel bundle were performed. The nondestructive examinations included visual examinations of the exterior surface, gross and isotopic gamma scans of the overall fuel bundle, and neutron radiographs at two perpendicular orientations through the fuel bundle. The fuel bundle was then sectioned to provide 21 transverse cross-sectional surfaces. These were quartered and polished to provide 84 samples for examination and photography, of which 42 samples were examined in detail on the metallograph. Approximately 30 small core bore samples were obtained from these metallographic samples for scanning electron microscope/wavelength dispersive spectroscopic (SEM/WDS) examination, as well as elemental and radiochemical analyses.

This section summarizes the major results from these PIEs. Additional detailed information is provided elsewhere (Jensen et al. 1989). Related information on other aspects of this experiment are also provided elsewhere (Carboneau et al. 1987, 1989, and 1990; Modro and Carboneau 1990), as are comparisons of the LP-FP-2 results with other severe core damage integral tests (Hobbins 1990).

5.1 Qualitative Analysis

This section describes in general the overall condition of the LP-FP-2 fuel bundle following irradiation. This description is primarily based upon visual examinations, gross and isotopic gamma scans, neutron radiography, and representative metallographic cross sections through the fuel bundle. This is followed by descriptions of specific types of material behavior, such as control rod behavior, zircaloy and fuel behavior, and melt behavior. These descriptions are based primarily upon the detailed metallography and SEM/WDS examinations.

Visual Examinations. The LP-FP-2 CFM was vertically lifted out of its underwater storage location in the Test Area North (TAN) water pit for visual examinations in January 1986. The fuel bundle was slightly discolored, and marginal oxidation of the zircaloy shroud was apparent in the area just above core midplane (Carboneau, 1987). A portion of the shroud in the northeast corner had cracked and broken off, exposing the ZrO2 insulation layer. It is not clear whether the broken shroud occurred during irradiation or after the test when the module was removed from the reactor and transported to the TAN water pit.

Ceramic debris was observed in the upper end box. Subsequent analyses indicated this debris was fuel and melt particles that were blown upward by the large amount of steam generated during the reflood stage.

Examinations of the bottom of the CFM indicated that no material had relocated out the bottom.

Gross and Isotopic Gamma Scans. Gross and isotopic gamma scans of the LP-FP-2 fuel bundle were conducted in September 1986 to provide some early insights into the posttest internal condition of the fuel bundle. Many of the conclusions and observations from these examinations (Jensen et al. 1989) were supported by subsequent examinations. However the reasons for observed behavior are now better understood, and two particularly pertinent facts from these examinations are discussed here.

It was observed during the gamma scans that significant amounts of material had been relocated from the upper portion of the bundle on the eastern side. Although this was later observed in the neutron radiographs and the metallographic cross sections, the significance of the gamma scan observation is that, since the module was always in the vertical position until after the gamma scans were completed, fuel handling did not significantly affect the posttest distribution of material in the fuel bundle.

Only a small fraction of the total fission product bundle inventory was released and deposited in the upper support structure above the fuel bundle.

Neutron Radiography. Neutron radiography was performed at Argonne National Laboratory-West (ANL-W) in September 1987 at two perpendicular orientations over the entire fuel bundle and a portion of the upper support structure. A schematic representation of the CFM damage state is shown in Figure 17. Axial elevations are referenced from the bottom of the 25 instrumented fuel rods, which were 0.1 m above the bottom of the CFM. The bottom of the instrumented fuel rods was 2.54 cm above the bottom of the 75 uninstrumented fuel rods. This reference system is used throughout this section.

Six distinctive regions were identified from the radiographs, and representative metallographic cross sections are used in the following discussion to illustrate these various regions.

Region 1 (< 0.1 m). The region below approximately 0.1 m encompasses the bottom spacer grid and below. The material in this region was intact, and only minor amounts of control rod droplets had relocated and solidified in this region. A representative quarter section of the transverse section through the lower spacer grid is shown in Figure 18. Some of the insulation on this sample, and other samples from the lower half of the fuel bundle, fell out during bundle sectioning and handling of the samples. It is known to have been intact because the inner liner was still intact in these regions, and the neutron radiographs showed the insulation to be intact prior to sectioning.

Region 2 (~0.1 to 0.23 m). Relocated material solidified in the region above the bottom spacer grid, forming a large blockage from approximately 0.1 to 0.23 m. This blockage was composed of metallic melts and small fuel debris. The metallic melts were primarily composed of silver-zirconium (Ag-Zr), with smaller amounts of iron (Fe), chromium (Cr), and nickel (Ni) mixed in. A representative quarter section through this blockage region is shown in Figure 19. The relocated material was generally not hot enough to damage the rods in this region, with the exception of a few rods near the center of the bundle.

Region 3 (~0.23 to 0.44 m). The rod array was essentially intact throughout this region, with only small amounts of metallic melt between the rods. Only two fuel rods near the center of the fuel bundle had failed. A representative quarter section is shown in Figure 20.

Region 4 (~0.44 to 0.85 m). Relocating material resulted in the formation of a large blockage throughout this region. The second spacer grid was at the lower extent of this blockage region, and metallic melt and fuel debris much like that found in the lower blockage region had accumulated on this spacer grid. However, unlike the situation at the lower spacer grid, the relocated material at this spacer grid was hot enough to cause significant liquefaction as a result of Ni-Zr eutectic interactions. A representative quarter section through the second spacer grid is shown in Figure 21. The spacer grids impeded material relocation; and, as discussed later, the largest flow blockages were located through, or just above, the two remaining spacer grids.

Above the second spacer grid, the relocated material was composed of high temperature $(U,Zr)O_2$ ceramic melt. The full cross section through the middle of this ceramic blockage region is shown in Figure 22. The ceramic melt surrounded the remaining fuel rod remnants except in the central region, where temperatures were sufficient to completely melt the fuel and oxidized cladding (> 3120 K). Temperatures in this region are discussed in more detail later, but the metallographic evidence indicates that a temperature gradient existed, with lower temperatures towards the periphery of this ceramic melt region. This suggests the formation of a solidified crust of $(U,Zr)O_2$ surrounding a central pool of molten $(U,Zr)O_2$, much like what

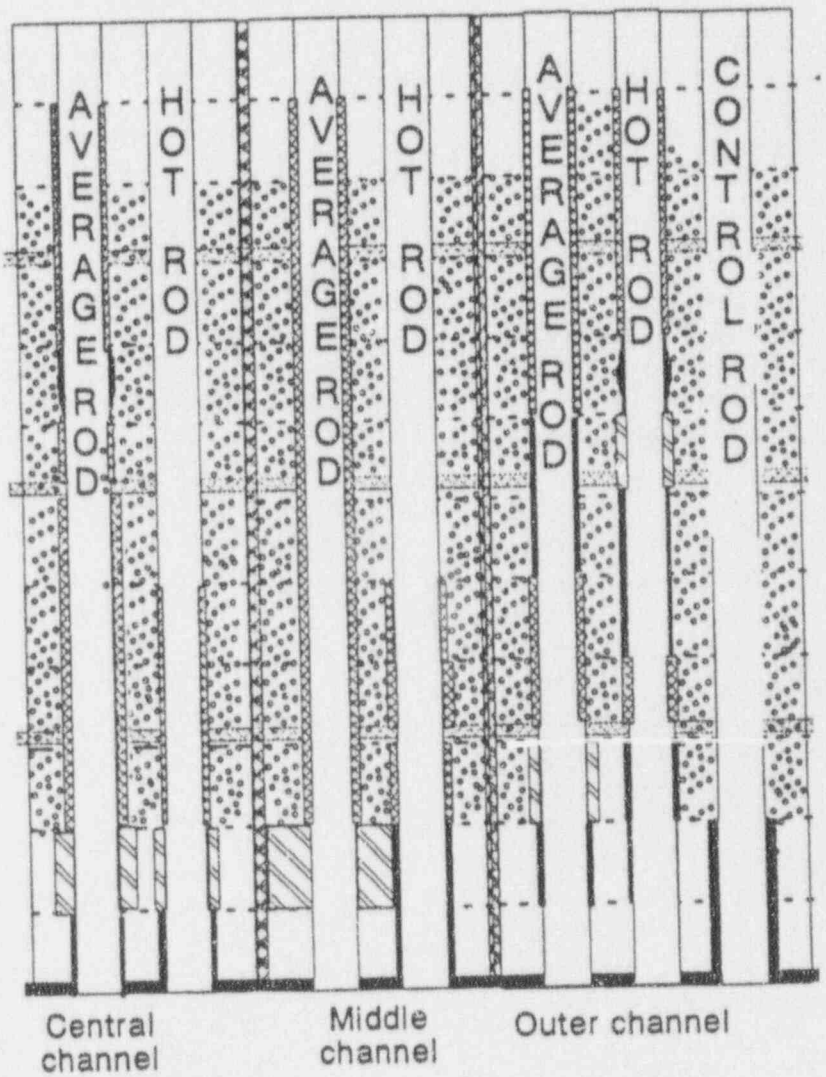

Figure 17. Schematic of CFM damage state.

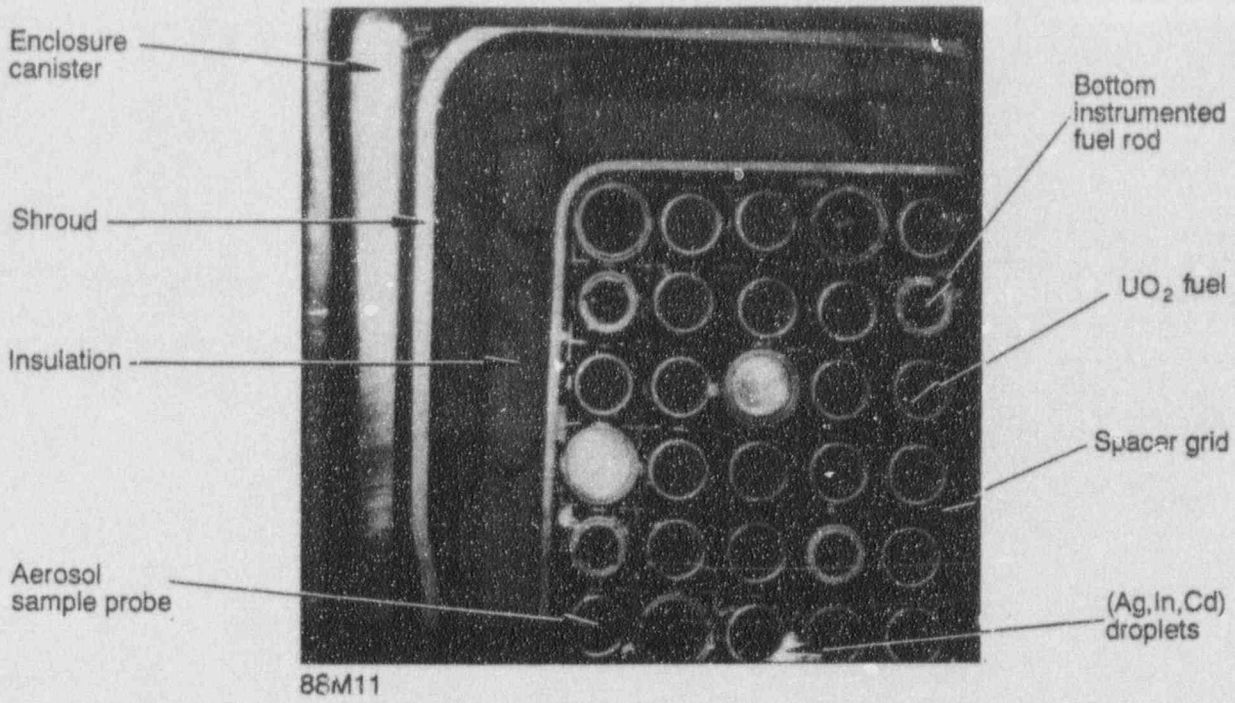

Figure 18. Quarter cross section through bottom spacer grid (0.03 m).

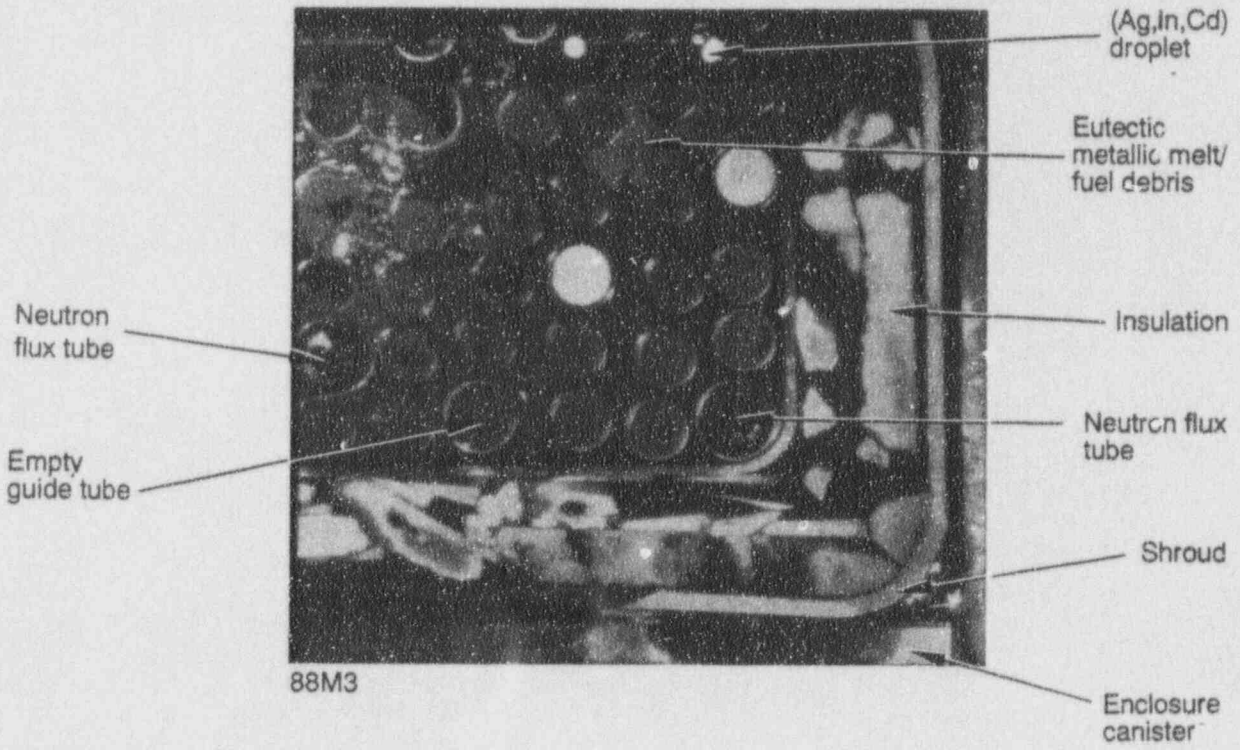

Figure 19. Quarter cross section through lower blockage (0.22 m).

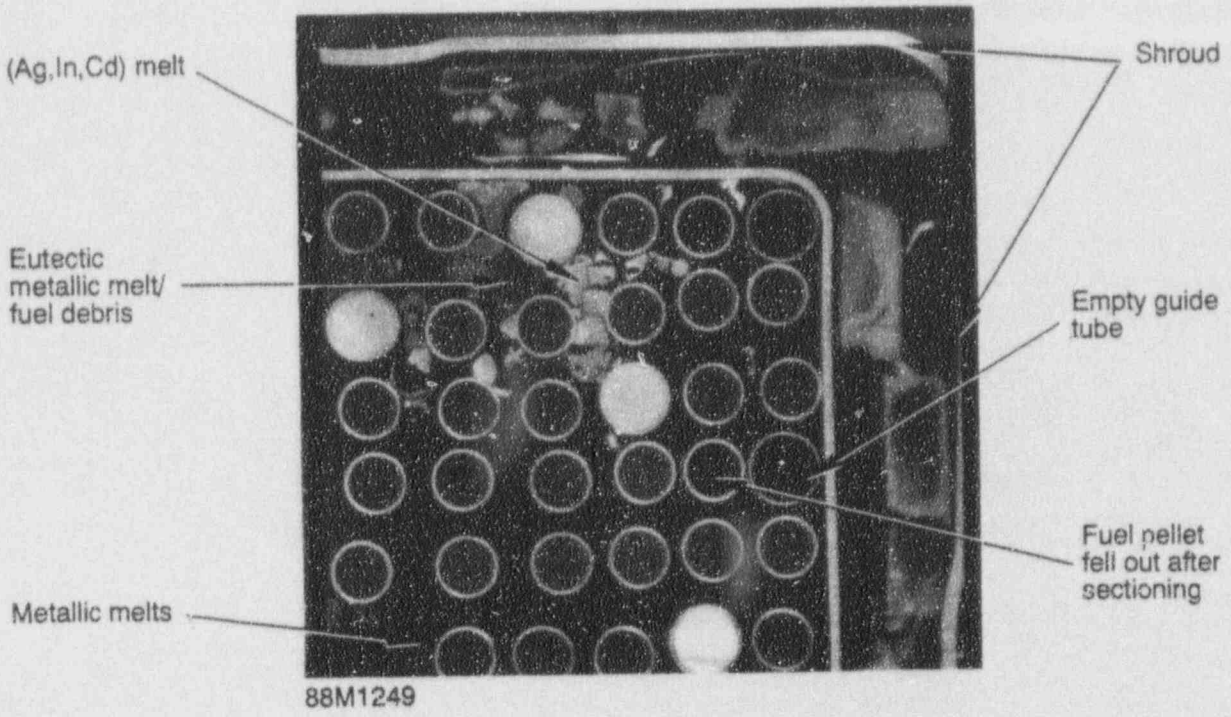

Figure 20. Quarter cross section through intact region between blockage (0.36 m).

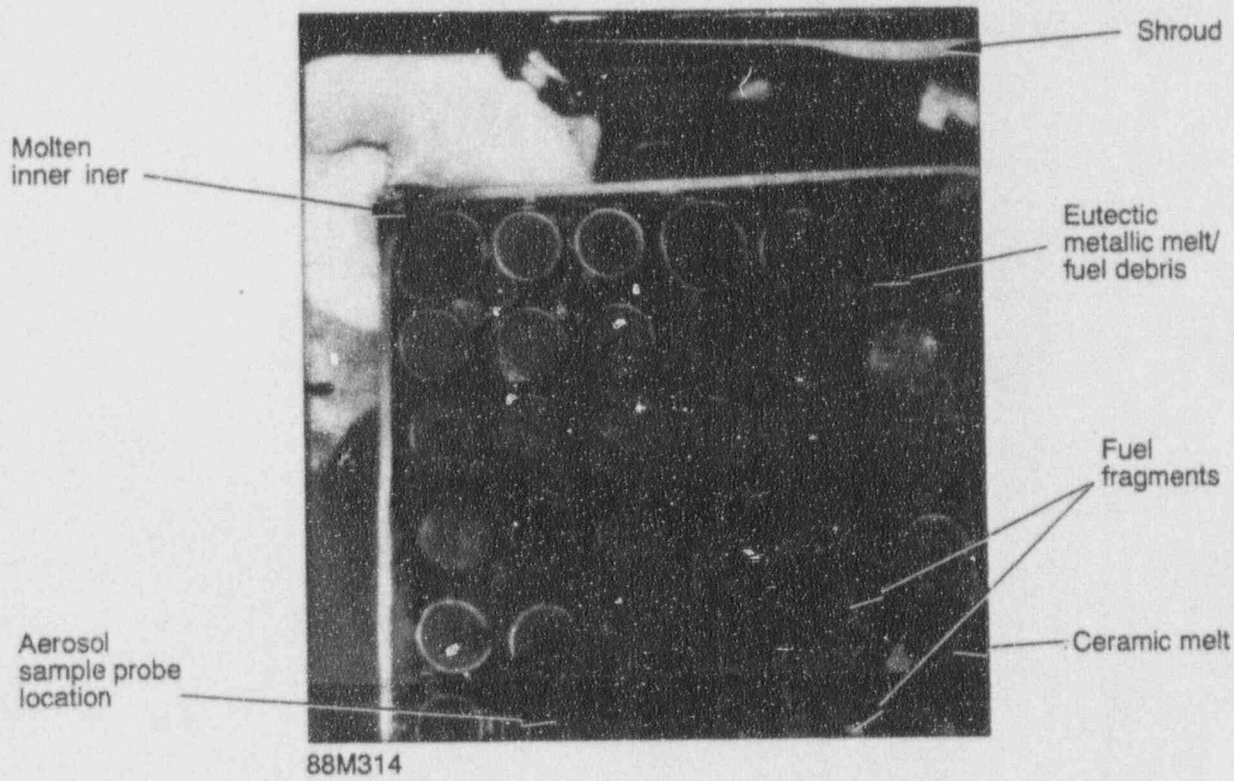

Figure 21. Quarter cross section through second spacer grid (0.46 m).

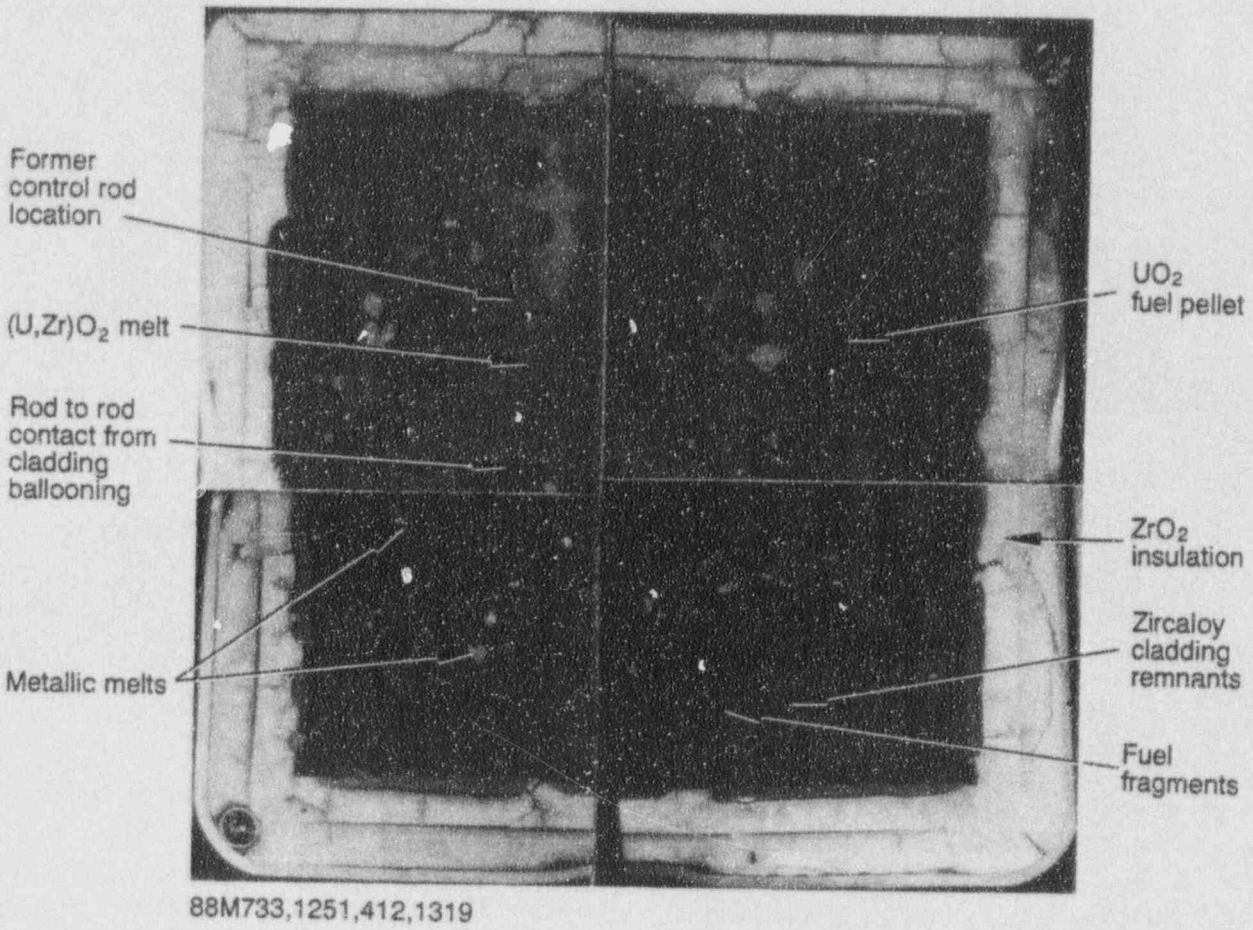

Figure 22. Full cross section through ceramic upper blockage (0.77 m).

occurred during the TMI-2 accident (Broughton et al. 1989).

In the region above the second spacer grid, the inner liner was completely liquefied and melt was able to penetrate into the insulation. Zircaloy oxidation also became significant above this elevation, and essentially all the remaining zircaloy at and above 0.66 m was completely oxidized. Cladding ballooning and rupture also became significant above the second spacer grid, reflecting the increased cladding temperatures associated with zircaloy oxidation. At and above the 0.58 m elevation, all the control rods had completely failed, releasing all the Ag-In-Cd control material above this location.

Region 5 (~0.85 to 1.15 m). The rod array in this region above the upper blockage exhibited extensive cladding ballooning and rupture. Rod-to-rod contact and fusion of oxidized cladding remnants was observed. Relocated $(U,Zr)O_2$ ceramic melt surrounded some of the fuel rods and partially blocked the flow channels. A representative quarter section is shown in Figure 23.

Region 6 (~1.15 to 1.70 m). This region consisted primarily of a rubble bed of fuel pellets

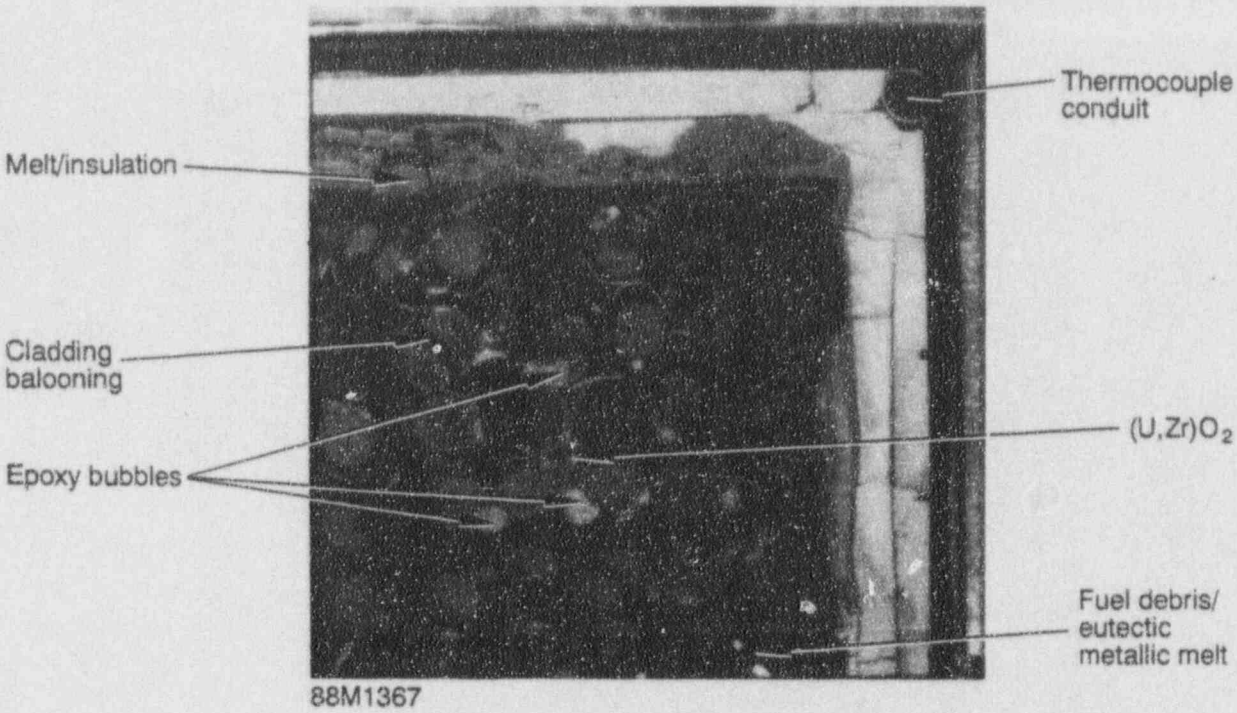

Figure 23. Quarter cross section above the upper blockage (1.04 m).

without any intact cladding to restrain them. Ceramic melts, from molten zircaloy cladding and the upper tie plate, had flowed down around the fuel debris. A lot of material was missing on the eastern side of the CFM, including much of the insulation. Some fuel pellet stacks (without any intact cladding) remained intact on the western side of the module. As described previously, comparison of the gamma scan results with the observed material distribution indicates that posttest handling did not affect the posttest configuration within the module; the solidified ceramic melt held the fuel debris in place. A representative quarter section through this region is shown in Figure 24.

Upper End Box Region (1.70 to ~1.8 m). Relocated material was observed in the upper end box during both the visual examinations and in the subsequent neutron radiographs. Figure 25 shows a representative quarter section through the middle of the stainless steel upper tie plate. The upper tie plate was only intact on the periphery of the bundle; in the center, it had liquefied and oxidized. Intact fuel pellet fragments were also observed in this area. As described in more detail in Carboneau et al. (1989), the liquefaction and oxidation of the upper tie plate, and the relocation of melt and fuel debris to this region, could only have occurred during the reflood period. During the transient, the temperatures and steam mass flow rates were too low to account for the observed behavior; but during the reflood period, both the temperature and steam mass flow rates increased dramatically.

5.2 Qualitative Material Descriptions

This section discusses the behavior of specific categories of materials. Supporting information and photographs are found in Jensen et al. (1989).

Spacer Grids. The LP-FP-2 CFM contained five Inconel 718 spacer grids. Only the bottom

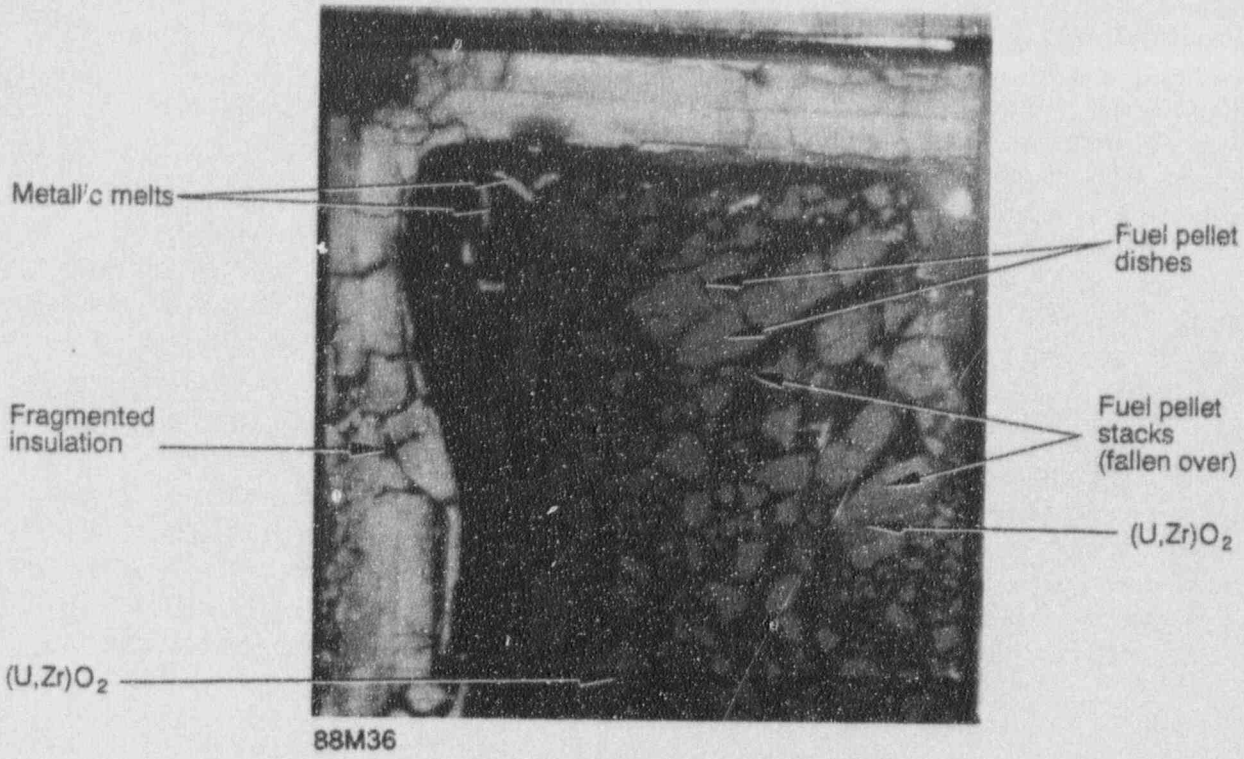

Figure 24. Quarter cross section through the fuel debris bed (1.2 m).

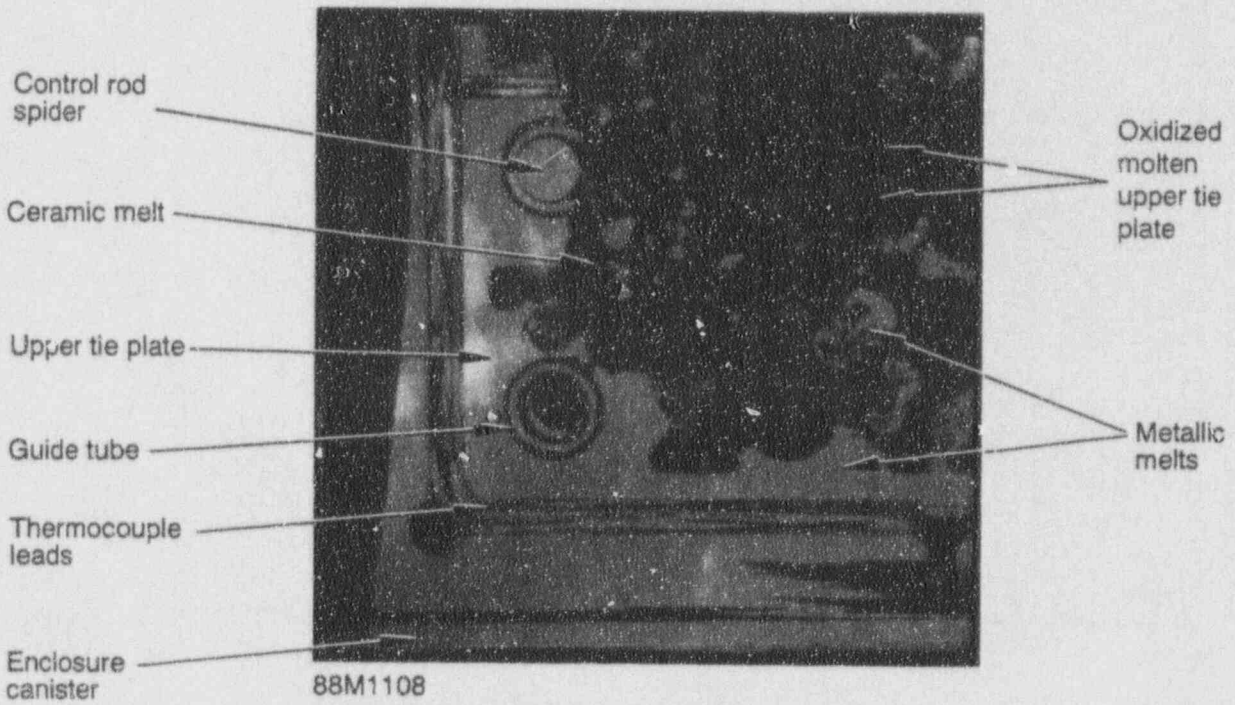

Figure 25. Quarter cross section through the upper tie plate (1.8 m).

spacer grid was still completely intact at the completion of the experiment. The second highest spacer grid was partially intact, and the other three spacer grids had completely liquefied. Relocating material accumulated at the second spacer grid, which suggests that the spacer grids served as traps for relocating material until they ultimately failed. Both of the large blockage regions were located just above the two remaining spacer grids. Representative photographs of the two remaining spacer grids were presented in Figures 18 and 21.

SEM/WDS examinations of areas of typical interaction between melts and spacer grids revealed the presence of a Zr-Nb phase along the grain boundaries of the intact spacer grid. The previously molten region adjacent to the intact spacer grid was a complex mixture of zircaloy components [Zr, tin (Sn)] interacting with the Inconel components [Ni, Fe, Cr, niobium (Nb), molybdenum (Mo), titanium (Ti)], with small amounts of Ag from the control rods.

As shown in Figures 26 and 27, the Zr-Ni and Zr-Fe phase diagrams indicate that liquid phases between these elements can form at temperatures as low as 1220 to 1233 K. A series of eutectic melts can also form between Zr and Ni over wide compositional ranges at temperatures between 1233 and 1443 K. Since the majority of Inconel 718 is nickel (~50 wt%), this suggests that rapid liquefaction of the spacer grids can be expected at temperatures of approximately 1400 to 1500 K, well below the 1720 K melting point of Inconel 718. This is consistent with the SEM/WDS examinations,

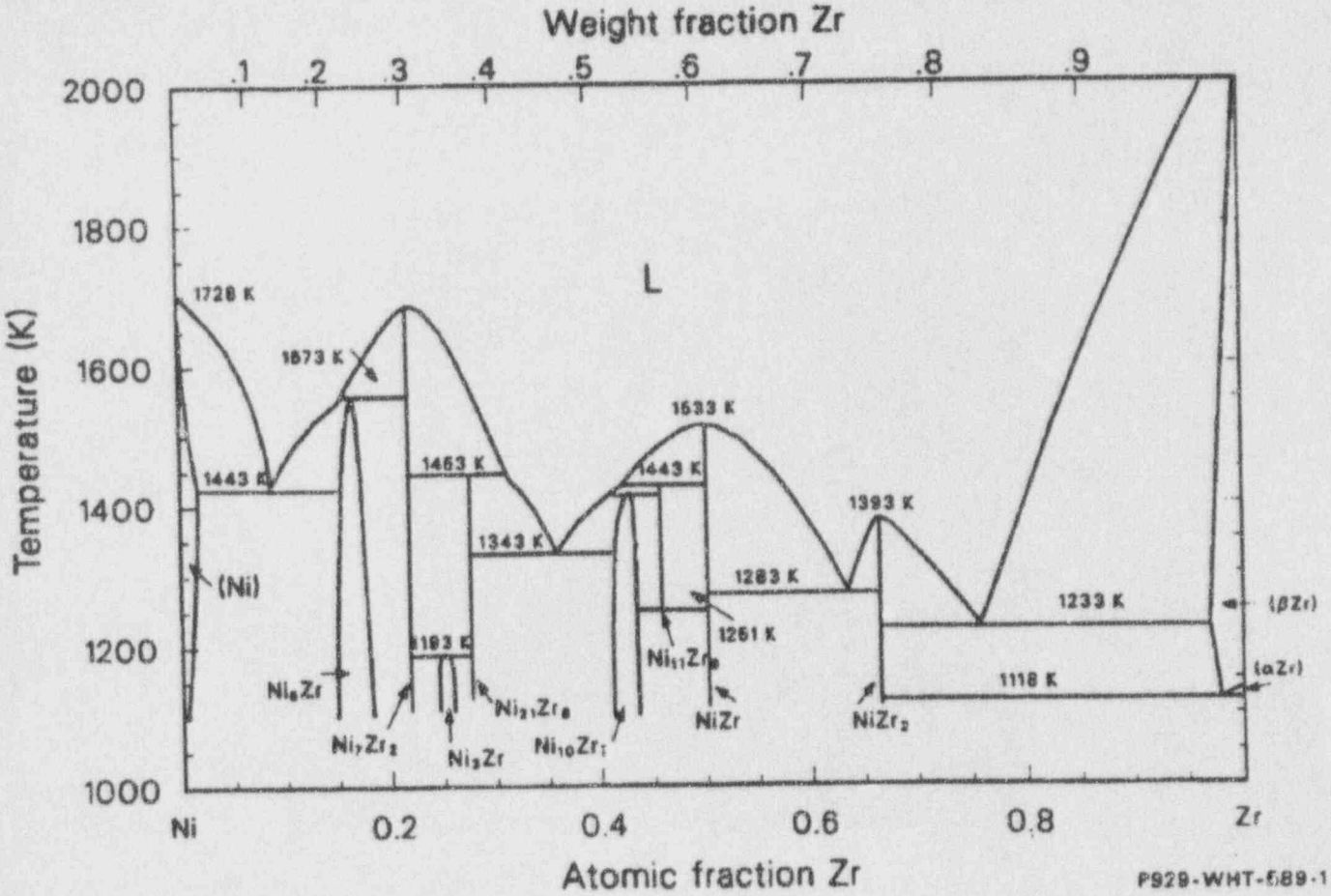

Figure 26. Ni-Zr phase diagram.

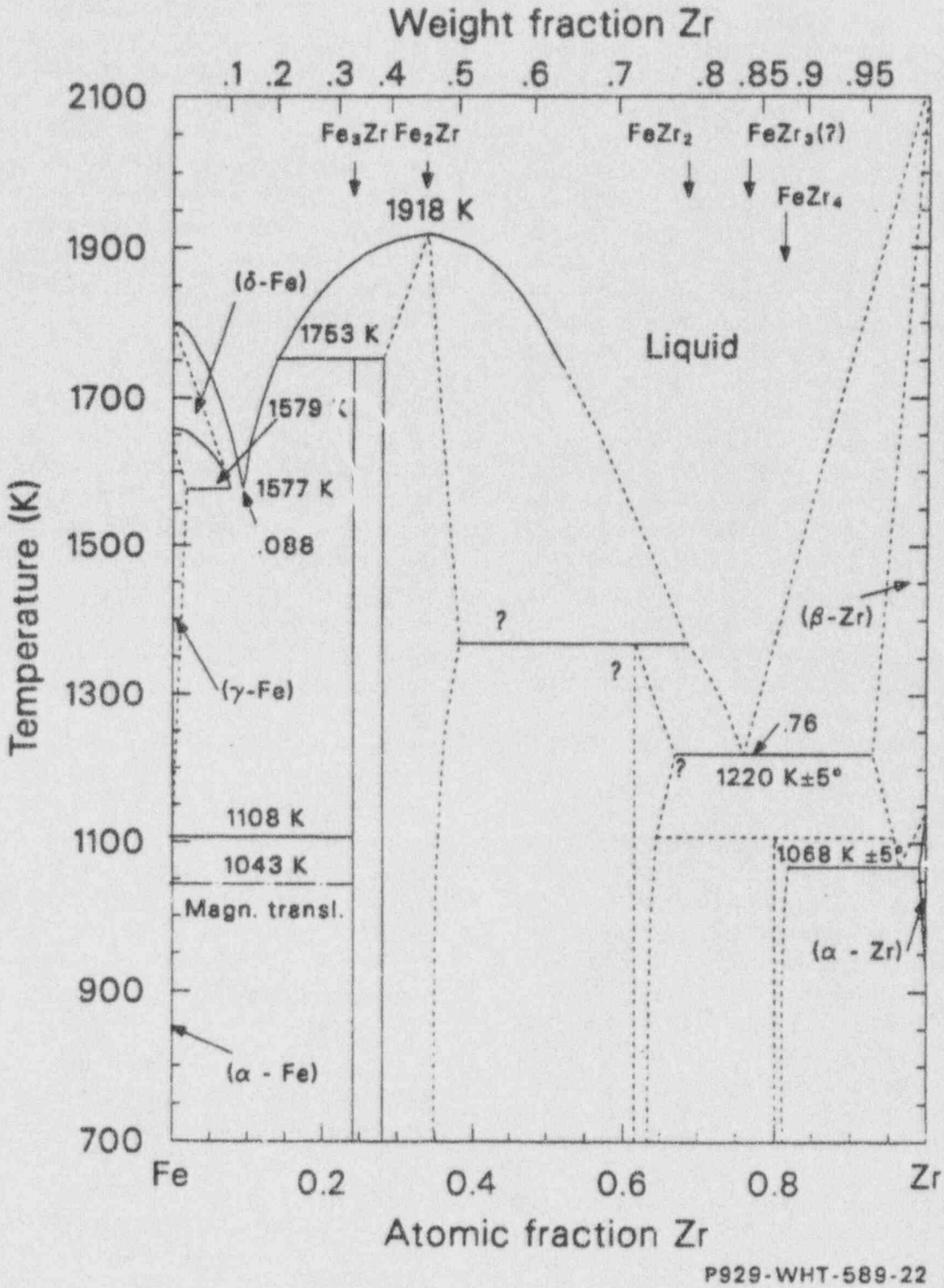

Figure 27. Fe-Zr phase diagram.

which show Zr interacting with the Inconel to form eutectic and multiphase compounds.

Control Rod Behavior. The LP-FP-2 Experiment utilized 11 Ag-In-Cd control rods. These rods used 304 stainless steel cladding, and each was contained within a zircaloy guide tube. All the control rods were intact at the second spacer grid elevation (0.46 m), but all had failed at the next elevation examined (0.58 m). Approximately 70% of the available control material (10 kg) was therefore released to the bundle either as an aerosol spray, when the cladding initially failed, or later as a melt. Approximately 8 kg of Ag were therefore available to interact with other bundle constituents. The Ag-Zr phase diagram shown in Figure 28 indicates that Ag can dissolve up to 67 atom% Zr above 1400 K, and that eutectic phases can form as low as approximately 1200 K. This indicates that Ag would be expected to liquefy the zircaloy cladding at temperatures well below the 2030 K melting point of zircaloy. As described later, the accumulation of large amounts of Ag-Zr bearing melts in the lower region of the bundle indicates that this liquefaction process resulted in significant amounts of early material relocation in LP-FP-2.

Molten Ag-In-Cd control material was observed within the partially liquefied remains of its stainless steel cladding. Examination of the cladding inner surface indicated that the molten control material did not interact with the cladding. However, metallic melts that flowed down the exterior of the cladding did interact with the stainless steel. An intergranular interaction zone was apparent on the outer surface of the cladding, and the liquefaction of the stainless steel had resulted in the formation of a eutectic melt structure. SEM/WDS examinations of this area revealed the presence of low melting point Zr-Ni intermetallic phases along the grain boundaries. The eutectic melt structure was also composed primarily of Zr and Ni, with smaller amounts of Fe and Cr mixed in. This behavior is consistent with the Zr-Ni phase diagram shown in Figure 26, indicating that Zr-bearing melts were responsible for the liquefaction of the stainless steel cladding.

Another example of melt interactions with stainless steel cladding was subjected to SEM/WDS examination, which revealed a Zr-Ni intergranular interaction zone and eutectic melts similar to the previous example. However, these photographs also showed the multiphase metallic melt structure breaking apart in a laminar structure. Similar laminar structures were observed in the lower blockage region, indicating that some of the material in the lower blockage formed in this manner.

Zircaloy Behavior. At the bottom of the CFM, the zircaloy cladding was in the as-fabricated condition, but recrystallized zircaloy was apparent at and above the 0.12 m elevation. The presence of recrystallized zircaloy indicates temperatures in excess of 925 K. Minor amounts (< 100 ppm) of Zr hydrides were also observed in the recrystallized regions. At higher elevations (0.27 to 0.58 m), prior-beta zircaloy structure was present, indicating temperatures in excess of 1245 K. At and above the 0.66 m elevation, essentially all the remaining zircaloy cladding was fully oxidized to ZrO_2. (The only unoxidized zircaloy was on a few rods in one corner near the very top of the fuel bundle.) Minor amounts of zircaloy oxidation were observed below the 0.66 m elevation on the surface of some of the fuel rods and guide tubes. The lowest extent was on some of the centrally located fuel rods at the 0.12 m elevation.

Cladding ballooning and rupture became significant above the second spacer grid. The oxidized cladding shells in this region came into contact and fused together in many instances. The axial transition in the degree of cladding ballooning was associated with a transition in the amount of zircaloy oxidation. This suggests that the exothermic zircaloy oxidation process caused cladding temperatures to increase and resulted in enhanced ballooning and rupture in these regions of the pressurized fuel rods.

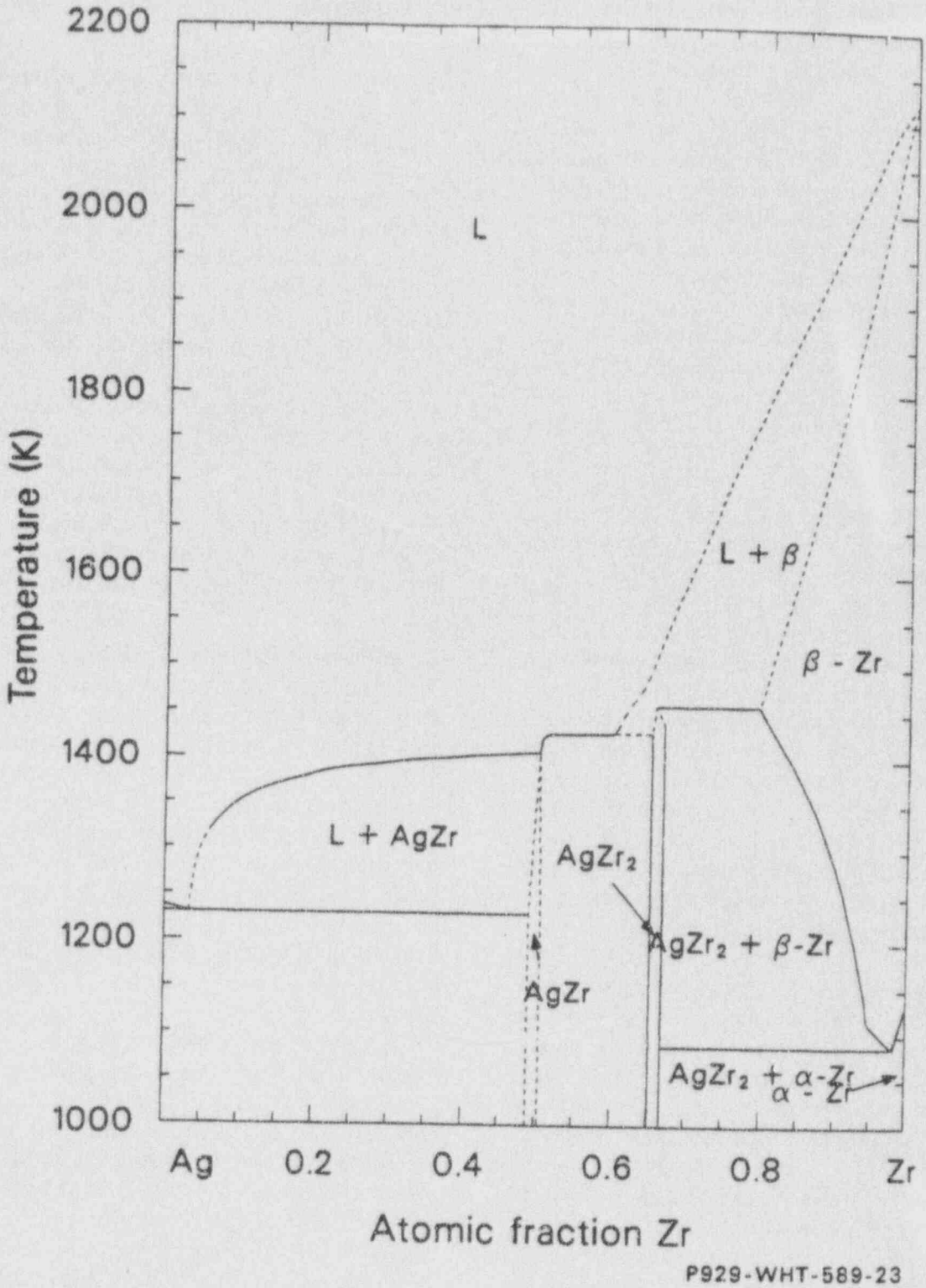

Figure 28. Ag-Zr phase diagram.

At and above the 0.58 m elevation, fully oxidized cladding shells were all that remained of the zircaloy. During the transient, the outer surface of the cladding fully oxidized to ZrO_2, which melts at 2960 K. Under this was a layer of partially oxidized alpha-Zr(O), which melts at approximately 2245 K; and beneath this was the unoxidized zircaloy, which melts at 2030 K. As temperatures in the bundle increased, primarily as a result of the exothermic zircaloy oxidation process, the unoxidized zircaloy on the cladding inner surface melted and was able to flow downward. On lower cross sections, this melt was observed filling the fuel/cladding gap and penetrating along cracks in the fuel. This molten zircaloy was also able to escape from ruptured portions of the fuel rods.

In regions where the zircaloy cladding was not completely oxidized, relocating metallic melts containing Ag were able to interact with the cladding and cause liquefaction below the melting point of the zircaloy. An example of this was found at the 0.43 m elevation, just below the second spacer grid. This example showed the formation of the laminar-type eutectic structures observed in the lower blockage region. These Ag-Zr laminar structures from zircaloy/melt interactions appear very similar to the Zr-Ni-Fe-Cr laminar melt structures from stainless steel/melt interactions, which suggests that both of these interactions were responsible for the early relocation of materials.

The zircaloy inner liner remained intact up through the 0.46 m elevation, but was partially liquefied at the 0.58 m elevation and completely gone at above the 0.66 m elevation. The molten liner and other metallic melts were able to penetrate into the insulation in these regions.

Examinations of the zircaloy shroud indicated only intermittent small oxide layers in the hotter regions near core midplane. Prior-beta zircaloy was observed in the region from 0.77 to 1.14 m, indicating temperatures in excess of 1245 K. This agrees with peak thermocouple measurements of 1620 K in this region (Carboneau et al. 1989). Examination of the cracked region of the shroud did not reveal any unusual features or evidence of overtemperature conditions.

Behavior in the Lower Blockage Region. The material in the lower blockage region was primarily composed of Ag-Zr-Fe-Cr-Ni metallic melt and fuel debris. Small amounts of oxidized cladding remnants and other metallic melts were also present. The eutectic metallic melt in this region resulted from liquefaction of zircaloy, stainless steel, and Inconel. Some laminar melt structure was also observed separating from the liquefied portion of the zircaloy cladding.

This lower blockage region solidified in an egg-shaped form with a central cavity region containing only the intact fuel rods. Although the outer crust of this blockage had extensive porosity on a microscopic scale, it was sufficiently agglomerated that the epoxy was unable to penetrate into the central cavity region.

Ceramic Melt Behavior. Ceramic melt was not located below the second spacer grid. Most of the $(U,Zr)O_2$ ceramic melt solidified in a large mass to form an upper blockage, which extended from approximately 0.58 to 0.88 m. SEM/WDS quantitative analysis confirmed that the ceramic melt was fully oxidized $(U,Zr)O_2$. $(U,Zr)O_2$ melt was also present around individual rods and fuel debris above the upper blockage. Near the top of the bundle, some of the ceramic melt contained oxidized melt from the stainless steel upper tie plate in addition to $(U,Zr)O_2$.

A typical ceramic melt structure was glassy in appearance, with some cracking and porosity. In one case, the $(U,Zr)O_2$ melt was hot enough to melt the oxidized cladding on one side of the fuel pellet, but not quite hot enough to completely dissolve all the oxidized cladding remnants on the other side of the pellet. Temperatures in excess of 2810 K are required to create molten $(U,Zr)O_2$, with temperatures above 2960 K required to melt oxidized ZrO_2 cladding. Temperatures were less than the 3120 K required to melt the UO_2 fuel. The melt penetrated along cracks in the fuel, and some grain growth in the center of the fuel pellet was observed.

Fuel Behavior. Several factors affected the behavior of the fuel in the LP-FP-2 Experiment. The different aspects of fuel behavior are divided into four categories: (a) grain size, (b) fuel reduction by metallic melts, (c) fuel fragmentation and powdering, and (d) fuel liquefaction and melting.

Grain Size. The nominal as-fabricated fuel grain size was 14 μm. A total of 107 measurements were made in typically representative fuel over the entire axial length of the fuel assembly. These measurements indicated an average grain size of 14 μm, with a 2-sigma standard deviation of ± 4 μm, indicating that grain growth did not occur in the majority of the fuel. However, grain growth was observed in the center of some of the fuel pellets in the hotter portions of the bundle. Thirty measurements in these grain growth regions indicated an average grain size of 27 μm, with a 2-sigma standard deviation of 17 μm.

Fuel Reduction by Metallic Melts. Areas of enhanced grain boundary separation and fragmentation were associated with the presence of metallic melts. There was evidence that this phenomenon was not simply a thermal effect, because in some instances, where ceramic and metallic melts were both in contact with the fuel, the grain boundary separation was limited to the areas near the metallic melt. This may be due to reduction of the fuel by the Zr-bearing metallic melts, resulting in slightly hypostochiometric fuel along the adjacent grain boundaries. As shown in the U-O phase diagram in Figure 29, this could result in the formation of a U-rich liquid phase along the grain boundaries at temperatures above approximately 1470 K. The presence of such a film could result in grain boundary separation and fragmentation, and similar dissolution and breakup of the fuel has been previously observed (Hofmann et al. 1988). In that instance, molten zircaloy contained in a UO_2 crucible resulted in partial disintegration of the crucible. However, any metallic U that may have formed on the grain boundaries in Experiment LP-FP-2 as a result of this process would have oxidized to UO_2 by the time this sample was prepared and examined and would be indistinguishable from the rest of the fuel.

Several SEM/WDS samples were examined to investigate this phenomenon. No second phase material was ever found in the separated grain boundary regions. These examinations did show that the melt was indeed metallic (low in oxygen), that the melt contained significant amounts of Zr (the only major bundle constituent capable of reducing the fuel), and that U was segregated in the melt. These results are consistent with fuel reduction. In all cases, the metallic melt did not penetrate into the grain boundary separation regions, which indicates that the melt solidified before the grain boundary separation occurred.

Fuel Fragmentation and Powdering. Fuel fragmentation and powdering (the breakup of fuel into individual grains) was observed throughout the LP-FP-2 fuel assembly on failed fuel rods that were exposed to water during reflood. It was not observed on intact portions of fuel rods (in the lower portion of the bundle) or fuel rods that were completely surrounded by melt material that restrained the fuel. This suggests that the thermal shock to the fuel during reflood contributed to breakup of the fuel; however, fuel fragmentation and powdering also occurred prior to reflood because fuel debris was intermixed with the melt material in the lower blockage. Fuel that had experienced grain boundary separation would have been particularly susceptible to fuel fragmentation and powdering.

Fuel Liquefaction and Melting. Areas of fuel with a foamy morphology were observed on the periphery of some fuel pellets in the midcore region and above. On the outer periphery of the foamy fuel region, the grain structure was obliterated, whereas farther inward, a grain structure was still apparent in the foamy fuel. Elemental dot maps from SEM/WDS examinations of a similar sample indicated the presence of Fe, Cr, and Ni in the fuel. Review of U-Fe-O phase diagrams indicates that eutectic interactions can take place between these materials, although the data are very limited,

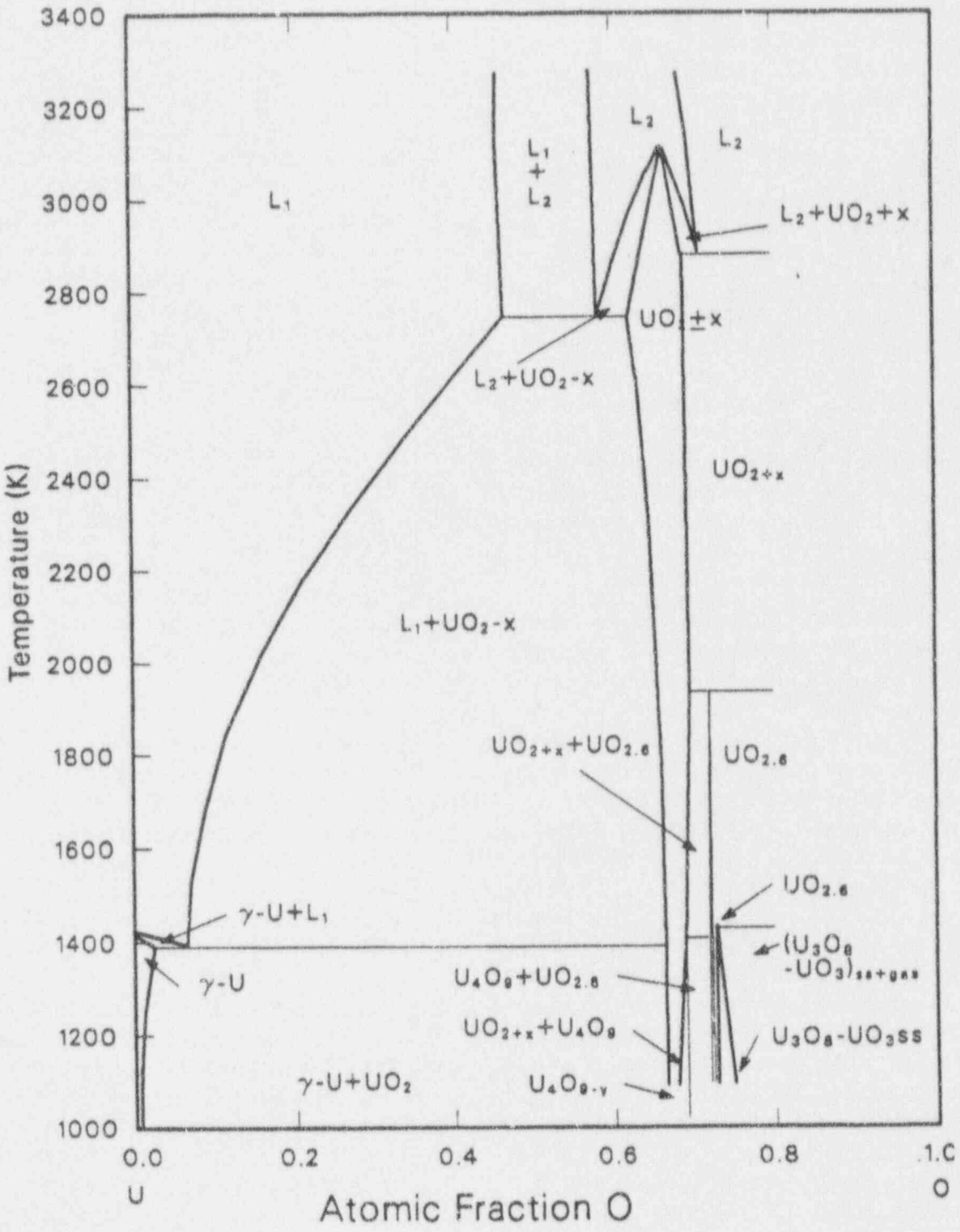

Figure 29. U-O phase diagram.

which suggests that the observed foamy fuel morphology may be due to fuel liquefaction by Fe oxides.

The foamy fuel regions discussed above were no longer surrounded by any molten material. However, porous fuel regions were also observed on some fuel pellets in the high temperature upper blockage region which were surrounded by $(U,Zr)O_2$ ceramic melt. Elemental dot maps from SEM/WDS examinations of a similar area indicated that these porous fuel regions did not contain any Fe oxides or other elements. This suggests temperatures very near the 3120 K melting point of the fuel. The lack of oxidized ZrO_2 cladding shells in these regions further indicates temperatures above the 2960 K melting point of ZrO_2. This behavior was observed on many of the fuel pellets in the center of the ceramic upper blockage region and was a prime indicator of melt temperatures in this region.

5.3 Quantitative Data Analyses

This section discusses the flow blockage and material redistribution measurements, provides estimates of oxidation and hydrogen generation and peak bundle temperatures, and discusses the results from the radiochemical and elemental analyses of the retained fission product samples.

Flow Blockage and Material Redistribution. The cross-sectional areas of various types of materials at each metallographic elevation were measured to provide axial distributions. Interpolation of these values provided integral volumes of materials. Density and elemental analyses of bulk samples were then used to estimate material compositions in the melt regions and to calculate material balances for U and Zr. Details of the measurement techniques and uncertainties are described elsewhere (Jensen et al. 1989); however, in general, the uncertainties were < 15%.

Intact and Fragmented Fuel. For these purposes, the term intact fuel refers to fuel pieces of sufficient size that they could be accurately characterized, generally on the order of 1/4 to 1/8 the size of a fuel pellet. As used here, this term is not meant to infer that the fuel was not cracked or fragmented; it is only meant to describe a categorical type of material observed metallographically. The term fuel fragments refers to a category of material consisting of fuel particles that were too small to accurately reproduce using manual planimetry techniques. This category generally consisted of an agglomeration of very small fuel particles that could not be individually distinguished from the cross-sectional photographs. However, higher magnification photographs showed significant amounts of open porosity separating the individual particles; consequently, the measured cross-sectional areas were reduced in half and the remainder was added to the measured open flow values.

The axial distribution of intact and fragmented fuel is shown in Figure 30, as well as the as-fabricated values. Below the second spacer grid, the fuel was essentially intact. (The bottom two elevations passed through the end caps of the instrumented fuel rods.) Above the second spacer grid (0.58 m) near the bottom of the large ceramic melt region, a lot of the fuel was not surrounded by any relocated melt material. Cladding ballooning and rupture in this region left the exposed fuel unrestrained and susceptible to fragmentation. Above this region (0.58 to 0.88 m), there was very little fragmented fuel; most of the fuel rods were surrounded by the ceramic melt, which held them in place. Above the upper blockage region, the array of ballooned and ruptured fuel rods was held together by cladding remnants and ceramic melt, which surrounded the individual rods and minimized fuel fragmentation. However, above this region, the cladding had been completely stripped from the fuel, allowing a debris bed of intact and fragmented fuel particles to form. The fuel from the upper portions of the bundle relocated downward and congregated on top of the remaining rod stubs.

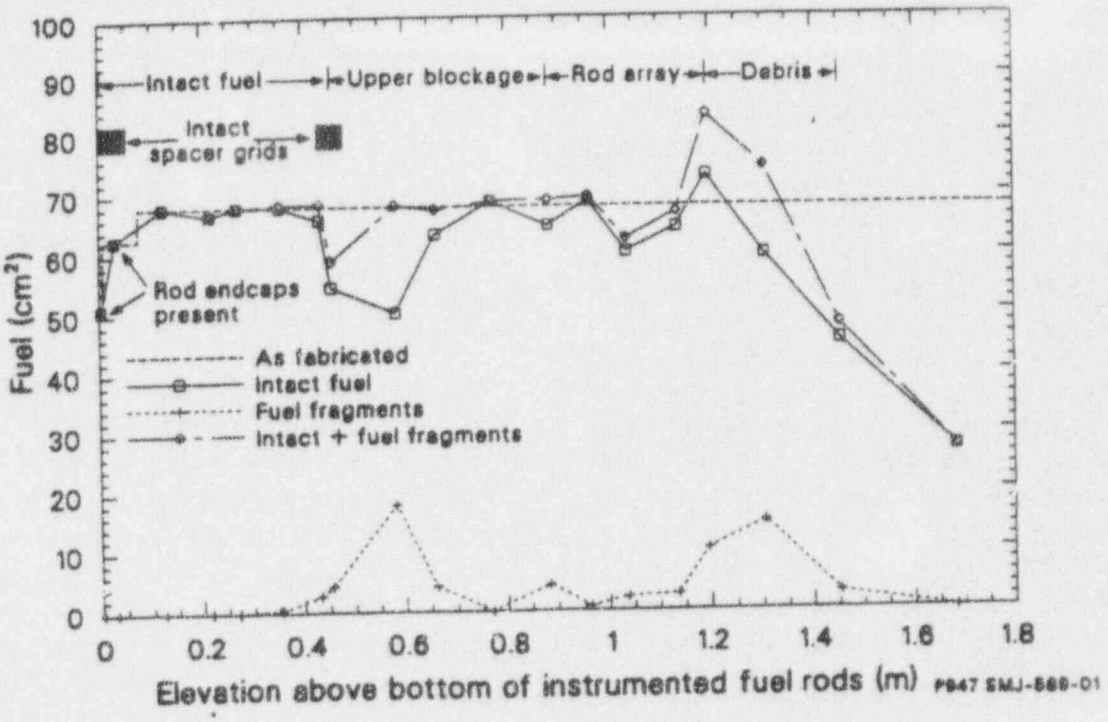

Figure 30. Fuel distribution.

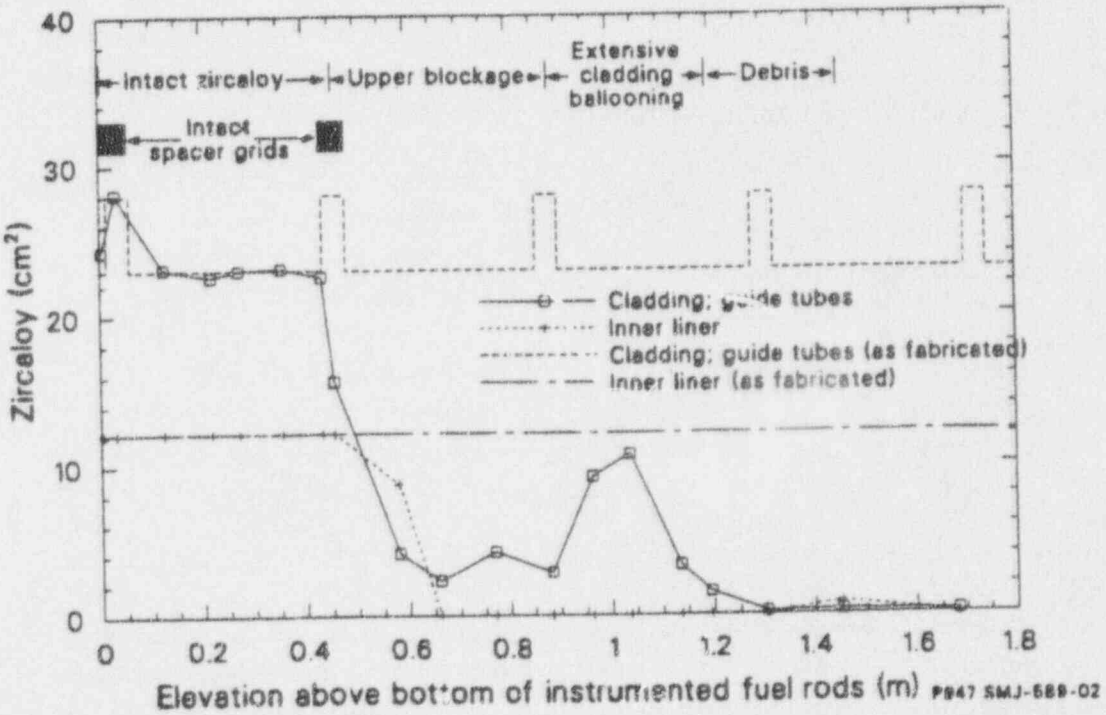

Figure 31. Zircaloy distribution.

Zircaloy. Zircaloy components included fuel rod cladding, guide tubes, lock rings surrounding the guide tubes at spacer grid locations, and the zircaloy inner liner. The posttest axial distribution of these components is shown in Figure 31, along with the as-fabricated values.

The zircaloy cladding, guide tubes, and lock rings were essentially intact below the second spacer grid. Melting of the cladding inner surface and fragmentation of the oxidized cladding shells accounted for the decrease in the amount of zircaloy above the second spacer grid. At and above the 0.66 m elevation, all of the zircaloy was fully oxidized to ZrO_2, except for a minor amount at the 1.45 m elevation. Very little zircaloy remained in the high temperature ceramic melt region (0.58 to 0.85 m) or in the uppermost region of the bundle; however, a significant amount of oxidized cladding surrounded rod stubs in the region between the upper blockage and the debris bed (0.96 to 1.14 m).

The inner liner, which separated the rod array from the insulation region, was also intact below the second spacer grid. However, it was completely liquefied at and above the 0.66 m elevation except for a minor amount in one corner at the 1.45 m elevation (the same region a minor amount of unoxidized zircaloy was located).

Control Rod Materials. The posttest distribution of Ag-In-Cd control rod alloy contained in its stainless steel cladding is shown in Figure 32. The stainless steel cladding was generally intact below the second spacer grid, with partial liquefaction occurring near the second spacer grid. Release of all the control material from all 11 control rods occurred between the 0.46 and 0.58 m elevations.

Insulation. It was necessary to measure the amount of insulation present at each elevation because the inner liner had melted in the upper portion of the fuel bundle and the insulation was able to fall out and relocate into the fueled portion of the bundle. This significantly affected the open flow distribution in the upper portion of the bundle. Melt was also able to penetrate into the low density (~20%) ZrO_2 insulation where the inner liner had melted. The amount of this melt material had to be accounted for in the Zr mass balance estimates for the bundle and for subsequent estimates of the amount of zircaloy oxidation in the bundle. As described below, the distribution of the melt penetration into the insulation also provides some insight into the sequence of events that occurred during this experiment.

The data for the intact insulation (area unaffected by melt penetration) and the melt/insulation areas are shown in Figure 33. These data show that all the insulation was intact and unaffected by any melt below the second spacer grid in the regions where the inner liner remained intact. Melt penetration into the insulation occurred throughout the central portion of the fuel bundle, with the greatest amount in the region above the ceramic melt blockage. Only very minor amounts were observed in the topmost regions of the bundle. A possible explanation for this behavior may be that the inner surface of the inner liner was oxidized in the central portion of the bundle, much like the outer surface of the fuel rod cladding in this region. As temperatures increased, the oxide layer on the inner liner would have subsequently held molten unoxidized zircaloy adjacent to the insulation and allowed the melt to penetrate into the insulation. This is analogous to melting of the unoxidized inner surface of the fuel rod cladding. The upper extent of the melt penetration into the insulation also corresponds to the upper extent of oxidized cladding remnants (see Figure 31). The oxidized cladding remnants at these upper elevations were also limited to exterior positions, near the inner liner, which suggests that steam was diverted to these exterior bundle positions after one or both of the blockages had formed. These data all suggest that zircaloy oxidation of intact rods and liner extended only to the 1.2 m elevation. Above this elevation, the zircaloy cladding and liner was liquefied and relocated before an oxide layer could develop. This liquefaction would have started on the inner surface of the inner liner; hence, melt would not

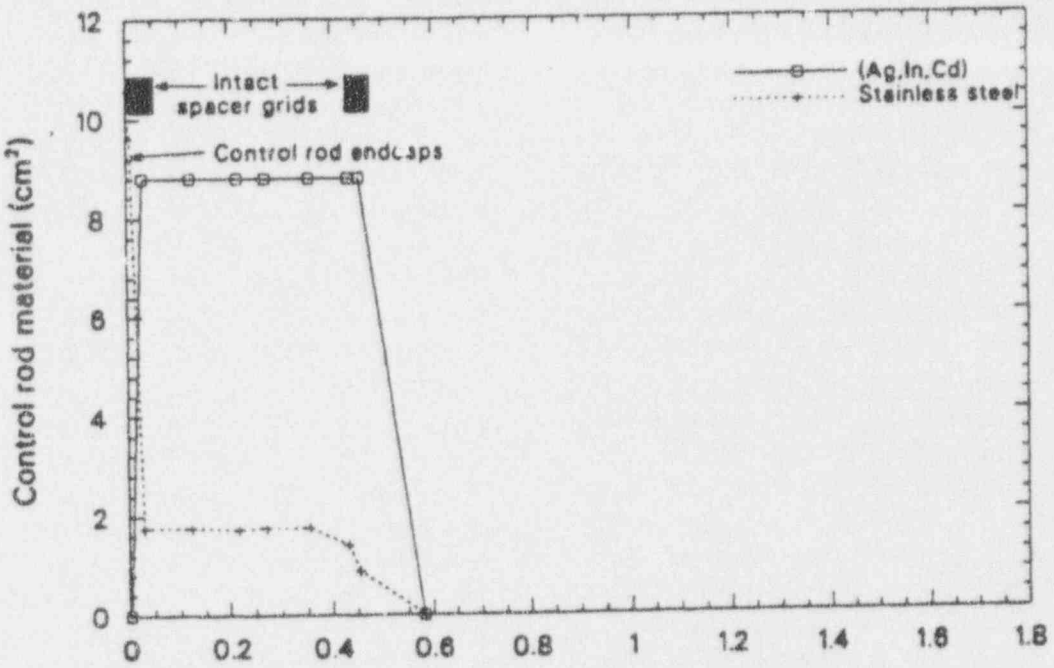

Figure 32. Distribution of control rod materials.

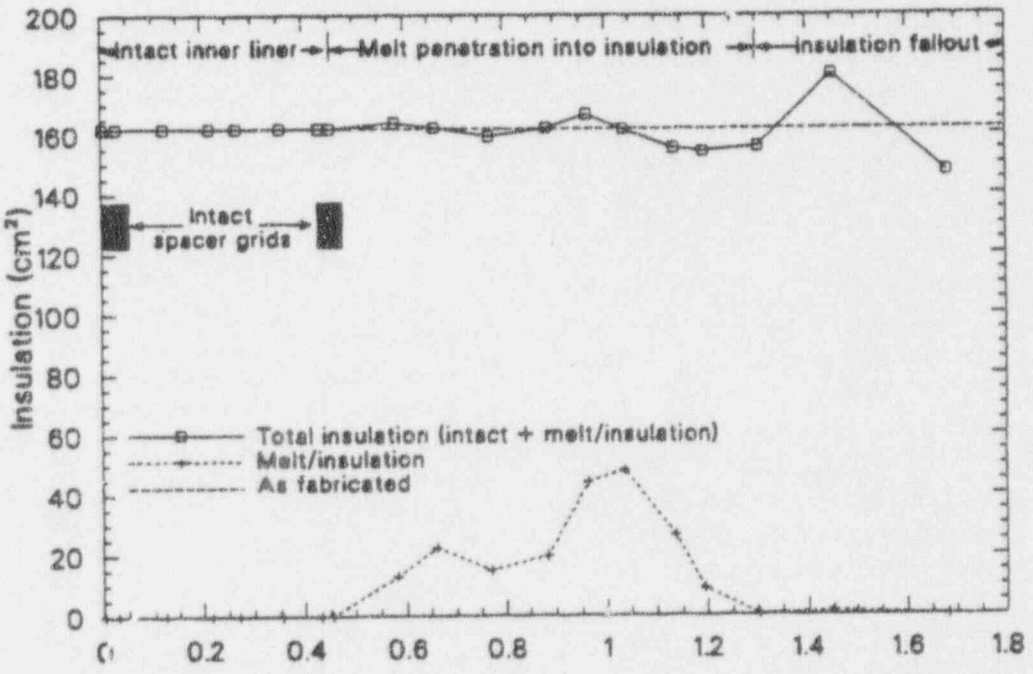

Figure 33. Distribution of insulation.

be held against the insulation and have an opportunity to penetrate into the insulation. This liquefaction probably resulted from dissolution of the zircaloy by Ag released upon control rod failure, and later perhaps resulted from simple melting of the unoxidized zircaloy.

Ceramic Melt. Most of the ceramic melt in the LP-FP-2 CFM was composed of $(U,Zr)O_2$, with relatively small amounts of bundle constituents mixed in. The exception was near the top of the fuel bundle, where the stainless steel upper tie plate had melted, relocated, and oxidized. The material distribution data for the ceramic melt are shown in Figure 34. The melt was only found above the second spacer grid, with the greatest accumulation between approximately 0.66 and 0.88 m. In this region, the melt formed a large solidified mass; whereas above this, the melt was limited to isolated regions around the remaining rod stubs and fuel debris.

Eutectic Metallic Melt/Fuel Debris. This material was primarily composed of an agglomeration of very small eutectic metallic melt particles (primarily Ag, In, Zr, Fe, Cr, and Ni), fuel grains and fragments, and small amounts of other assorted fuel bundle debris (cladding remnants, larger metallic melt droplets, and fuel fragments). On a microscopic scale, there was also considerable porosity between the particles. As shown in Figure 35, this material formed the lower blockage region just above the bottom spacer grid. It also accumulated on the second spacer grid.

Metallic Melts. Most, if not all, of the metallic melts at and below the second spacer grid consisted of droplets of Ag-In-Cd control rod alloy. Above this elevation, the majority of the metallic melts consisted of multiphase elemental mixtures. As shown in Figure 36, the amount of these melts was relatively small; and their distribution was very irregular throughout the fuel bundle. The large increase in metallic melt near the top of the fuel bundle is due to metallic melts relocating from the upper tie plate and other portions of the upper end box.

Open Flow. The measured open flow axial distribution is shown in Figure 37. Near the bottom of the CFM was the lower blockage region, consisting primarily of eutectic metallic melt and fuel debris. The solid line in this region is based solely on the material present, whereas the dotted line takes into account the fact that there was a cavity region within the lower blockage without steam access. The flow area reduction in this region corresponds to 86% of the area within the inner liner, assuming that steam was diverted around the lower blockage.

The second greatest flow area reduction was through the second spacer grid and corresponded to 78% of the area within the inner liner. The reduction in open flow due to the presence of the large solidified ceramic melt can be seen in the region from 0.58 to 0.88 m. Above this ceramic melt region, the open flow increased; the region consisted of ballooned and ruptured rod stubs surrounded by small amounts of ceramic melt. The decrease in open flow at 1.2 m was due to fuel debris resting on top of the rod stubs, and the increase in open flow above this reflects the loss of material from this region.

Integration of the as-fabricated and posttest open flow measurement data indicates an 11% reduction in the open flow volume (using the solid line in Figure 37). This corresponds to a 15% volume expansion of the material initially contained within the inner liner. This is a result of the porosity within the various melt regions. The reduction in the open flow volume is 12%, if it is assumed that steam was diverted around the lower blockage (using the dotted line in Figure 37).

Integral Material Distribution Data. Interpolation of the cross-sectional measurement data provided integral volumes of material in the bundle. These data are provided in Tables 4 and 5, along with upper and lower limits based on the uncertainties in the measurement data. These limits assumed that all the measurement data for

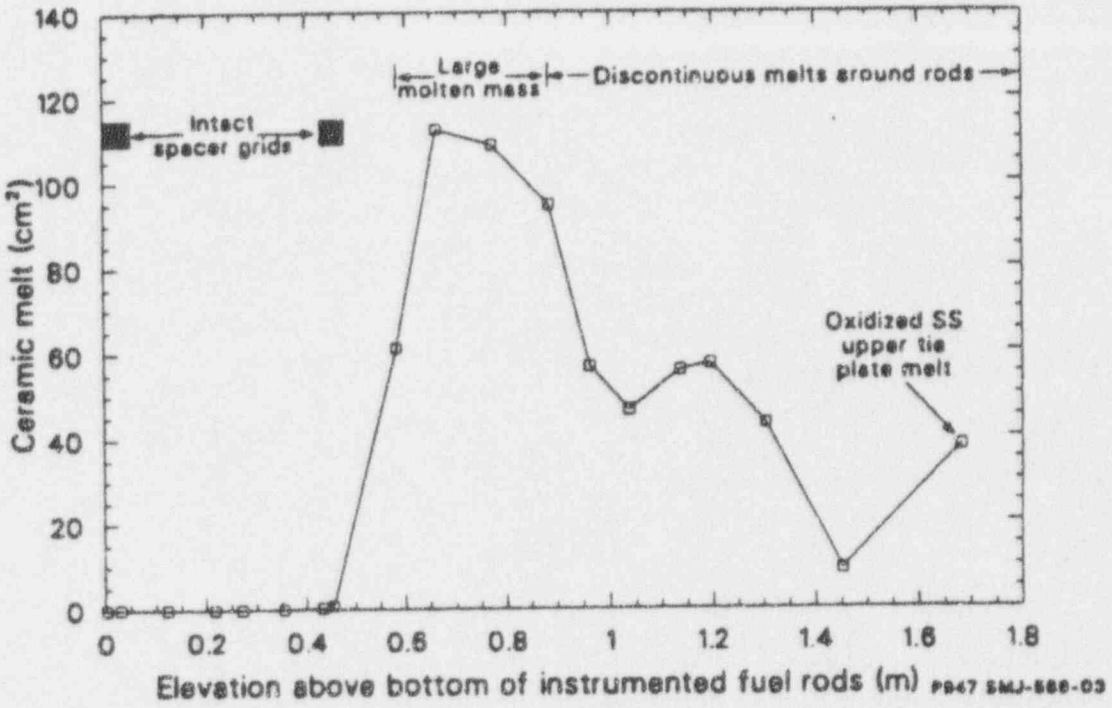

Figure 34. Distribution of ceramic melt.

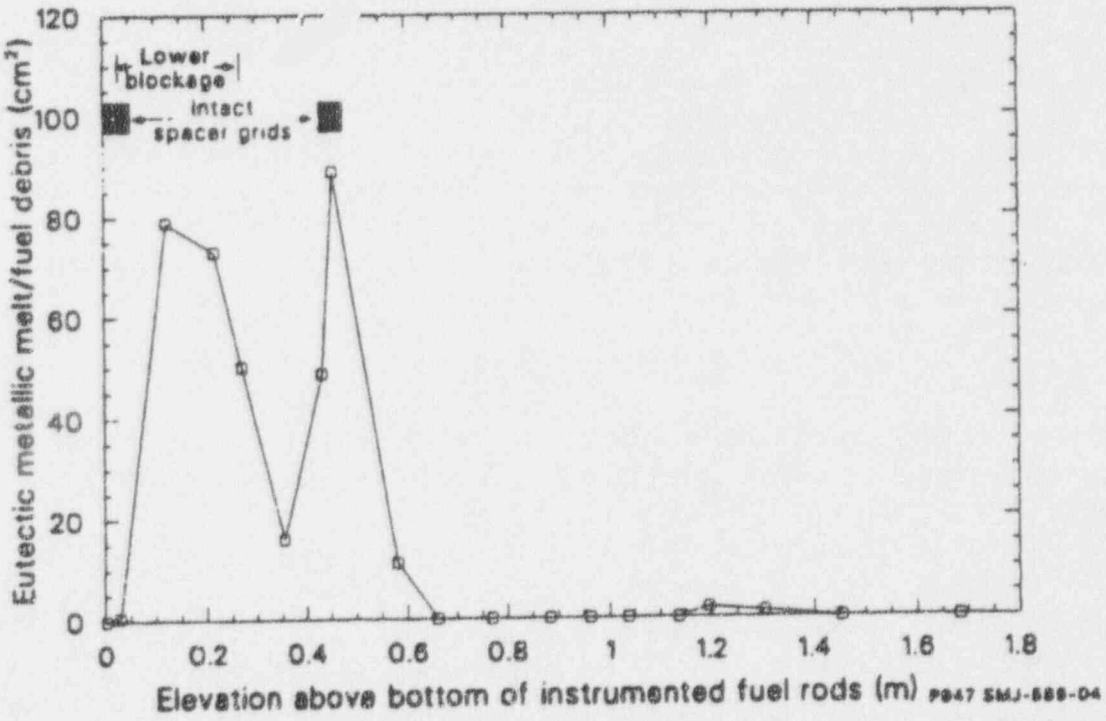

Figure 35. Distribution of eutectic melt/fuel debris.

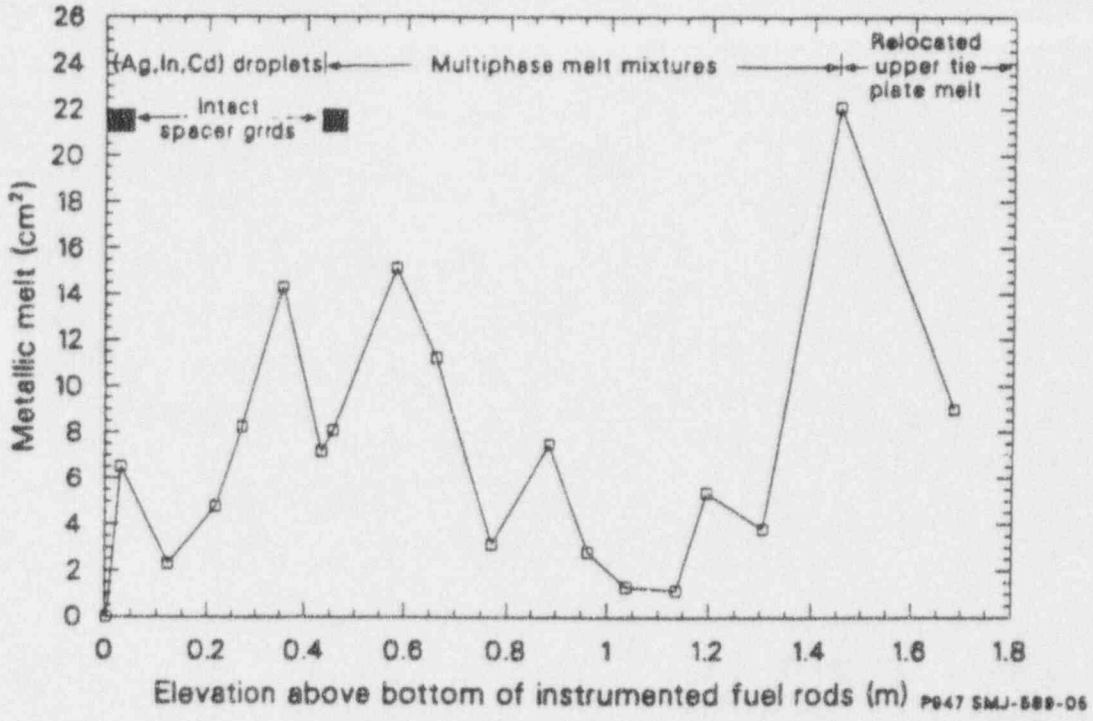

Figure 36. Distribution of metallic melt.

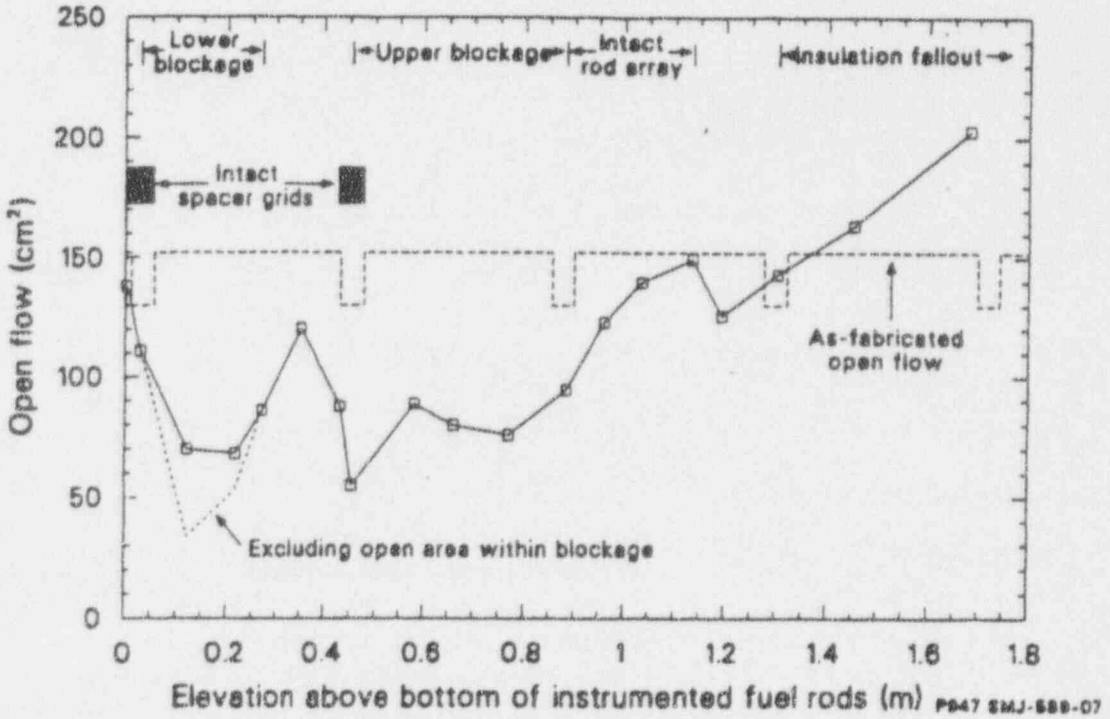

Figure 37. Posttest open flow distribution.

Table 4. Integral volumes of material in LP-FP-2 Experiment.

Material	Pretest (cm^3)	Lower limit (cm^3)	Nominal (cm^3)	Upper limit (cm^3)
		Fuel		
Intact		8919 (79%)	10025 (89%)	11133 (99%)
Fuel fragments		495 (4%)	688 (6%)	908 (8%)
Total	11273	9414 (84%)	10713 (95%)	12041 (107%)
		Zircaloy		
Cladding	4163	1363 (33%)	1575 (38%)	1806 (43%)
Liner	2207	758 (34%)	767 (35%)	776 (35%)
		Control material		
Ag-In-Cd	1475	386 (26%)	442 (30%)	498 (34%)
Stainless steel	319	88 (28%)	88 (28%)	88 (28%)
Spacer grid	366	124 (34%)	126 (34%)	129 (35%)
		Insulation		
Intact		25974 (91%)	27251 (95%)	28528 (100%)
Melt/insulation		1495 (5%)	1760 (6%)	2024 (7%)
Total	28585	27469 (96%)	29011 (101%)	30552 (107%)

Table 5. Integral volume of melt and debris in LP-FP-2 Experiment.

Material	Lower limit (cm^3)	Nominal (cm^3)	Upper limit (cm^3)
Ceramic melt	6070	6744	7418
Metallic melt	1181	1389	1598
Eutectic metallic melt/fuel debris	2517	2796	3076
Miscellaneous debris	10	20	30

a given component were biased high or low; thus, these limits are very conservative.

The integral results indicate that much more zircaloy liquefied than fuel and approximately 70% of the control rod material was released to the bundle. All the insulation is generally accounted for, which indicates that very little, if any, was dissolved in the melt regions. This suggests that the insulation relocated after the bundle had cooled, perhaps even during subsequent handling of the fuel bundle. The largest volume of melt was in the ceramic melt regions.

Posttest Mass Balances for Uranium and Zirconium. Core bore samples were obtained from representative regions within the fuel bundle, and elemental analysis was performed on these samples to provide bulk compositional information. Density measurements were also performed on the core bore samples from the ceramic melt and eutectic metallic melt/fuel debris samples to enable estimates to be made of the total amount of material distributed in these regions. From these data, it was possible to calculate material balances for the major bundle constituents of U and Zr, as well as provide information on the distribution of U and Zr in the fuel bundle. The Zr distribution data were subsequently used to calculate Zr oxidation and hydrogen generation, and the overall mass balances for these elements provided an internal consistency check on the material distribution measurements and methodology.

Details of the analysis methodology are described elsewhere (Jensen et al. 1989), and only the final results are presented in Tables 6 and 7. For the nominal conditions, the material balance overpredicts the amount of U but accurately predicts the amount of Zr. The overprediction in the U mass balance may be partially due to overestimating the amount of fuel present at each metallographic cross section due to the inclusion of fuel cracking and separation of the fuel. These data suggest that the lower estimated values for the cross-sectional and integral volumes of intact and fragmented fuel may be more accurate. However, the overall good agreement in these material balance calculations indicates that the material distribution measurements and methodology provide a reasonable approximation of the actual conditions.

These data also provide information on the amount of molten U and Zr and the partitioning of these elements among the various melts. Approximately 63 wt% of the zircaloy was liquefied; however, only about 15 wt% of the fuel was liquefied. Most of these liquefied materials were located in the ceramic melt region, although significant amounts of Zr were located in the eutectic metallic melt in the lower blockage and in the melt that penetrated the insulation. This reflects the dissolution of unoxidized zircaloy by Ag to form the lower blockage and the melting of the inner liner.

Oxidation and Hydrogen Generation. Oxidation of zircaloy, stainless steel, and Inconel components each contributed to hydrogen generation in the LP-FP-2 Experiment. The zircaloy oxidation was calculated from the PIE data using two methods--subtraction of unoxidized Zr from an upper oxidation limit and addition of oxidized Zr in the various regions of the bundle. The first method was considered to provide the best-estimate values; the second method also provided information on the distribution of oxidized Zr, as well as a comparison check with the first method. These distribution data were useful for developing a bundle scenario of events, based upon when the Zr in the various regions probably oxidized. Oxidation of molten stainless steel and Inconel components was also estimated from the PIE data, to provide an estimate of the total amount of hydrogen generated in LP-FP-2

Best Estimate of Zircaloy Oxidation and Hydrogen Generation. The best estimate of the zircaloy oxidation was calculated by establishing an upper limit and then subtracting the unoxidized amounts of Zr in the various melt regions. This was considered to be

Table 6. Uranium mass balance in LP-FP-2 Experiment.

Location	Low estimate (g)	Nominal estimate (g)	Upper estimate (g)
Ceramic melt	14,000 (14%)[a]	18,000 (15%)[a]	22,000 (16%)[a]
Eutectic melt/fuel debris	2,100 (2%)	2,300 (2%)	2,600 (2%)
Metallic melt	380 (.3%)	960 (1%)	2,100 (2%)
Intact fuel	79,000 (79%)	92,000 (77%)	100,000 (74%)
Fuel fragments	4,500 (4%)	6,300 (5%)	8,300 (6%)
Posttest total	100,000 (100%)	120,000 (120%)	140,000 (140%)
Pretest total	100,000 (100%)	100,000 (100%)	100,000 (100%)
Δ%	0	20	40

a Percentages are normalized to posttest total.

Table 7. Zirconium mass balance in LP-FP-2 Experiment.

Location	Low estimate (g)	Nominal estimate (g)	Upper estimate (g)
Ceramic melt	9,100 (28%)[a]	12,000 (29%)[a]	16,000 (32%)[a]
Eutectic melt/fuel debris	4,900 (15%)	5,400 (13%)	6,000 (12%)
Metallic melt	1,500 (5%)	3,000 (7%)	5,200 (10%)
Melt/insulation	4,100 (13%)	5,600 (14%)	6,900 (14%)
Intact cladding and liner	13,000 (40%)	15,000 (37%)	16,000 (32%)
Posttest total	33,000 (80%)	41,000 (100%)	50,000 (122%)
Pretest total	41,000 (100%)	41,000 (100%)	41,000 (100%)
Δ%	-20	0	22

a Percentages are normalized to posttest total.

superior to the method described in the next section because of reduced uncertainties.

The upper limit for zircaloy oxidation was determined from measurements of the amount of oxidized cladding and guide tube remnants in the bundle, assuming that all the previously molten zircaloy had fully oxidized. The amount of hydrogen generated as a result of zircaloy oxidation was calculated based upon the following chemical equation:

$$Zr + 2H_2O \rightarrow ZrO_2 + 2H_2 \qquad \text{(EQ 1)}$$

Thus, for every mole of molten Zr or intact ZrO_2, 2 moles of H_2 could be produced. From this, an upper limit of 1226 g of hydrogen from zircaloy oxidation was calculated.

Determination of the amount of unoxidized Zr in the melt regions was based upon density measurements and elemental analysis of core bore samples from the various melt regions, to provide the total amount of Zr present, along with SEM/WDS examinations to determine the extent of unoxidized Zr in those regions. Additional details on the methodology are described elsewhere (Jensen et al. 1989).

Table 8 summarizes the results of this analysis. The estimated amount of hydrogen from zircaloy oxidation was 862 g, with lower and upper limits of 575 and 1064 g, respectively. For the nominal case, this corresponds to an oxidation of 49% of the Zr in the inner liner, cladding, and guide tubes, with the lower and upper limits corresponding to 32 and 60%. The large uncertainties are due to the conservatism incorporated in minimizing and maximizing these estimates. However, as discussed in the following section, good agreement between these calculations and two alternative methods indicates that there is a high probability that the actual amount of hydrogen is near the nominal estimate.

Hydrogen Generation Based Upon Total Oxidized Zirconium. An alternative method for calculating the amount of zircaloy oxidation is based upon summing up the oxidized Zr in the various regions, as opposed to subtracting the unoxidized Zr from an upper limit. This method has larger uncertainties associated with it, but it has the advantage of providing information on the distribution of oxidized Zr. This information can be used in conjunction with postulated bundle scenarios to provide information on heat generation in the various regions of the bundle at various times during the experiment. It also provides a check on the amount of zircaloy oxidation and hydrogen generation calculated in the previous section.

The estimated amounts of hydrogen generated from Zr oxidation in the various

Table 8. Best estimate of hydrogen generation from zircaloy oxidation.

Location	Hydrogen (g)		
	Lower	Nominal	Upper
Upper limit from zircaloy oxidation			1226
Unoxidized zirconium in eutectic metallic melt	-197	-118	-54
Unoxidized zirconium in melt/insulation	-226	-114	-42
Unoxidized zirconium in metallic melts	-228	-132	-66
Total hydrogen from zircaloy oxidation	575	862	1064

Table 9. Hydrogen generation from zircaloy oxidation in various regions of LP-FP-2

Location	Hydrogen[a] (g)		
	Lower	Nominal	Upper
Oxidized ZrO_2 cladding shells	36	63	93
Eutectic metallic melt	54	118	197
Ceramic melt in large blockage (< 0.92 m)	225	327	471
Ceramic melt above large blockage (> 0.92 m)	175	195	214
Melt/insulation	56	133	229
Total from zirconium	546	836	1204

a. These values were calculated using alternative methods than those used to estimate the hydrogen from zircaloy oxidation in Table 8.

regions of the fuel bundle are summarized in Table 9. The total amounts are in very good agreement with the hydrogen estimates given in Table 8. The greater limits shown in Table 9 reflect the increased uncertainties associated with calculating the amount of oxidized Zr in the ceramic melt region, as opposed to calculating the amount of unoxidized Zr in the smaller metallic melt regions using the first method. The conservatism incorporated in determining the lower and upper limits in Table 9 is apparent in comparing the upper limit of 1204 g of hydrogen with the absolute fuel bundle upper limit of 1226 g estimated in the previous section. Since there are significant amounts of unoxidized Zr in the various melt regions, this comparison indicates that the upper and lower limits are, indeed, very conservative.

The results in Table 9 indicate that very little oxidation was associated with oxidized zircaloy cladding shells. Most of the zircaloy oxidation was associated with previously molten zircaloy in one form or another. The oxidation of the cladding shells had to have occurred relatively early in the experiment before significant material relocation, because these oxidized shells were surrounded by the melts. *It can also be assumed that the oxidation of the Zr in the eutectic metallic melt regions probably occurred during the transient.* This is based upon their position low in the bundle, where they would have been exposed to any steam flow before the rest of the bundle; the probability that they experienced their hottest temperatures as they were relocating to form the lower blockage; and the fact that these would be the first regions quenched by reflood. The data from the melt/insulation regions indicate that a significant amount of the Zr in these regions was unoxidized. This is probably due to the relatively lower temperatures in these regions of the bundle. These data also indicate that the greatest amount of oxidized Zr was located in the ceramic melt regions, particularly in the large mass that made up the upper blockage. The partitioning of the Zr oxidation and hydrogen generation in these various regions provides some valuable information on the possible sequence of bundle events, when these data are compared to measured and calculated hydrogen concentrations in the BST and the PCS. These comparisons are described in detail elsewhere (Carboneau 1990, Modro and Carboneau 1990).

Oxidation of Stainless Steel and Inconel Components. In addition to the zircaloy, major portions of the type 304L stainless steel upper tie plate were molten and/or oxidized. An example of this is shown in

Figure 25 on page 35. Based upon area fraction measurements, and SEM/WDS examinations that indicated Fe and Cr were oxidized in these regions, it was possible to estimate the amount of hydrogen generated from this source. Similar calculations were performed to estimate the hydrogen generated from the oxidation of Fe and Cr in the molten stainless steel cladding and Inconel spacer grids. Details are provided elsewhere (Jensen et al. 1989).

The hydrogen contribution from these sources is shown in Table 10. A total of 163 ± 83 g of hydrogen was calculated from these

Table 10. Oxidation of nonzircaloy components.

Location	Hydrogen (g)		
	Lower	Nominal	Upper
Oxidation of stainless steel upper tie plate	51	103	155
Oxidation of molten stainless steel cladding	20	40	60
Oxidation of molten spacer grid	9	20	31
Total hydrogen from nonzircaloy components	80	163	246

Table 11. Best estimate of total hydrogen production in LP-FP-2 Experiment.

Location	Hydrogen (g)		
	Lower	Nominal	Upper
Upper limit from zircaloy oxidation			1226
Unoxidized zirconium in eutectic metallic melt	-197	-118	-54
Unoxidized zirconium in melt/insulation	-226	-114	-42
Unoxidized zirconium in metallic melts	-228	-132	-66
Total hydrogen from zircaloy	575	862	1064
Oxidation of upper tie plate	51	103	155
Oxidation of molten stainless steel cladding	20	40	60
Oxidation of molten spacer grid	9	20	31
Total hydrogen from nonzircaloy components	80	163	246
Total hydrogen generation in LP-FP-2	655	1025	1310

sources, of which the oxidation of the upper tie plate was the most significant.

Total Hydrogen Generation and Discussion of Results. The best estimate of the total oxidation and hydrogen generation in the LP-FP-2 fuel bundle is the sum of the contributions from the zircaloy and nonzircaloy components. These data are summarized in Table 11, which indicates that 1025 g of hydrogen were generated in the nominal case, with lower and upper limits of 655 and 1310 g, respectively. This is in excellent agreement with an independent analysis based upon grab samples from the BST and calculated amounts in the PCS, which indicated 1024 ± 364 g of hydrogen. Details of this independent analysis are provided elsewhere (Carboneau, 1989 and 1990; Modro and Carboneau 1990), but the results are summarized here to demonstrate the good agreement between the two different analyses.

The amount of hydrogen calculated to be in the BST, based upon grab samples, was 205 ± 11 g. The amount in the PCS, based upon pressure and temperature measurements and calculated gas compositions, was 819 ± 364 g. These values provide an indication of the amount of hydrogen generated during the transient and the reflood period, because the BST was isolated just prior to reflood.

The data on the distribution of oxidized Zr indicated that nominally 181 g of hydrogen were generated from the cladding oxide shells and the oxidized Zr in the lower blockage. As discussed previously, these materials had to have oxidized during the transient. This value is in very good agreement with the 205 ± 11g found in the BST, which must have been generated during the transient. Correspondingly, 818 g of hydrogen were estimated to have been generated from the ceramic melt regions, the melt which penetrated the insulation, and the oxidation of the nonzircaloy components (Tables 9 and 10). This is also in excellent agreement with the 819 g of hydrogen estimated to be in the PCS, most of which had to have been generated during reflood.

In summary, the results of two independent analyses show excellent agreement as to the partitioning of the hydrogen generation between the transient and reflood periods and in regards to the total amount of hydrogen generated (1024 versus 1025 g). Excellent agreement was also found between two alternative methods of estimating the zircaloy oxidation and hydrogen generation from the PIE data (836 versus 862 g). The agreement among all these values suggests that the best-estimate nominal values closely reflect the actual conditions and provide a greater degree of confidence in the data than the separate estimates with their individually large uncertainties would imply.

Estimate of Fuel Bundle Peak Temperatures. Temperatures within the fuel bundle were estimated based upon metallographic observations of changes in the zircaloy microstructure and the presence of molten materials and their interaction with other materials. Thermocouple data obtained during the experiment provided information up until failure and shunting occurred. However, cladding thermocouples in this experiment generally failed at around 2000 to 2200 K; and only a limited number of fuel centerline thermocouples were available to provide higher temperature data (up to 2970 K). Consequently, metallographic examinations provided the only data on peak temperatures in many regions of the fuel bundle.

The axial profile of peak bundle averaged temperatures in Experiment LP-FP-2 is presented in Figure 38. The primary purpose of this temperature distribution is to provide modelers of this experiment with a single cross-sectional average temperature to benchmark their codes. Localized temperatures at a given cross section varied above and below these peak bundle average temperatures. Details of how this profile was determined are described elsewhere (Jensen et al. 1989), and only a summary of the methodology is provided here.

At and below 0.36 m, the peak bundle averaged temperature could be determined from changes in the zircaloy microstructure

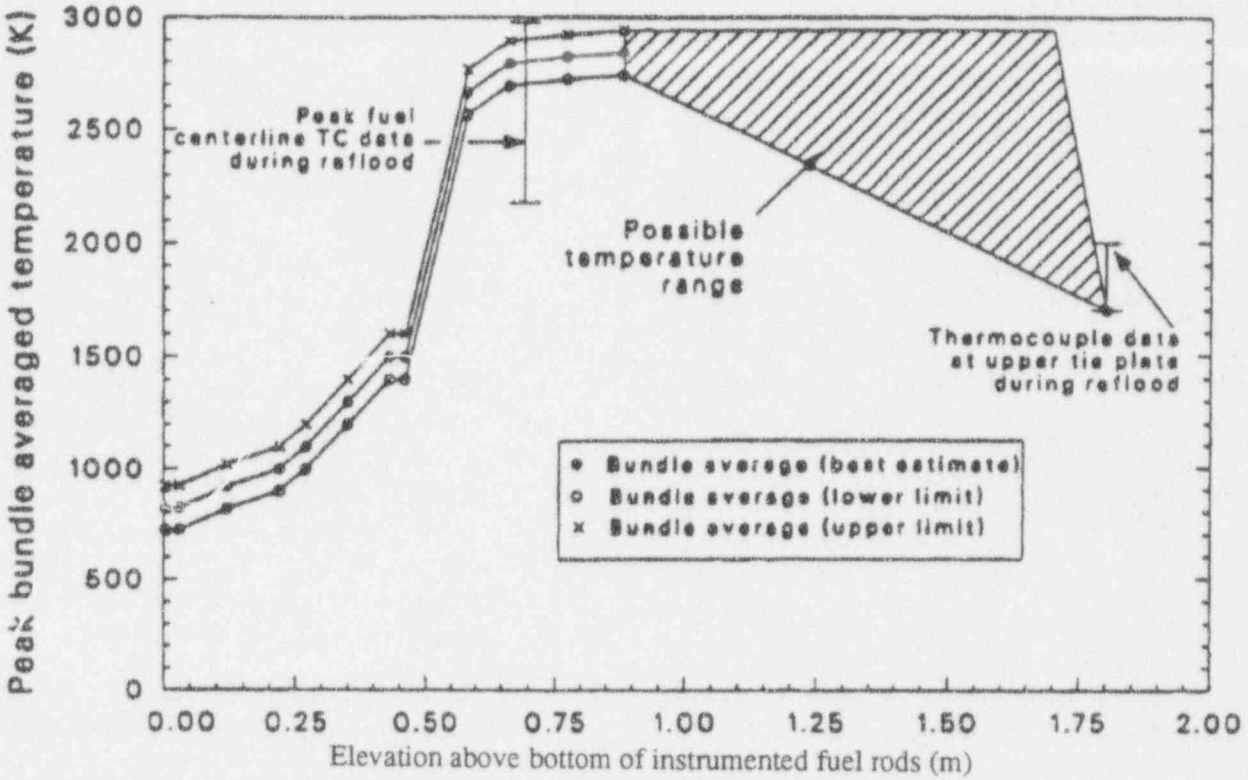

Figure 38. Peak bundle averaged temperature distribution.

(recrystallization above 920 K and the formation of prior-beta microstructure above 1245 K). From 0.43 to 0.46 m, the peak bundle average temperatures were based upon material interactions with the spacer grid (primarily Zr-Ni eutectic interactions, which become significant above approximately 1400 to 1500 K).

From 0.58 to 0.88 m, the peak bundle average temperatures were based upon material weighted temperatures for the various regions in the ceramic melt. For example, Figure 22 on page 33 shows the entire cross section through the 0.77 m elevation through the middle of the ceramic upper blockage region. In the center of this ceramic melt, temperatures were sufficient to cause fuel melting (> 3120 K); but on the periphery of the melt, the temperatures were above the melting point of $(U,Zr)O_2$ (2810 K) but below the melting point of the oxidized ZrO_2 cladding remnants (2960 K). Fuel centerline thermocouple readings supported these temperatures and also indicated that peak temperatures were approximately 2200 K in the peripheral regions of the bundle away from the ceramic melt regions. Average temperatures for each of these temperature regimes were weighted by the amount of material present to calculate the peak bundle average temperature at each cross section.

In the region above 0.88 m, the temperatures were difficult to estimate from the metallographic data because there were very few indicators and the range of possible temperatures was relatively large. Consequently, temperature ranges were based on interpolations between temperatures in the high temperature ceramic blockage and the upper tie plate. The peak bundle average temperature of 1700 K for the upper tie plate was based upon the fact that the stainless steel plate had melted in the central regions but was still intact on the periphery; consequently, the peak bundle average temperature straddled the 1720 K melting point of the stainless steel. Although the temperature profile must decrease at some point in this region, large uncertainties arise as to the actual shape of the profile; i.e., whether there is a

smooth transition or whether there is an abrupt change at some point.

Retained Fission Product and Elemental Analysis. Thirty core bores (approximately 6 and 10 mm in diameter) were drilled from specific regions in the metallographic samples for radiochemical analyses. The objective of these analyses was to determine the distribution of core materials and the retention of fission products in various materials.

Elemental analysis (using inductively coupled plasma spectroscopy) was performed for the 27 elements that made up the principal components of the bundle; however, only the major constituents of U and Zr were present in sufficient quantities to allow for extrapolation of the data to bundle inventories. This information was used in conjunction with the material distribution data to estimate integral volumes of material and to provide mass balance information, as described previously. The Zr distribution data were also used to determine the distribution of zircaloy oxidation in the fuel bundle.

The radionuclide concentrations were determined from isotopic gamma spectroscopy for ^{100m}Ag, ^{144}Ce, ^{60}Co, ^{134}Cs, ^{137}Cs, ^{152}Eu, ^{54}Mn, ^{144}Pr, ^{103}Ru, ^{106}Ru, and ^{125}Sb; beta spectroscopy for ^{90}Sr; and neutron activation of ^{129}I and subsequent gamma spectroscopy for ^{130}I. The fissile/fertile content was also measured by neutron activation/delayed fission neutron analysis.

Details of these analyses are described elsewhere (Jensen et al. 1989); however, the major conclusions and observations are summarized as follows:

- Sn apparently concentrated in the metallic melts, as evidenced by Sn/Zr ratios greater than the as-fabricated zircaloy.
- Fuel and control materials were positively identified in the upper end box, confirming results from the metallographic and SEM/WDS examinations that these materials were transported to this region. The fuel materials exhibited low retention of all major fission products, which suggests high temperatures or optimum release conditions.
- Antimony (Sb) accumulated in the metallic melt phases in the lower portion of the bundle.
- Cs was generally retained within intact and fragmented fuel. Iodine was retained in the intact fuel pellets; however, significant losses were calculated in fragmented fuel at temperatures of approximately 2200 to 2600 K. Significant losses of both Cs and I were measured in partially liquefied fuel.
- Significant losses of both Cs and I were measured in the ceramic melt samples, ranging from essentially complete release to less than 50% retention. These fission product releases could not be correlated solely to peak temperature, which indicates that other factors (such as time at temperature and surrounding materials) affected the release.

5.4 Summary and Conclusions

The major results and conclusions from the PIEs of the LP-FP-2 fuel bundle are summarized in this section.

The material relocation and stratification in the LP-FP-2 fuel bundle resulted in low melting point metallic melts near the bottom, a high temperature $(U,Zr)O_2$ ceramic melt region above this, and a debris bed of fuel pellets near the top. This is very similar to material relocation and stratification found in smaller scale integral severe fuel damage tests and observed in examinations of the TMI-2 core (Petti et al. 1989; Broughton et al. 1989; Hobbins 1990).

Material interactions between Ag and zircaloy resulted in liquefaction of the zircaloy well below the melting point of the zircaloy.

The Zr in these Ag-Zr melts interacted with the stainless steel cladding on the control rods and the Inconel spacer grids to cause liquefaction of these materials. Ag-Zr, Zr-Fe, and Zr-Ni interactions can all cause liquefaction of these materials above approximately 1200 K, but they become particularly significant above ~1400 to 1500 K.

The distribution of oxidized cladding shells indicates that the upper extent of significant cladding oxidation, prior to massive material relocation, was approximately 1.04 to 1.14 m. Above this elevation, the cladding shells were limited to a few rods on the periphery of the bundle. Upon control rod failure, Ag aerosols were released, which liquefied the unoxidized zircaloy in the upper portion of the bundle. The resultant melt relocated to form the lower blockage, diverting steam flow to the periphery of the bundle. The presence of these materials near the bottom of the fuel bundle, and the relatively low temperatures required for their liquefaction, indicates that these were the first materials to massively relocate during the transient.

The largest flow blockages (78 to 86%) were located through or just above the two remaining spacer grids. This indicates that the spacer grids tended to impede material relocation.

Integration of the posttest open flow measurement data indicated that the total volume of open area within the fuel bundle was reduced by 11% as a result of porosity trapped in the various melt regions. This corresponds to a 15% volume expansion of the material initially contained within the inner liner.

Fuel grain boundary separation was associated with the presence of metallic melts. This suggests that fuel reduction may have occurred adjacent to these metallic melts, resulting in the formation of a liquid U phase along these grain boundaries. The effect was not observed where high temperature ceramic melts were in contact with the fuel. Fuel fragmentation was also observed in areas that were not surrounded by any melt material, which suggests that the thermal shock associated with reflood may have contributed to fuel fragmentation.

Foamy fuel structures occurred as a result of Fe oxides liquefying the fuel. However, porous fuel structures were also observed on fuel pellets surrounded by the high temperature ceramic melt, and SEM/WDS examinations confirmed that this was pure UO_2. This indicates that peak temperatures near the center of the ceramic upper blockage exceeded fuel melting (> 3120 K).

The nominal grain size for most of the fuel was the same as in the as-fabricated condition (14 μm), although some grain growth did occur in the center of some of the fuel pellets in the hotter regions of the fuel bundle. The grain size in those regions averaged 27 μm. *The relatively large as-fabricated grain size and general lack of grain growth may have been an important factor in the small release of Cs and I from intact fuel pellets in this experiment.*

The PIEs identified fuel debris and melt materials in the upper end box, as well as extensive melting and oxidation of the upper tie plate. The relocation of these materials, and the damage to the upper tie plate, could only have occurred during the reflood period, when steam mass flow rates and temperatures were sufficient to have caused the observed behavior.

Approximately 63% of the zircaloy cladding and inner liner had liquefied, as compared to approximately 15% of the fuel. Most of the molten material was contained in the ceramic melt region, and Zr was the most abundant element in this region. Large amounts of Zr were also present in various metallic melts.

The best estimate of the hydrogen generated from zircaloy oxidation was 862 g. This corresponds to 49% of the zircaloy cladding and inner liner. An alternative methodology resulted in an estimate of 836 g, showing good agreement between the two estimates. An additional 163 g of hydrogen was nominally estimated to have been generated from oxidation of stainless steel and Inconel components, resulting in a best-estimate total of 1025 g of hydrogen. This

total is also in excellent agreement with measurement data based upon grab samples taken from the BST, which indicated 205± 11 g of hydrogen, and from an estimated amount of 819± 364 g in the PCS, for a total amount of 1024 g (Modro and Carboneau 1990; Carboneau et al. 1989). Analysis of the PIE data also indicated that 181 g of hydrogen were nominally generated during the transient phase from the oxidation of zircaloy cladding and the material in the lower blockage. This is in reasonable agreement with the 205 g in the BST, which is indicative of the amount of hydrogen generated during the transient since this tank was isolated from the system just prior to reflood. The hydrogen that resulted from the oxidation of the ceramic melt material, the melt that penetrated into the insulation, and the oxidation of the molten stainless steel and Inconel components, totals 818 g, which agrees with the 819 g estimated to be in the PCS, where all the hydrogen generated during reflood would have migrated (Modro and Carboneau 1990; Carboneau et al. 1989). These data indicate that most of the hydrogen in the LP-FP-2 test was generated during the reflood period.

Cesium was generally retained within intact and fragmented fuel pellets. Iodine was retained in the intact fuel pellets; however, significant losses were calculated in fragmented fuel at temperatures of approximately 2200 to 2600 K. Significant losses of both Cs and I were measured in partially liquefied fuel. Significant losses of both Cs and I were measured in the ceramic melt regions, ranging from essentially complete release to less than 50% retention. However, fission product release in these melt regions could not be correlated solely to peak temperature, which indicates that other factors (such as time at temperature and the nature of the surrounding material) probably affected fission product release.

6. SCDAP/RELAP5 ANALYSIS

This section describes an analysis of the OECD LOFT LP-FP-2 Experiment using the SCDAP/RELAP5 computer code [Allison 1993]. This analysis has had three objectives. The first was to confirm event timing and condition estimates from both on-line and post-irradiation examination (PIE) measurements. Of particular interest was the timing and magnitude of: (a) ballooning; (b) control rod melting; (c) metallic melting; (d) ceramic melting; (e) hydrogen production; and (f) fission product release. There was also significant interest in the code's prediction of oxide condition during reflood. The second objective was to establish the influence of key experimental and modeling parameters on the progress of the transient. The third objective was to assess the early phase core damage progression models in the code.

The SCDAP/RELAP5 analysis is presented in four sections, a discussion of (a) the input model; (b) the transient analysis; (c) the reflood analysis; and (d) an assessment of SCDAP/RELAP5.

6.1 Input Model

There is a long history of analysis of the OECD LOFT LP-FP-2 Experiment with SCDAP/RELAP5. Several analysts with multiple input models have used many versions of the code to analyze the experiment (Adams et al. 1985; Carboneau et al. 1989; Guntay et al. 1991). In the course of performing these calculations, a number of modifications have been made to the original LP-FP-2 model. These revisions were made to permit the code to handle the transient more smoothly and to better represent a particular aspect of the facility. For the analysis described here, the author has endeavored to make the best use possible of the previous analyses. This has consisted of reviewing the analyses and utilizing the best of the model revisions.

Primary Coolant System Model. The primary system model for the current analysis is similar to LOFT facility models that have been developed in the past, with several revisions intended to establish a best-estimate thermal-hydraulic model. The most significant of these modifications are:

a. The downcomer model was changed to a split (two-channel) downcomer model and was renodalized to allow volume boundaries to have the same elevation as core volume boundaries. Analysts have oscillated between the use of single channel and split downcomer models. Advocates of the single-channel downcomer claim calculational simplicity with minimal impact on hydraulic response during a large break. However, the reactor vessel mass inventory is sufficiently critical during the small- break portion of this calculation that the split downcomer model has been reinstituted. The downcomer elevations were renodalized because previous calculations have shown that when the downcomer and core have different elevations, oscillations in liquid level can occur.

b. The upper plenum structure surface areas were modified to reflect detailed surface area calculations (Carboneau et al. 1987, Appendix P). Also the upper plenum thickness was modified to reflect estimates of the upper plenum structural mass. This modification was introduced to better simulate the fission product transport phenomena observed during the transient.

c. RELAP5 heat structures representing the center fuel module (CFM) high-, medium-, and low-power fuel rods, control rods, guide tubes, and thermal shroud were all replaced with SCDAP components. Also, the RELAP5 single-channel model of the CFM was replaced with a three-channel model. This allows

significantly better simulation of core blockage and relocation and their impact on coolant flow diversion.

d. RELAP5 heat structures representing peripheral module fuel rods were replaced with SCDAP components representing high- and average-power fuel rods.

The SCDAP/RELAP5 model of the LOFT reactor vessel is shown in Figure 39, while the ex-vessel PCS is shown in Figure 40. This nodalization, representative of a Westinghouse 4-loop plant, models all components in the PCS, such as the intact and broken loops, steam generator and secondary system, and reactor vessel.

Core Model. The reactor core was modeled as four separate channels, one representing the peripheral fuel bundles and three representing the CFM, as shown in Figure 41. The center fuel module (CFM) was modeled using nine SCDAP components, as shown in Figure 42.

The center fuel module fuel rods were modeled with six components. These six components were divided into three pairs of rods, each pair representing a bank of fuel rods different only in power. This was necessary because these rods were enriched to 10%, causing significant thermal neutron depletion, and therefore a depression in the radial power profile of approximately 13%. A pair of identical fuel rod components were used to model each bank, because it has become a standard practice to bound the oxidation response with a pair of components, the first modeling oxidation limited only by steam availability, and the second modeling oxidation limited by the diffusion of steam through a hydrogen boundary layer. Although modeling these bounding phenomena had little impact on the analysis of the transient phase of LP-FP-2, it can impact the results if significant quantities of hydrogen are being generated by the oxidation process. Three additional components were used to model the Ag/In/Cd control rods, the guide tubes, and the zircaloy-lined insulating shroud surrounding the CFM. Figure 42 illustrates the CFM nodalization, showing the three banks of fuel rods, as well as the locations of the guide tubes and Ag/In/Cd control rods. The thermal shroud surrounding the CFM was, of course, modeled as a separate component.

As discussed earlier, the CFM was divided into three parallel flow channels, each surrounding a single group of fuel rods. In the past (Carboneau 1989), the thermal-hydraulic representation of the LOFT core used a hot-channel approach. This approach consisted of using one hydraulic channel to model flow conditions for the average flow channel and a second hydraulic channel to model flow conditions in the hottest channel. This hot-channel approach had been used successfully in the past to model large- and small-break experiments. Unfortunately, because of the implied assumption that all fuel rods within the same flow channel behave independently of one another, this approach has been shown to be inaccurate during any transient where fuel rod geometry changes (Coryell 1992). Basically, as the flow through the unit cell around a fuel rod is disrupted, additional coolant flow is diverted into adjacent channels, making them less likely to undergo geometry change. This violates the assumption that each fuel rod within the hydraulic channel is independent. For this reason, the CFM was divided into three parallel flow channels. Since the peripheral modules experienced no deformation, the assumption of independence remains valid; and the hydraulic model was left unchanged, with one channel representing all modules.

Initial Conditions. Reactor conditions at the start of the transient were established in the usual manner used with RELAP5 in that the initial core power was defined and a set of steady-state controllers were applied to the primary coolant pumps, pressurizer spray and heaters, feed system, and secondary system. Several hundred seconds of null transient were then performed with the model to allow the steady-state controllers to bring the system to an equilibrium condition.

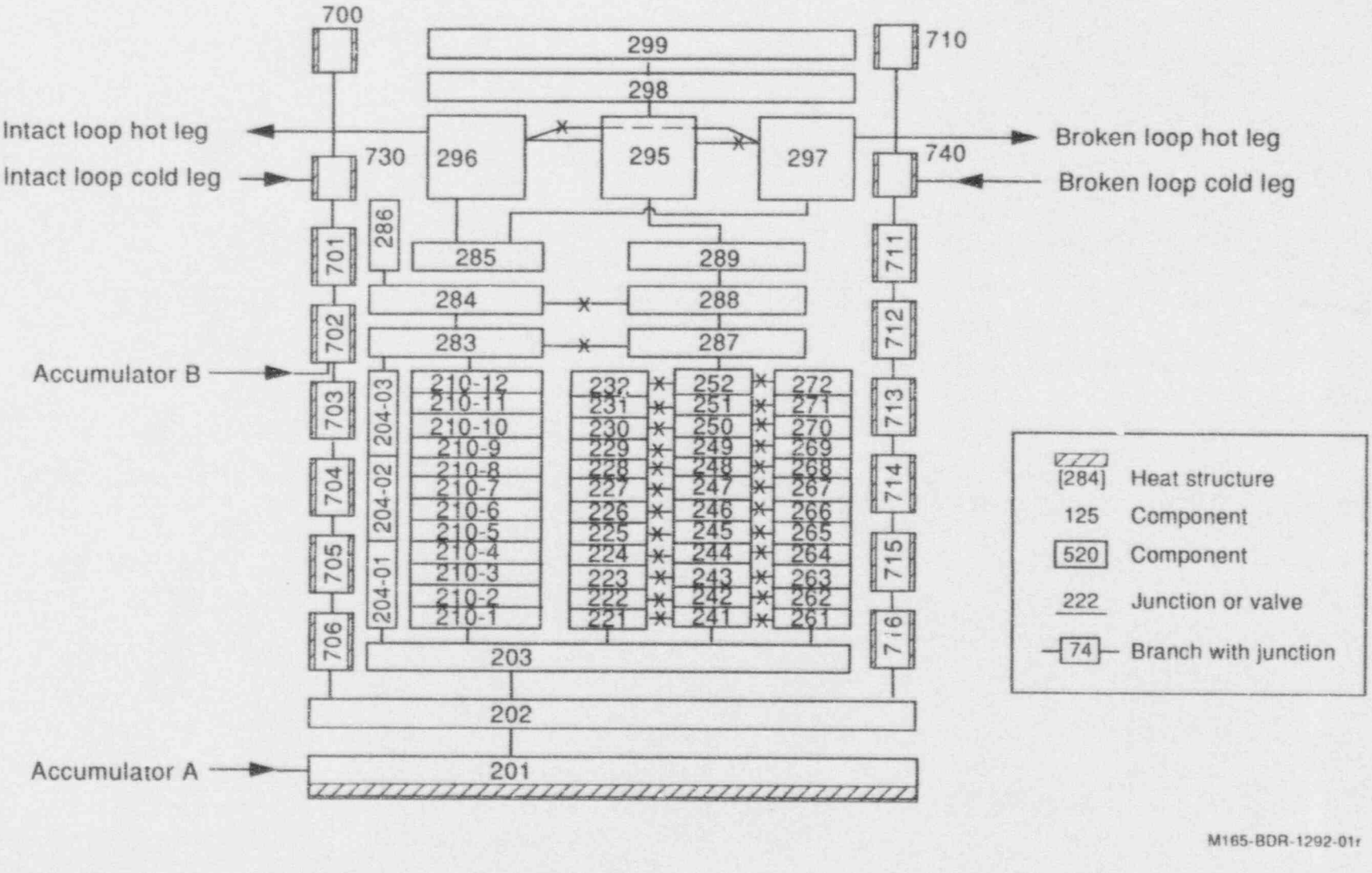

Figure 39. SCDAP/RELAP5 nodalization diagram of LP-FP-2 reactor vessel.

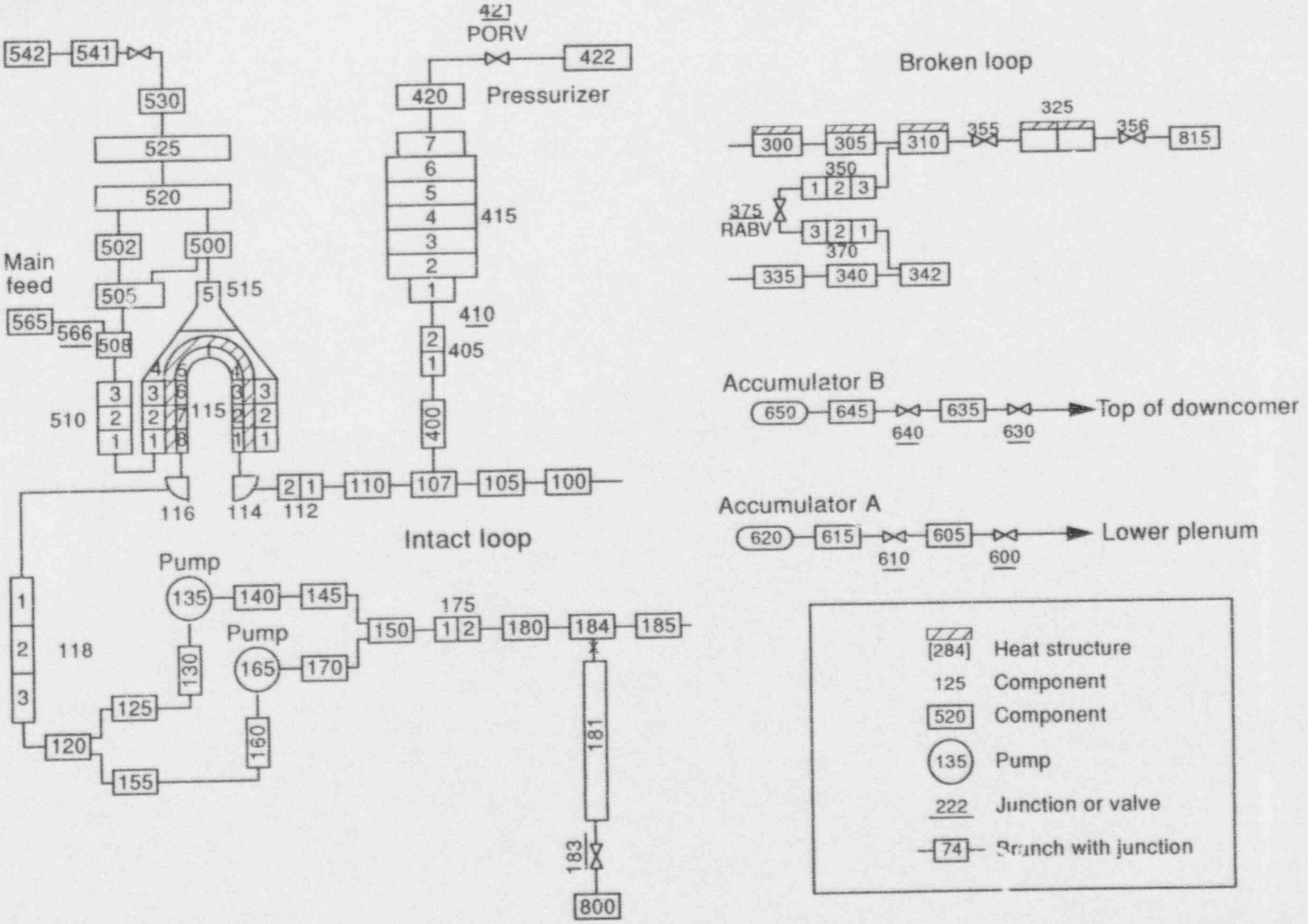

M165-BDB-1292-002

Figure 40. SCDAP/RELAP5 nodalization diagram of LP-FP-2 primary system.

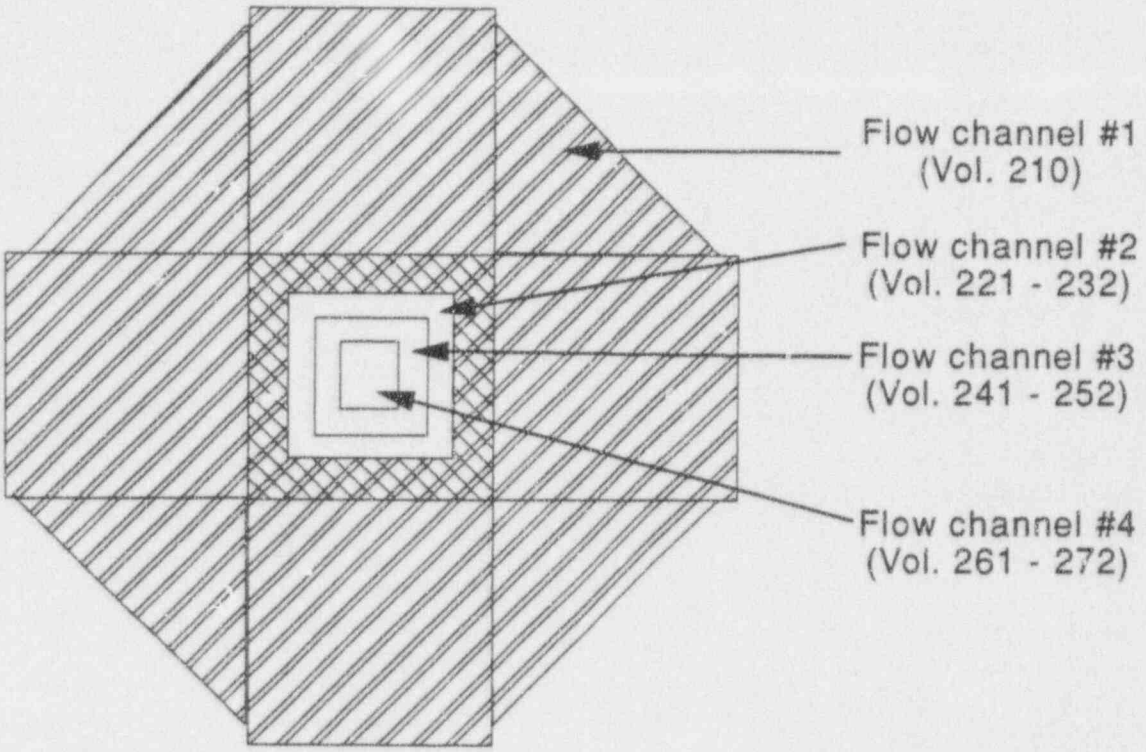

Figure 41. Radial core hydrodynamic nodalization.

7	5	5	8	5	5	5	7	5	5	7
5	3	3	3	3	7	3	3	3	3	5
5	3	8	3	3	3	3	3	8	3	5
8	3	3	1	1	1	1	1	3	3	8
5	3	4	1	2	1	1	1	3	3	5
6	7	3	1	1	7	1	1	3	8	5
5	3	3	1	1	1	1	1	3	3	5
8	3	3	1	1	1	1	1	3	3	7
5	3	8	3	3	3	3	3	8	3	5
5	3	3	3	3	8	3	3	3	3	5
7	5	5	7	5	5	5	8	5	5	7

1 Low power fuel rod limited by diffusion.

2 Low power fuel rod limited by steam availability.

3 Medium power fuel rod limited by diffusion.

4 Medium power fuel rod limited by steam availability.

5 High power fuel rod limited by diffusion.

6 High power fuel rod limited by steam availability.

7 Guide tube.

Figure 42. SCDAP center fuel module nodalization.

Table 12. Comparison of calculated and measured initial conditions.

Parameter	Measured value	Calculated value
Primary coolant system		
Core delta T (K)	11.7 ± 1.4	11.35
Primary system pressure (MPa)	14.98 ± 0.1	15.08
Hot leg temperature	571.6 ± 0.8	570.5
Cold leg temperature (K)	559.9 ± 1.1	559.9
Loop mass flow (kg/s)	475 ± 2.5	475.01
Reactor vessel		
Power level (MW)	26.8 ± 1.4	26.8
Decay heat at 200 s (kW)	684.8	695.19
Maximum linear heat generation (kW/m)	42.6 ± 3.6	43.0
Secondary system		
Secondary pressure (MPa)	6.38 ± 0.08	6.09
Pressurizer		
Liquid volume (m^3)	0.57 ± 0.03	0.57
Steam volume (m^3)	0.37 ± 0.03	0.37
Water temperature (K)	616.9 ± 2.1	605.9
Pressure (MPa)	15.1 ± 0.1	15.05
Liquid level (m)	1.06 ± 0.06	1.06
Boron suppression tank		
Pressure (kPa)	95 ± 3	100

After reaching equilibrium, the thermal and hydraulic conditions (mass flow, internal energy, pressure, and so on) and initial temperature distributions for heat structures and SCDAP components were transferred into a second input deck, through the use of PYGMALION, a utility available to all RELAP5 newsletter subscribers. Table 12 compares the initial measured and calculated hydraulic conditions for several significant parameters.

Boundary Conditions. Boundary Conditions for experiments in the LOFT facility were usually very well defined, because experiments in this facility were routinely used for thermal-hydraulic code development or assessment. The boundary condition with the greatest uncertainty in experimental facilities is nearly always environmental heat losses. LOFT environmental heat losses, however, have been parametrically defined over a series of 26 experiments, covering a wide range of break sizes and are therefore well-characterized. The heat losses during the LP-FP-2 transient were modeled as three separate quantities, from the reactor vessel, the steam generator, and the intact loop piping.

The remaining boundary conditions for the OECD LOFT LP-FP-2 Experiment were, unfortunately, not as well defined as previous LOFT experiments. Because the objectives of this experiment were directed exclusively towards early phase severe core damage phenomena and fission product transport, definition of thermal-hydraulic boundary conditions was sacrificed to provide added confidence in meeting the core damage objectives. The primary analytical difficulty is that the intermediate size break on the intact loop cold leg, through which 80% of the system coolant inventory was expelled, was merely a non-instrumented, non-orificed pipe. Although maximizing early coolant depletion, as intended, the lack of an orifice at this break has forced all

subsequent analyses to rely on secondary indications, such as time of core uncovery, to characterize the PCS mass balance.

Radial and axial power profiles were measured with traversing in-core probes (TIP's), and decay heat has been well defined by detailed reactor physics calculations. Pressure in the BST, the simulated containment, was modeled as a constant. Although pressure in an effluent tank 13 times as large as the PCS will increase marginally as the system experiences blowdown, it has no significant effect on primary system response.

The remaining boundary conditions, specifically the specification of significant thermal-hydraulic events such as valve and pump operation, were modeled using a RELAP5 control system based primarily on the measured timing of each operation. The specification of these events to the facility control room were based upon system pressure, and attempts were made early in the analysis of this experiment to specify operator action based upon pressure. However, in a transient such as the interfacing systems LOCA which this experiment simulated, when the system pressure decreases slowly, it was determined that a small discrepancy in pressure could significantly impact the timing of valve operation. Wherever possible, then, the effects of operator actions were simulated based upon the experiment time.

6.2 Transient Analysis

SCDAP/RELAP5 has been used to analyze the LP-FP-2 Experiment as early as the experiment's planning stages. However, in the seven years since the experiment, a number of significant improvements have been made to SCDAP/RELAP5[a]. For this reason, an analysis of the experiment was performed with the objective of assessing the state of the code against experimental and identifying parameters which are key to the analysis.

a. SCDAP/RELAP5/MOD3, configuration control version 8ae.

System Thermal-Hydraulic Behavior. In most severe accident analyses, the uncertainty in the thermal-hydraulic behavior of the PCS dominates the uncertainty of the analyses. This is emphasized in the analysis of the LP-FP-2 Experiment because the experiment focused exclusively on early phase severe accident phenomena prior to corium relocation into the lower vessel.

As was mentioned in the discussion of boundary conditions, the primary difficulty in analyzing the LP-FP-2 Experiment has always been the evaluation of the primary system mass balance. The best-estimate analysis presented here has been no exception. It has not been difficult in the past to tune the loss coefficients on both the intact loop cold leg break and the simulated LPIS line such that the PCS pressure is matched exactly. Unfortunately, for all system models used to date, this causes the system to retain too much fluid in the reactor vessel, thereby delaying the start of core uncovery by as much as 500 seconds. Two hypotheses have been advanced to explain the inability of the model to predict both system pressure and time of core uncovery: first, that the mass balance has been correctly tracked but has been distributed incorrectly about the system; or, secondly, that the distribution is roughly correct but that the input model does not correctly characterize the reactor vessel internals and has therefore caused the energy deposition to the coolant to be too low. Although it should be possible to modify the input model to examine these two hypotheses, the additional resources required would not significantly benefit the assessment of severe accident code models, which remains the primary goal of this analysis. In order to evaluate the severe accident models, more emphasis was placed on correctly predicting the time of core uncovery than on duplicating system pressure. Figure 43 compares the calculated and measured system pressure during the transient phase of the experiment.

Figure 44 shows the core dryout time as a function of elevation above the bottom of the active core. This figure illustrates that SCDAP/RELAP5 predicts that the top of the core is low

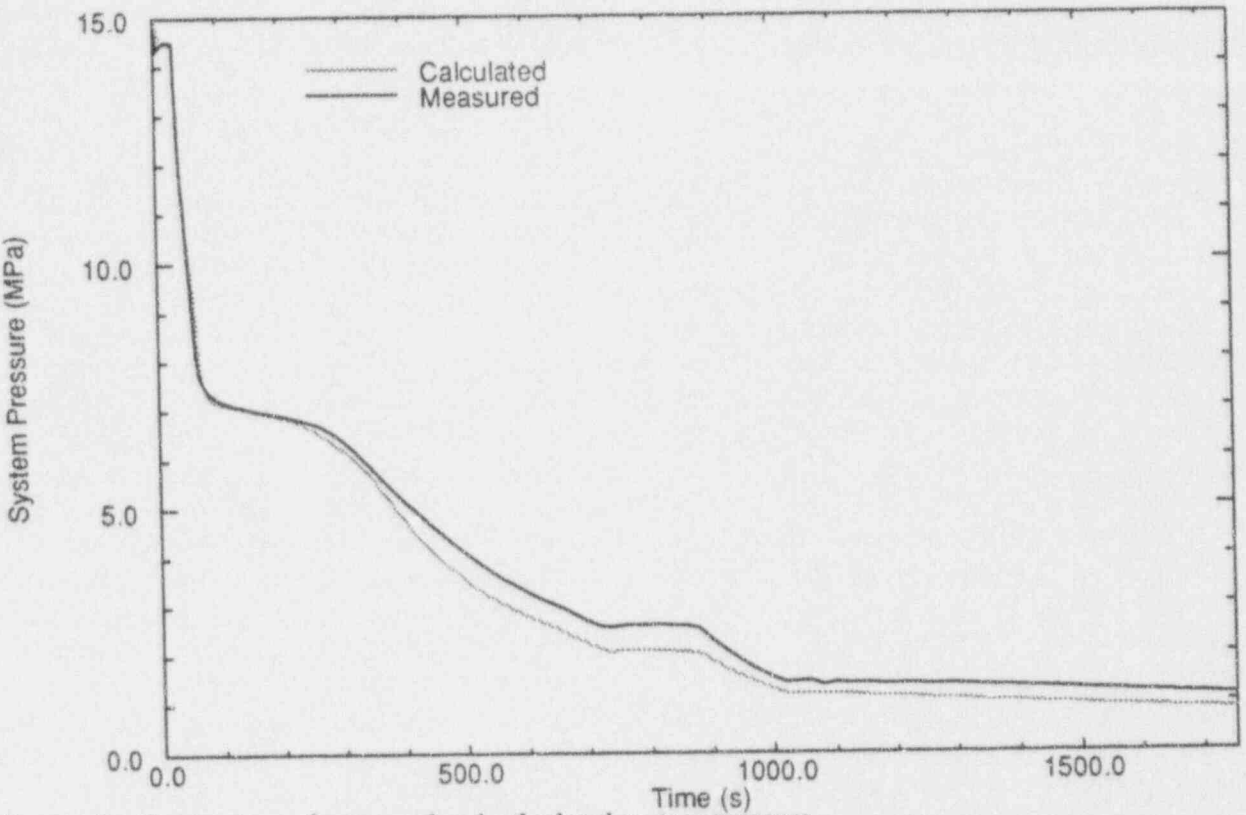

Figure 43. Comparison of measured and calculated system pressure.

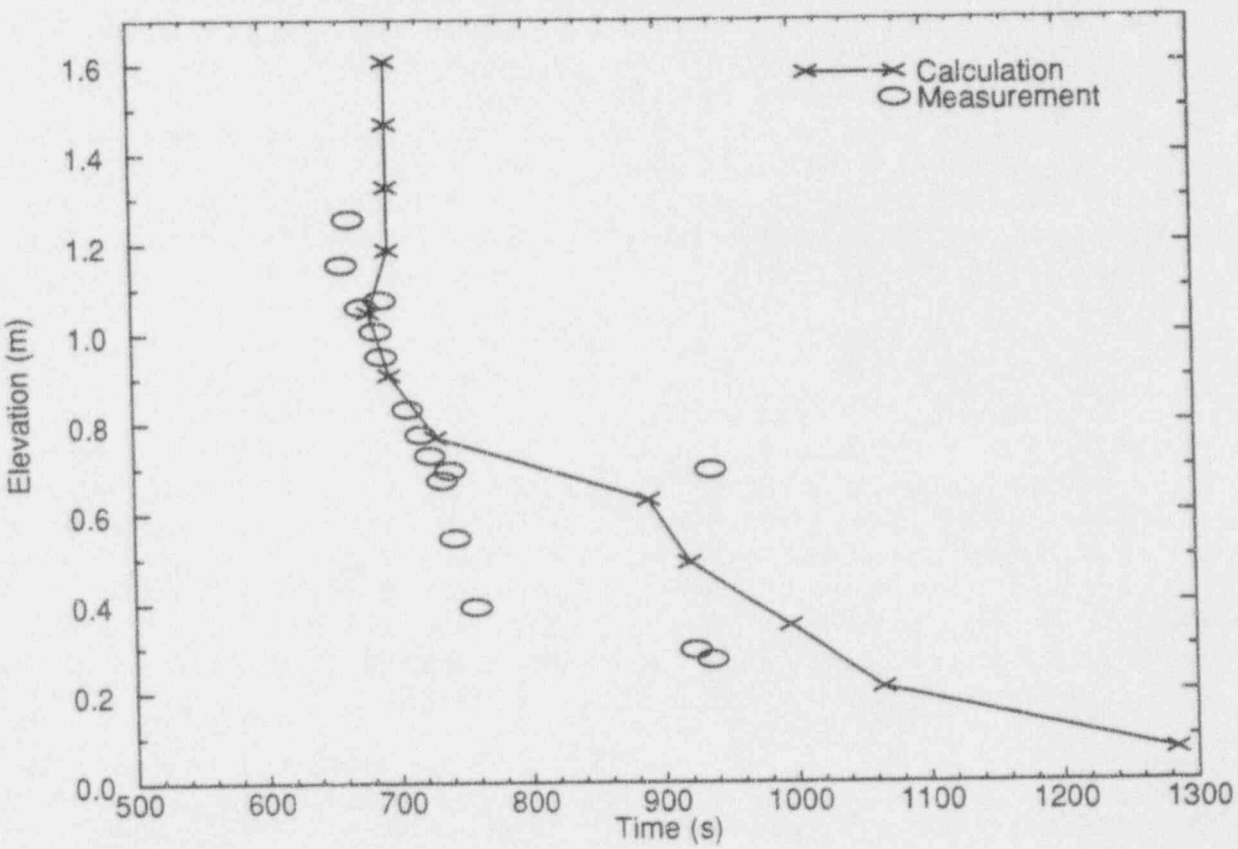

Figure 44. Comparison of calculated and measured core dryout time.

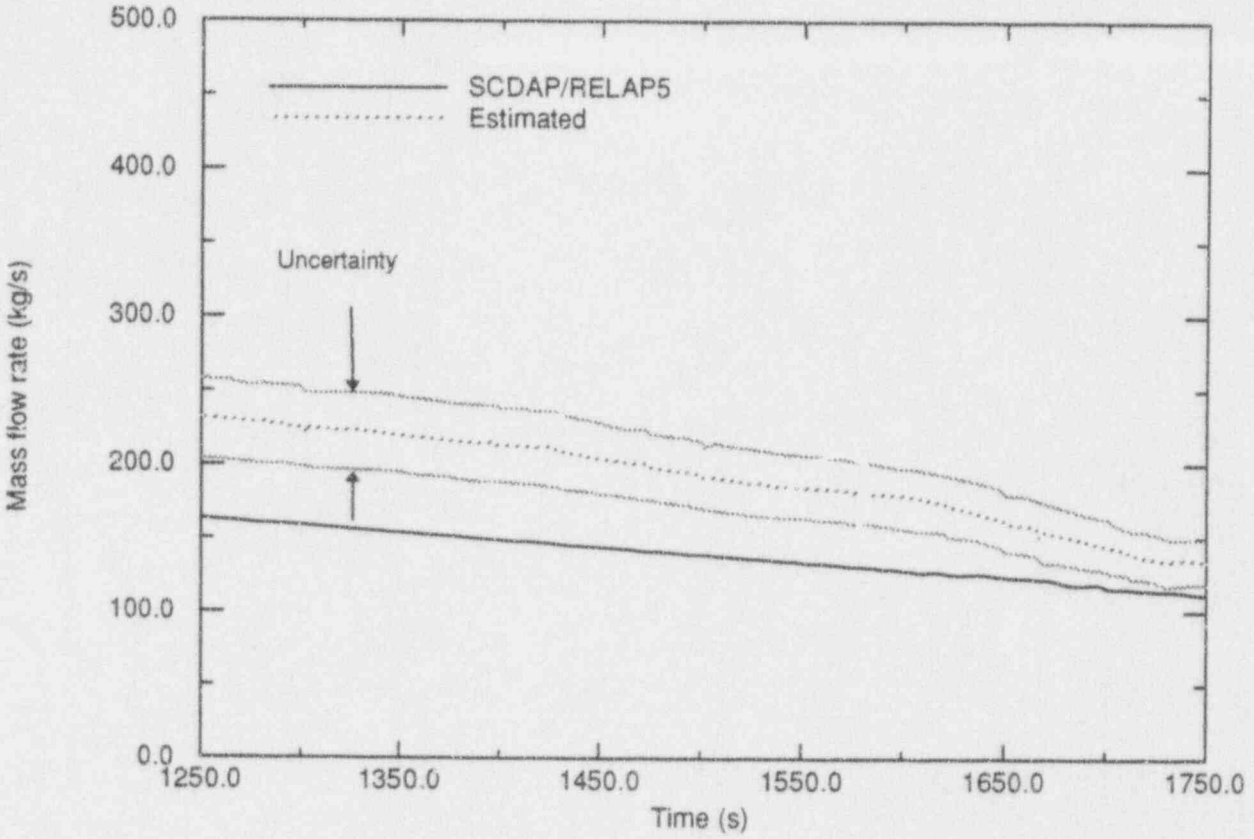

Figure 45. Calculated and estimated LPIS mass flow rate.

enough in power that it is initially cooled by steam/entrained liquid until the liquid level drops to an elevation of 0.9 m. The code tracks core dryout very well until valve cycling causes perturbations in the liquid level. The code predicts core dryout in the bottom-most portion of the core later than measured.

One of the locations where estimates of coolant system mass flow is available is in the simulated LPIS line. This mass flow has been estimated from pressure, temperature, and differential pressure data associated with the LPIS venturi, [Carboneau 1989]. The result of this estimate is compared to the mass flow calculated for the simulated LPIS line by SCDAP/RELAP5 in Figure 45. As seen in this figure, the predicted flow rate during the later phase of the experiment is less than the expected value. Since the driving force for this flow is the pressure differential between the reactor vessel and the simulated containment, such an underprediction is consistent with the underprediction of system pressure.

One of the key parameters in an assessment of the ability of SCDAP/RELAP5 to predict core damage phenomena is the core temperature history. Figure 46 compares the calculated cladding response with that measured at the 10 inch elevation. As seen in this figure, the time of core uncovery at the bottom of the core is late and the core heatup rate is too fast. This difference in thermal response is caused by the discrepancy in the vessel liquid inventory just discussed. Figure 47 compares the calculated cladding temperature at the 27 inch elevation (the peak power zone) with that measured during the experiment. This figure shows that the time of core uncovery at the center of the core is predicted very well. The cladding heatup rate is also predicted very well until 877 s, when the operators began a series of valve operations to lower the system pressure to prevent fission

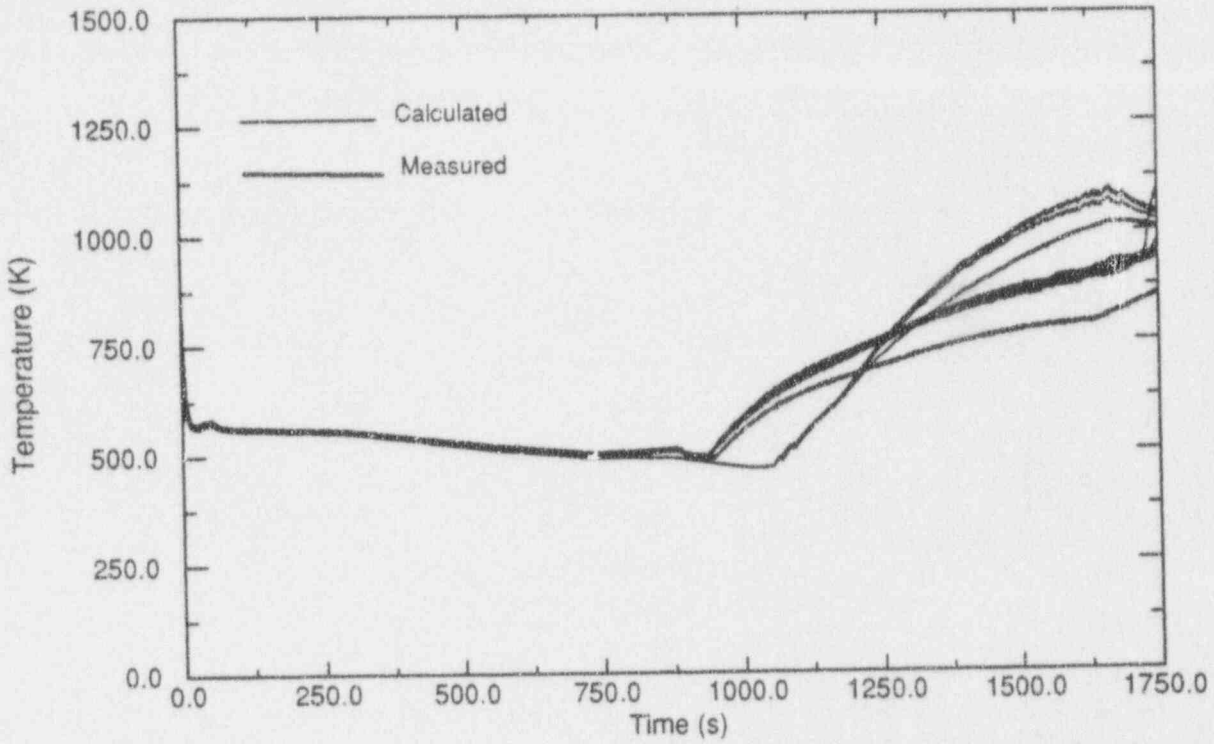

Figure 46. Calculated and measured cladding temperature at the 10 inch elevation.

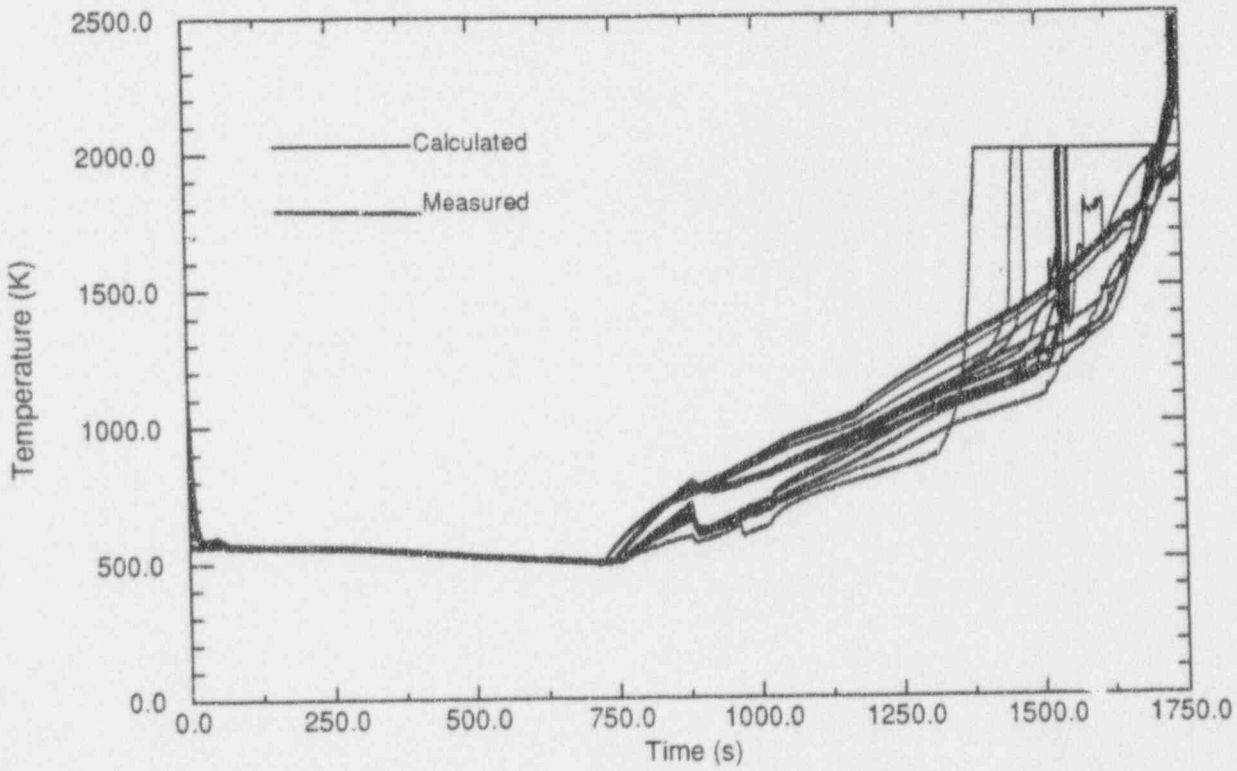

Figure 47. Calculated and measured cladding temperature at the 27 inch elevation.

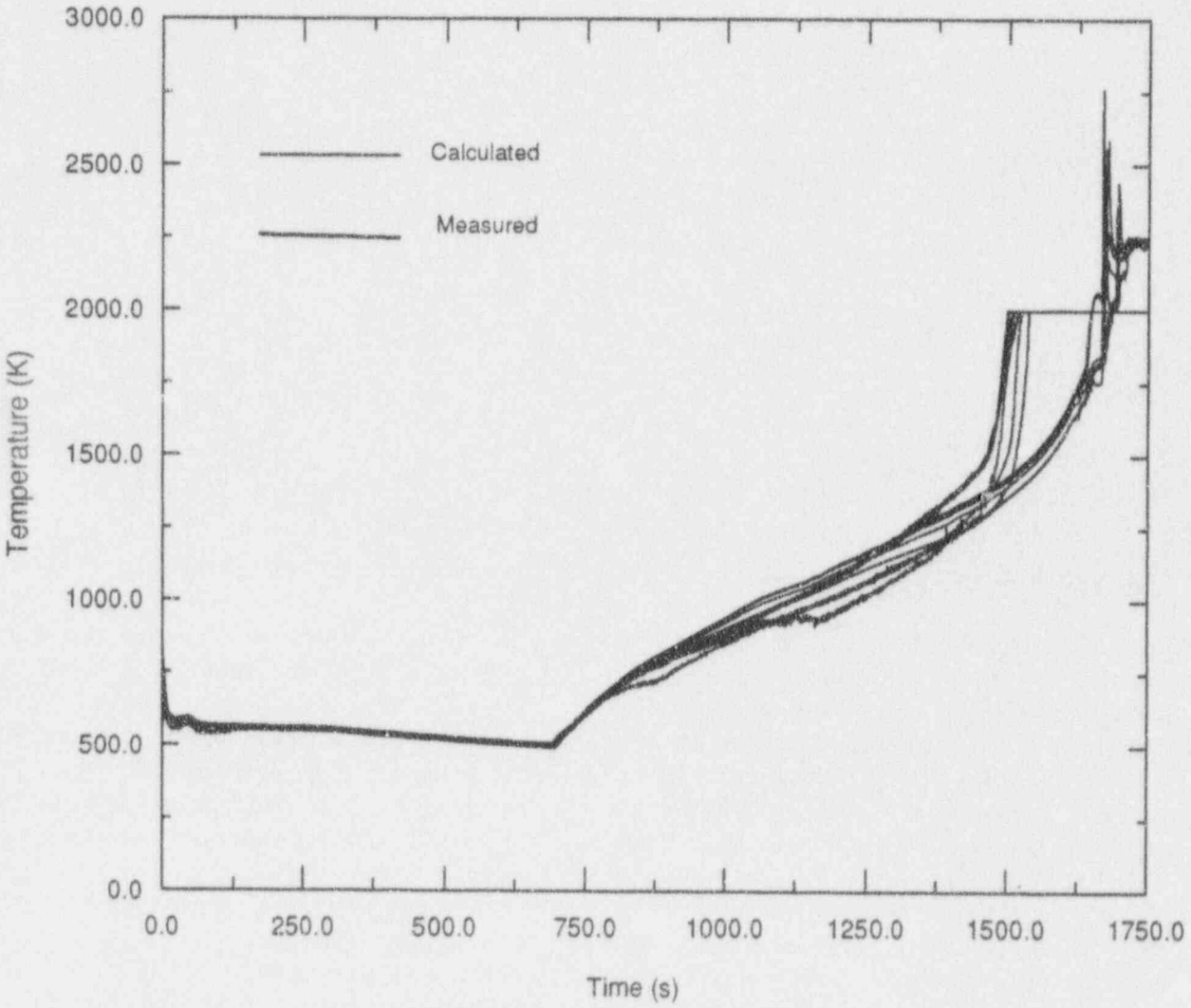

Figure 48. Calculated and measured cladding temperature at the 42 inch elevation.

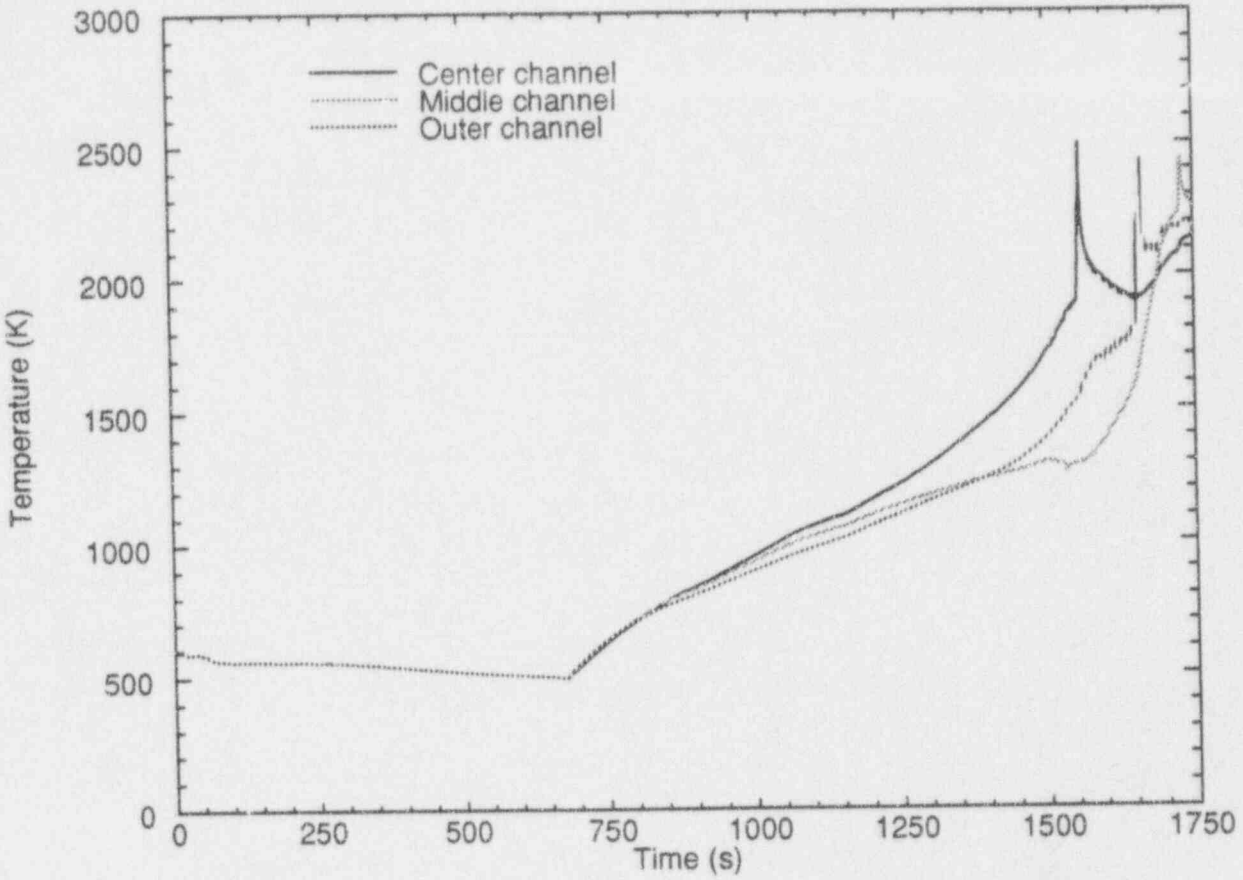

Figure 49. Radial temperature profile across the center fuel module at the 42 inch elevation.

product instrumentation damage. This valve operation (reopening of the intact loop cold leg break and PORV) caused some cooling of the thermocouples. Whether this measured cooling was representative of what occurred throughout the core or only on the instrumented rods is unknown, but the current combination of input model and code was unable to model it. Figure 48 compares the calculated cladding temperature with that measured at the 42 inch elevation. Although the instrumentation in this part of the core did not survive to experience the early severe accident phase of the experiment, early indications show that the calculated cladding behavior is within the uncertainty of the measurement. It should be noted on all comparisons to experimental data that as the thermocouple indicates rapid oxidation rates and temperatures in excess of 1800 K, the instrument is probably no longer tracking local cladding response.

Figure 49 illustrates the radial temperature across the center fuel module at the 42 inch elevation. This node is the highest temperature node, and is the node at which cladding rupture is predicted. The response at this elevation is just as expected, with the core heatup beginning universally across the module at the same point in time, the response remaining very similar until radiation heat transfer and fuel rod geometry changes begin to cause distinctions across the module. At approximately 1150 s the fuel rod in the center channel is predicted to rupture. This matches the first measurement of fission product gap release of 1200 s. After fuel rod rupture at this elevation, SCDAP/RELAP5 models double-sided oxidation at the failure elevation. After 1500 s, core damage and blockage due to material relocation cause the middle channel to heatup less rapidly than the channels on either side of it. At approximately 1550 s, the cladding in the average channel is completely oxidized at this location and the lack of oxidation heat

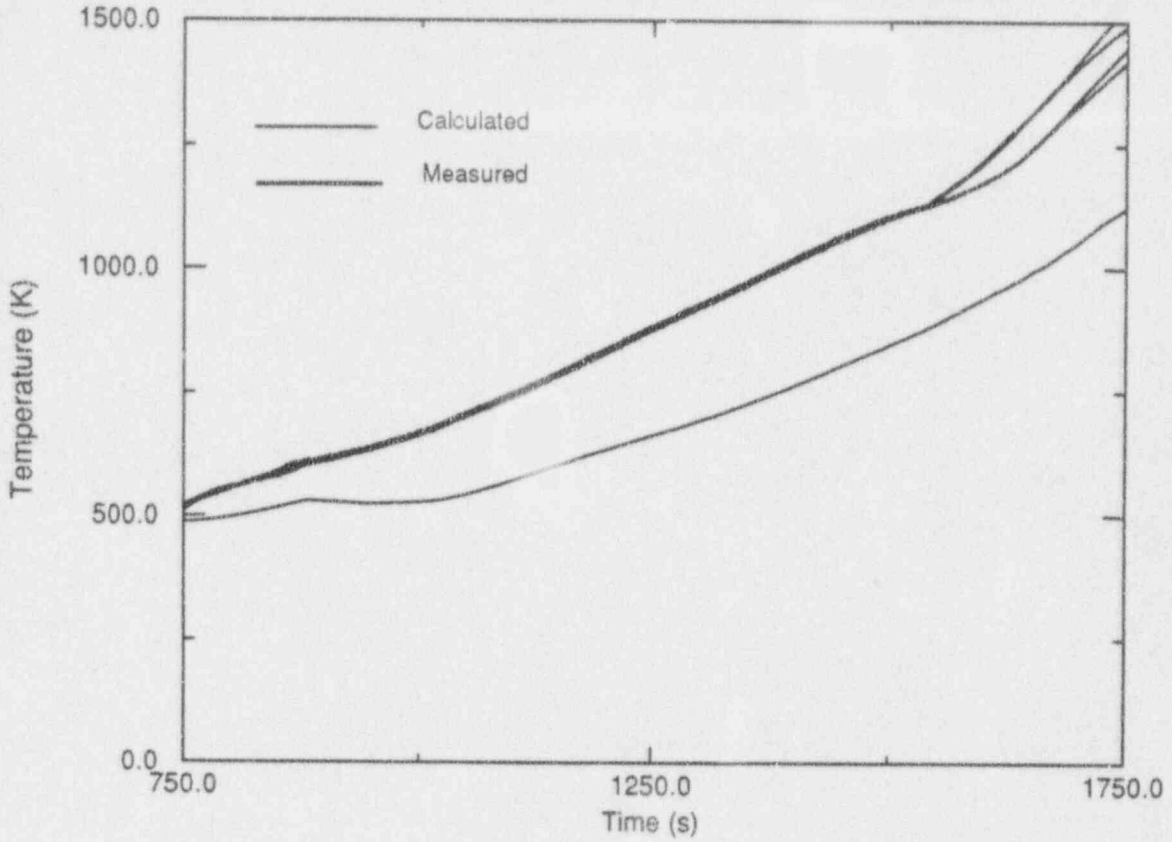

Figure 50. Calculated and measured outer shroud temperatures at the 42 inch elevation.

generation causes the component to cool to the coolant temperature. At approximately 1665 s the Ag/In/Cd control rods are predicted to fail. This is only slightly later than the estimated failure time of 1520 s, indicated by relocation of molten material to the lower portions of the core.

Figure 50 shows a comparison between the calculated and measured response on the outer surface of the flow shroud at the high core temperature elevation (42 in.). This comparison indicates that the heat conduction through the flow shroud is underpredicted. This underprediction is probably caused by the uncertainty in the time-of-failure of the shroud liner and the consequent uncertainty in the time-dependent thermal conductivity of the ZrO_2 insulation as coolant penetrated the insulation. The same underprediction of CFM heat loss through the thermal shroud is shown on all elevations of the shroud. An underprediction of heat loss was expected at the top and bottom of the core, due to the fact that SCDAP/RELAP5 can only model a single thermal conductivity for all elevations of the shroud, when in reality the designers specified different density ZrO_2 at the top and bottom of the shroud.

In summary, SCDAP/RELAP5 is modeling the thermal and hydraulic response of the core reasonably well. Even though dryout at the bottom-most portion of the center fuel module is being predicted slightly late, it has little effect on the transient analysis, and the boundary conditions to the core damage models are accurately tracked.

Key Transient Parameters. One of the objectives of this analysis was to identify modeling parameters which had an impact on the calculated response during the transient phase of the LP-FP-2 Experiment. Two parameters were identified during this portion of the analysis (1) the threshold for double-sided oxidation, and (2)

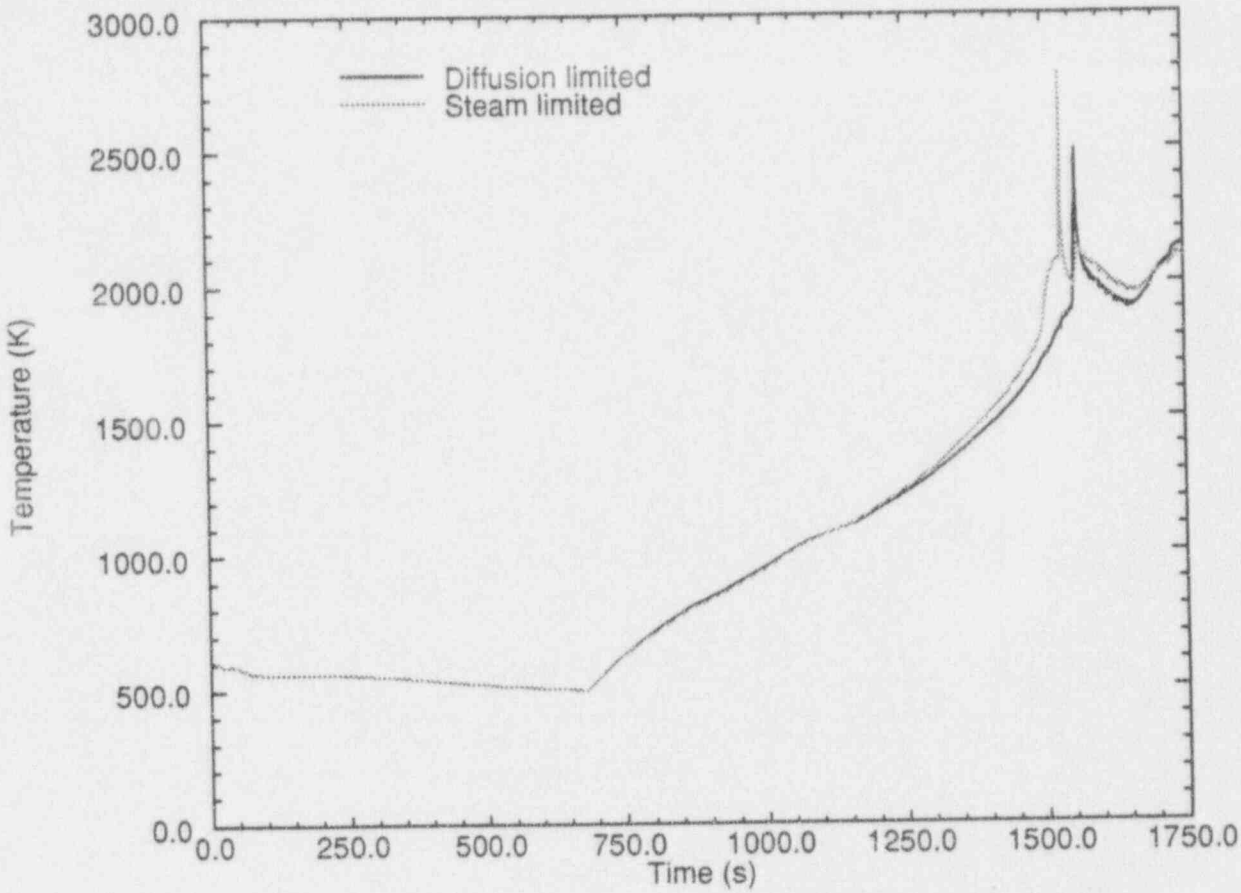

Figure 51. Effect of oxidation rate limit on identical fuel rod components.

the oxidation limiting model.

It is interesting to note that early calculations of the LP-FP-2 transient allowed double-sided oxidation to occur over too great a length of the fuel rod. This model uses a threshold local hoop strain to determine whether or not double-sided oxidation is occurring. Early calculations used a threshold hoop strain of 2%, resulting in too rapid a heatup below the peak temperature node and delayed the heatup at higher elevations due to steam starvation. It also caused a significant over-prediction of the transient hydrogen generation. The current calculation uses a threshold local hoop strain equal to the rupture strain, thereby allowing double-sided oxidation only at the ruptured node. This increase in the threshold for double-sided oxidation may be an artifact of either the low burnup fuel, or the non-prototypical fuel rod pre-pressurization. However, this analysis suggests that the default threshold for double-sided oxidation be increased to the rupture strain.

One of the parameters which was identified as potentially impacting the calculated transient response was the type of oxidation limit imposed on the fuel rods. SCDAP/RELAP5 has traditionally allowed the zircaloy cladding to oxidize at a rate limited only by the availability of steam. A recent extension has added the capability of limiting the oxidation rate by the limit of steam diffusion through a hydrogen boundary layer. The analysis described here modeled the fuel rods in each coolant channel with a pair of fuel rod components which were identical except for the oxidation rate limit imposed. The results of this bounding analysis are shown in Figure 51. As could be expected the difference in the oxidation limiting models does not become apparent until rapid oxidation begins, and even then the LOFT core is

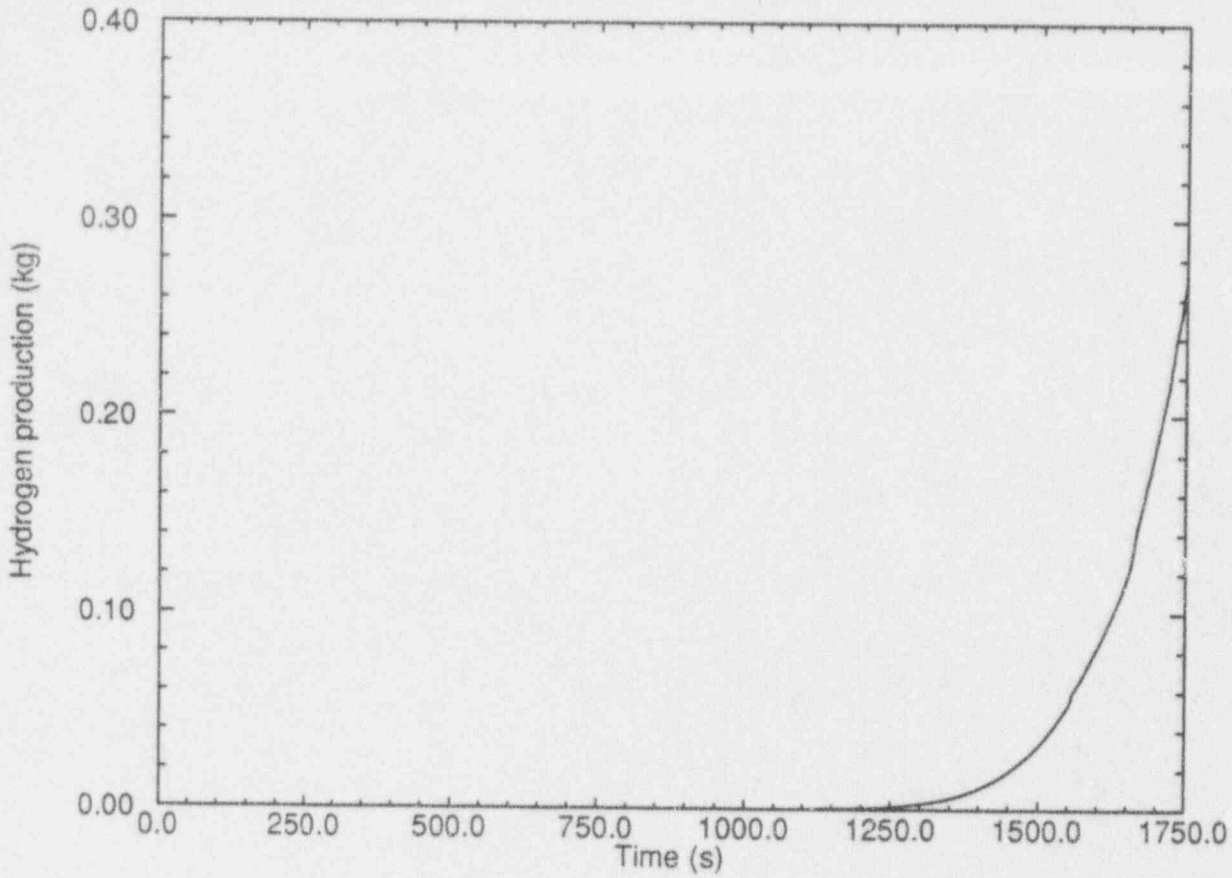

Figure 52. Calculated hydrogen production.

sufficiently steam rich that the diffusion limit does not lag significantly behind the steam availability limit.

Transient Damage Progression. The ability of SCDAP/RELAP5 to predict core damage during the transient phase of LP-FP-2 has been and will continue to be of keen interest to the code developers. A facility which provided experimental evidence of core damage during the early phases of a severe accident is invaluable to the code development and assessment process.

One of the more interesting parameters to characterize the integral response of a damaged core is the hydrogen production rate, both because of it's significance to the risk evaluation process and because it represents an integral measurement of core response. Figure 52 shows the hydrogen production calculated by SCDAP/RELAP5 for the transient portion of the experiment. The cumulative hydrogen production during the transient portion is predicted to be approximately 270 g. This compares very well with the estimated transient production of 205± 11 g.

Figure 53 illustrates the overall condition of the LOFT CFM just prior to the initiation of reflood. This figure illustrates the condition of the three primary fuel rod groups, as well as the Ag-In-Cd control rods. As seen in this figure, all three fuel rod groups have ballooned and failed at axial node eight, which represents the hottest portion of the CFM. This corresponds with measurements of the temperature at the 42 in. elevation As is typical in damage progression in the LOFT core, this elevation is just above the peak power zone. It can be observed that the cladding ballooning is as localized as the axial nodalization will allow, and that there has been no significant fuel rod damage other than localized deformation and cladding failure. No significant ceramic fuel rod melting has been

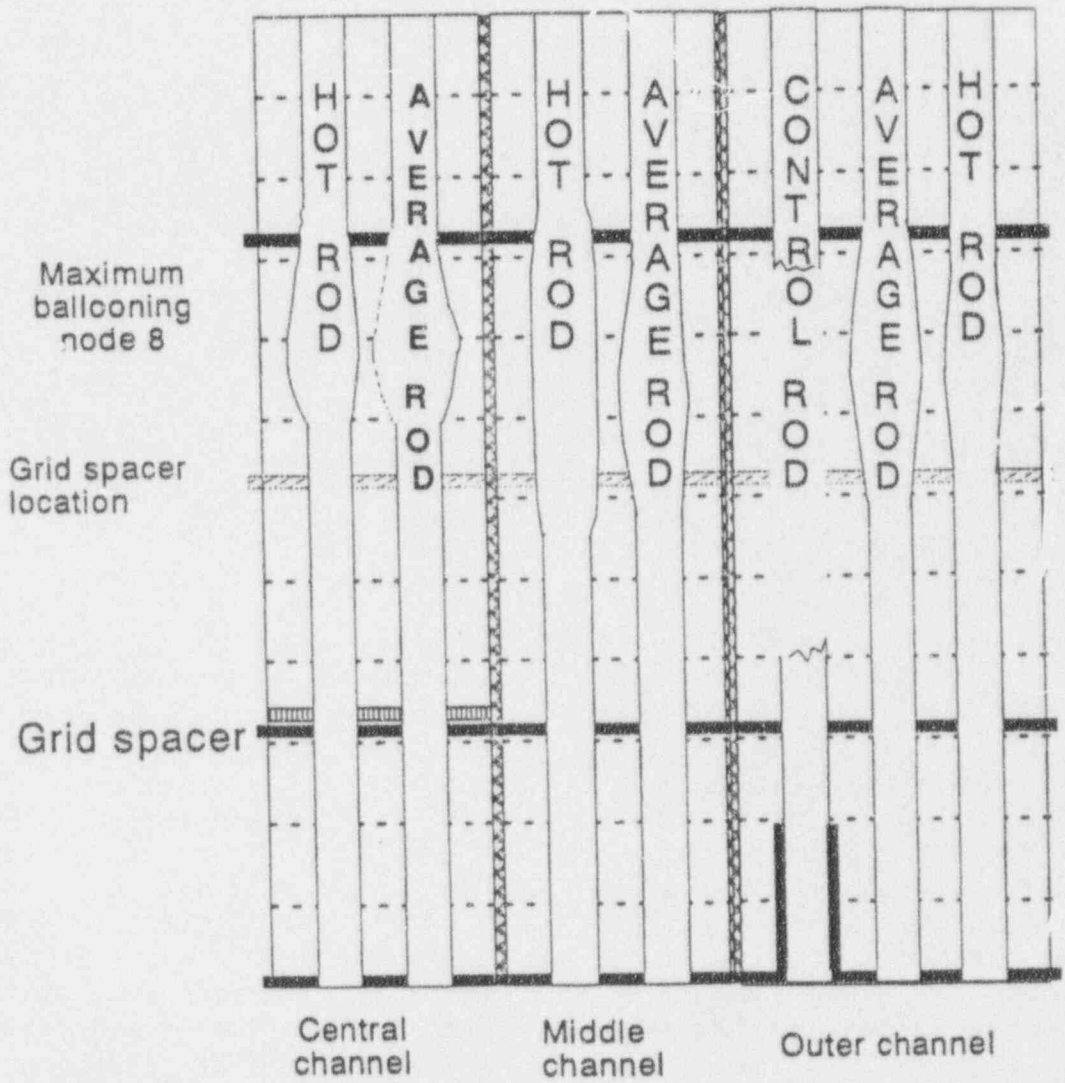

Figure 53. Calculated core end state prior to reflood.

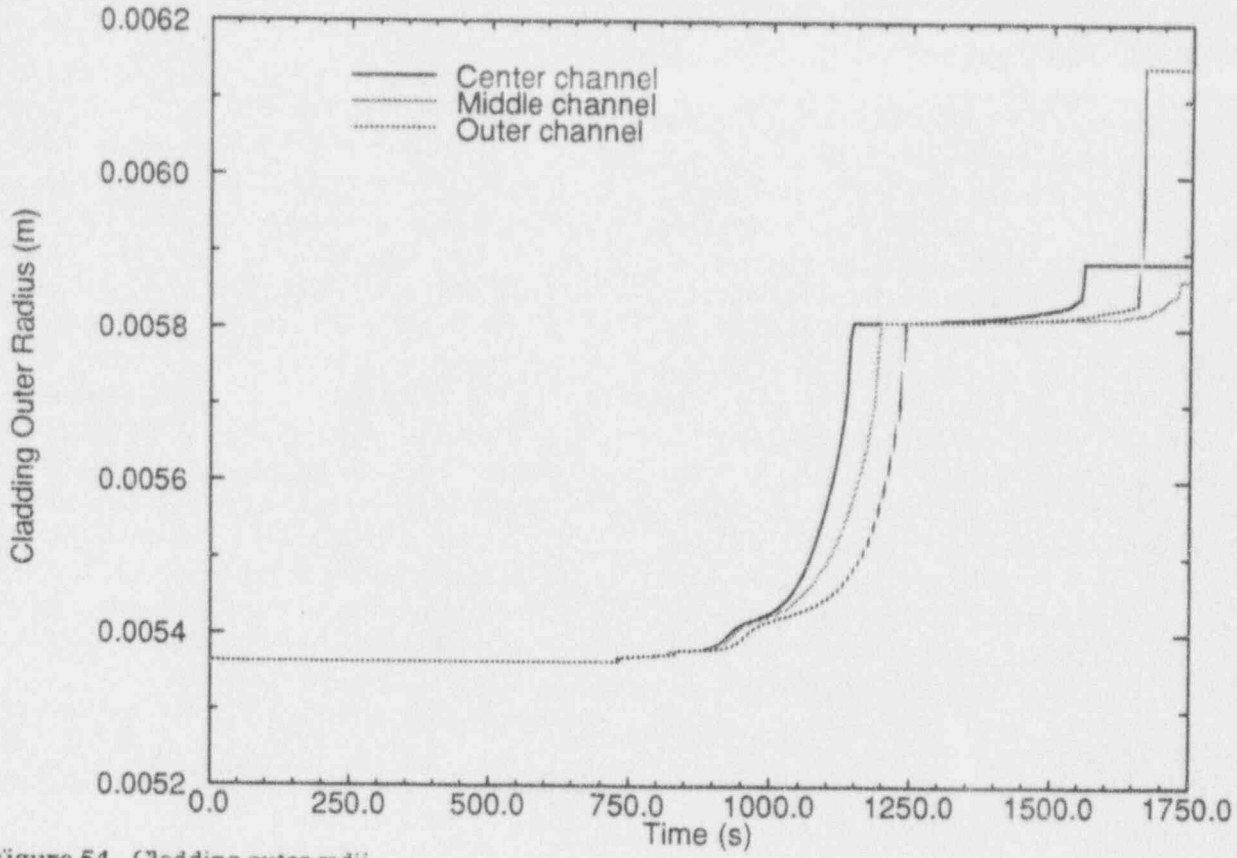

Figure 54. Cladding outer radii.

predicted to occur. This core condition coincides quite well with posttest examination of the bundle, although it does not adequately describe the eutectic formation which is believed to have occurred when molten absorber material was sprayed onto adjacent fuel rods.

Figure 53 also illustrates the predicted control rod damage. As shown, all of the Ag-In-Cd absorber material has melted and voided axial zones five through nine. All experimental data support the theory that the central region of the Ag-In-Cd control rods melted and generated sufficient internal pressure to breach the stainless steel sheath as well as the zircaloy guide tube. The molten absorber material was then sprayed onto adjacent hot fuel rod cladding, causing fuel rod metallic melting by eutectic formation as well as providing a cloud of vaporized absorber material for fission product transport. A significant portion of the absorber material was observed to relocate to the bottom of the fuel module, where it resolidified approximately 0.15 to 0.3 m above the coolant level. Since SCDAP/RELAP5 does not have the capability of modeling the phenomena of absorber material spraying onto adjacent fuel rods, the code predicted that the relocating absorber material would flow down the outside of the guide tube to the bottom of the fuel module and solidify in the volume just above the coolant level. Since RELAP5 predicted the coolant level to be slightly lower than measured, the calculated solidification occurred slightly lower than measured.

The ability of the code to predict fuel rod ballooning and rupture is illustrated in Figure 54, which shows the fuel rod cladding outer radius predicted for each of the three fuel rod groups, each of which were within a separate flow channel in the CFM. Previous analysis (Coryell 1992) has shown that the capability added to SCDAP/RELAP5 to model multiple flow channels within a single enclosure can impact the phenomena observed during the early phases of a

severe accident. If the CFM is modeled as a single hot channel, as has been done in the past, flow diverted by the deforming fuel rods is channeled into the peripheral module, thereby imposing coplanar blockage and overestimating the CFM flow blockage. Now that the radiation enclosure representing the CFM can enclose multiple flow channels, flow diverted by deforming fuel rods in one channel is directed into an adjacent flow channel within the CFM, thereby causing additional cooling in that channel and reducing or delaying the deformation in that channel. This capability also allows the code to model cold wall effects, due to the presence of the cold walls of the shroud. Although no measurements were made of fuel rod cladding deformation, an indirect measure of channel blockage can be inferred by the fact that sufficient coolant flow was maintained through the CFM to maintain zircaloy oxidation.

6.3 Reflood Analysis

One of the objectives of the analysis described here was to examine the ability of the code to model the core damage progression during the reflood phase of the LP-FP-2 Experiment. During the LP-FP-2 Experiment, the CFM experienced an oxidation excursion sufficient to drive fuel rod temperatures above the melting point of ceramic UO_2 (3100 K). It has been estimated that approximately 60% of the zircaloy oxidation/hydrogen production that was experienced during this experiment occurred during the reflood phase of the experiment. This application of SCDAP/RELAP5 to the LP-FP-2 reflood is sufficiently challenging to the code that it has been of significant interest to both code developers and program participants.

Thermal-Hydraulic Response. The ability of SCDAP/RELAP5 Mod3 to model the thermal-hydraulic response of the LOFT system during the reflood phase has dramatically improved since the EASR calculation (Carboneau 1989) was performed. The most significant improvement is the addition of the capability of modeling non-condensables, which occurred in the transition between MOD2.5 and MOD3.

One of the models within earlier versions of SCDAP/RELAP5 which the LP-FP-2 Experiment cast doubt upon was the durability of the oxide shell around the fuel rod cladding. Experimental evidence indicates that the protective oxide shell can experience sufficient stress, particularly during reflood conditions, that the shell spalls and fresh zircaloy surface is exposed to steam. LP-FP-2 measurements indicate that significant fractions of unoxidized zircaloy were exposed to the high-temperature steam atmosphere at the time of reflood. It seems likely that the additional zircaloy was available for oxidation because (a) a portion of the CFM had experienced some degree of steam starvation during the transient phase and (b) additional fresh zircaloy surface was exposed at the time of reflood due to oxide shattering. In the past the code has had no mechanism to expose additional zircaloy at the time of reflood, since the only failure mechanism for the protective oxide shell was that of reaching the oxide failure temperature. A task was undertaken to extend the ability of the code to model reflood by the addition of a model to shatter the oxide shell under reflood conditions [Coryell and Katsma, 1992]. The new model is detecting the conditions necessary to shatter the oxide, and is exposing fresh cladding surface for oxidation during reflood.

Although the new oxide shattering model does correctly predict shattering when reflood reaches the core components, SCDAP/RELAP5 provides sufficient cooling to limit the oxidation excursion, and terminate the transient prior to ceramic melting. This may be caused by inherent assumptions of stability in the heat transfer correlations which are violated by the chaotic conditions of reflood, as is illustrated in Figure 55. This figure illustrates the chaotic flow conditions that exist between 1780 s, when reflood reaches the core, and 1800 seconds, when the flow stabilizes. In order to assess the ability of the code to model the oxidation excursion, an input option to shatter all in-core oxide upon reflood initiation was used. The maximum cladding thermal response to this

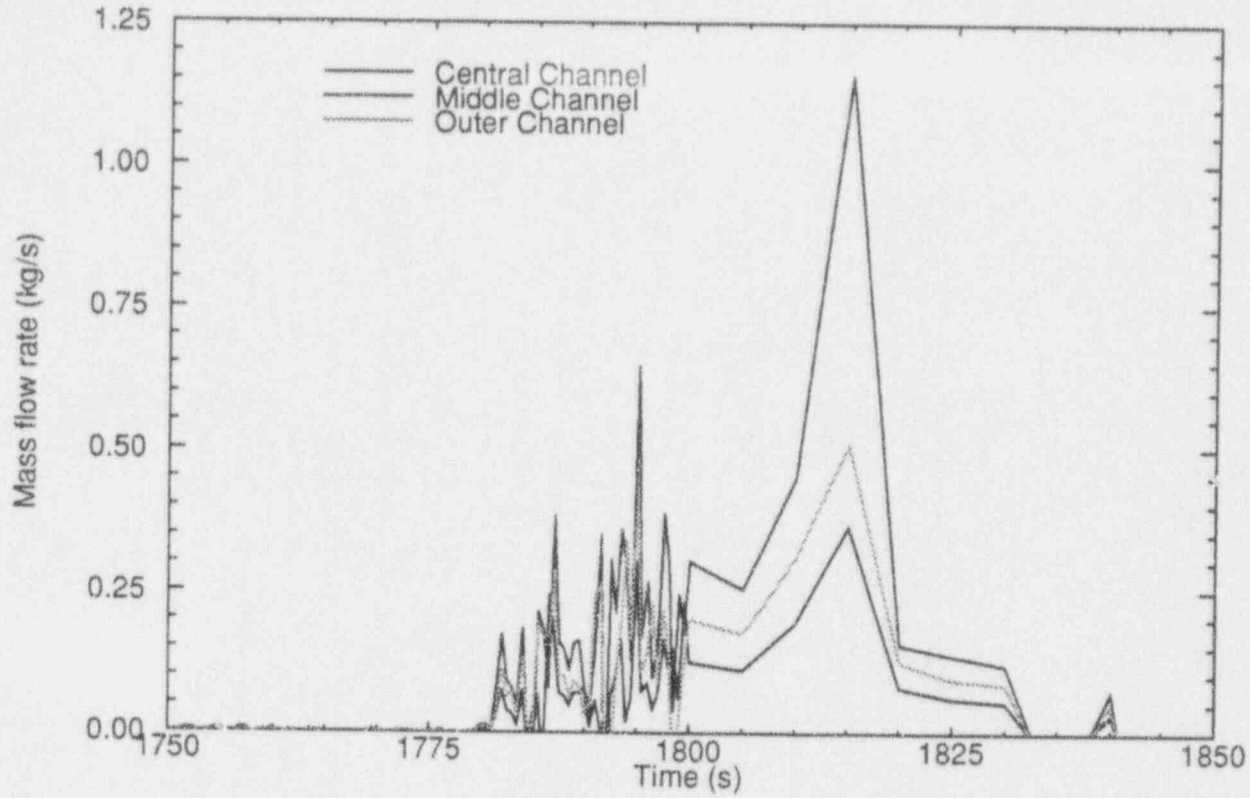

Figure 55. Center fuel module flow rate during reflood oxidation.

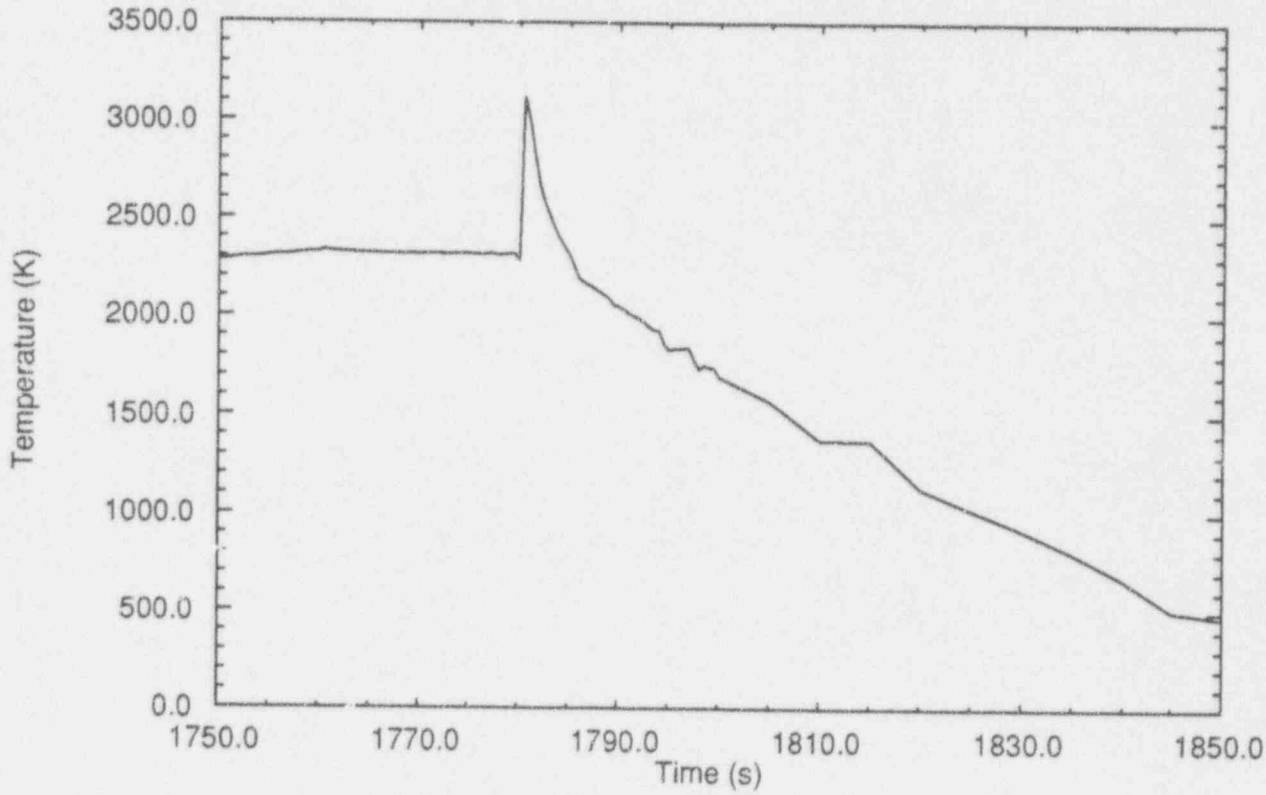

Figure 56. Component 1 cladding temperature response during reflood.

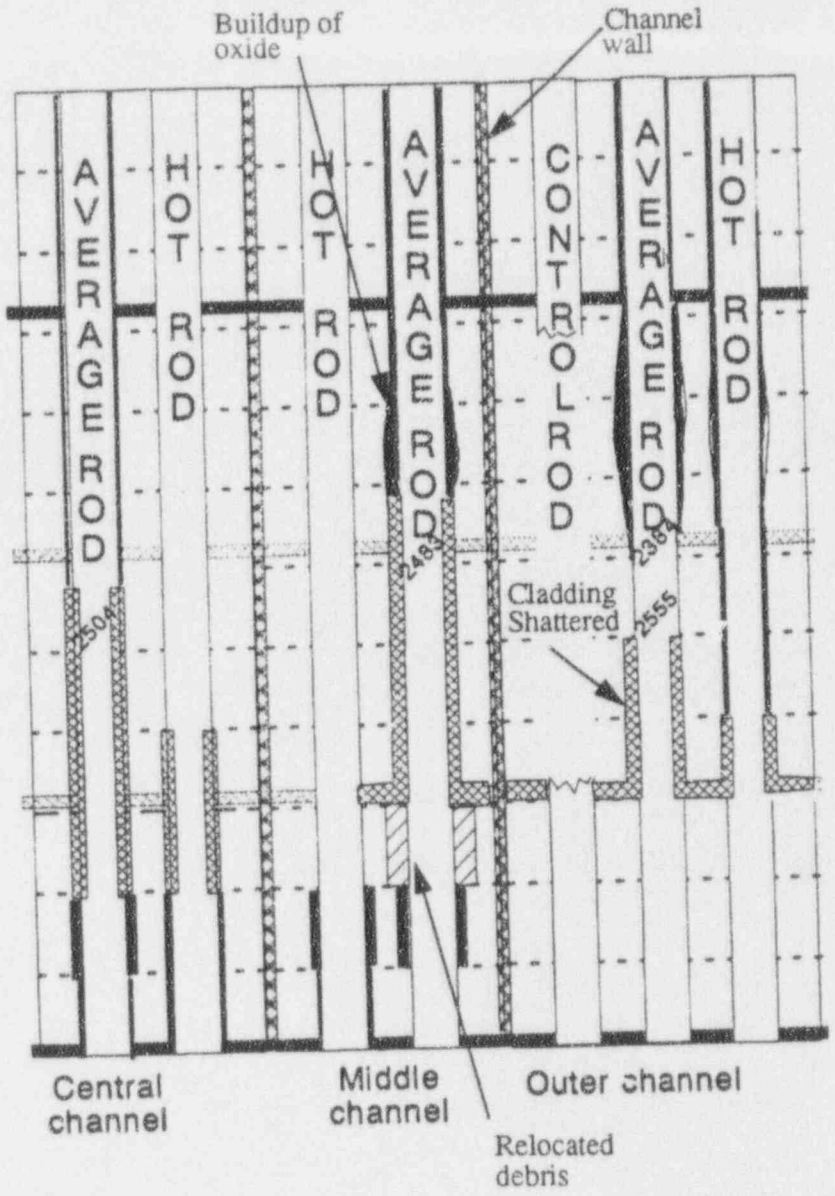

Figure 57. Core condition after reflood.

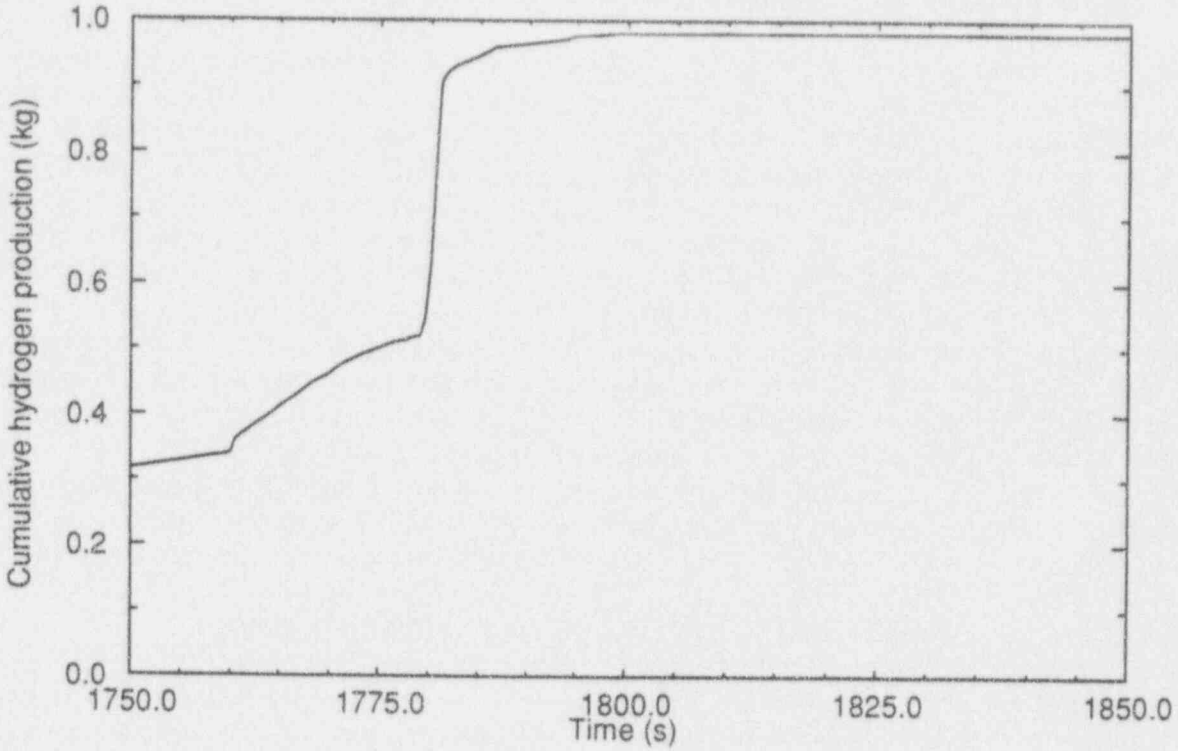

Figure 58. Cumulative hydrogen production during reflood.

oxidation excursion is shown in Figure 56, which shows the reflood response of Component 1 at the 42 inch elevation. As reflood exposes fresh zircaloy an oxidation excursion begins which drives the fuel rod to melting, at which point the oxidation calculation is terminated.

Reflood Damage Progression. Figure 57 shows the condition of the core after reflood. As illustrated by this figure, there has been some fuel rod melting and fragmentation, with a subsequent relocation and resolidification into a porous debris bed in node three at the center of the fuel module, and node four at the outer edge of the module. All fuel rods above this location are predicted to have fragmented during reflood, forming a rubble debris bed.

The code prediction of hydrogen production during reflood is shown in Figure 58. As shown in this figure the cumulative hydrogen production predicted for this analysis is approximately 980 g. Although slightly low, this value is within the uncertainty of the total hydrogen production for this experiment, estimated to be 1024 ± 364 g.

6.4 Assessment of SCDAP/RELAP5

The analyses of severe accident transients continues to be dominated by uncertainties in the thermal-hydraulic conditions. The ability of SCDAP/RELAP5/MOD3 to predict core temperatures remains as reliable as that experienced by SCDAP/RELAP5/MOD2.5, provided the thermal-hydraulic boundary conditions are realistic. The mechanics of heat conduction and oxidation are handled in a manner that produces results within the uncertainties encountered during the LP-FP-2 Experiment. Each core damage phenomena observed during the transient portion of the experiment was triggered within the correct temperature range with the possible exception of the onset of rapid oxidation. The codes late

prediction of this onset may be just an artifact of the LOFT thermocouple effect, which would not be applicable to uninstrumented fuel rods. Transient thermal results tracked observed phenomena quite well, with the exception of phenomena related to the eutectic interaction between control rod absorber material and zircaloy. The lack of a model examining the interaction between Ag and zircaloy has not significantly impacted the prediction of temperatures but would significantly impact any fission product transport analysis. The impact on fission product transport is significant because a cloud of vaporized control rod material would be created at the same time and location as massive cladding disruption, causing significant interaction between iodine and the vaporized absorber material.

The ability of SCDAP/RELAP5/MOD3 to model hydrogen production and transport has improved since MOD2.5, although this phenomenon is highly dependent on the reliability of the hydraulic prediction. SCDAP/RELAP5/MOD3 has accurately predicted core damage progression within the limits of the hydraulic calculation for this analysis. The onset of cladding deformation and its subsequent failure appear to be predicted within reasonable uncertainty. As previously mentioned, the lack of a model to examine the potential for spraying molten control rod absorber material onto adjacent rods will cause the code to underpredict the amount of zircaloy eutectic formation, prior to melting, but appears to impact only the fission product transport analysis in the LP-FP-2 analysis.

One of the objectives of this task was to perform an assessment of the ability of SCDAP/RELAP5/MOD3 to examine core damage progression during the reflood portion of the LP-FP-2 Experiment. The hydrodynamic portion of the code has made significant advances in modeling the thermal and hydraulic response of a reactor to reflood conditions, although the heat transfer conditions during the chaotic reflood phase are not well understood. It should also be noted, that difficulties are still encountered when non-condensable quality approaches unity. The model for the shattering of the cladding oxide upon reflood does appear to be working correctly, and can provide an oxidation excursion. There is insufficient experimental data to determine if the oxidation excursions are typical of the physical response, but the integral measurements, such as hydrogen production and debris formation, appear to match experimental quantities within the experimental uncertainty.

6.5 Conclusions

The ability of the SCDAP/RELAP5 code to model both the transient and reflood phases of the LP-FP-2 transient has improved dramatically over the years since the experiment was performed. It now seems likely that if the input model can provide reasonably realistic boundary conditions, the severe accident models within SCDAP/RELAP5 are capable of yielding best-estimate results, without resorting to the use of user-specified input parameters which may lie outside the defensible range of the parameters. The uncertainty in the LP-FP-2 transient analysis is dominated by uncertainties in the thermal-hydraulic response of the primary coolant system (PCS), and the greatest uncertainty remains the experimental uncertainties, such as the break flow. A lack of instrumentation on the most significant break flow path, the intact loop cold leg break line, has led to the necessity for parametric studies of break flow resistance.

7. RELATIONSHIP TO SEVERE ACCIDENT DATA BASE

This section discusses how the LP-FP-2 Experimental results relate to those obtained in other severe fuel damage experiments and through analysis to the damaged TMI-2 reactor core.

7.1 The Relationship of LP-FP-2 Test Results to Other Severe Accident Data

The accident at TMI-2 stimulated research to understand how such severe accidents progress, how to mitigate their consequences, and how to terminate them. Of central importance in addressing the above concerns is the behavior of the fuel and fission products during an accident. The LP-FP-2 Experiment was the last of several integral in-pile experiments conducted at the INEL to investigate severe accident phenomena.

This section summarizes results from the LP-FP-2 Experiment that are important to understanding severe accident phenomena and provides a consistent interpretation with results obtained in the severe fuel damage (SFD) test series carried out in the Power Burst Facility (PBF) at the INEL and results from the examination of the damaged core of the TMI-2 reactor. Melt progression, the effect of spacer grids, energy and hydrogen generation upon reflood, damage to core support structures, fission product transport and deposition, and the retention of fission products in high-temperature melts are considered.

Experimental Conditions. Information on the scale and experiment/accident conditions among the LOFT LP-FP-2 Experiment (Carboneau et al. 1989; Jensen et al. 1989), the PBF-SFD tests (Knipe et al. 1986; Martinson et al. 1986; Martinson et al. 1989; Petti et al. 1989; Osetek 1987), and the TMI-2 accident (Broughton et al. 1989) presented in Table 1? indicates that the LP-FP-2 Experiment has much in common with the TMI-2 accident; namely, decay heating, reflooding, excess steaming rate, control materials, and low burnup. Differences include the lower system pressure and much smaller scale of the LP-FP-2 Experiment relative to the TMI-2 accident. The SFD-ST test shares the method of cooldown (reflooding) and an excess steam supply rate (incoming steam not totally converted to hydrogen by reaction with zircaloy in the bundle) with the LP-FP-2 Experiment and the TMI-2 accident. All the experiments listed in Table 1?, as well as the TMI-2 reactor, contained Inconel spacer grids. The SFD experiments were conducted at a system pressure (6.9 MPa) within the range of pressures measured in the TMI-2 accident (5 to 15 MPa) and greater than the pressure during bundle heatup and damage in the LP-FP-2 Experiment (1.1 MPa). Two of the SFD experiments utilized fresh fuel irradiated to only trace levels to produce measurable quantities of short-lived fission products prior to the transient, and two contained fuel rods previously irradiated to high exposures (30 GWd/tU). All four SFD experiments were heated by fissioning (fission power from the driver core), as opposed to decay heat in LP-FP-2 and the TMI-2 accident. Three of the SFD tests were terminated with a slow, power-controlled cooldown. The cooldown in Test SFD 1-1 was with steam, whereas in Tests SFD 1-3 and SFD 1-4 it was with argon. One SFD experiment, SFD 1-4, contained Ag-In-Cd control materials; but the coolant in this experiment did not contain the H_3BO_3 present in the LP-FP-2 Experiment and the TMI-2 accident. Due to the central location of the test bundle in the LOFT core, the bypass flow area relative to the flow area within the bundle was much larger in the LP-FP-2 Experiment (80%) than in TMI-2 (1.5%) and the PBF-SFD tests (0.5%). Although small relative to the TMI-2 core, the LP-FP-2 bundle was considerably larger in scale than the SFD tests. The two SFD tests of particular interest for comparison with LP-FP-2 and TMI-2 are SFD-ST (reflooded) and SFD 1-4 (contained Ag-In-Cd control rods).

Relationship to Studies in PBF and TMI-2. The damage zones produced in the LP-FP-2

Table 13. Experiment/accident conditions and scales.

Attribute	SFD-ST	SFD 1-1	SFD 1-3	SFD 1-4	LP-FP-2	TMI-2
Geometry						
Number of rods	32	32	32	32	121	39,825
Rod length (m)	0.91	0.91	0.91	0.91	1.87	4.0
Bypass (%)	0.5	0.5	0.5	0.5	80	1.5
Heating method	Fission	Fission	Fission	Fission	Decay	Decay
Cooldown method	Reflood	Slow	Slow	Slow	Reflood	Reflood
Steaming rate	Excess	Limited	Limited	Limited	Excess	Excess
Pressure (MPa)	6.9	6.8	6.85/4.7	6.95	1.1	5-15
Fuel burnup (GWd/tU)	Trace	Trace	30	30	0.45	3
Control rod material	None	None	None	Ag-In-Cd	Ag-In-Cd + H_3BO_3	Ag-In-Cd + H_3BO_3
Spacer grids	Inconel	Inconel	Inconel	Inconel	Inconel	Inconel
Time above 2100 K (s)	750	315	1000	1425	270	3600

CFM are very similar to those produced in the PBF-SFD tests and in the TMI-2 core despite quite large differences in scale, system pressure, steam supply, water elevation in the vessel, bypass flow area, fuel burnup, duration of transient, method of heating, and method of transient termination. In Tests SFD-ST, SFD 1-4, LP-FP-2, and the TMI-2 accident, a metallic blockage formed at the lower spacer grid, a ceramic blockage occurred above the lower blockage, and a rubble bed of fuel fragments rested on top of the ceramic blockage. In the PBF-SFD tests and in the TMI-2 accident, the lower metallic blockages occurred near the level of the coolant. However, in the LP-FP-2 Experiment, the water level was below the fuel bundle; and the metallic blockage occurred well above the water level in a region where the temperature was less than the solidification temperature of the relocating melt.

The ceramic blockages in the PBF-SFD tests and the LP-FP-2 test appear to be precursors of the large ceramic molten pool that formed in the TMI-2 accident. The additional time at temperature in the accident evidently contributed to the larger mass (about 45% of the core) of ceramic melt in the TMI-2 reactor vessel. The rubble beds of fuel fragments above the ceramic melt formed with either excess or limited steam supply conditions and with either reflooding or slow power reduction methods of transient termination. The common factor appears to be the loss of restraint of the fuel due to the melting and relocation of its zircaloy cladding.

The particle size distribution in the rubble is set primarily by the crack distribution within fuel stacks in the fuel rods prior to the transient. Cracks in the fuel pellets develop as a result of thermal stresses in the fuel pellets during power changes in the reactor, particularly during reactor start-ups and shutdowns. The largest fragments (about 2 mm) occurred in the SFD-ST test as a result of a minimum of power cycling and a slow heatup in a steam-rich environment. The minimum power cycling produced relatively coarse crack patterns, and the slow heatup enhanced oxidation prior to zircaloy melting and resulted in oxygen-rich zircaloy melts that were wet and thereby tended to glue fragments together. In the TMI-2 core, the debris bed consisted of fuel fragments that were mainly about 1 mm in size. The particle sizes in the loose rubble in the SFD 1-4 and LP-FP-2 Experiments were intermediate between the above two cases.

The metallic blockages in SFD-ST, SFD 1-4, LP-FP-2, and TMI-2 occurred at the lowest spacer grid. An analysis of the influence of spacer grids on trapping relocating debris indicates that if the spacer grid is at a temperature below the solidification point of the relocating melt, it can strongly influence trapping of the debris (Gasser et al. 1990). The spacer grid provides an increased mass for heat transfer (80% of that of the fuel rod cladding), an increased surface area for heat transfer (220% of that of the fuel rod cladding), and a decreased cross-sectional flow area. (The largest diameter of a drop that can pass without impacting a solid surface is 3 mm with a spacer grid versus 8 mm without.)

Despite the large flow blockages of the LP-FP-2 bundle and the large bypass available for steam flow, extensive oxidation of zircaloy occurred. The bypass flow around the LOFT CFM was 80%, compared to a bypass flow of 1.5% for TMI-2 and 0.5% for PBF; yet the zircaloy oxidation (58%) was comparable to other experiments (64% in SFD-ST and 32% in SFD 1-4) and to the TMI-2 accident (50%). Thus, the LP-FP-2 Experiment is confirmation of observations made from earlier experiments that flow blockages do not prevent continued zircaloy oxidation and hydrogen production (Cronenberg et al. 1989).

The production of energy and hydrogen during reflood of a damaged fuel bundle or core is not unique to the LP-FP-2 Experiment. An analysis of the increase in system pressure measured during the B-loop pump transient in the TMI-2 accident and the associated energetics suggests that up to 32% of the hydrogen generated in the accident may have been produced during this event (Kuan et al. 1989). Hydrogen peaks following reflood have also

been measured during SFD-ST and in the CORA (Hagen et al. 1989) out-of-pile severe fuel damage test (in which a temperature excursion was also measured).

As in the case of LP-FP-2, localized damage occurred to structures immediately above the fueled region in the TMI-2 accident. The stainless steel upper core support plate sustained localized melting and foaming oxidation. An assessment of possible mechanisms and the energetics associated with the damage to the upper core support plate in the TMI-2 core suggests that the damage likely occurred during the B-loop pump transient as a result of high-temperature steam and hydrogen generated by zircaloy-steam reaction (Kuan et al. 1989).

Because the fission product release pathway in the TMI-2 accident was through water and, in addition, the reactor was reflooded, little information on fission product deposition in the RCS is available. Also, quantitative measurement of total fission product deposition on the deposition rod (simulated plenum surfaces) in the SFD 1-4 test was unreliable. However, quantitative measurement of fission product deposition was made in the LP-FP-2 Experiment with deposition coupons that were protected from wash-off during reflood and within the LPIS line that was closed off prior to reflood. The fission product deposition measured in the upper plenum of the LOFT reactor was considerable (~65%) for I and Cs, where the residence time was about 7 seconds and surface temperatures were about 650 K, but was much less in the LPIS line (10-27%), where the residence time was only 0.2 seconds and wall temperatures were about 520 K.

The formation of AgI in the LP-FP-2 Experiment was not unexpected based on thermodynamic considerations (Hahn and Acree 1984), the burst mode of control rod failure at low system pressure (Petti 1989a), and the low fuel burnup. No other integral-effects in-pile experiments have generated these conditions, so the LP-FP-2 Experiment is unique in having confirmed the theoretical expectations for the formation of AgI as a dominant chemical form of I under specific conditions.

The general features of fission product retention in ceramic melts are common to the SFD 1-4 experiment, the LP-FP-2 Experiment, and the TMI-2 accident (Hobbins et al. 1991). Sr and Ce are stable as low-volatility oxides soluble in the ceramic melt and are understandably present at large fractions of inventory levels. Other medium- and low-volatility fission products (Sb and Ru) are largely absent from the ceramic melt phase, but are found concentrated in metallic phases within the melt. Small, but significant, amounts (2% - 15%) of the volatile fission products I and Cs remain in the ceramic melts.

Summary and Conclusions. The LP-FP-2 Experiment extended severe accident experience into the realm of a large-break LOCA and permitted measurements of core melt progression phenomena under low system pressure in a decay-heated bundle and fission product transport through a scaled upper plenum and a simulated LPIS line. The principal damage zones observed under small-break LOCA boiloff conditions in PBF-SFD tests and in the TMI-2 accident were confirmed under large- break LOCA blowdown conditions in the LOFT LP-FP-2 Experiment. A coolant level within the core is not necessary for the formation of blockages within the core due to the solidification of relocating melts. As in previous experiments and the TMI-2 accident, spacer grids were found to collect relocating debris and act as preferential sites for the formation of flow blockages. The LP-FP-2 Experiment, having a much larger bypass flow than previous experiments or the TMI-2 core, provided excellent confirmation of the inability of flow blockages to prevent continued zircaloy oxidation and hydrogen production in a core melt accident.

As in the TMI-2 accident, considerable energy and hydrogen were produced during the reflood in the LP-FP-2 Experiment. Hydrogen generation upon reflood has been measured in the SFD-ST test and in the CORA-12 test in

which a temperature excursion as a result of reflood was also measured. The energy produced in the LP-FP-2 CFM during reflood caused melting within the bundle, and the hot effluent gases caused localized melting and foaming oxidation of the stainless steel tie plate directly above the fuel bundle. The narrow axial zone of stainless steel damage above the fueled region in LP-FP-2 is comparable to the localized melting and foaming oxidation in upper end boxes and the upper core support plate in the TMI-2 reactor. This evidence suggests that energy produced by steam oxidation during reflood is deposited within the fueled region and within a narrow axial region above the fuel.

The LP-FP-2 Experiment demonstrates that fission product deposition can be significant where temperature and flow conditions permit, as was the case in the LOFT upper plenum. However, when residence times are very short, as in the case of the LPIS line, deposition is minimal. Iodine behaves as AgI in the LP-FP-2 Experiment and confirms theoretical predictions for the specific conditions (low system pressure and low fuel burnup) that prevailed in this experiment. Cesium behaves as CsOH rather than $CsBO_2$ even though H_3BO_3 was present in the coolant. The retention of fission products in melts in the LP-FP-2 Experiment is consistent with results from the SFD 1-4 test and the TMI-2 accident and confirms that small, but significant, amounts of I and Cs are retained.

8. CONCLUSIONS

The LP-FP-2 experiment provided information on the release, transport, and deposition of fission products and aerosols during a V-sequence large-break LOCA accident scenario that resulted in severe core damage. The following are the most significant conclusions derived from posttest analysis:

8.1 Core Damage Progression

- All measurements, observations, and analyses of the LP-FP-2 data indicate that most of the CFM damage occurred during the reflood phase of the experiment.
- The highest temperatures in the CFM (> 3120 K) were reached during reflood and were caused by rapid metal-water reaction.

8.2 Distribution of Fuel and Control Materials

- The stratification of material in LP-FP-2 was similar to that observed in TMI-2 and the SFD series of experiments in PBF; i.e., metallic melts, ceramic melts, and a debris bed were formed.
- The presence of spacer grids impeded material relocation, resulting in the greatest flow blockages.
- Upward material relocation to the upper end box region occurred during reflood.
- Approximately 15% of the fuel and 63% of the zircaloy cladding and liner were liquefied.
- Approximately 70% of the control rod alloy (Ag-In-Cd) was released to the fuel bundle.
- The large amount of silver detected in the upper plenum suggests that the control rods failed by overpressure and sprayed silver onto adjacent rods.

8.3 Hydrogen Production

- Approximately 205 g of hydrogen were detected in the BST; and 819 g are estimated to have been trapped in the PCS. The total amount of released hydrogen was ~1024 g, which is equivalent to an oxidation of 58% of the CFM. This estimate agrees with that determined by PIE.
- Most of the 1024 g of hydrogen released during the experiment are believed to have been released during reflood.
- The distribution of hydrogen is similar to the noble gas distribution; i.e., 20% of the hydrogen and 18% of the noble gases were found in the BST; and 80% of the hydrogen and 82% of the noble gases were found in the PCS.

8.4 Fission Product Behavior

- The primary fission product chemical species were AgI and CsOH.
- The major release of fission products occurred during reflood.
- The BST fission product inventory accounted for 2% of the krypton; 1.7% of the xenon; 1% of the iodine; and 0.23% of the cesium detected. The release fractions to the PCS following reflood were 9% for xenon and krypton; 13% for iodine; and 16% for cesium.
- The primary reason for the small transient release fractions is probably due to the initially large grain structure of the fuel (approximately 14 μm) and the limited fuel temperatures (< 2700 K).

8.5 SCDAP/RELAP5 Code Comparisons

- SCDAP/RELAP5 MOD3 is now able to predict the behavior of the facility during the reflood phase, although the code still predicts far too much cooling during the core quench. However, the code is capable of predicting the renewed heating and melting, changes in geometry, and dramatic increases in hydrogen production.
- SCDAP/RELAP5 MOD3 modeled key components of the transient phase of the experiment well.
- Although the dryout times and heatup of the CFM are impacted by the uncertainties in break flow, the calculated and observed behavior appear to be within the experimental uncertainties of the measurements and test thermal-hydraulic boundary conditions. Default values were used for all damage progression models.Reflood significantly increased core damage.

8.6 The Relationship of LP-FP-2 Test Results to Other Severe Accident Data

- The principal damage zones observed under small-break LOCA boiloff conditions in the PBF SFD tests and in the TMI-2 accident were confirmed under large-break LOCA blowdown conditions.
- The LP-FP-2 experiment provided excellent confirmation of the inability of flow blockages to prevent continued zircaloy oxidation and hydrogen production in a core melt accident.
- Fission product deposition can be significant where temperature and flow conditions permit; however, when residence times are very short, deposition is minimal. The retention of fission products in melts is consistent with results from the SFD 1-4 test and the TMI-2 accident and confirms that small, but significant, amounts of iodine and cesium are retained.

9. BIBLIOGRAPHY

Adams, J.P., et al, *1985, Quick-Look Report on OECD LOFT Experiment LP-FP-2*, OECD LOFT-T-3804, September 1984.

Allison, C.M, et al, 1993, SCDAP/RELAP5 Code Manual, Volumes I - V, NUREG/CR-6150, December 1993.

Bowsher, B. R. and S. Dickinson, 1986, *The Interaction of Cesium Iodide With Boric Acid: Vapor Phase and Vapor-Condensed Phase Relationships*, AEEW-R2102, May 1986.

Broughton, J. M., et al., 1989, "A Scenario of the Three Mile Island Unit 2 Accident," *Nuclear Technology, 87*, 34, 1989.

Carboneau, M. L. et al., *1987, OECD LOFT Fission Product Experiment LP-FP-2 Data Report*, OECD LOFT-T-3805, May 1987.

Carboneau, M. L., V. T. Berta, and M. S. Modro, 1989, *Experiment Analysis and Summary Report for OECD LOFT Project Fission Product Experiment LP-FP-2*, OECD LOFT-T-3806, June 1989.

Carboneau, M. L., 1990, "Highlights of the OECD LOFT LP-FP-2 Experiment, Including Hydrogen Generation, Fission Product Chemistry, and Transient Fission Product Release Fractions," *Proceedings of an Open Forum Sponsored by the OECD Nuclear Energy Agency with the Support of the OECD/LOFT Spanish Consortium, Madrid, Spain, May 9 - 11, 1990.*

Coryell, E.W. and K.R. Katsma, 1992, *Design Report: Modifications to Examine the Influence of Cold Wall Effects on Core Damage Progression*, EGG-SSRE-10221, April 1992.

Coryell, E.W., et al, 1992, *Design Report: SCDAP/RELAP5 Reflood Oxidation Model*, EGG-RAAM-10307, October, 1992.

Cronenberg, A. W., et al., 1989, "Severe Accident Zircaloy Oxidation/Hydrogen Generation Behavior Noted from In-Pile Test Data," *Proceedings Seventeenth Water Reactor Safety Information Meeting, Rockville, Maryland, October 22-25, 1989.*

Guntay, S., et al., 1991, *A Post Test Analysis of the OECD LOFT Experiment LP-FP-2 Using the Computer Programs SCDAP/RELAP5, TRAP-MELT2.2, and PULSE*, PSI-Bericht Nr. 95, April 1991.

Gasser, R. D., et al., 1990, *Damaged Fuel Relocation Experiment DF-1: Results and Analyses*, NUREG/CR-4668, SAND86-1030, January 1990.

Hagen, S., et al., 1989, "Results of the CORA Experiments on Severe Fuel Damage with and without Absorber Material," *National Heat Transfer Conference, Philadelphia, Pennsylvania, August 6-9, 1989*, AIChE Symposium Series 269, Vol. 85, 1989.

Hahn, R. and H. J. Ache, 1984, "Thermodynamical Calculations on the Behavior of Gaseous Iodine Species Following a Hypothetical Severe Light Water Reactor Accident," *Nuclear Technology, 67*, 407, 1984.

Hobbins, R. R., et al, 1990, "Review of Experimental Results on LWR Core Melt Progression", *Proceedings Eighteenth Water Reactor Safety information Meeting, Rockville, Maryland, October 22-24, Vol. 2, 1990.*

Hobbins, R. R. and G. D. McPherson, 1990, "A Summary of Results from the LOFT LP-FP-2 Test and Their Relationship to Other Studies at the Power Burst Facility and of the Three Mile Island Unit 2 Accident," *Proceedings of an Open Forum Sponsored by the OECD Nuclear Energy Agency with the Support of the OECD/LOFT Spanish Consortium, Madrid, Spain, May 9 - 11, 1990.*

Hofmann, P., et al., 1988, "Reactor Core Materials Interactions at Very High Temperatures," *Topical Meeting on the TMI-2 Accident Materials Behavior and Plant Recovery Technology, Washington, D.C., October 31 - November 4, 1988.*

Jensen, S. M., D. W. Akers, B. A. Pregger, 1989, *Postirradiation Examination Data and Analyses for OECD LOFT Fission Product Experiment LP-FP-2*, OECD LOFT-T-3810, Vol. 1, December 1989.

Jensen, S. M. and D. W. Akers, "Postirradiation Examination Results from the LP-FP-2 Center Fuel Module," 1990, *Proceedings of an Open Forum Sponsored by the OECD Nuclear Energy Agency with the Support of the OECD/LOFT Spanish Consortium, Madrid, Spain, May 9 - 11, 1990.*

Knipe, A. D., S. A. Ploger, D. J. Osetek, 1986, *PBF Severe Fuel Damage Scoping Test - Test Results Report*, NUREG/CR-4683, EGG-2413, March 1986.

Kuan, P., J. L. Anderson, E. L. Tolman, 1989, "Thermal Interactions During the Three Mile Island Unit 2 2-B Coolant Pump Transient," *Nuclear Technology, 87*, 977, 1989.

Martinson, Z. R., D. A. Petti, B. A. Cook, 1986, *PBF Severe Fuel Damage Test 1-1 Test Results Report*, NUREG/CR-4684, EGG-2463, Vol. 1, October 1986.

Martinson, Z. R., et al., 1989, *PBF Severe Fuel Damage Test 1-3 Test Results Report*, NUREG/CR-5354, EGG-2565, October 1989.

Modro, S. M. and M. L. Carboneau, 1990, "The Severe Fuel Damage Scenario. Discussion of the Relative Influence of the Transient and Reflood Phase in Affecting the Final Condition of the Bundle," *Proceedings of an Open Forum Sponsored by the OECD Nuclear Energy Agency with the Support of the OECD/LOFT Spanish Consortium, Madrid, Spain, May 9 - 11, 1990.*

Osetek, D. J., 1987, "Results of the Four PBF Severe Fuel Damage Tests," *Proceedings Fifteenth Water Reactor Safety Information Meeting, Gaithersburg, Maryland, October 26-30, 1987*, NUREG/CP-0090, 1987.

Petti, D. A. et al., 1989, *Power Burst Facility (PBF) Severe Fuel Damage Test 1-4 Test Results Report*, NUREG/CR-5163, EGG-2542, April1989.

Petti, D. A., 1989a, "Silver-Indium-Cadmium Control Rod Behavior in Severe Reactor Accidents," *Nuclear Technology, 84*, 128, 1989

Appendix A
The LOFT Facility

Appendix A

The LOFT Facility

A-1. Facility Description

The LOFT experimental facility was a 50 MW(t), volumetrically scaled, pressurized water reactor (PWR) system. The LOFT facility was designed to study the engineered safety features (ESF) in commercial PWR systems as to their response to the postulated loss-of-coolant accident (LOCA). With recognition of the differences in commercial PWR designs and inherent distortions in reduced scale systems, the design objective for the LOFT facility was to produce the significant thermal-hydraulic phenomena that would occur in commercial PWR systems in the same sequence and with approximately the same time frames and magnitudes. Experiments conducted in the LOFT facility provided "integral" system data for assessment of analytical licensing techniques and for identification of unexpected thresholds or events that may occur during a LOCA. The term integral implies that the entire system is modeled and the entire LOCA sequence is carried out as opposed to separate effects tests in which specific phenomena, components or single systems are studied during a particular phase of the LOCA.

Figure A-1 shows the LOFT facility in comparison with the ZION commercial nuclear reactor and the Semiscale experimental facility.

The LOFT facility was also intended for experiments and acquisition of data on operational transients that may occur in a commercial or generic reactor. Such transients as loss of feedwater, loss of primary coolant flow,

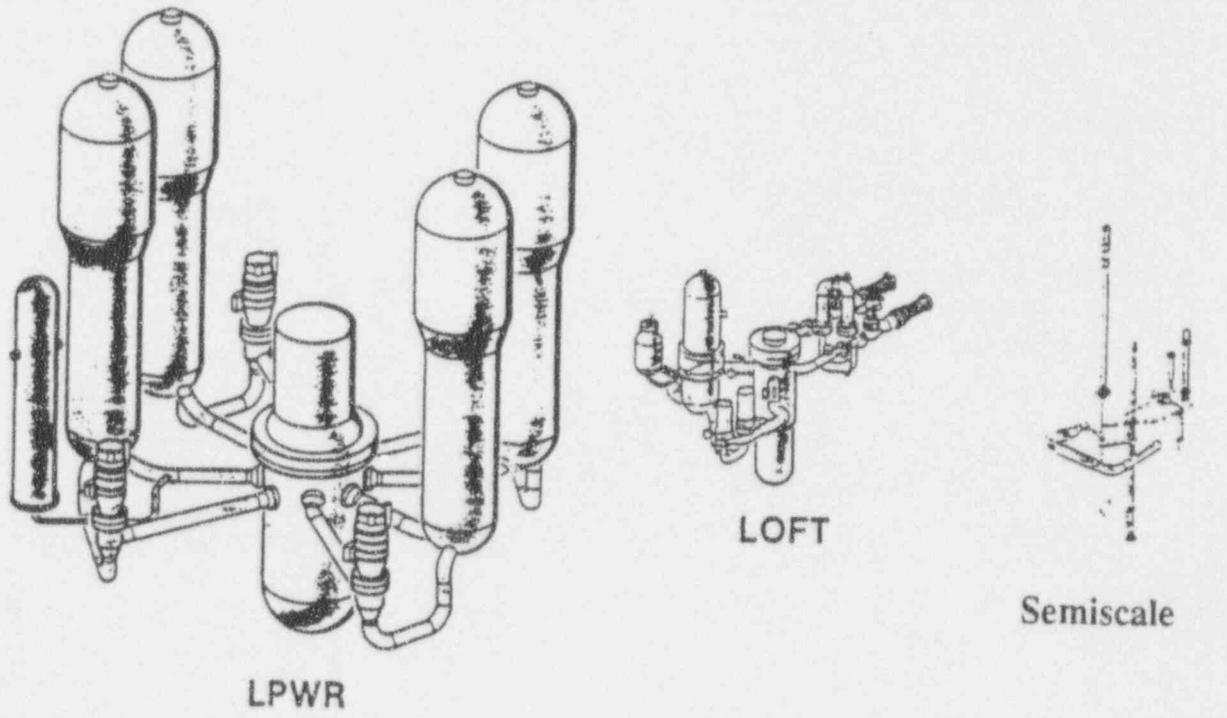

Figure A-1. Scale comparison of LOFT facility.

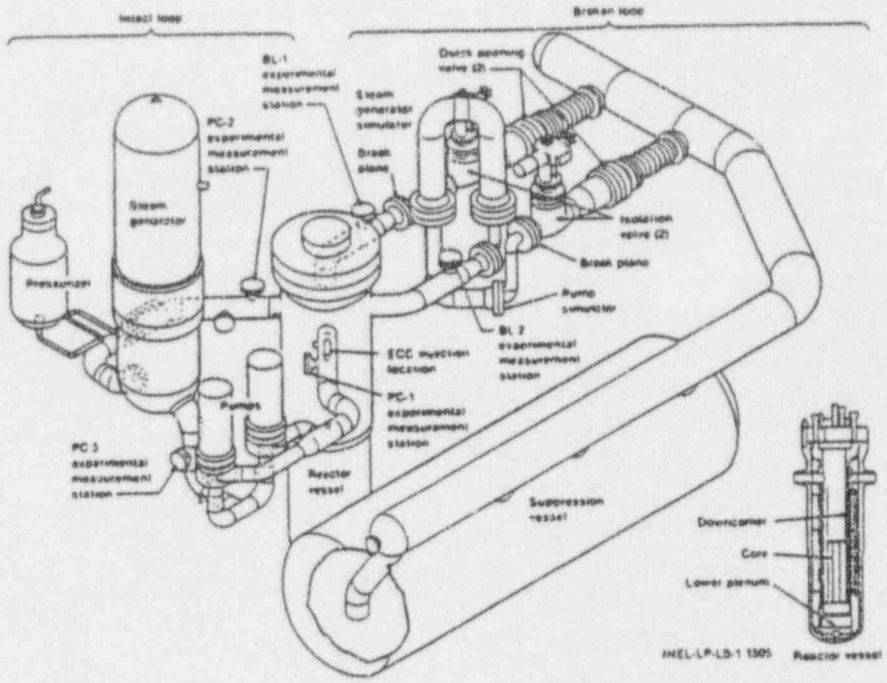

Figure A-2. Axonometric projection of the LOFT system.

and loss of steam load may lead to pressure relief valve setpoints being exceeded. Relief valves then actuate and vent primary system coolant. Improper relief valve operation can lead to loss-of-coolant transients as occurred at Three Mile Island.

The LOFT Experimental Facility shown in Figure A-2 is described in detail in Reference A-1. The facility consisted of five major systems:

1. Primary Coolant System.
2. The Reactor System that contained the 1.68-m high nuclear core.
3. Blowdown Suppression System.
4. Emergency Core Cooling System.
5. Secondary Coolant System.

These systems were instrumented extensively to measure the system parameters.

The LOFT Primary Coolant System, shown in Figure A-2, consisted of an intact loop containing active components to simulate three unbroken loops of a four-loop PWR, a reactor vessel containing a nuclear core, and a broken loop to simulate the single broken loop of a PWR. The broken loop contained passive steam generator and pump components (simulators) and did not have appreciable flow prior to loss-of-coolant experiment (LOCE) initiation. The pump and steam generator simulators contained orifice plates to simulate the pressure drops of their counterparts. The broken loop terminated in two quick-opening blowdown valves which simulate the pipe break. The break area was sized with orifice plates located at the break planes.

The reactor system (Figure A-3) contained a 1.68-m nuclear core that was about one-half the length of typical reactor cores (3.7 m long) in commercial plants. However, this was the only compromise made in the nuclear fuel for the LOFT core. PWR fuel rod assemblies were used in the geometry shown in Figure A-4. The triangular corner assemblies were partial square assemblies and had reactor control rods in the guide tubes. The center fuel assembly was the most heavily instrumented assembly with instruments placed in the vacant guide tubes as

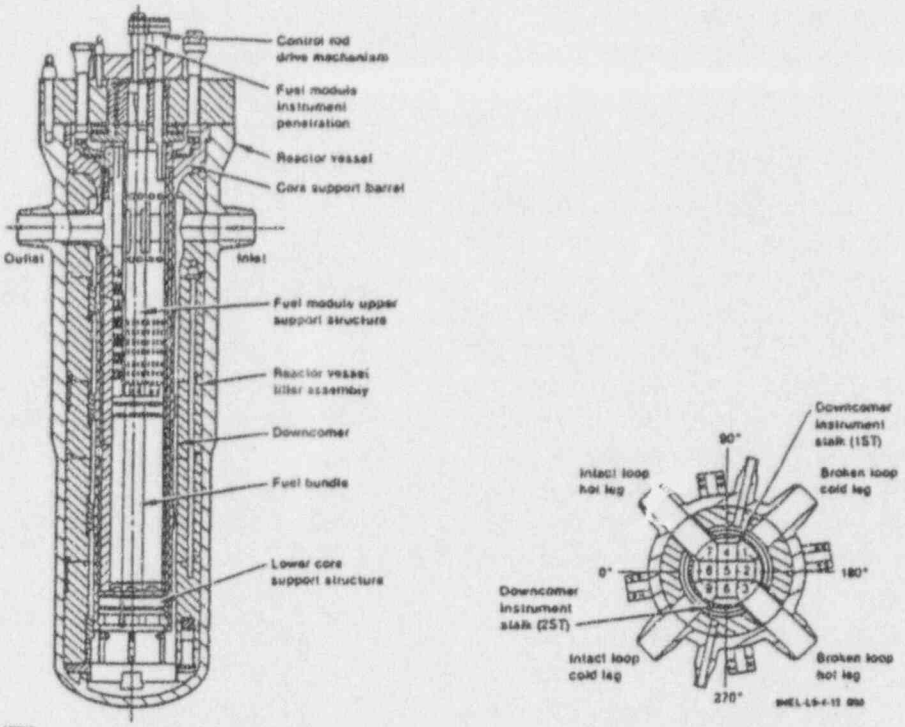

Figure A-3. LOFT reactor vessel assembly.

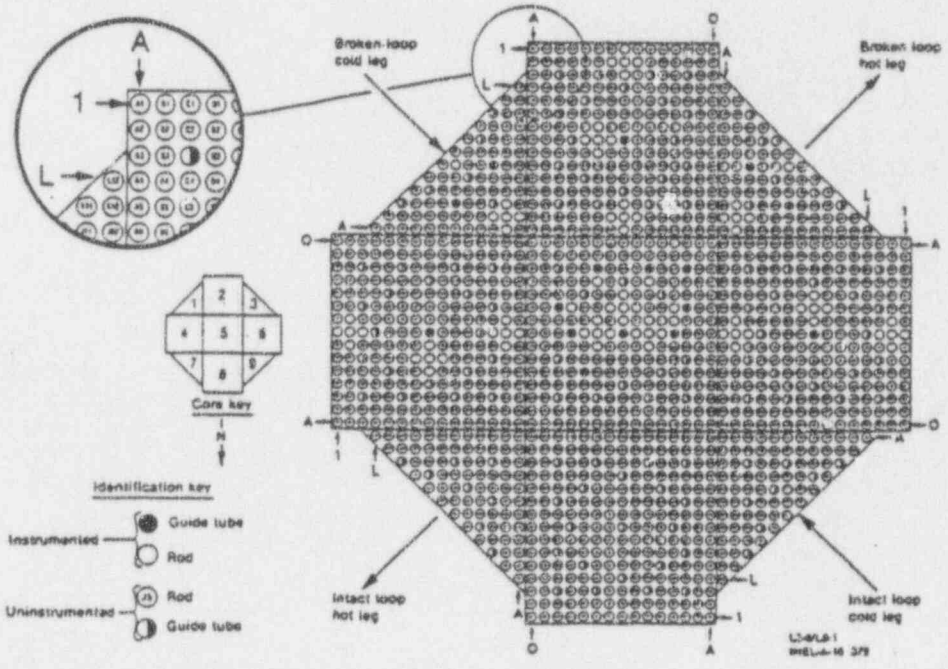

Figure A-4. LOFT core arrangement.

well as on the fuel rods. The LOFT fuel assemblies were complete with upper and lower end boxes and fuel rod spacer grids at five elevations. More specific detail of the LOFT core design is contained in Reference A-1.

The LOFT nuclear core can be considered a segment of a generic PWR core which is subjected to the same transient or off-normal conditions that a generic PWR would undergo in the event of a LOCA or operational transient. Thus, the core geometric size, peaking factors, and power generation lead to primary coolant system volumes via the criteria of maintaining, as close as possible, the coolant volume-to-total core power ratio in order to create the same transient and off-normal conditions that a generic PWR core would be subjected to. This view of the LOFT model was explicit in the early planning and design.

The Blowdown Suppression System was designed to simulate the containment back pressure in large PWR's during LOCA events. It consisted of a large pressure suppression vessel, downcomers and a header connected to the primary system via the quick-opening blowdown valves (see Figure A-2).

The Emergency Core Cooling System (ECCS) consisted of the same three systems currently in commercial PWR's--the high pressure injection system (HPIS), the accumulators, and the low pressure injection system (LPIS). The systems were actuated similar to their generic counterparts and injected scaled amounts of emergency core coolant typical of the ECC delivery behavior in commercial PWR's. The LOFT ECCS had the capability of injecting ECC to any of several locations including the intact loop hot or cold legs, and the reactor vessel downcomer, lower plenum, or upper plenum. An identical backup ECCS was also available which functioned separately from the ECCS used in a LOCE.

The Secondary System was designed to remove the heat transferred into the steam generator to the environment. This system, however, could not be controlled for full simulation of secondary system response in large PWR's.

A-2. LOFT Facility Scaling

The LOFT facility was scaled to generic PWR's by maintaining the system and component coolant volume-to-total-power ratio whenever possible.[A-2] Inherent in scaling are some compromises of geometric similarity. Scaling compromises must be such as to not adversely affect the requirements for typicality, defined in Table A-1, that must exist between the LOFT facility and the generic PWR. The LOFT scale model of the generic PWR that resulted is summarized in Table A-2, which contains comparisons of geometric and physical parameters between LOFT and commercial

Table A-1. Typicality requirements for the LOFT model design.

Item	Reason
System volume to core power ratio	Distribution of energy
Break area to system volume ratio	Depressurization of event time similarities
Length-to-diameter ratios (system resistance)	Pressure drop balance
Elevation	Pressure distribution
Surface area to volume ratios	Heat transfer distribution
Core power distribution	Thermal response

Table A-2. Comparison of LOFT and commercial PWR.

Item	LOFT		TROJAN	
	Volume (m^3)	Total (%)	Total (%)	Volume (m^3)
Reactor Vessel				
Outlet Plenum	0.95	12.51	15.95	55.47
Core and Bypass	0.31	4.12	7.50	26.0
Lower Plenum	0.71	9.32	8.58	29.73
Downcomer and Inlet Annulus	0.69	9.00	5.89	20.42
Subtotal		34.95	37.95	
Intact Loop[a]				
Hot Leg Pipe	0.35	4.60	1.94	6.71
Cold Leg Pipe	0.37	4.85	2.08	7.22
Pump Suction Pipe	0.33	4.38	309	1 0.70
Steam Generator	1.45	18.97	26.40	91.49
Pump	0.20	2.60	1.96	6.80
Subtotal		35. '0	35.47	
Broken Loop				
Cold Leg to Break[b]	0.16	2.16	1.72	5.97
Vessel to Steam Generator	0.15	1.98	0.65	2.24
Steam Generator	0.52	6.88	8.80	30.50
Pump	0.05	0.72	0.65	2.27
Additional Volume				
Part of Outlet Plenum	0.19	2.46	N/A	N/A
Part of Inlet Plenum	0.22	2.83	N/A	N/A
Pressurizer	0.96	12.62	14.7	50.97
Total	7.63	100.00	100.00	346.60

a. TROJAN values are for three loops combined.
b. Includes pump suction piping.

Table A-3. Comparison of LOFT core to commercial PWR core.

Item	LOFT	TROJAN
Fuel rod number	1300	39372
Length (m)	1.68	3.68
Inlet flow area (m^3)	0.16	4.96
Coolant volume (m^3)	0.295	20.227
Maximum linear heat generation rate (kW/m)	39.4	39.4
Coolant temperature rise (K)	32.2	32.2
Power (MW)	36.7	3540.5
Peaking Factor	2.34	1.60
Power/coolant volume (MW/m^3)	124.4	175.0
Core volume/system volume	.038	.057
Mass flux ($Kg/s-m^2$)	1248.8	3707.3
Core mass flow/system volume ($Kg/s-m^3$)	25.6	51.7

PWR's. The comparison between the scaled LOFT core and a commercial PWR core is shown in Table A-3. The physical parameters listed in Table A-2 and Table A-3 are for nominal operating conditions in the Westinghouse four-loop ZION PWR and in the LOFT model prior to the LOCE designated L2-3.

A-3. Instrumentation

The LOFT facility was augmented with an extensive "experimental" measurements system[A-1] in addition to the normal PWR instrument systems for reactor operation and control. The following parameters were measured with the experimental instrumentation: temperature, pressure, differential pressures, density, coolant velocity, coolant momentum flux, liquid levels, pump speed, and neutron flux.

State measurements of the coolant in the primary system provided the capability of following the redistribution of mass and energy in the primary coolant system following the initiation of a transient. Extensive thermal measurements in the nuclear core provided detailed information on the thermal response of the fuel cladding and fuel centerline temperatures. Nuclear measurements in the core assisted in determining the initial or steady state energy distribution. The philosophy followed on measurement locations in the nuclear core, as shown in Figure A-4, was to instrument one-half of the core on a circularly symmetric basis with emphasis on the center fuel assembly. The intent was to permit determination of the thermal and mechanical effects of instrumentation on the fuel rods during post-irradiation analysis. Utilizing circular symmetry simplified the core structure by permitting identical fuel assemblies to be used in fuel assemblies 2, 4, 6, in assemblies 1 and 3, and in assemblies 7 and 9.

Experimental measurements were also located on the ECC systems, the secondary coolant system, the pressure suppression system, and on components such as pumps, valves, and control

rod drive mechanisms for mechanical operation measurements during a transient.

Temperatures were measured in LOFT using three types of thermocouples: Type K - chromel versus alumel; Type S - platinum versus platinum 10% rhodium; Type T - copper versus constantan. There were two groups of mechanical design of the thermocouples: the grounded spade junction and the grounded weld junction. The spade junctions were used as metal surface temperature measuring devices and the grounded weld junctions thermocouples were primarily used as coolant temperature measuring devices.

Pressure measurements were made by two types of transducers: free field and standoff absolute. The free field transducers were used for the subcooled portion of the blowdown. This type of transducer is characterized with very fast response time but is also sensitive to temperature changes. The standoff transducers were used for pressure measurements during the two-phase part of the transient, since they are less temperature sensitive, but slower in response.

Differential pressure was measured using transducers similar to the standoff absolute pressure transducers with the diaphragm separating the high and low pressure fields.

Coolant density was measured in the hot and cold legs of the primary system using three beam gamma densitometers. A 22Ci ^{60}Co, source was used. The source was collimated into three beams as indicated in Figure A-5. NaI scintillation cells with photomultiplier tubes were used as detectors. There was also a fourth detector used to measure the background radiation thereby allowing it to be subtracted from the actual measurement. The density measurement with the three beams allowed recognition of flow regimes in the piping and could be used to infer liquid level measurements.

Coolant velocity, momentum flux and flow direction were measured using drag disk-turbine (DDT) assemblies. Such assemblies located in the hot and cold legs of the primary coolant piping consisted of three drag disk and turbine groups and a thermocouple as shown in Figure A-6. The drag disk device consisted of cylindrical drag body and a linear variable differential transformer to detect motion. The drag disk measured coolant momentum flux and indicated flow direction. The turbine was a six bladed turbine with graphite bearings and eddy current coil to pick up blade movement. Additional drag disk turbine assemblies were installed at the inlet and outlet of the core. The DDT turbine was calibrated to measure velocity in either direction.

Liquid level in the reactor vessel was measured at several locations using electrical conductivity probes consisting of several electrodes at various intervals in a tube. The tube was perforated at each electrode to provide good communication between the electrode and surrounding fluid. The absence of liquid was determined by measuring the electrical conductivity of the surrounding fluid.

The primary coolant pump speed was monitored with a transducer consisting of an eddy current pickup coil mounted in the pump bearing cavity on the elevation of a tachometer plate mounted to the shaft with radial slots. The direct current readout was converted to revolutions per minute.

Displacement transducers were used in LOFT to measure the dynamic vertical motion and thermal displacement of the central fuel assembly in the core. The device used a linear variable differential transformer with two coils and a floating core attached to the upper core support structure sleeve. The transducer core was attached to the upper core support structure.

The neutron flux was measured with two types of transducers: scanning and fixed location detectors. The scanning detector, a traversing incore probe, provided graphs of the axial flux distribution at four different locations in the core. The fixed detectors used ^{60}Co neutron flux detectors for fast response. These detectors are called self-powered gamma detectors, because they use the current generated by decay of cobalt to indicate power level.

A-4. OECD LOFT Experimental Configuration

For each experiment, the facility was

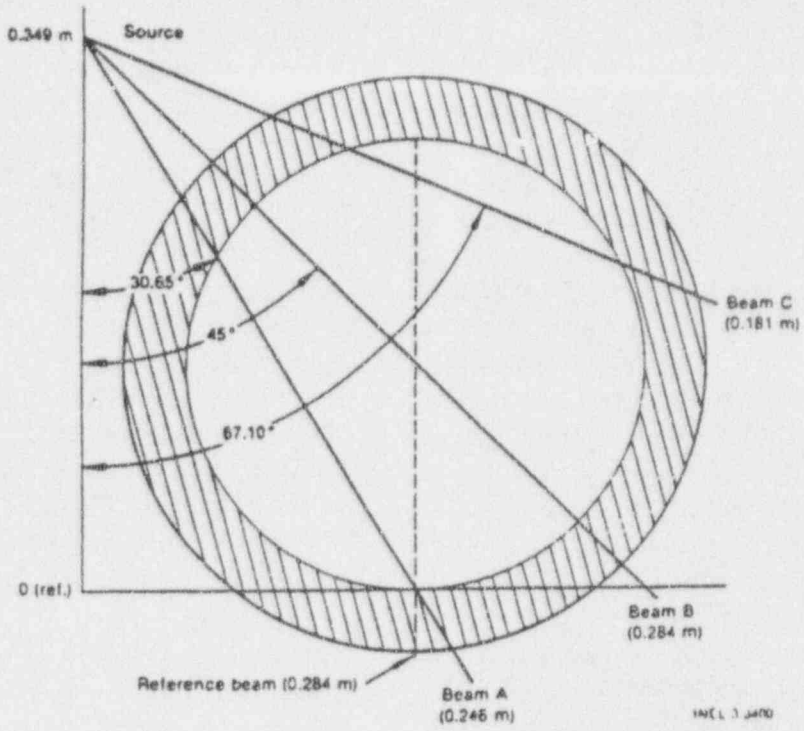

Figure A-5. Gamma densitometer arrangement in the hot leg of the intact loop.

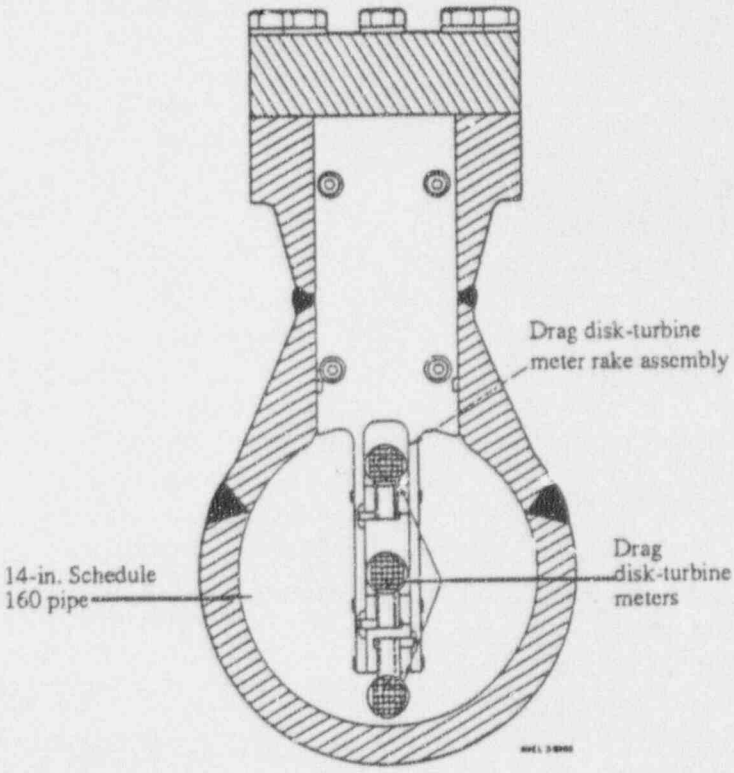

Figure A-6. Drag and Disk-Turbine (DDT) assembly.

configured according to the experiment objectives. The following indicates system changes that were made for individual experiments. A standard LOFT large-break LOCA and anticipated transients configuration is assumed. Also, special instrumentation used in fission product Experiments LP-FP-1 and LP-FP-2 is presented.

A-4.1 Experiment LP-FW-1:

Standard LOFT configuration, as shown in Figure A-2.

A-4.2 Experiment LP-SB-1:

The configuration of the LOFT primary system for Experiment LP-SB-1 is shown in Figure A-7. The break location was in the hot leg of the intact loop between the steam generator and the reactor vessel. The break nozzle was in the break piping connecting the midplane of the intact loop hot leg to the blowdown suppression tank. The break piping and the relative location of the instrumentation in the line are shown in Figure A-8.

A-4.3 Experiment LP-SB-2:

Same as Experiment LP-SB-1.

A-4.4 Experiment LP-SB-3:

The configuration of the LOFT Facility for Experiment LP-SB-3 is shown in Figure A-9. The break location was in the cold leg of the intact loop between the primary coolant pumps and the reactor vessel. The break nozzle was in a pipe that connected the intact loop cold leg to the blowdown suppression tank. Figure A-10 shows the configuration of the break piping and the relative location of the experiment

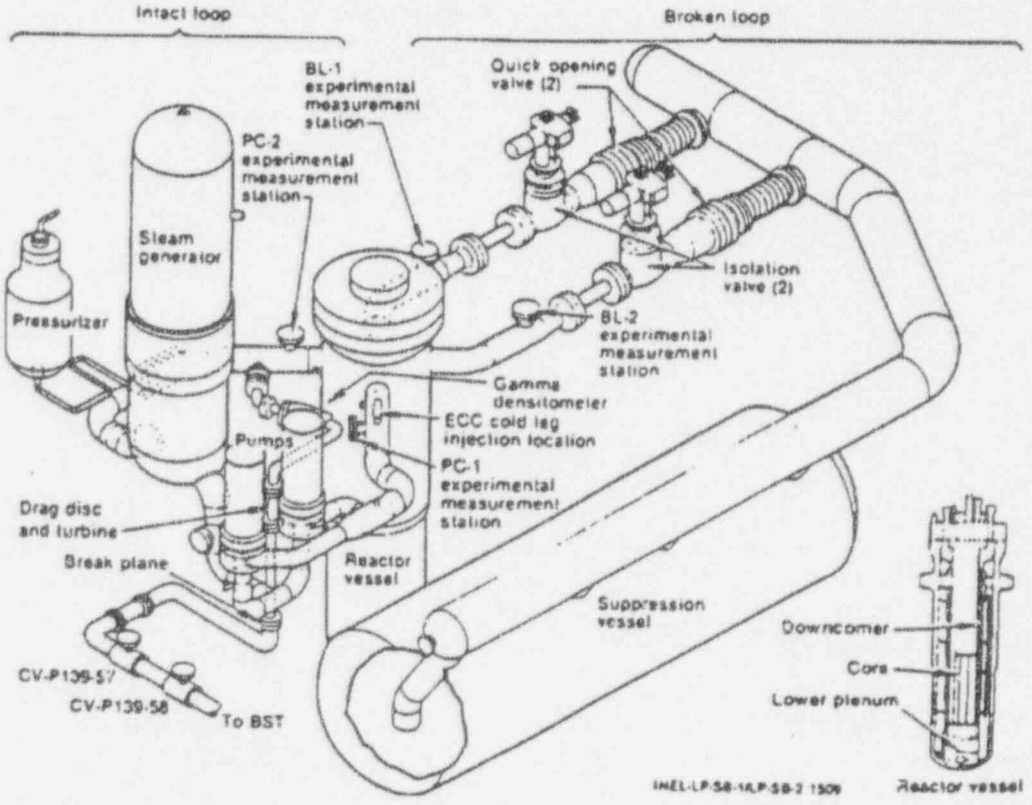

Figure A-7. LOFT system configuration for Experiments LP-SB-1 and LP-SB-2.

instrumentation.

A-4.5 Experiment LP-02-6:

Standard LOFT configuration, Figure A-2. A new center fuel module was provided with prepressurized fuel pins.

A-4.6 Experiment LP-LB-1:

Standard LOFT configuration, Figure A-2. Center fuel module with unpressurized pins.

A-4.7 Experiment LP-FP-1:

Standard LOFT configuration, Figure A-2 For this experiment a special center fuel module

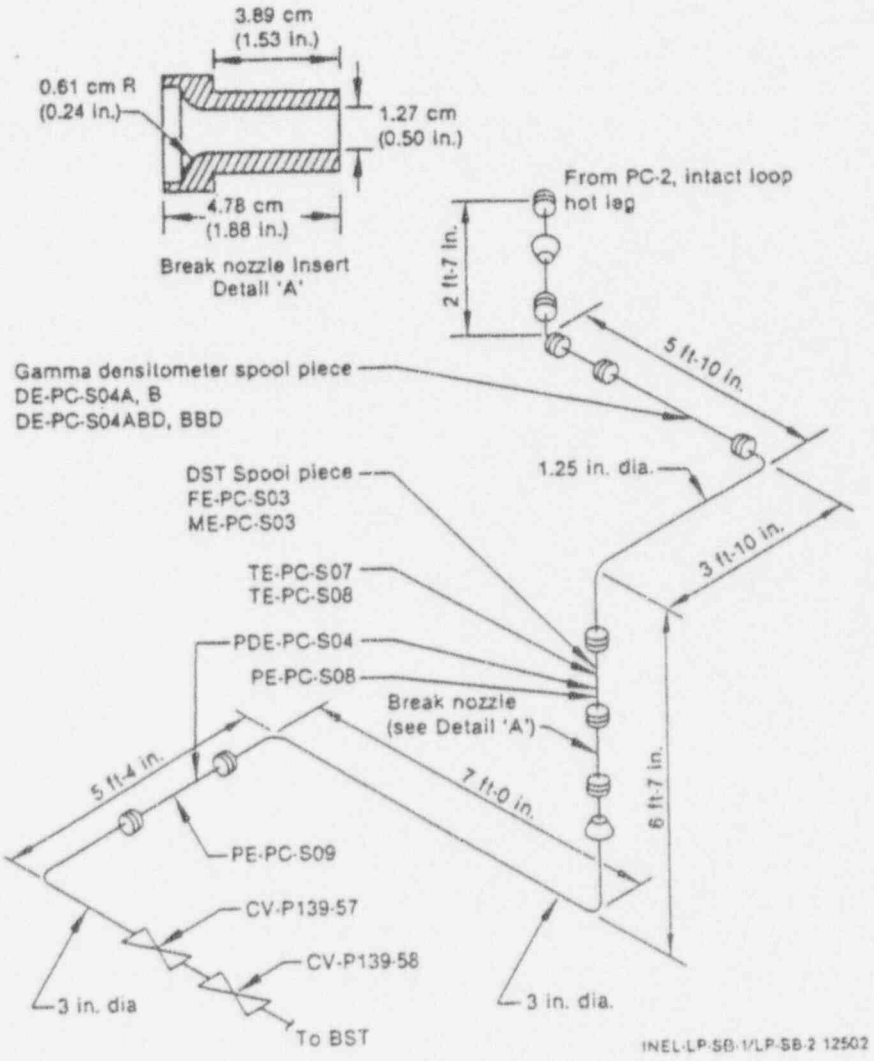

Figure A-8. Experimental spool piece configuration for hot leg break piping.

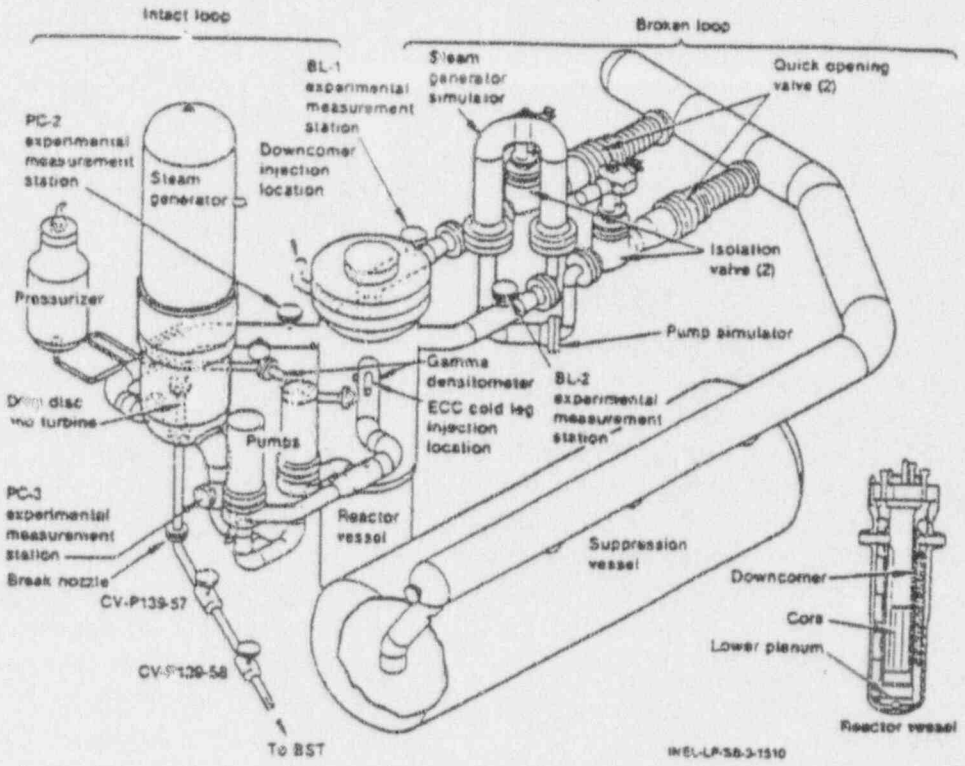

Figure A-9. LOFT configuration for small break experiment LP-SB-3.

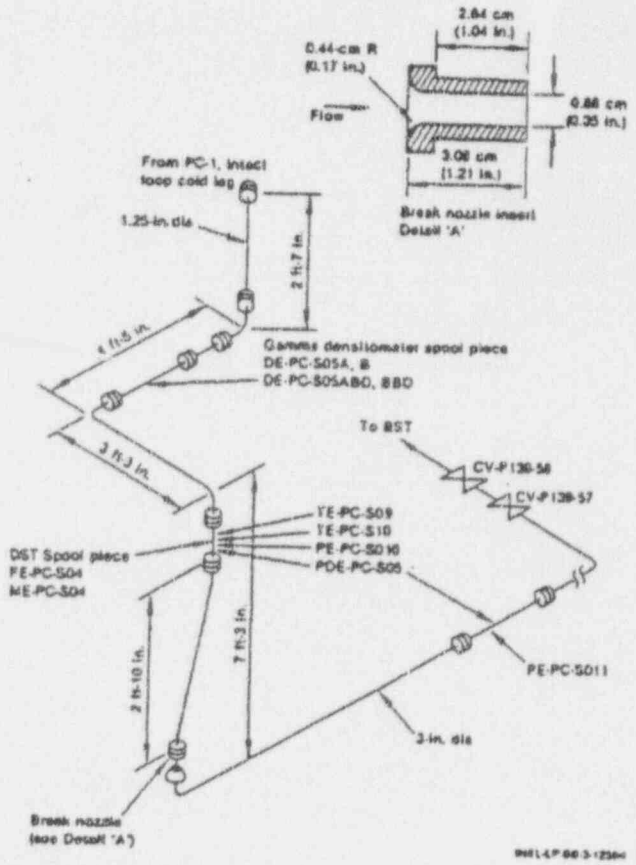

Figure A-10. Break piping configuration.

was manufactured with a zircaloy shroud. This fuel module included 24 fuel rods enriched to 6 weight% ^{235}U (regular fuel enrichment in LOFT was 4-weight% ^{235}U). Figure A-11 shows a cross-section of the center fuel module and indicates the instrumentation in the module. Twenty-two of these were prepressurized at cold conditions to 2.41 MPa.

A special fission product measurement system (FPMS) was designed for this experiment. The FPMS consisted of three basic systems: the steam sample system, which was operated during the transient phase of the experiment; the gamma detection system, which was operated during the 12 hour post-transient phase, and the deposition coupons, which collected samples during both phases. Figure A-12 shows the FPMS schematically.

The steam sample system had four sampling locations:

- S1 - in upper plenum about 7 cm above the center fuel module upper tie plate and directly below the upper plenum ECC injection port.
- S2 - in the center fuel module, 171 cm above the top of the lower tie plate.
- S3 - two samples drawn from center fuel module 115 cm above the lower tie plate.
- S4 - broken loop hot leg upstream of the steam generator simulator.

The sample lines were routed from the sample points to the instrumentation and processing equipment mounted on a movable skid. The lines were heat traced and kept to a minimum length to maximize the fission product transport to the instrumentation. The instrumentation on the skid included gross gamma detectors, flow meters, iodine species samplers, steam condensers, liquid traps and temperature and pressure measurements.

The deposition coupons were located in the reactor vessel upper plenum on three elevations: 15, 61, and 165 cm above the upper tie plate. On each elevation were two coupons and both were exposed to the reactor environment during the heatup phase. One coupon at each elevation was isolated and sealed prior to initiation of reflood, while the second coupon remained exposed.

Three gamma spectrometers were used in the experiment to provide a real time quantitative measurement of the radio isotopes present in the LOFT system during the 12 hour post-transient

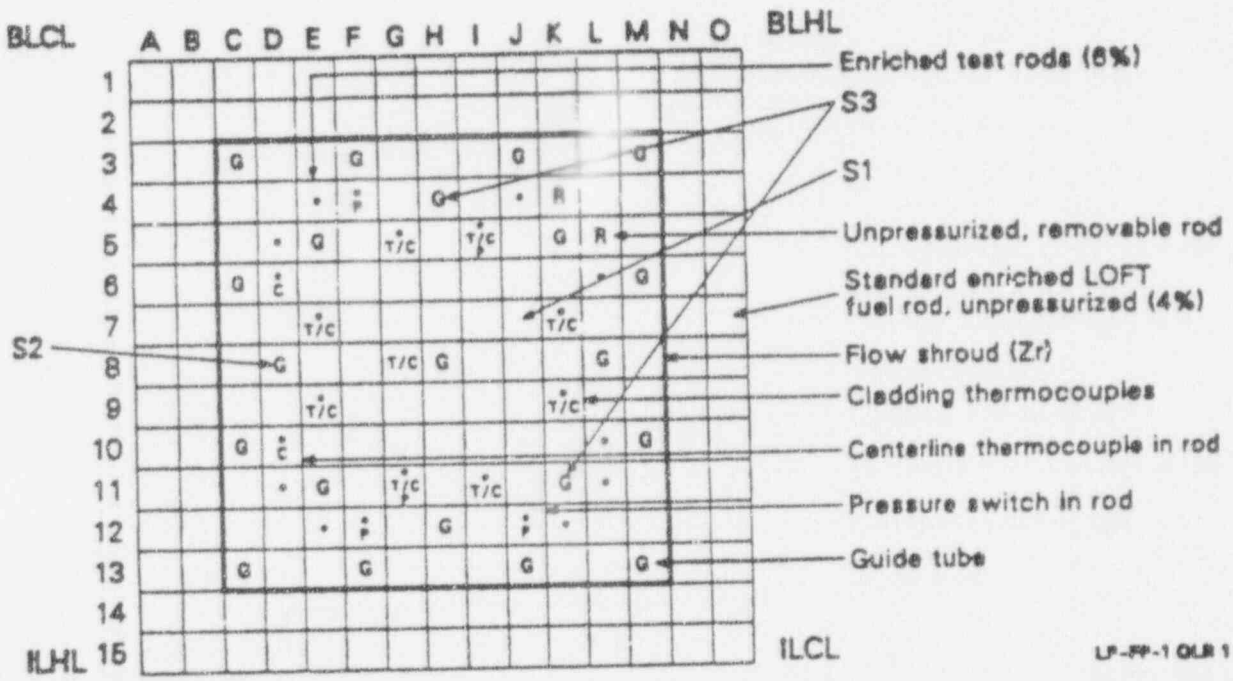

Figure A-11. Central fuel assembly instrumentation locations.

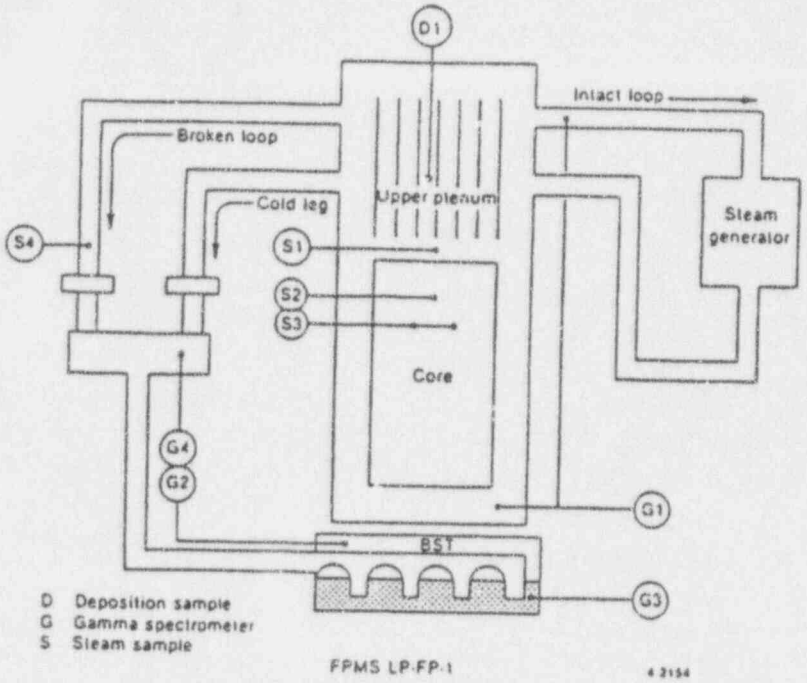

Figure A-12. Fission product sampling locations.

sampling period. The sample points are shown in Figure A-12.

A-4.8 Experiment LP-FP-2:

The configuration of the LOFT facility for Experiment LP-FP-2 is shown in Figure A-13. Important changes were made to the LOFT facility in order to conduct the LP-FP-2 Experiment. These changes included removal of the broken loop cold leg piping and the simulated steam generator, removal of the blowdown valves and the blowdown header, installation of a simulated LPIS line at the broken loop hot leg, a

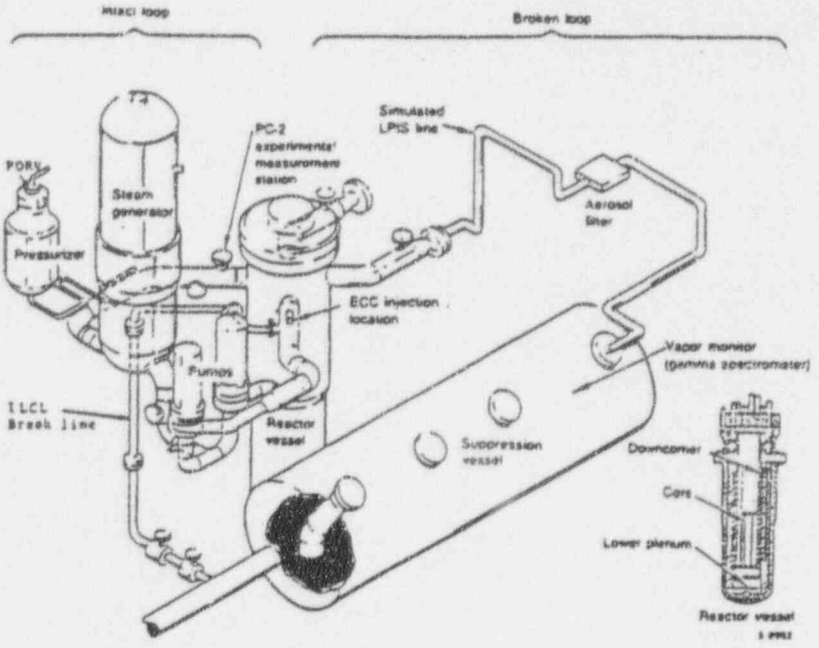

Figure A-13. LP-FP-2 LOFT system configuration.

special center fuel module and addition of the fission product measurement system (FPMS).

The simulated LPIS line (shown in Figure A-14) was scaled to represent correctly a LPIS line of a commercial power plant. The required scaling parameters included the break path flow area and LPIS line length. Break area scaling provided representative thermal-hydraulics, and specifically, similar coolant velocities for transport of fission products and aerosols. LPIS pipe length scaling was necessary to provide similar residence times for transport and retention phenomena in the LPIS piping. The scaling rationale is described in Appendix A of the EASR.[A-3]

Design of the center fuel module for Experiment LP-FP-2 is shown in Figure A-15. The outer two rows of fuel rods in the standard 15 by 15 array were replaced with a shroud that provided thermal insulation and hydraulic separation of the remaining 11 by 11 array of fuel rods from the peripheral modules. The shroud consisted of zircaloy walls with zirconium oxide ceramic internal insulation. The fuel rods within the CFM were enriched to 9.74 weight% 235U. The purpose of increasing the enrichment was to provide at least three minutes of cladding temperatures above 2100 K before the peripheral fuel rods reach the damage limit of 1462 K.

The fission product measurement system, illustrated in Figure A-16, consisted of three basic subsystems: (a) four gamma spectrometer systems and one gross gamma detector, (b) a deposition sampling system, and (c) filter sample systems.

The four on-line gamma spectrometers and the

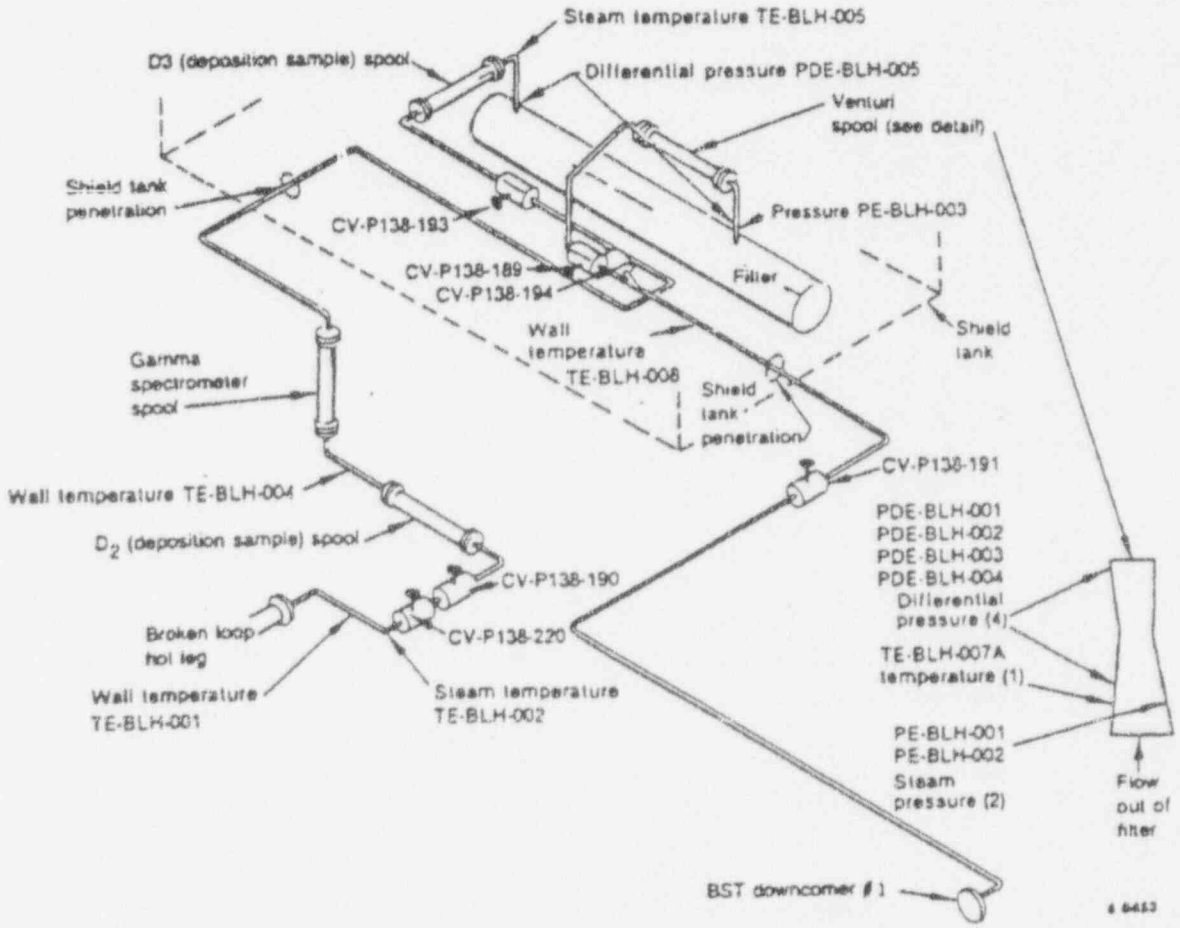

Figure A-14. LOFT simulated LPIS line.

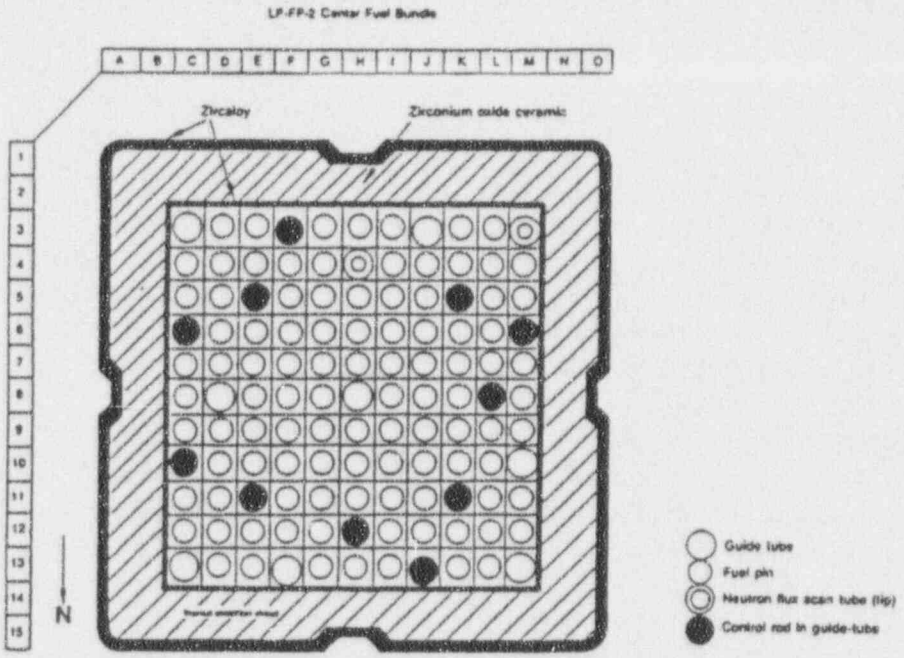

Figure A-15. LOFT center fuel module design.

G6 gross gamma monitor were located at five different sample locations: (a) G1 sampled from the reactor vessel lower plenum or, alternatively, from the intact loop hot leg; (b) G2 sampled from the blowdown suppression tank vapor spaces during the post-transient, and from the combined F1+F2 sample lines during the transient phase of the experiment; (c) G3 sampled from the blowdown suppression tank liquid space; (d) G5 sampled from the simulated LPIS line during the transient and post-transient; and (e) G6 sampled the F1 line at the top of the reactor vessel. The G4 detector was used during Experiment LP-FP-1 and was not used in this experiment. Each gamma

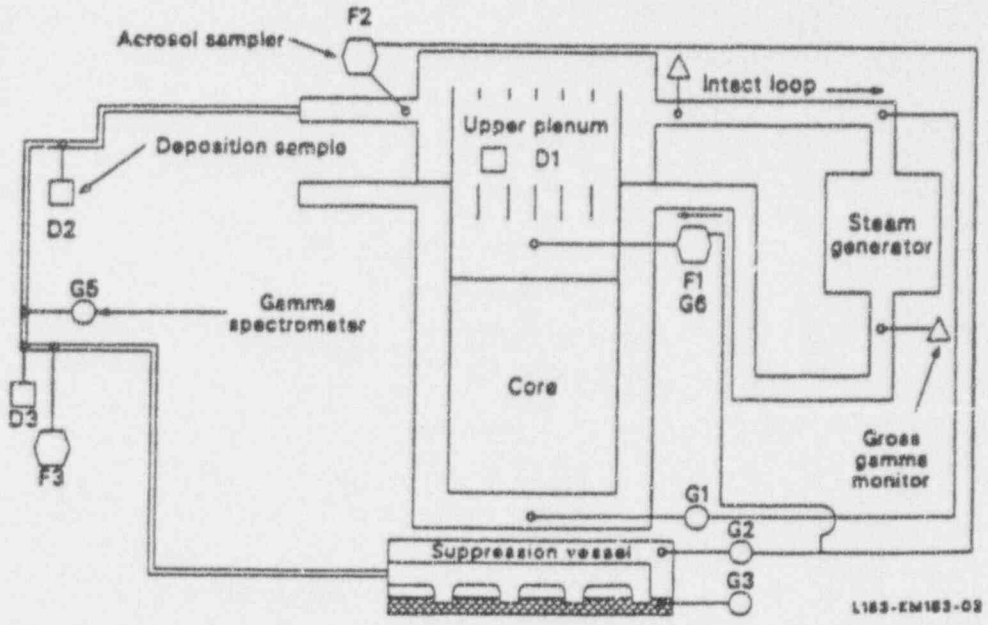

Figure A-16. LOFT LP-FP-2 FPMS instrumentation.

spectrometer was designed to operate remotely and could be calibrated using a ^{228}Th source mounted on a collimator wheel. With the exception of G5 and G6, this system operated only during the post-transient phase.

The deposition sampling system consisted of six stainless steel coupons and two deposition spool pieces. Two coupons were located at each of three elevations above the central fuel module (for a total of six coupons, collectively designated D1). At each elevation, both coupons were exposed to the fluid stream during the transient. One coupon at each elevation was to be isolated from the PCS prior to initiation of reflood while the other coupon remained exposed to the fluid. However, the protective cover did not seal around the lowest level coupon and contact with reflood water occurred. The other coupons functioned as planned. The two deposition spool pieces, located instrumentation line header, were designated D2 and D3 respectively. These spool pieces were designed to provide a measurement of the primary coolant system surface deposition of volatile fission products during the heatup or transient. Since this line was isolated prior to reflood, these coupons were protected from the reflood wa[illegible] therefore did not experience postexperin[illegible]sition, leaching, or removal of reversibly plated fission products.

The final FPMS subsystems consisted of two aerosol/steam sampling lines with corresponding equipment and an aerosol filter system on the LPIS line. These sample lines were designed to provide a continuous sample of the vapor and aerosols generated during the heatup phase of the experiment. The Fl sampling line consisted of the following major components:

1. Sample line probe placed above the CFM.
2. Argon dilution gas supply.
3. Dual cyclone separator/isolation valves.
4. Dilution filter.
5. Virtual impactor.
6. Collection filters.
7. Infrared moisture detectors.
8. Hydrogen recombiner.

The F2 sampling line was similar to the Fl line, except that there were no dilution gas supply and moisture detectors. The F3 filter sampling system consisted of the D2 and D3 deposition spool pieces, a filter, and a flow venturi. The three sample line locations are: Fl, 180 cm. above the top of the lower tie plate and located directly above the center fuel module; F2, the broken loop hot leg spool piece just outside of the upper plenum, and F3, the exit of the simulated LPIS line header.

A-5. REFERENCES

A-1. D. L. Reeder, LOFT System and Test Description (55 Foot Nuclear Core LOCEs) NUREG/CR-0247 TREE-1208, Change 1, September 1980.

A-2. L. J. Ybarrondo et al., "Examination of LOFT Scaling," ASME 74-WAIHT-53, Annual Meeting, November 17-22,1974.

A-3. M. L. Carboneau et al., Experiment Analysis and Summary Report for OECD LOFT Fission Product Experiment LP-FP-2, OECD LOFT-T-3806, June 1989.

Appendix B

The Planning and Conduct of Experiment LP-FP-2

APPENDIX B

THE PLANNING AND CONDUCT OF EXPERIMENT LP-FP-2

This appendix describes the planning and conduct of Loss-of-Fluid Test (LOFT) Facility Experiment LP-FP-2.

B-1. Experiment Planning

OECD LOFT Experiment LP-FP-2 was one of two experiments dealing with the release and transport of fission products. The first experiment, LP-FP-1[B-1,B-2] provided information on fission product release and transport from the fuel gap. Experiment LP-FP-2[B-3,B-4,B-5,B-6] provided information on the release and transport of fission products and aerosols in a severe fuel damage scenario. The specific accident scenario governing the design of LP-FP-2 was to be a hypothetical event that has a significant contribution to the total risk of nuclear power plant operation. Within this framework, the nature of the observed phenomena governing fission product and aerosol release and transport could be linked to potential pressurized water reactor (PWR) system thermal-hydraulics and core thermal response leading to fuel failure and fission product transport behavior. The following sections describe the design of the experiment and the design and modification of the LOFT system for conduct of the experiment.

B-1.1 Experiment Design.

Probabilistic risk assessment studies[B-7] revealed that the interfacing systems loss-of-coolant accident (LOCA), a hypothetical event first postulated in the Reactor Safety Study[B-8] and labeled the V sequence, has a significant potential contribution to the total risk from operation of nuclear power plants. This accident sequence was selected as the governing mechanism under which severe fuel damage phenomena would be studied in Experiment LP-FP-2. The specific interfacing systems LOCA was a pipe break in the low pressure injection system (LPIS), also called the residual heat removal system. This system typically serves two functions: (a) it provides emergency coolant injection for core recovery during intermediate and large LOCAs, and (b) it provides for decay heat removal during normal shutdown. The LPIS represents a potential path by which a LOCA external to the containment could occur, discharging primary system coolant outside the containment. If core cooling cannot be maintained during such an event, fission product release to the environment could occur through failure of the auxiliary building.

In the V-sequence scenario, the effectiveness of the emergency core cooling system (ECCS) in supplying cooling water to the primary coolant system (PCS) is not a principal factor in the outcome, or end result. The ECCS only influences the time to core uncovery. The limiting consideration for fission product release is that the ECCS, at some point, fails to maintain core cooling, which results in a core uncovery and subsequent heatup to severe fuel damage temperatures. Therefore, the conduct of a V-sequence scenario in the LOFT facility would not include operation of the ECCS. Based on this decision, the LP-FP-2 transient was conducted to predetermined termination conditions, at which time a plant recovery phase commenced,

utilizing the full capacity of the LOFT ECCS under the direction and control of the Reactor Operations Group. Plant recovery with ECCS, therefore, was defined to be a programmatic function and not a part of the V-sequence scenario. In order to preserve fission product data (in a time-integrated form), all affected systems, including plant and measurement systems, were isolated prior to ECCS initiation.

The existing LOFT ECCS connected to the intact loop and reactor vessel downcomer and lower plenum.[B-9] The simulated LPIS piping could not be interconnected with the existing LOFT ECCS, therefore leaving the broken loop as the region for the connection location. An additional important consideration affecting the location of the simulated LPIS piping was the ability to make thermal-hydraulic and fission product measurements in the LOFT PCS for determination of the source-term characteristics. To make such measurements in the lower plenum and downcomer in LOFT (for a simulated LPIS line connection in the broken loop cold leg) would have been very difficult and was judged to be beyond the scope of the program. Therefore, the simulated LPIS piping was connected to the broken loop hot leg. This location also was valid for the intended purpose of studying fission product and aerosol transport behavior under representative geometric and thermal-hydraulic boundary conditions, as will be clarified in Section B-1.3.

B-1.2 Source Term Design. The intent of Experiment LP-FP-2 was to study release and transport of fission products from the fuel matrix in the presence of aerosols from control rods. The nuclear core in the LOFT PWR, which contains fuel assemblies identical to commercial fuel except for length, would provide the fission product source with the correct timing of thermal response events and behavior. However, a full core involvement in fission product source production could not be handled within the scope of the OECD LOFT Program. The postexperiment plant cleanup and decontamination and decommissioning tasks required a well-defined starting point that would allow completion of these tasks within program cost and schedule parameters. An open-ended severe fuel damage transient in the LOFT core similar to the TMI-2 accident could not be allowed. Therefore, the fission product source term was limited to a specially designed central fuel module (CFM) that incorporated physical features of (a) higher power density than the peripheral fuel modules; (b) thermal and hydraulic separation from the peripheral fuel modules; and (c) control rods for the aerosol source term. In addition, the following requirements and termination criteria were imposed on the core thermal transient:

- The structural integrity of the peripheral fuel modules must be maintained to facilitate their removal from the reactor vessel. The transient termination condition to meet this requirement was a maximum peripheral fuel cladding temperature of 1462 K.
- The structural integrity of the CFM, exclusive of the fuel rods and control rods, must be maintained to facilitate removal from the reactor vessel. The transient termination condition to meet this requirement was based on the use of zircaloy in a shield on the CFM for thermal and hydraulic insulation and was an outer shroud surface maximum temperature of 1573 K.

The design of the CFM would be such as to cause the CFM fuel rods and control rods to reach severe fuel damage temperatures at least three minutes prior to the occurrence of either of the two transient temperature termination conditions. A time limit of seven minutes was imposed administratively as the maximum time allowed before plant recovery with the ECCS would commence. As indicated in References B-5 and B-6, the CFM temperature was above

2100 K for approximately 4.5 minutes before plant recovery began.

Experiment LP-FP-2 studied only the initial phase of severe fuel damage as a result of a V-sequence accident scenario. Further, the source term in the initial severe fuel damage phase was constrained by design to originate from a single fuel module located at the center of the LOFT core. Because of the hydraulic isolation of the fuel rods in the CFM from the remainder of the core, the source term must exit the core at the top of the CFM. The source term was further constrained by the design of the upper support structure of the peripheral fuel modules to flow almost entirely through the CFM upper support structure to the elevation of the hot leg pipes, where flow is relatively unrestricted across the reactor vessel to the hot leg pipes. The design constraints on the source term generation and flow path provided a more definable environment and boundary condition for the measurement of fission product and aerosol transport and retention phenomena. This degree of definition could be achieved only if the simulated LPIS piping (break flow path) were connected to the broken loop hot leg. This configuration was judged to be the only possibility for a successful experiment within the program scope.

B-1.3 Transient Thermal-Hydraulics. Scaling considerations for the experiment centered on the V-sequence phenomena that were calculated to occur in commercial PWR's. The required scaling parameters included only the break flow path area (LPIS pipe size scaling) and LPIS line length. Break area scaling provided representative thermal-hydraulics and, specifically, similar coolant velocities for transport of fission products and aerosols. LPIS pipe length scaling was necessary to provide similar residence times for transport and retention phenomena in LPIS piping. A scaled representative LPIS piping system, completely separate from the existing LOFT ECCS LPIS, was required to conduct the V-sequence transient. The need for this piping system came not only from scaling considerations but also from programmatic considerations, as explained in Section B-1.1.

A survey of commercial PWR LPIS designs showed that LPIS pipe sizes varied in the 6- to 10 in. (Schedule 160) size, having inside diameters of 0.13 to 0.22 m. The break flow area/system volume ratio was used to determine the LOFT break area range of 0.009 to 0.031 m. Volumes used were 355.1 m3 for a typical PWR[B-10] and 7.36 m^3 for LOFT. The pipe size selected for the LOFT simulated LPIS line was 1.25-in. Schedule 160 with an inside diameter of 0.0295 m. A pipe size near the upper end of the allowable range was selected in order to minimize the effect of differences in surface-to-volume ratios in the LPIS pipes between LOFT and commercial PWR's.

The 1.25-in. Schedule 160 pipe size selection for the simulated LPIS piping was the same size as that used for small-break simulations in the intact loop cold leg (Experiment LP-SB-3) in which a break flow orifice was inserted along with an instrumented pipe section.[B-11] This break location and piping flow path to the blowdown suppression tank (BST) was rejected for use as the break location for LP-FP-2 because of the difficulties with definable fission product transport geometries and measurements, as discussed previously. However, initiating the LP-FP-2 transient from this location was observed to be advantageous for the following reasons:

- PCS mass distribution and depletion (up to core uncovery) would be more representative of a true V-sequence scenario.
- Component and instrument design requirements on the simulated LPIS line would be less demanding, since the line

could be opened at a pressure lower than steady state pressure required for plant operation.

- Delaying the opening of the simulated LPIS line until only a high-quality steam flow occurred in the line would provide a less severe and more definable environment for fission product measurements.

These advantages led to the development of an operational scenario wherein the unorificed line in the intact loop cold leg would be utilized to initiate the transient. At a time (determined to be 220 s in Reference B-3) when the hot leg piping was sufficiently voided, the simulated LPIS line would be opened. The intact loop cold leg break path would be closed prior to onset of core uncovery. The remainder of the transient from core uncovery onward would be in response only to the simulated LPIS line break path in the broken loop hot leg. An additional advantage of this operational sequence was the earlier time to core uncovery that maximized the use of the decay heat difference between the CFM and peripheral fuel modules.

Returning to the second scaling consideration of LPIS line length, the development of the experiment design paralleled the LOFT simulated LPIS line system and component design following the decision to locate the line in the broken loop hot leg. The final system designed explained here and described in Section B-1.4 was based on consideration of PWR LPIS line residence time, surface-to-volume ratios, LOFT plant structures, design standards, and the development of fission product measurements.

The survey of PWR LPIS lines revealed a large variation in line lengths (19.5 to 61 m). If the LOFT simulated LPIS line were to have the surface area equivalent to that in a commercial PWR, the LOFT line would have to be in the range of 3.3 to 10.4 m. This was based on a factor of 6.9 difference between the LOFT-PWR surface-to-volume ratios in the LPIS lines. The final design length (effective) of the LOFT simulated LPIS line was 9.75 m. This value was near the upper end of the allowable range for surface area consideration. The residence time, however, assuming equal velocities, would be approximately one-half that in a PWR LPIS line at best. The final LOFT design was judged to be at or near the optimum possible based on all considerations identified above. Similar steam velocities and effective surface areas were judged to be essential and more important to understanding fission product behavior than the preservation of residence time (line length). This position was supported by the design decision to capture all particulate fission products in a filter inserted at the end of the effective length of the simulated LPIS line. Steam and gaseous fission products and other noncondensible gases would continue to flow to the BST following passage through the filter.

Transient calculations for experiment planning were done with the RELAP5/MOD1 code.[B-3] A V-sequence calculation in the Surry PWR[a] was used as a reference and a guide for the LOFT LP-FP-2 Experiment design. Figure B-1 shows the defined scenarios leading to severe core damage used in the Surry calculation and the LOFT experiment plan. The calculations showed that severe core damage would occur approximately 8000 seconds later in Surry than in LOFT. However, comparisons of thermal-hydraulic parameters in the upper plenum and LPIS lines in the two facilities beginning at fuel cladding temperatures of 2100 K showed good similarity. Examples of importance to fission product transport analysis where good similarity occurred were the steam mass flow per fuel rod and the upper plenum steam velocity. Surry

a. The Surry V-sequence calculation was performed in 1983 with the MARCH and PSTAC codes by Science Applications, Inc., Palo Alto, CA. The results of the calculation were provided to EG&G Idaho, Inc. by R. L. Ritzman, SAI, and P. R. Davis, Intermountain Technologies Inc., Idaho Falls, ID.

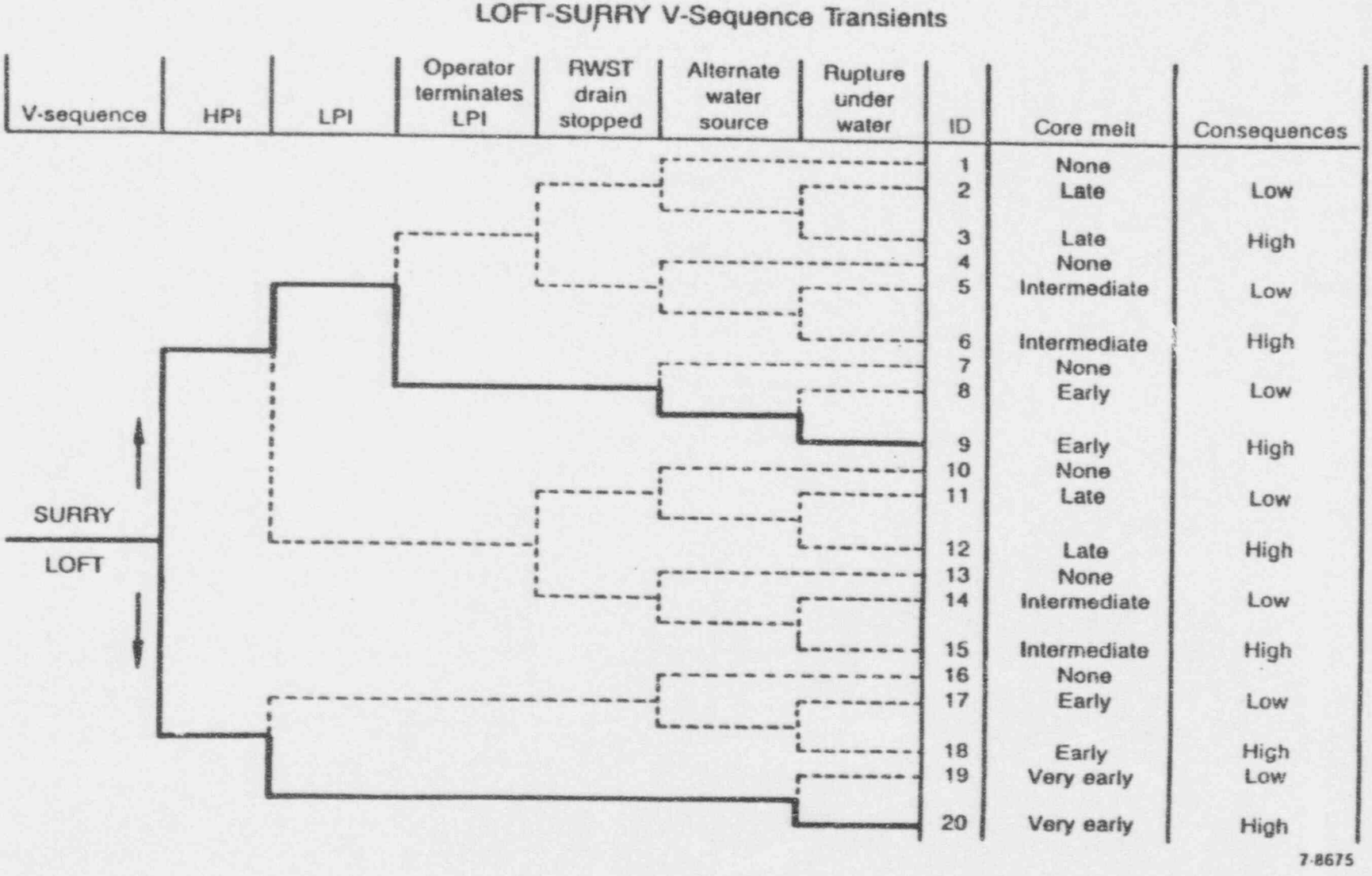

Figure B-1. V-sequence scenario map, showing LOFT and SURRY scenarios.

upper plenum model surfaces were approximately 10% cooler than in LOFT. This was due to the partial use of the ECCS and the relatively long time to core heatup in Surry. The LPIS line velocity in Surry was larger than in the LOFT calculation by almost a factor of two. This was due to the Surry LPIS line size being 6-in. Schedule 160, whereas the scaled size based on the LOFT LPIS line size would be about 10% larger than an 8-in. Schedule 160 pipe. The flow area difference is approximately a factor of two. The residence time in the Surry LPIS line at a core temperature of 2200 K was calculated to be 0.4 seconds, as compared to the predicted LOFT LPIS residence time of approximately 0.24 seconds. Thus, residence times will be short in all PWR LPIS lines, which decreases the importance of line length preservation and increases the importance of surface area to volume.

In summary, the design for the LP-FP-2 Experiment was concluded to meet the objective of providing data on the initial phase of a severe fuel damage transient resulting from a high-risk accident scenario. However, the LP-FP-2 Experiment must be viewed not as a study or simulation of an actual V-sequence transient, but rather as an experiment in which V-sequence thermal-hydraulic and fission product/aerosol transport phenomena were created with timing and magnitude within the range expected for V-sequence phenomena in commercial PWR's.

B-1.4 LOFT PCS Design. The plan view of the LOFT PCS is shown in Figure B-2. The shaded region indicates those broken loop components that were removed for LP-FP-2. A blind flange was placed on the broken loop cold leg pipe. The simulated LPIS line was located between the flange on the broken loop hot leg and Vent No. 4 in the BST. The other three BST vents were blindflanged. In addition, all other systems and hardware in containment that were not needed for plant operation or postexperiment cleanup operations were removed from the facility.

The design of the simulated LPIS line is shown in Figure B-3 and Figure B-4. A bypass line around the filter was included in response to the concern that the effectiveness of the particulate filter might be lessened if the depressurization from 220 seconds (when the line is opened) to the onset of severe fuel damage vented through the filter. The bypass line was used to vent PCS mass during most of this time interval to maintain filter effectiveness. The filter line was to be opened and the bypass line closed prior to fuel cladding failure in the CFM, and also with sufficient time to allow for heatup of the filter line to LPIS line temperature so that LPIS steam mass flow measurement data could be obtained downstream of the effective end of the LPIS line (the filter).

The LPIS line measurements are identified in Figure B-4. The D2 and D3 deposition spools are removable pipe sections for the study of fission product deposition. Steam temperature and inside pipe wall temperature were to be measured in pairs upstream and downstream of the removal pipe sections and downstream of the filter. Several of these measurements failed during the transient. Figure B-4 identifies those measurements that provided valid data.

B-1.5 LOFT Core Design. The design of the CFM for LP-FP-2 is shown in Figure B-5, and a summary of design characteristics is given in Table B-1. The outer two rows of fuel rods in the standard 15 by 15 array were replaced with a shield that provided thermal insulation and hydraulic separation of the remaining 11 by 11 array of fuel rods from the peripheral fuel modules. The shield consisted of zircaloy walls with zirconium oxide ceramic internal insulation.

The fuel rods in the 11 by 11 array were enriched to 9.74 weight% ^{235}U, which is more

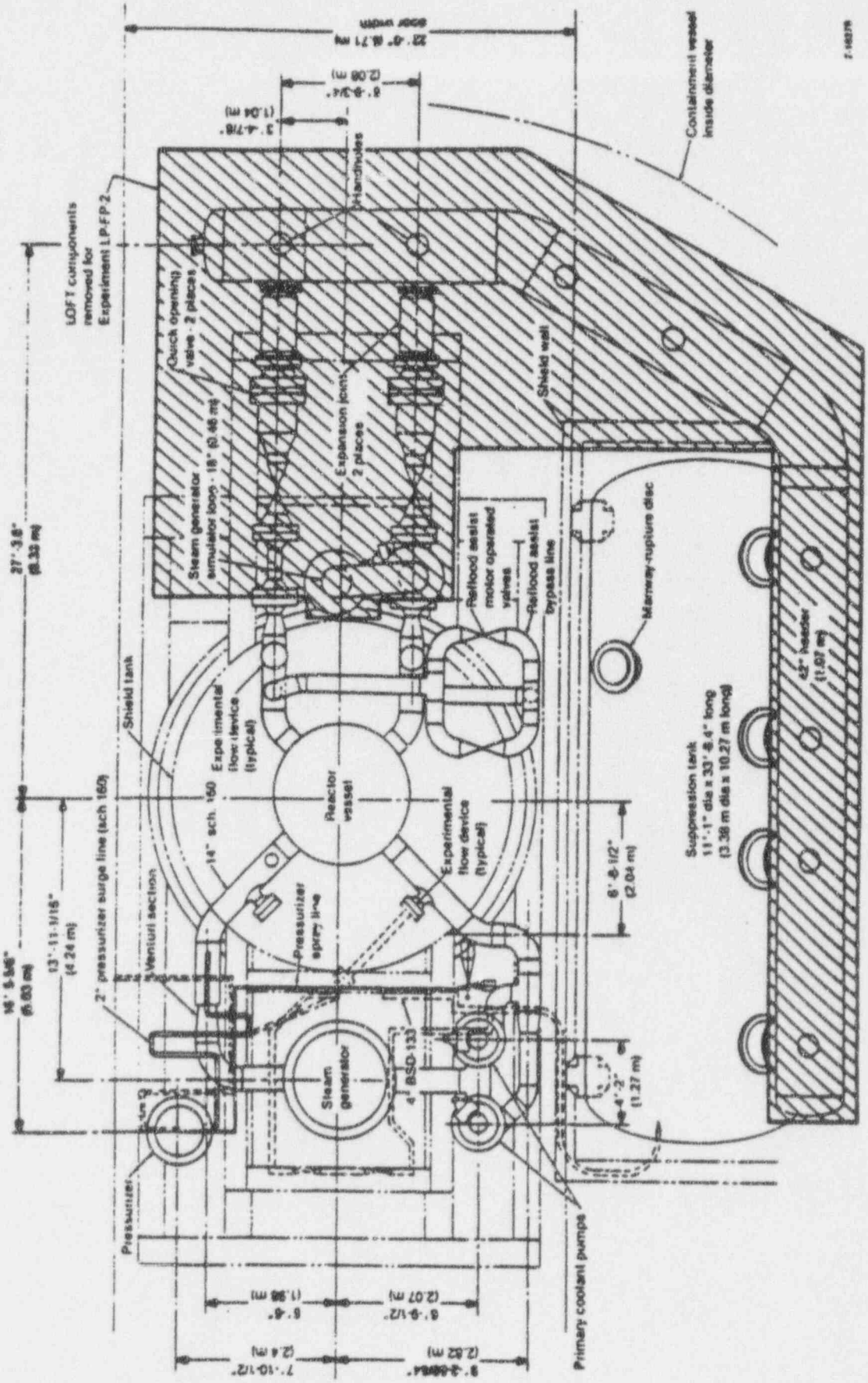

Figure B-2. LOFT Primary Coolant System for Experiment LP-FP-2.

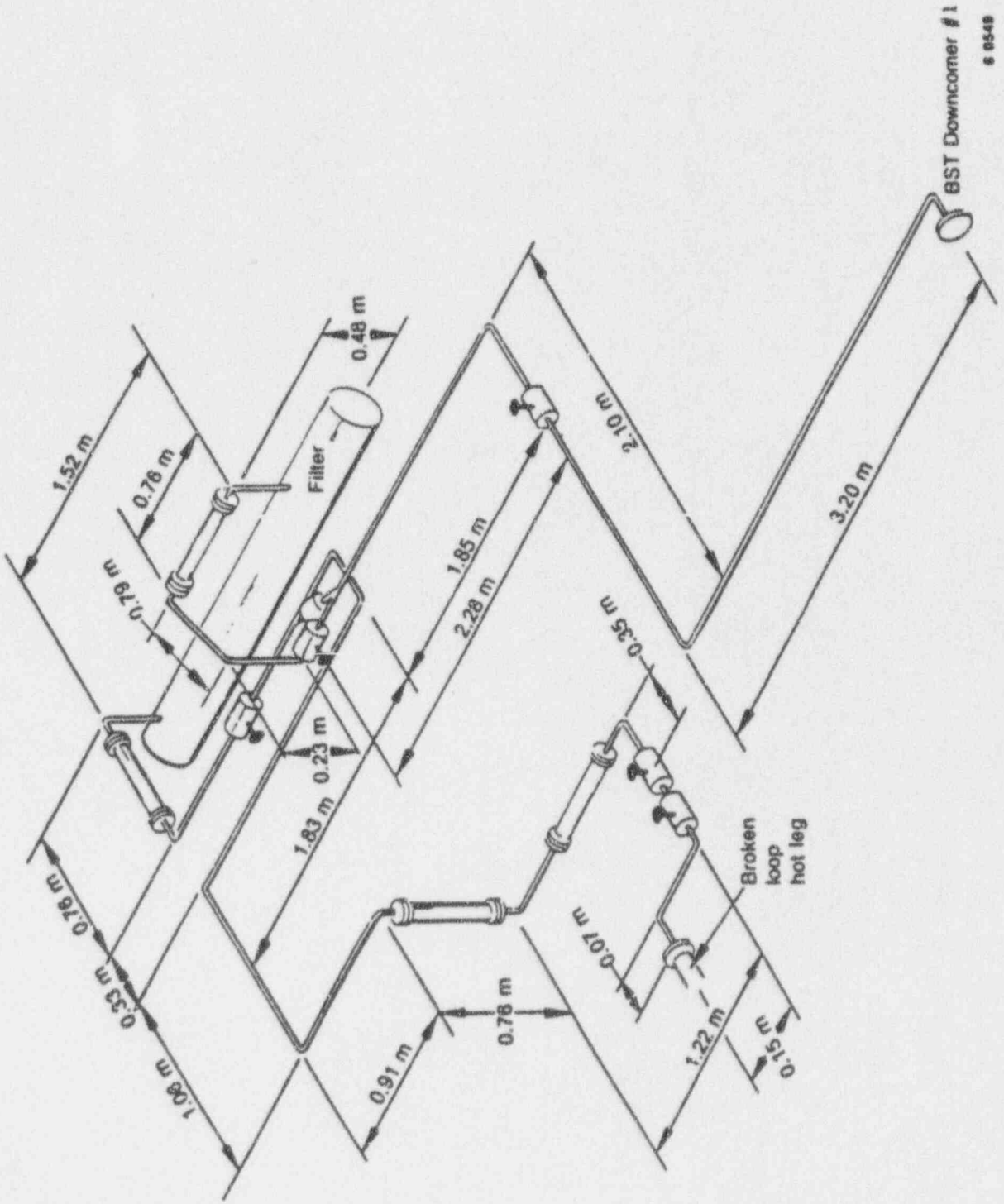

Figure B-3. LOFT simulated LPIS line design and dimensional data.

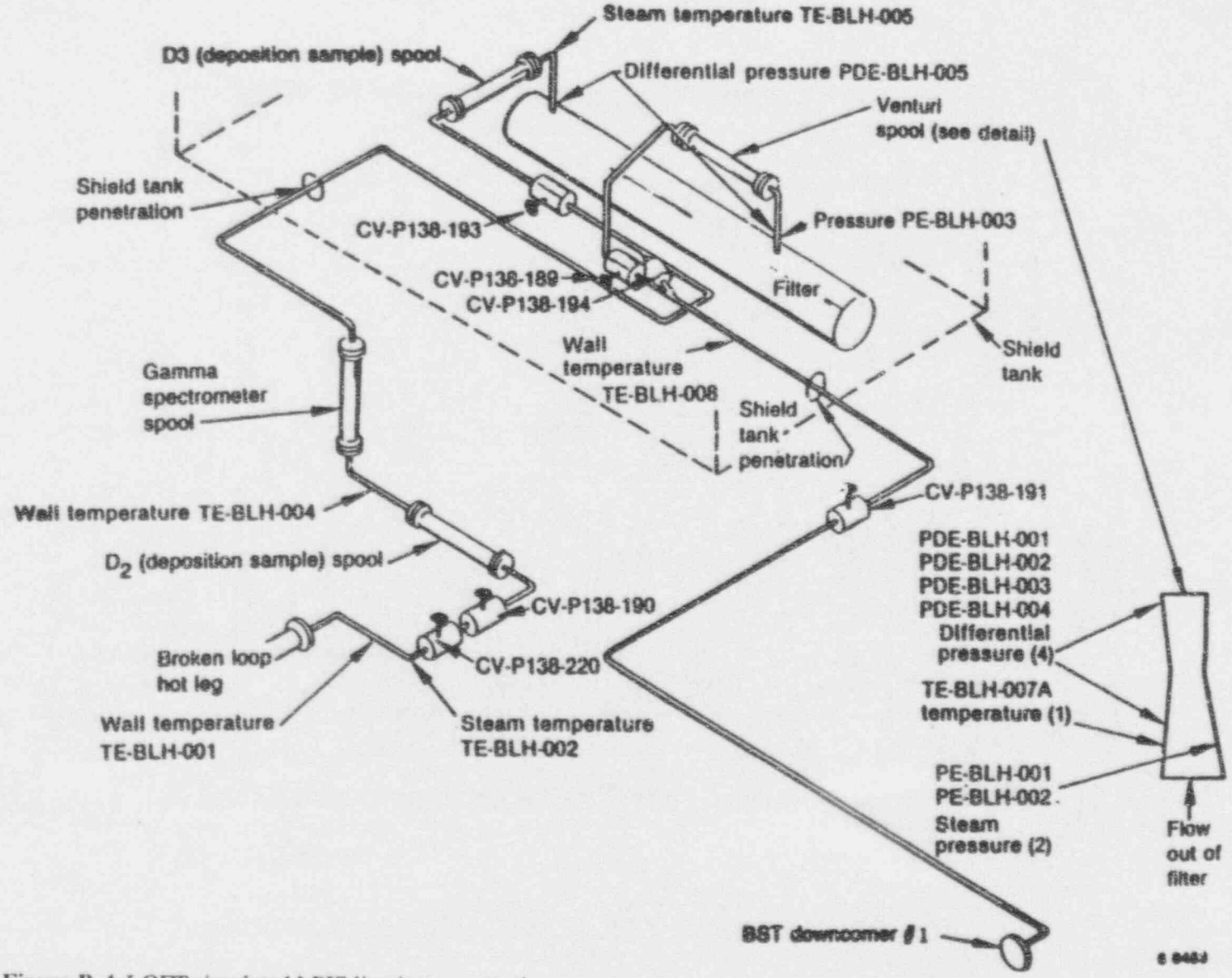

Figure B-4. LOFT simulated LPIS line instrumentation.

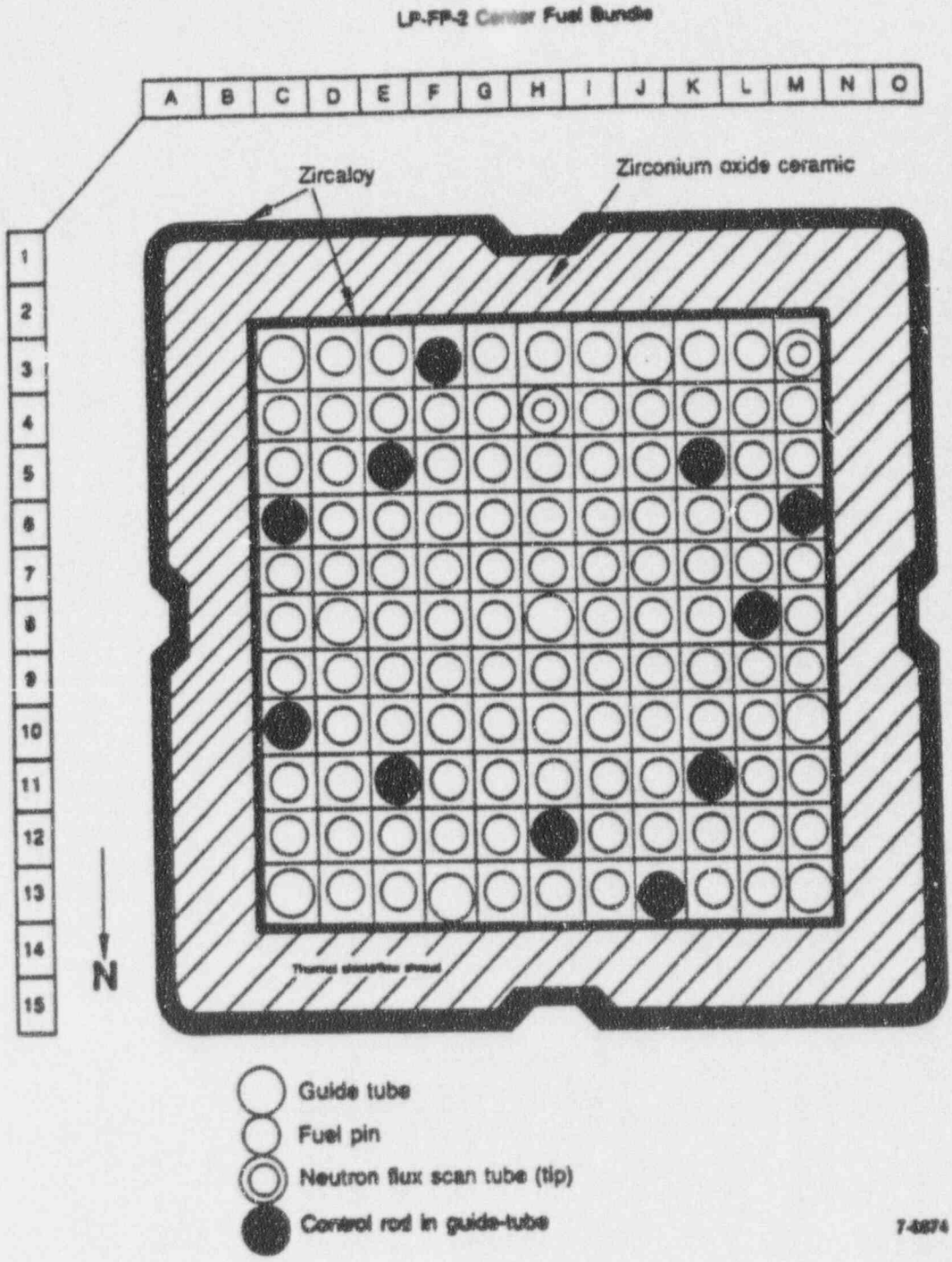

Figure B-5. LOFT center fuel module design.

Table B-1. LP-FP-2 test design parameters.

Parameter	Definition
Fuel Rods	
Number of fuel rods	100
Outer diameter	10.72 mm
Cladding thickness	0.62
Length	1.8 m
Cladding material	zircaloy-4
Fill gas	helium (2.4 MPa)
Enrichment	9.74 wt% ^{235}U
Fuel density	94.7± 0.4% TD
Control Rods	
Number of control rods	11
Outer diameter	11.23 mm
Cladding thickness	0.51 mm
Cladding material	204 stainless steel
Neutron absorber	80 wt% Ag, 15 wt% In, 5 wt% Cd
Guide Tubes	
Number of guide tubes	6 empty, 15 on non-fueled rods
Outer diameter	13.84 mm
Inner diameter	12.98 mm
Material	zircaloy-4
Spacer Grids	
Material	Inconel 718
Shroud	
Wall material	zircaloy-4
Outer wall thickness	3.18 mm
Inner wall thickness	1.52 mm
Insulation	solid ZrO_2 (20% TD)
Insulation thickness	22.35 mm

than a factor of three above the standard LOFT fuel enrichment. The purpose of increasing the CFM enrichment was to provide for at least three minutes of cladding temperatures above 2100 K before the peripheral fuel rods reached the limit of 1462 K. The thermal design of the shield was intended to decrease the heat transfer rate from the CFM to the peripheral fuel modules. Calculations of fuel cladding heatup rates and heat transfer rates[B-3] showed that, with all conservatism accounted for, the CFM would be above 2100 K for at least three minutes. The three-minute design objective resulted from the time predicted for release of aerosols, fuel rod gap fission products, and fuel rod matrix fission products; the time for transport of those materials through the LOFT PCS and simulated LPIS line; and the time required for fission product measurement system (FPMS) operation.

The outer wall of the CFM shield was the primary structural member of the CFM. In order to meet the requirement that the structural integrity had to be maintained to facilitate CFM removal, a temperature limit was placed on the outer wall of the shield. This limit was 1573 K, as noted previously. The termination criterion for the LP-FP-2 transient was either this limit or the peripheral module fuel cladding limit of 1462 K.

The CFM contained 11 control rods to provide approximately the same fuel rod/control rod ratio as in a standard fuel module with control rods. The upper support structure was a modified standard LOFT upper structure for fuel modules with control rods, which contained the 11 control rods in a fully withdrawn position until the initiation of the experiment. Thus, the CFM control rods did not interfere with or influence power operation but were in the full insertion position (core scrammed) prior to core heatup.

CFM measurements consisted exclusively of thermocouple temperature measurements during the experiment. The locations, with elevations given in inches above the bottom of the active core, are shown in Figure B-6; and the axial orientations of both instrumented and uninstrumented fuel rods are shown in Figure B-7. The two neutron flux scan tubes were used for traversing neutron detector power profile measurements during preexperiment power operations. The tubes were sealed during a reactor shutdown interval prior to final power operation and establishment of experiment initial conditions.

B-1.6 LOFT FPMS Design.

The final design of the FPMS is illustrated in Figure B-8. The FPMS consisted of three basic systems: the aerosol sampling system which was operated during the transient phase only, and the gamma detection and deposition coupon systems, which collected data during both transient and posttransient phases. Each of these systems is described herein.

B-1.6.1 Deposition Sampling System

Stainless steel deposition coupons were positioned in the reactor vessel upper plenum region to provide postexperiment information on fission product plateout. These are designated D-1 on Figure B-8. Two coupons were located at each of three axial elevations, corresponding to 0.152, 0.61, and 1.65 m above the upper tie plate. Both coupons at each elevation were exposed to the reactor environment during the heatup. One coupon at each elevation was isolated and sealed prior to initiation of reflood, while the second coupon remained exposed. Thus, the plateout during the heatup phase was to have been distinguished from the plateout/leaching during the reflood phase.

The D-1 deposition device is a hollow rod containing deposition coupons. At experiment initiation, the D-1 deposition device was full of liquid water. A nitrogen purge gas system was connected to the rod to ensure dry coupons for fission product plateout. The hollow rod was pushed down before reflood to isolate the protected coupons. At that time, the nitrogen gas purge was restarted to remove steam, which

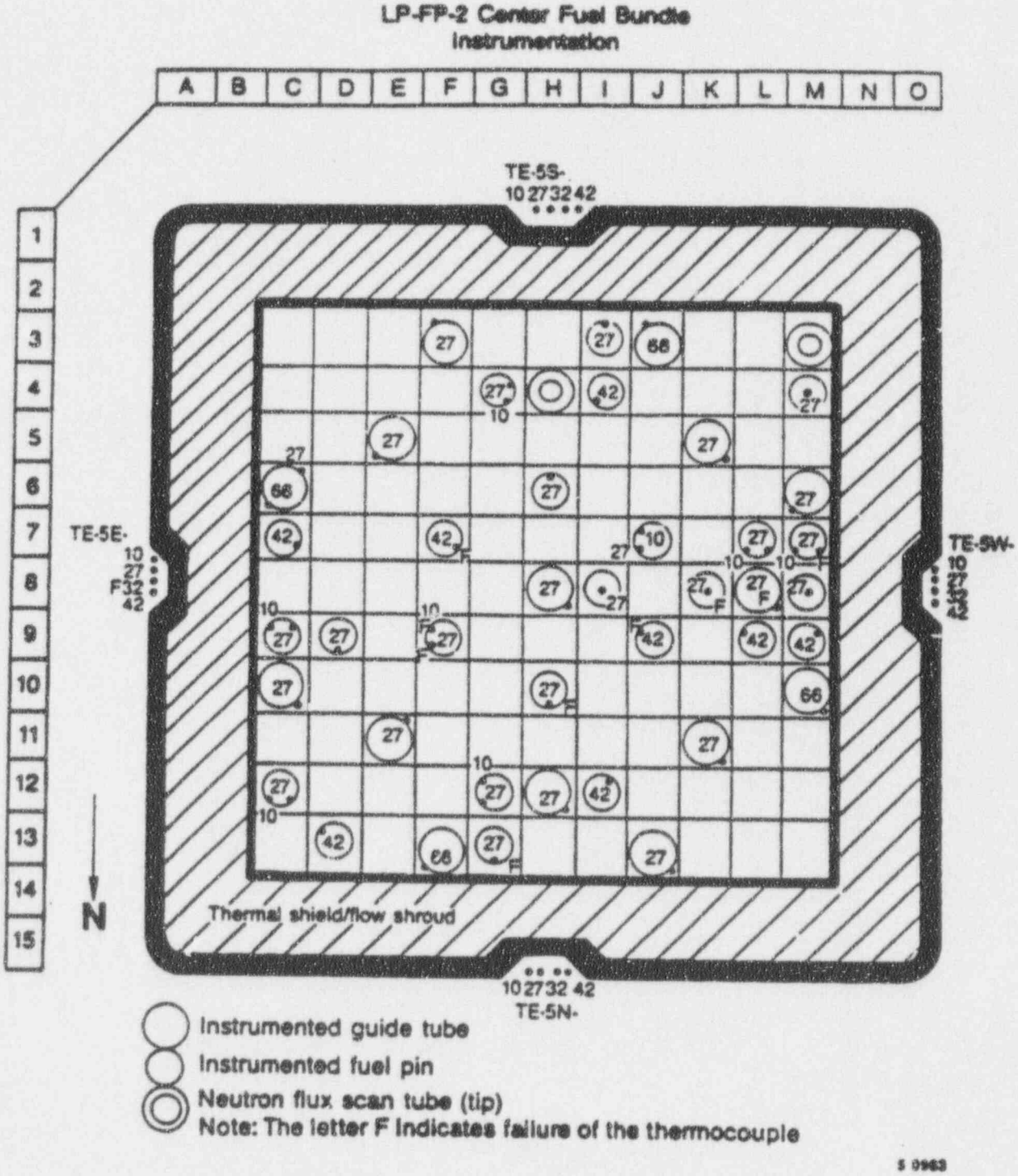

Figure B-6. LOFT center fuel module temperature measurements.

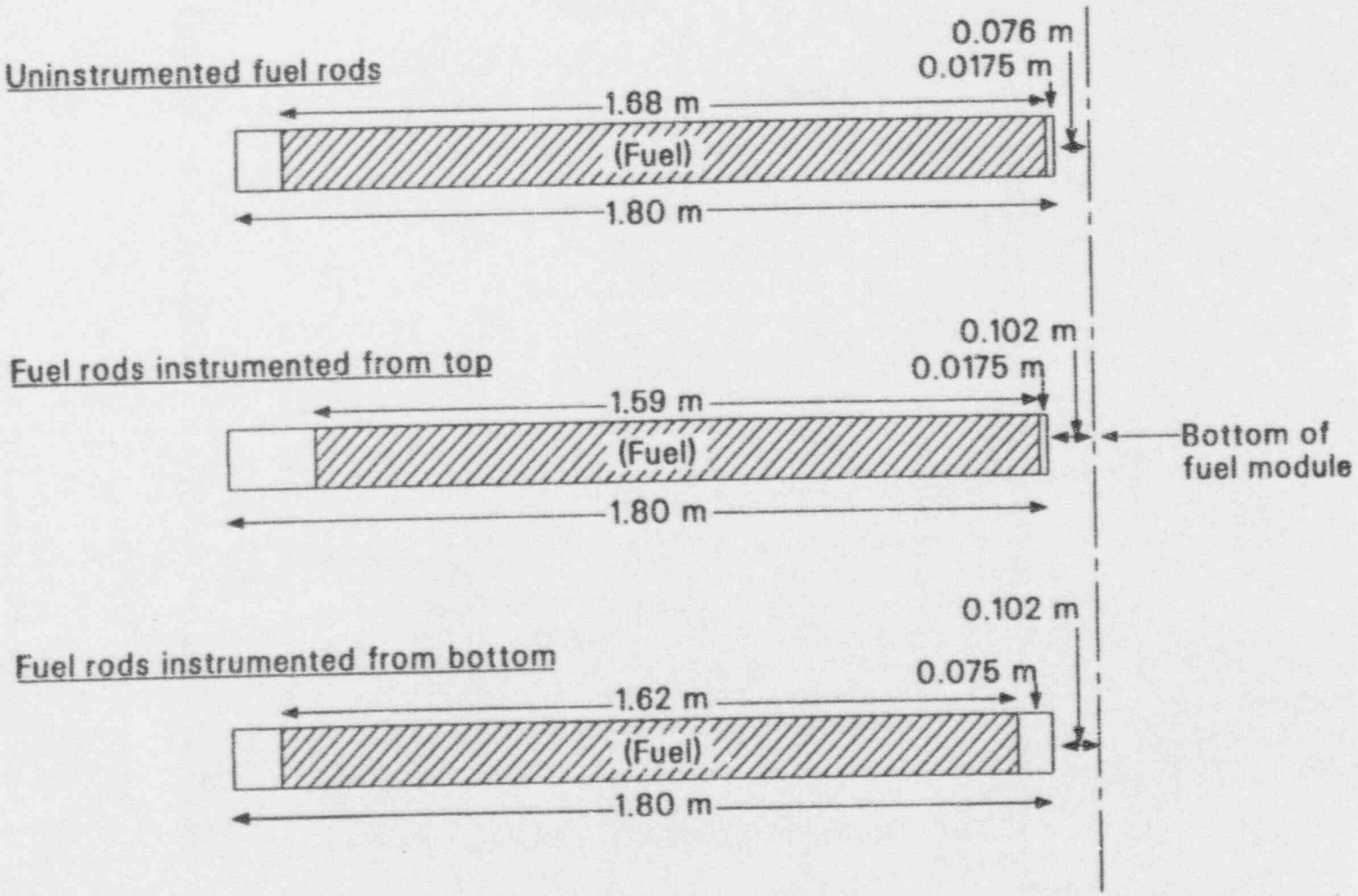

Figure B-7. Axial orientations of instrumented and uninstrumented fuel rods.

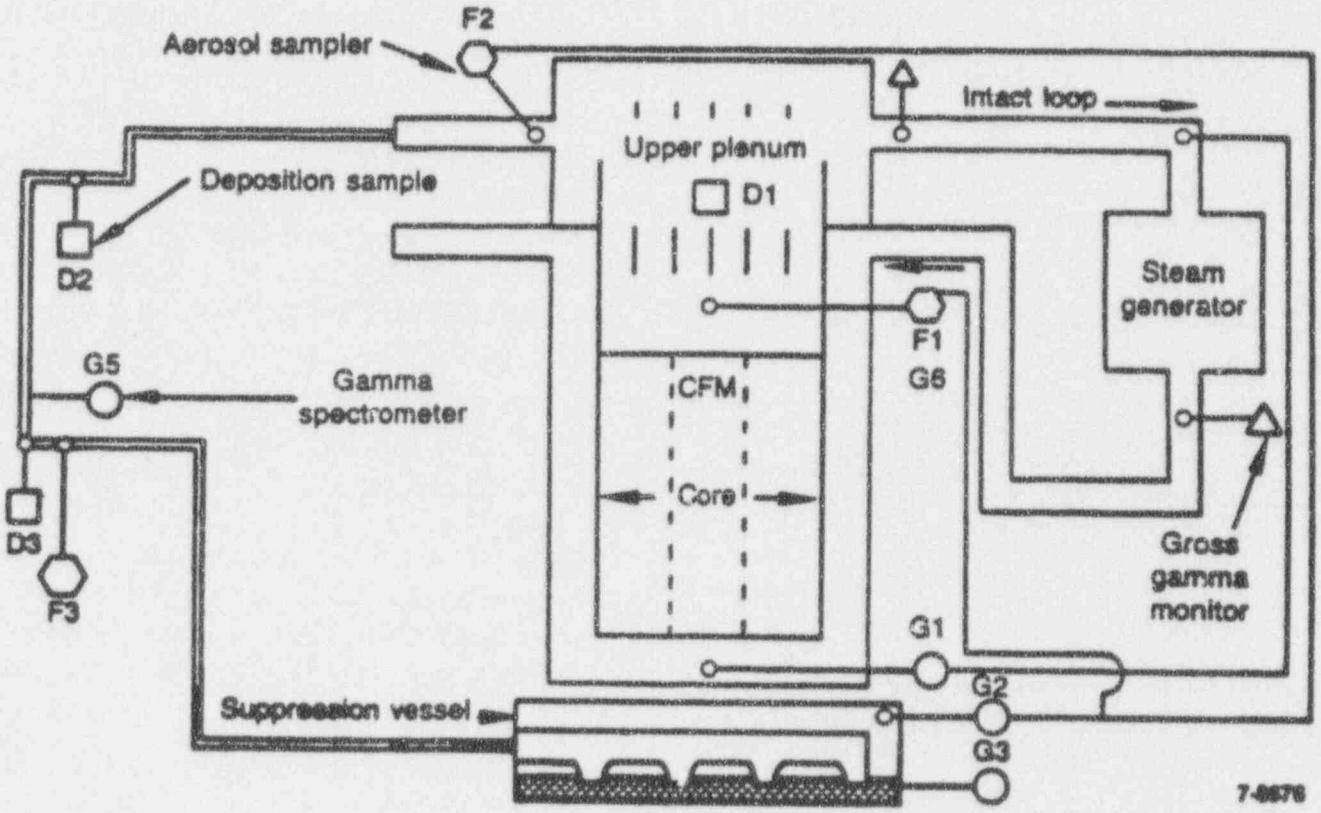

Figure B-8. LOFT Experiment LP-FP-2 Fission Product Measurement System.

could condense onto the coupons. The nitrogen gas supply to the rod was then to have been controlled at 1.4 MPa above reactor pressure to ensure that any leakage of the deposition rod seals was outward, thereby maintaining a dry atmosphere for the protected coupons.

The D2 and D3 coupons were located upstream and downstream of the simulated LPIS header, respectively. To allow only high-quality steam to flow into the line, it was not opened until the primary system mass inventory had decreased. In addition, the line was isolated prior to reflood so that these deposition coupons were protected from water flow

B-1.6.2 Filter Sampling System. There were three filter sampling systems installed for this experiment. These systems provided samples of the vapor and aerosols generated during the heatup phase of the experiment. Both of these constituents were expected to combine to provide the medium for transport of the fission products. Figure B-9 is a schematic representation of the design of the F1 and F2 sample lines. The filter sample locations were:

- F1--in the reactor vessel upper plenum at 1.80 m above the top of the lower tie plate
- F2--in the broken loop hot leg spool piece just outside of the upper plenum
- F3--in the exit of the broken loop hot leg

The F1 system consisted of the following major components:

- Sample line probe
- Cyclone separator/isolation valve]
- Dilution filter
- Virtual impactor
- Collection filters
- Infrared moisture detectors
- Recombiner
- Critical flow orifice
- Gamma spectrometer.

The sample line probe, shown in Figure B-10, diluted the vapor/aerosol sample with an inert gas to minimize sample line deposition and to inhibit interactions within the sample. The cyclone separator/isolation valve, shown in Figure B-11, isolated the filter assembly before and after the heatup phase and removed particles with an aerodynamic diameter larger than 20 to 30 μm. The dilution filter reduced the mass loading of the aerosols to prevent plugging of the virtual impactor.

The filter train, shown in Figure B-12, consisted of the dilution filter, the three-stage virtual impactor (Figure B-13) and the collection filters. The train separated the aerosols into size ranges of 6 to 20 μm 1.7 to 6 μm, and less than 1.7 μm, with each size range being collected on a separate filter.

The recombiner contained cupric oxide, which converted the hydrogen to water. The infrared moisture detectors then provided quantitative data on the amount of argon, hydrogen, and steam entering and exiting the recombiner. These data provided the necessary input for calculating the amount of hydrogen and the dilution ratio of argon/ hydrogen sampled during the transient.

The critical flow orifice provided a mass flow out of the line during the transient.

The F2 line was similar to the F1 line except for the deletion of the moisture analyzers and inert dilution gas. The F3 line, also designated the simulated LPIS line and shown in Figure B-14, contained the following components:

- Deposition samples upstream and downstream of the gamma spectrometer (D1 and D2)
- Gamma spectrometer (G5)
- Filter (F3)
- Flow venturi.

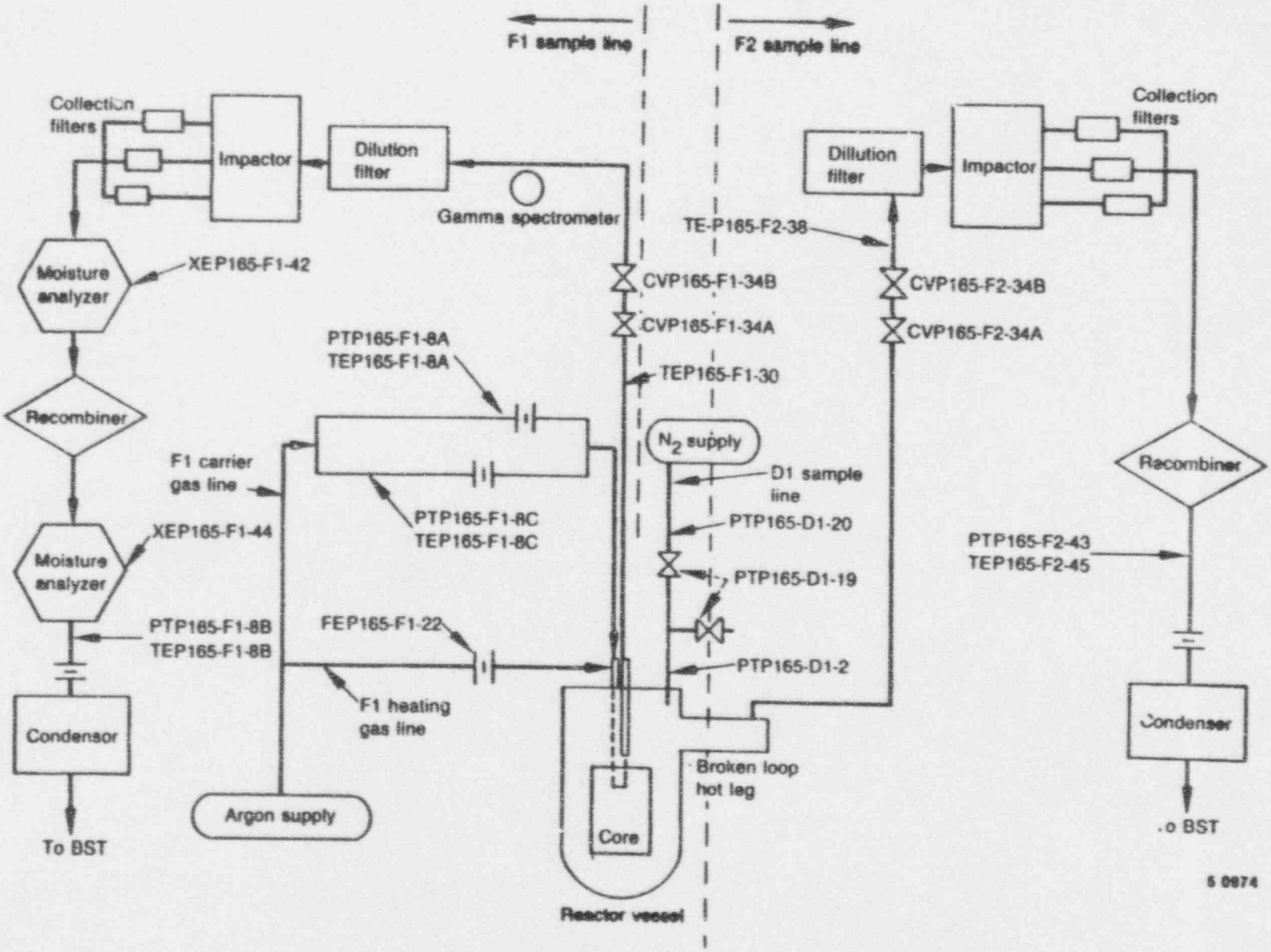

Figure B-9. Schematic of F1 and F2 aerosol sample systems.

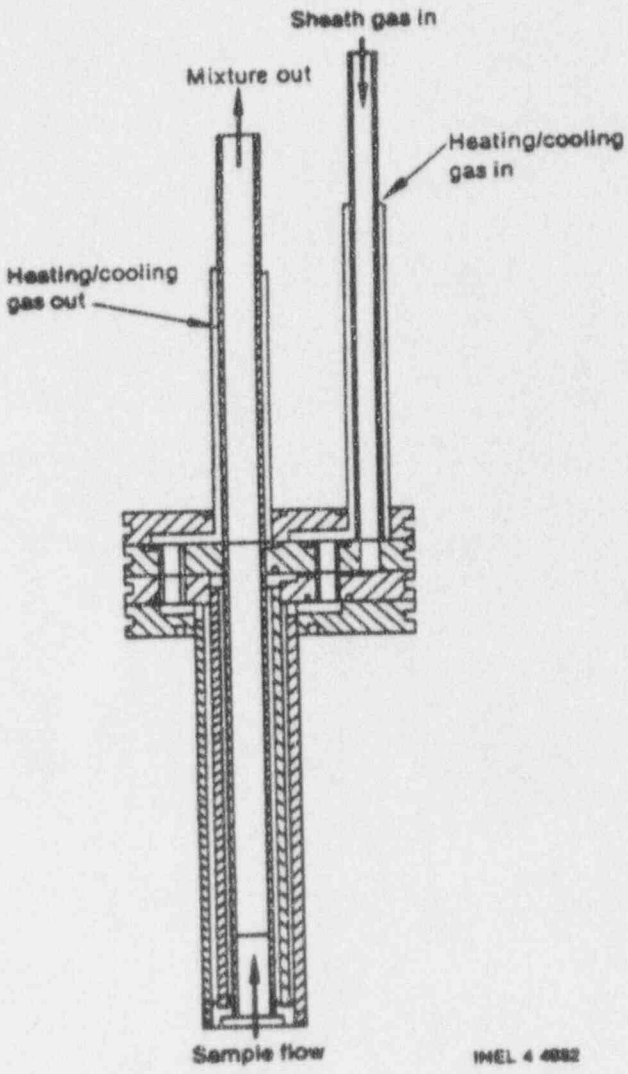

Figure B-10. Sample line probe.

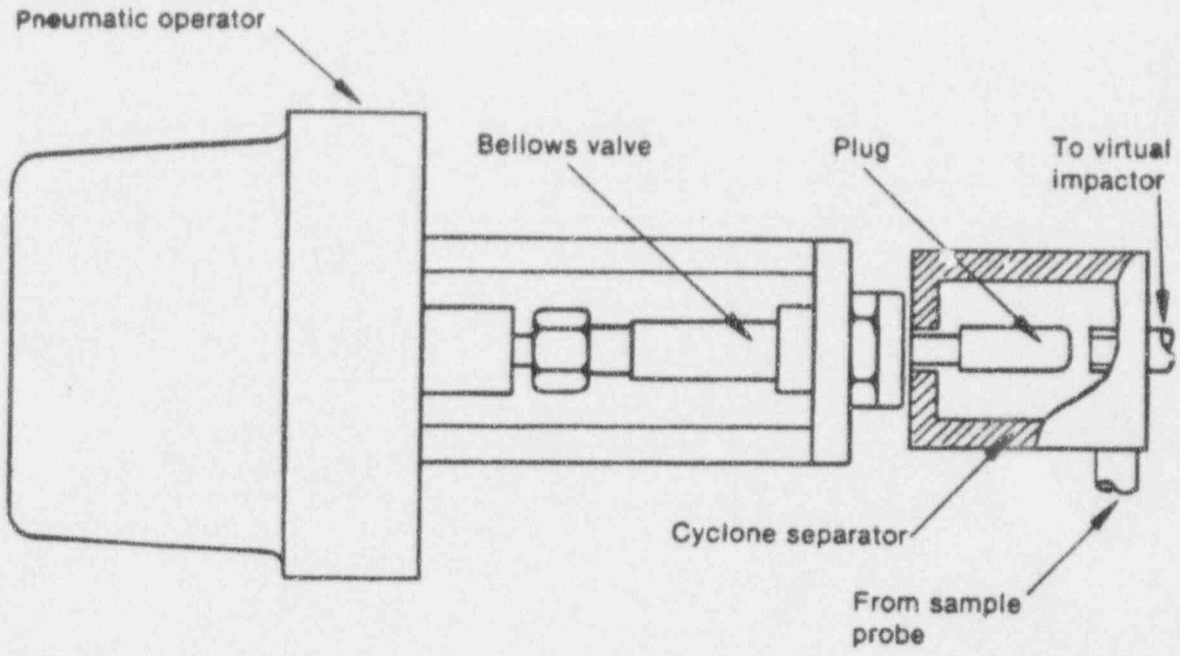

Figure B-11. Cyclone separator / isolation valve.

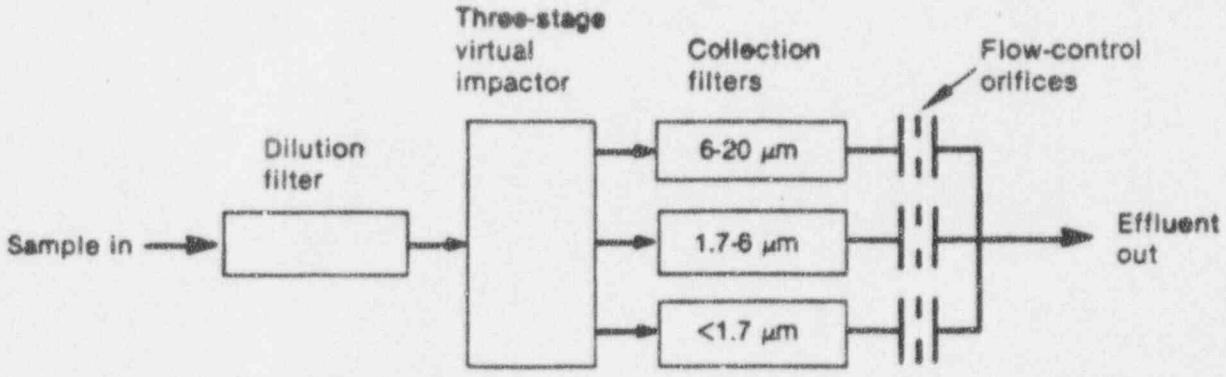

Figure B-12. Impactor and filter train.

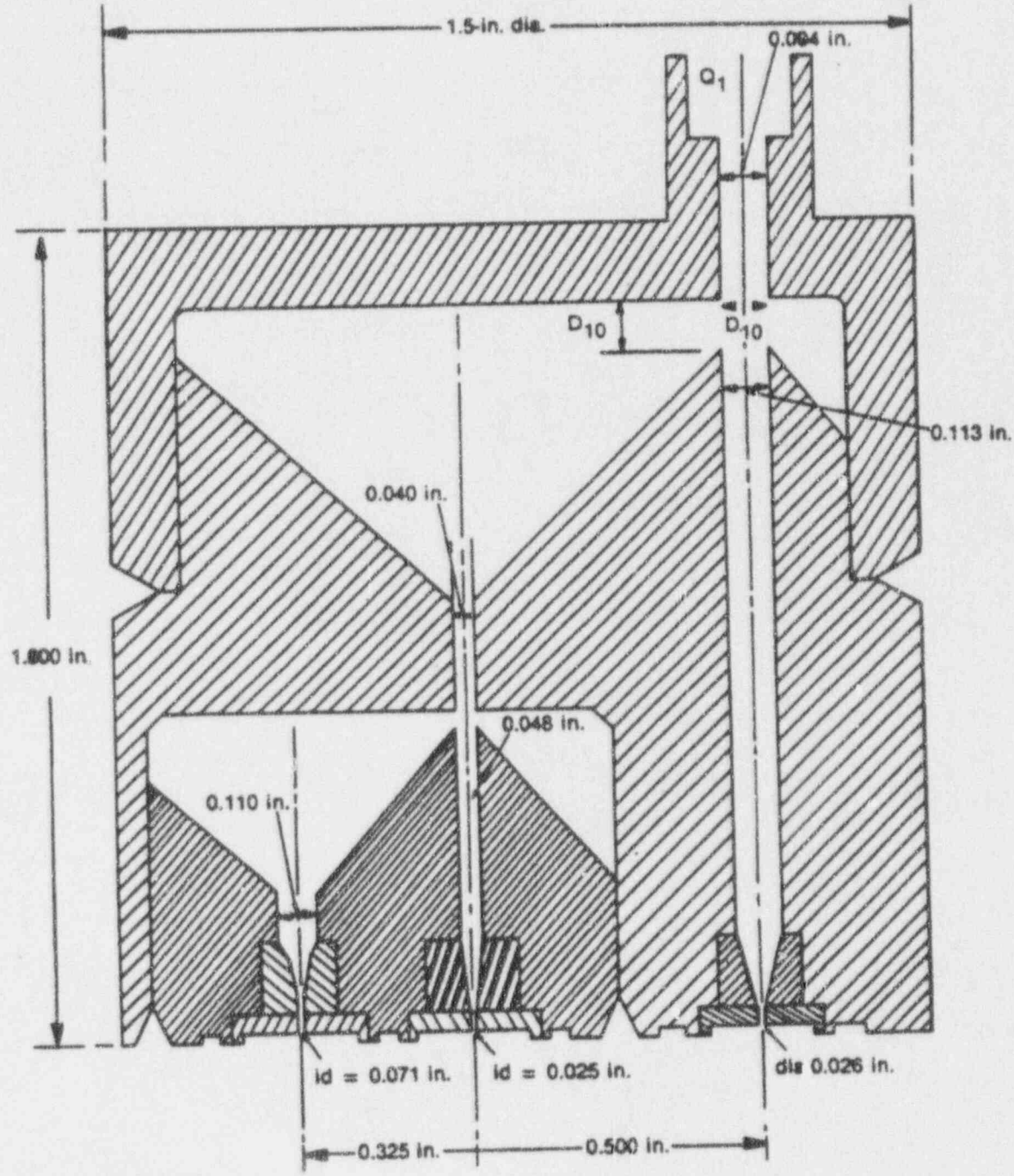

Figure B-13. Three stage virtual impactor.

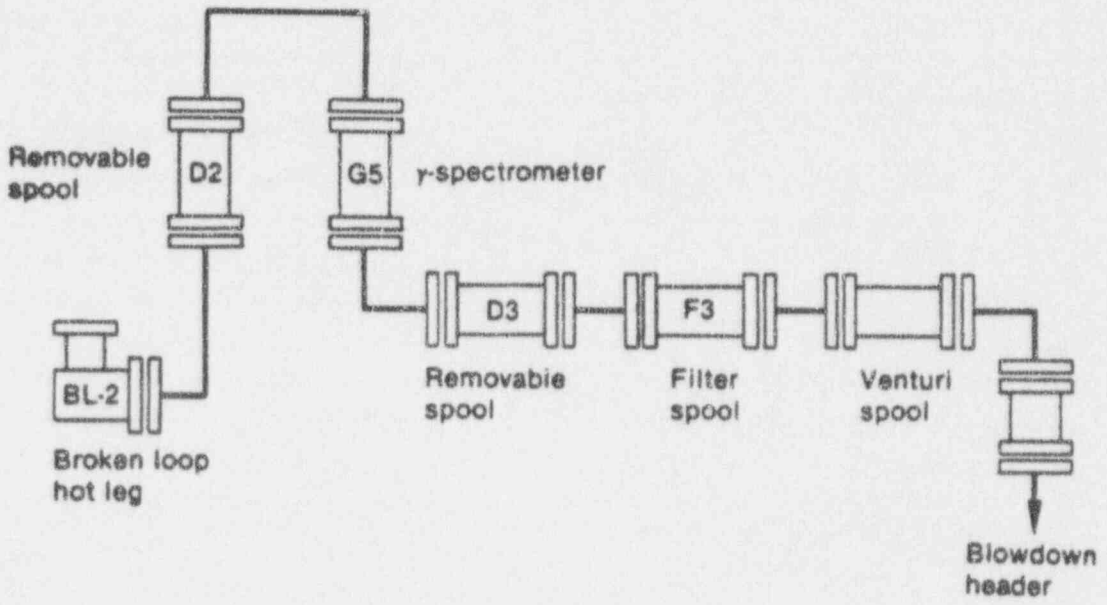

Figure B-14. Simulated LPIS line components.

B-1.6.3 FPMS Gamma Detection Sampling System. Four gamma spectrometers and one gross gamma monitor were used in the FPMS to provide a real-time quantitative measurement of the radioisotopes present in the LOFT system during the posttransient sampling phase. Two of the five were operated during the transient phase. The sample points are shown on Figure B-8 and are as follows:

- G1--spectrometer operated only during postexperiment, sampling either in the reactor vessel lower plenum at 0.584 m below the core or from the primary coolant hot leg in the horizontal PC-3 flange.
- G2--spectrometer operated during the transient, sampling the combined F1 and F2 sample lines effluent, and postexperiment, sampling the vapor space of the BST.
- G3--spectrometer operated only during postexperiment, sampling the liquid space of the BST.
- G5--spectrometer operated during the transient, sampling upstream of the filter in the simulated LPIS line.
- G6--gross gamma monitor operated during the transient; it viewed samples being drawn by the F1 sample line located in the reactor vessel upper plenum at 1.80 m above the lower tie plate.

The gamma spectrometer sample systems included valves for isolation and sample point selection, pumps to provide flow, and pressure and temperature instruments. The samples were returned to the same source that was being sampled. The G1, G2, and G3 spectrometers were enclosed in a tent to which an inert gas purge was applied to minimize the buildup of background contamination that occurred during Experiment LP-FP-1. Additionally, the liquid and gas sample lines were purged with clean water and inert gas, respectively, to measure plateout.

Each gamma spectrometer was designed to operate remotely over a broad range of sample intensities. To improve accuracy, the spectrometer was calibrated during the experiment (also remotely), using a 228^{Th} source mounted on the collimator wheel and background radiation levels were recorded.

B-2. Experiment Conduct

The operational procedure for the conduct of Experiment LP-FP-2 was based on four continuous phases, where the end of one phase was defined to be the beginning of the subsequent phase. These phases were (a) fuel preconditioning; (b) pretransient; (c) transient; and (d) posttransient. The conduct of the experiment is discussed in the following sections within the context of the four phases.

B-2.1 Fuel Preconditioning Phase. This phase was defined to provide the minimum burnup (with consideration of power operation in the pretransient phase) on the new CFM for generation of the fission product source within the fuel matrix. The burnup placed on the CFM in this phase was 252 MWd/tU. The operational history for this burnup was a core thermal power of 32 MW for ~84 hours. This phase is shown by the power operation prior to -200 hrs in Figure B-15. The remainder of the minimum burnup required for the experiment (325 MWd/tU) was obtained in the pretransient phase.

B-2.2 Pretransient Phase. The first part of this phase consisted of a 75-hour shutdown interval during which plant systems and fission product measurement systems underwent final preparations. The transversing in-core probe system guide tubes were cut and capped in order to prevent fission product release through the tubes to the outside of the containment.

Following the shutdown interval, power

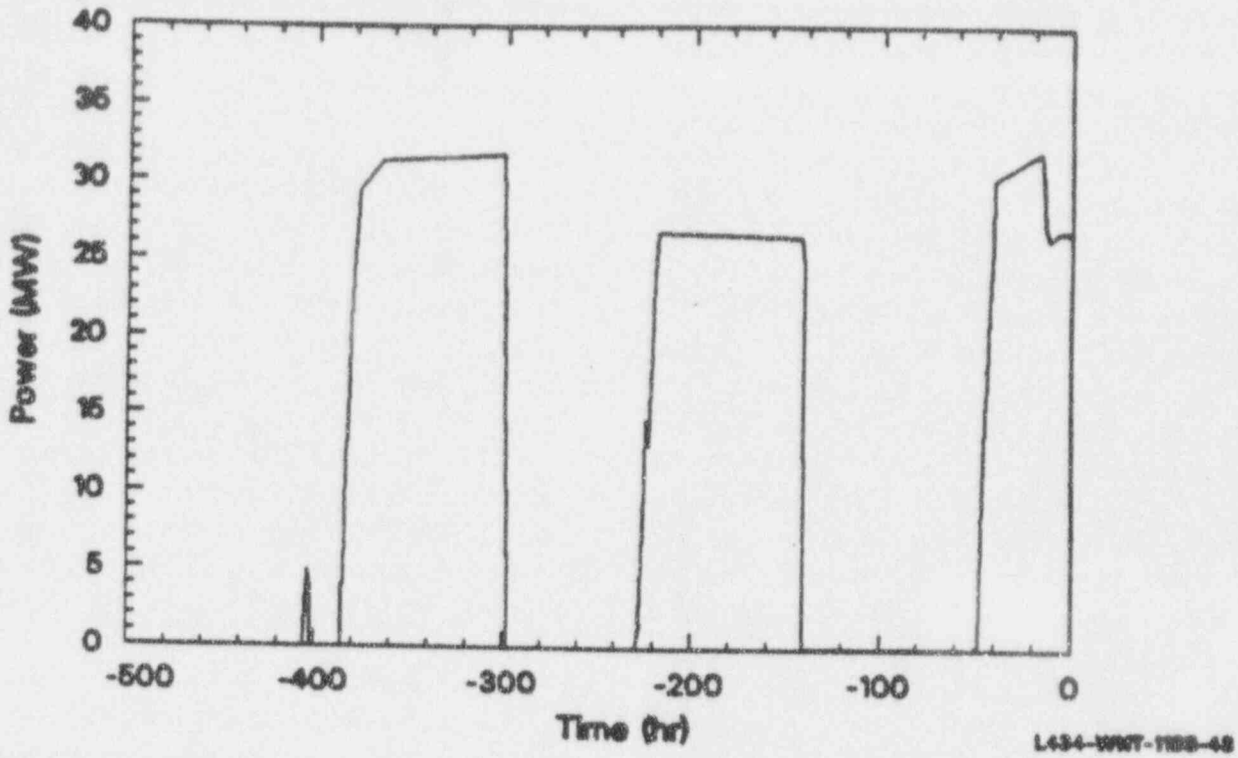

Figure B-15. LOFT core power operation prior to initiation of Experiment LP-FP-2.

operation commenced to acquire the remaining fuel burnup and establish experiment initial conditions. A power operation of 80 hours duration at the specified power level of 26.5 MW was achieved prior to transient initiation. This phase is shown by the second block of time-at-power, from -220 to -140 hours in Figure B-15. The total fuel burnup was 346 MWd/tU at the time the transient phase could be initiated.

The operational sequence defined for initiating the transient was first to drop the 11 CFM control rods, which would establish time zero. This step would be followed by scramming the reactor, then opening the break path in the intact loop cold leg, and finally tripping the primary coolant pumps (PCPs). This procedure would provide two independent indications that the CFM control rods were in--an indication of negative reactivity and core power decline, and an activation of limit switches on the CFM. This transient-initiating sequence also was based on prior operating experience, which verified that the control rods in the standard LOFT fuel modules will drop with the PCPs operating. The 11-control-rod assembly in the CFM was also calculated to drop with PCPs operating, but the margin for a control rod drop was small. The first step in the transient initiation sequence was taken; however, the CFM control rods did not drop and remained in the initial condition position. A variance to the operating procedure of this nature required experiment termination and a return to a safe shutdown state.

The CFM control rods were determined to be structurally sound. The control rods did not drop due to levitation caused by steady-state PCP operation. A new experiment-initiating sequence was defined, which consisted of scramming the reactor (time zero), tripping the PCPs, dropping the CFM control rods at a loop flow of 189 kg/s, and opening the intact loop cold leg break path following verification that the CFM control rods had dropped.

Reactor power operation commenced to reestablish the required decay heat level and to

establish the specified initial conditions for the experiment. The LOFT reactor was operated first at a thermal power of 31 MW for ~26 hours. The thermal power was then reduced to the specified initial condition value of 26.5 MW for 15 hours to complete the decay heat buildup and to allow the system to stabilize at the specified initial conditions. The total fuel burnup at the time of the transient initiation was 430 MWd/tU, with a decay heat level of 684.1 kW at 200 seconds. The power history up to transient initiation is shown in Figure B-15. The initial conditions for the experiment are listed in Table B-2. Except for the liquid level in the BST, all initial conditions were within the limits specified in the Experiment Specification document.[B-3] The single out-of-specification value did not affect the experiment, since an exact BST simulation of PWR containment was not part of the experiment.

B-2.3 Transient Phase. The transient was initiated with the operational sequence described in the previous section. The chronology of events in the transient are listed in Table B-3. Those events that were defined to be operational setpoints are listed in Table B-4. These setpoints were determined from experiment prediction calculations.[B-4] A detailed event sequence for the fission product measurement systems is listed in Table B-5. Analysis of data on core damage[B-6] led to a chronology of core damage events, which is given in Table B-6.

The system depressurization was not as rapid as had been predicted in the two-phase region extending to high-quality (steam) conditions. A variance from prediction in this area was recognized as a possibility because of the difficulties encountered in the modeling of the simulated LPIS line and in the application of the systems codes to this transient. A variance of this nature is not detrimental to the success of the experiment relative to simulation of the V-sequence thermal-hydraulics; however, an operational design limit of 1.38 MPa was used for the FPMS. In the event that the system pressure exceeded this value during the time the fission product measurements were on-line, then the success of the experiment would be in doubt and dependent on the success or failure of the fission product measurements. Operational procedures were defined that allowed the reactor operators to reopen the intact loop cold leg break path and also open the PORV, if the system pressure exceeded the design value during the early part of the core heatup. These actions would be taken at a CFM cladding temperature of 800 K and would be terminated (all vent paths closed except for the LPIS line) at a CFM cladding temperature of 1050 K. These actions were needed, as indicated in Table B-3, and were successful in reducing system pressure within the design range of the fission product measurements prior to fission product release.

The design objective of the transient was to produce CFM cladding temperatures above 2100 K for a minimum of three minutes. As indicated in Table B-3, approximately 4.5 minutes elapsed from the time the temperature was reached until initiation of the ECCS. The FPMS (D1, F1, and F2) and the simulated LPIS line were isolated within 5 seconds of ECCS initiation in accordance with operational specifications. The experiment termination procedure, starting with the isolation of the simulated LPIS line, began when the temperature limit of 1517 K on the CFM outer wall was reached at 1776 seconds.

B-2.4 Posttransient Phase. The initiation of plant recovery at 1776 seconds was the beginning of the posttransient phase. All events listed in Tables B-3, B-4, and B-5 following 1776 seconds are the result of plant recovery procedures to bring the plant to a controlled steady-state shutdown with the PCS temperature maintained by primary-to-secondary heat transfer following PCS refill and establishment of loop natural circulation. Prior to

Table B-2: Initial conditions for Experiment LP-FP-2.

Parameter	Specified[a] Value	Measured Value
PRIMARY COOLANT SYSTEM		
Core delta T (K)	--	11.7 1.4
Primary system pressure (hot leg) (MPa)	14.95 0.1	14.98 0.1
Hot leg temperature (K)	571 1.1	571.6 0.8
Cold leg temperature (K)	--	559.9 1.1
Loop mass flow (kg/s)	479 19	475 2.5
Boron concentration (ppm)	--	499 15
Primary coolant pump injection (both pumps) (L/s)	0.127 0.016	0.128 0.003
REACTOR VESSEL		
Power level (MW)	26.5 0.5	26.8 1.4
Decay heat (200 s) (kW)	685 10	684.8
Maximum linear heat generation rate (kW/m)	40[b]	42.6 3.6
Control rod position(above full-in position) (m)	1.37 0.01	1.38 0.01
STEAM GENERATOR		
Secondary system pressure (MPa)	--	6.38 0.08
Water level[c] (m)	--	0.17 0.06
PRESSURIZER		
Liquid volume (m^3)	--	0.57 0.03
Steam volume (m^3)	--	0.37 0.03
Water temperature (K)	--	616.9 2.1
Pressure (MPa)	--	15.1 0.1
Liquid level (m)	1.12 0.1	1.06 0.06
SUPPRESSION TANK		
Liquid level (m)	1.19 0.051 - 0.0	1.18 0.06
Gas volume (m^3)	--	59.11 2.02
Water temperature (K)	< 311	295.6 0.5
Pressure (gas space)	100 20	95 3
Boron concentration (ppm)	--	3710 15

Table B-2: Initial conditions for Experiment LP-FP-2. (Continued)

Parameter	Specified[a] Value	Measured Value
EMERGENCY CORE COOLING SYSTEM		
Borated water storage tank temperature (K)	303 3	301.3 3
Accumulator A liquid level (m)	<2.17	1.81 0.02
Accumulator A pressure (MPa)	>4.21	5.1 0.06
Accumulator A liquid temperature (K)	303 3	303.1 0.7
Accumulator B liquid level (m)	<2.16	1.81 0.02
Accumulator B pressure (MPa)	>4.21	4.95 0.06
Accumulator B liquid temperature (K)	303 3	305.6 0.7

a. If no value is listed, none was specified.
b. Approximately.
c. Steam generator liquid level referenced to 2.95 m (116 in.) above the top of the tube sheet.

Table B-3. Chronology of events for Experiment LP-FP-2.

Event	Time (s)
Scram	0.0
Control rods fully inserted	2.4 ± 0.1
PCP coastdown initiated	9.7 ± 0.1
CFM control rods fully inserted	23.4 ± 0.5
ILCL break initiated	32.9 ± 0.1
PCP coastdown complete[a]	25.1 ± 0.1
End of subcooled blowdown[b]	53 ± 1
LPIS line break initiated	221.6 ± 0.1
Secondary pressure exceeded primary system pressure	260 ± 10
Earliest coolant thermocouple deviation from saturation	
Upper plenum	300 ± 10
Hot leg pipe	390 ± 10
Downcomer	730 ± 10
Lower plenum	800 ± 20
Fuel rod cladding heatup started in PFM	662 ± 2
Fuel rod cladding heatup started in CFM	689 ± 2
ILCL break closed	735.5 ± 0.1
ILCL break reopened	877.6 ± 0.1
PORV opened	882.0 ± 0.1
LPIS bypass closed	951.9 ± 0.1
FPMS lines opened	1013.1 ± 0.1
ILCL closed	1021.5 ± 0.1
PORV closed	1162.0 ± 0.1
First indication of (gap) fission products at F1 and F2	1200 ± 20
First indication of (gap) fission products at F3	1249 ± 60
Peripheral fuel cladding reached 1460 K (2172°F)	--[c]
Maximum upper plenum coolant temperature reached[d]	1495 ± 5

Table B-3. Chronology of events for Experiment LP-FP-2. (Continued)

Event	Time (s)
First indication of (fuel) FPs at F1, F2, and F3	1500 ± 10
Cladding temperatures reach 2100 K (3320°F)	1504 ± 1
1st shroud thermocouple reached trip setpoint	1743 ± 1
2nd shroud thermocouple reached trip setpoint	1766 ± 1
Maximum cladding temperature reached	--[e]
LPIS break closed	1777.6 ± 0.1
FPMS lines closed	1778.1 ± 0.1
Maximum upper plenum metal temperature reached[d]	1780 ± 5
Deposition coupons isolated	1780.6 ± 0.1
ECCS initiated	1782.6 ± 0.1
Accumulator flow stopped	1795 ± 2
Maximum LPIS line coolant temperature reached	1800 ± 5
Core quenched	1795 ± 5[f]

a. The pumps were allowed to coastdown under the influence of the motor generator flywheel until the pump speed reached 750 rpm. At that time, the flywheel was disconnected from the motor generator and the pumps quickly stopped adding energy to the fluid. The time at which the flywheel was disconnected is defined as the time the PCP coastdown was complete.

b. End of subcooled blowdown is defined as the time when the first measured fluid temperature outside of the pressurizer reaches saturation conditions.

c. None of the cladding thermocouples in the peripheral fuel bundle measured validated temperatures above the setpoint. The two that gave readings above this setpoint were failed before reaching the setpoint.

d. These temperatures represent the maximum measured temperatures before reflood at these locations. The thermocouple output during reflood could not be interpreted.

e. Because of the large number of cladding thermocouples in the central fuel module that failed at high temperatures during the transient, it is not possible to determine the precise maximum temperature or the time at which it occurred. The time is estimated to be between 1782 and 1795 s. The maximum temperature exceeded 2400 K (3860oF) based on extrapolations from valid temperature readings before thermocouple failure.

f. The peripheral fuel modules were quenched by 1793s. Most of the centrai fuel module cladding thermocouples were quenched by 1795 s. Some isolated thermocouples indicated persistent high (superheated) temperatures a few minutes longer. Interpretation of the temperature data is complicated by the large number of thermocouples in the center fuel module that failed during or just before reflood.

Table B-4. Operational setpoints for Experiment LP-FP-2.

Event	Specified (s)	Measured (s)
Scram reactor	0.0	0.0
Turn off primary pumps	8.0 ± 2	9.7 ± 0.1
Insert CFM control rods[a]	20.	22.4 ± 0.1
ILCL break opened[b]	23.	32.9 ± 0.1
LPIS break opened	220. ± 5	221.6 ± 0.1
ILCL break closed[c]	721.	735.5 ± 0.1
F1 and F2 opened[d]	905.	1013.1[h] ± 0.1
Open the LPIS line filter	945.	950.8 ± 0.1
Isolate gamma densitometer sources[e]	945.	262. ± 2
Close FPMS lines[f]	1766.	1777.1 ± 0.1
Close the LPIS line[f]	1766.	1777.6 ± 0.1
ECCS flow initiated[g]	1783.6 ± 0.5	1782.6 ± 0.1

a. Insertion of the CFM control rod was initiated when the primary coolant flow decreased to 189 kg/s (1.5 x 10^6 lb_m/h).

b. The ILCL break was opened upon verification that the CFM control rods were fully inserted.

c. The ILCL break was closed when cladding temperatures reached 566 K (560°F) or PCS pressure reached 1.2 MPa (160 psig).

d. The F1 and F2 lines were opened at 1013.1 and steam was first detected in the F1 line between 1013.1 and 1015.7 seconds.

e. The gamma densitometer sources were to have been isolated from the detectors when the cladding temperatures reached 840 K (1052°F).

f. The FPMS sampling line and LPIS line isolation valves were closed when shroud temperatures reached 1517 K (2272°F).

g. ECCS flow was initiated 6 seconds after initiation of closure of the LPIS line isolation valves.

Table B-5. Sequence of events affecting the FPMS .

Event	Time (s)
F1 Dilution gas line opened	-199.4
F1 and F2 vent line closed	-146.8
Reactor scram	0.0
D1 moved (to drop CFM control rods)	20.6
D1 initial purge started	750.6
D1 initial purge stopped	763.1
F1 steam analyzer external purge started	878.1
F1 steam analyzer external purge stopped	883.0
F1 annulus gas line opened	883.1
F3 line opened	950.8
F3 bypass line closed	951.9
F1 and F2 sample lines opened	1013.1
Fission products detected in the F1 line	1198.0
Fission products detected in the BLHL	1201.0
LPIS line closed	1777.6
F1 line closed	1778.0
F2 line closed	1778.1
Attempted closure of the D1 coupons	1780.6
D1 nitrogen backup on	1808.0
F1 and F2 vent line closed	1823.0
F1 dilution gas line closed	1833.1
D1 opened	2085.6
D1 nitrogen backup bypass opened	2143.1
D1 nitrogen backup bypass closed	2148.0
D1 nitrogen backup bypass opened	2933.1
D1 nitrogen backup bypass closed	2968.2
F1 annulus gas line closed	3401.6

Table B-6. Chronology of core damage events.

Events	Time (s)
Estimated time of initial fission product gap release	< 1200
Ag-Cd melt at 0.69 m elevation	1300
Metal-water reaction at 0.69 m elevation (guide tubes)	1430
Maximum measured temperatures reach 2100 K	1504
MWR spreads across 1.07 m elevation	1480 to 1530
MWR spreads across 0.69 m elevation	1450 to 1595
Control rod cladding rupture (about 1250 K)	1500
Relocation of molten material (downward)	1520 to 1680
Partial blockage	1550
Second blockage	1640

completion of refill and startup of natural circulation, the PORV was cycled twice to control system pressure.

The plant was maintained in a quiescent state for 14 days, during which time fission product measurements were made using the on-line measurement systems. Batch samples of the BST liquid and vapor and PCS liquid were taken during the next 44 days, when the posttransient phase was ended. The state of the PCS during the posttransient phase is discussed in Appendix F of Reference B-12.

REFERENCES

B-1. J. P. Adams et al., Quick Look Report on OECD LOFT Experiment LP-FP-I, OECD LOFT-T-3704, March 1985.

B-2. E. W. Coryell et al., OECD LOFT Fission Product Experiment LP-FP-1 Fission Product Data Report, OECD LOFT-T-3708, Rev. 1, November 1986.

B-3. V. T. Berta, OECD LOFT Project Experiment Specification Document, Fission Product Experiment LP-FP-2, OECD LOFT-T-3802, Rev. 1, Changes 1-5, May 1985.

B-4. S. Guntay, M. Carboneau, and Y. Anoda, Best-Estimate Prediction for OECD LOFT Project Fission Product Experiment LP-FP-2, OECD LOFT-T-3803, June 1985.

B-5. J. P. Adams et al., Quick Look Report on OECD LOFT Experiment LP-FP-2, OECD LOFT-T-3804, September 1985.

B-6. M.L. Carboneau et al., OECD LOFT Fission Product Experiment LP-FP-2 Fission Product Data Report, OECD LOFT-T-3805, May 1987.

B-7. P.R. Davis et al., "The Risk Significance of Transient Accidents from PRA Studies", ANS Topical Meeting on Anticipated and Abnormal Transients in Light Water Reactors, Jackson WY, September 1983, Vol. 2, pp. 911-919.

B-8. U.S. Nuclear Regulatory Commission, Reactor Safety Study--An Assessment of Accident Risks in U.S. Commercial Nuclear Power Plants, WASH-1400, October 1975.

B-9. D.L. Reeder, LOFT System and Test Description (5.5-ft Nuclear Core 1 LOCEs), NUREG/CRR-0247, TREE-1208, Change 1, September 1980.

B-10. Portland General Electric Company, TROJAN Final Safety Analysis Report, GE 006-50344-38, April 1, 1983.

B-11. M. Tanaka et al., Quick Look Report on OECD LOFT Experiment LP-SB-3, OECD LOFT-T-3604, March 1984.

B-12. M.L. Carboneau, V.T. Berta, and S.M. Modro, Experiment Analysis and Summary Report for OECD LOFT Project Fission Product Experiment LP-FP-2, OECD LOFT-T-3806, June 1989.

Distribution

U. S. Nuclear Regulatory Commission
Office of Nuclear Reactor Regulation
Washington, D.C. 20555
ATT: R. Barrett, OWFN
J. H. Flack, NLS324
A. C. Thadani, OWFN 8E2

U S. Nuclear Regulatory Commission
Office of Nuclear Regulatory Research
Washington, D.C. 20555
ATT: S. Basu, NLN 344
E. S. Beckjord, NLS007
F. Eltawila, NLN344
T. L. King, NLN370
R.L. Palla, Jr., OWFN 10 E 4
A. M. Rubin, NLN344
B. W. Sheron, NLN369
T. P. Speis, NLS007
C. G. Tinkler, NLN344
R. W. Wright, NLN344

U. S. Nuclear Regulatory Commission
Office of ACRS
Washington, D.C. 20555
ATT: M. D. Houston, PHIL P-315

U. S. Nuclear Regulatory Commission
Division of Technical Information and
Document Control
7920 Norfolk Avenue
Bethesda, MD 20014

Argonne National Laboratory
9700 South Cass Avenue
Argonne, IL 60439
ATT: B. Spencer

U S. Department of Energy
Idaho Operations Office
785 DOE Place
Idaho Falls, ID 83401-1134
ATT: W. H. Rettig

Idaho National Engineering Laboratory
EG&G Idaho, Inc.
P.O. Box 1625
Idaho Falls, ID 83415
ATT: C. M. Allison, MS 3840

Brookhaven National Laboratory
130 BNL
Upton, NY 11973
ATT: T. Pratt

Electric Power Research Institute
P.O. Box 10412
3412 Hillview Avenue
Palo Alto, CA 94303
ATT: M. Merilo

Fauske and Associates, Inc.
16W070 West 83rd Street
Burr Ridge, IL 60521
ATT: R. J. Hammersley

Oak Ridge National Laboratory
P 0. Box Y
Oak Ridge, TN 37830
ATT: T. Kress
S. Hodge
L. Ott

Frank E. Panisko
Reactor Systems, Fuels & Matls. P8-35
Pacific Northwest Laboratory
P.0. Box 999
Richland, WA 99352

Sandia National Laboratory
P 0 Box 5800
Albuquerque, NM 87185
ATT: D. Powers
S. Thompson
K. O. Reil

University of California Los Angeles
Nuclear Energy Laboratory
405 Hilgaard Avenue
Los Angeles, CA 90024
ATT: I. Catton

Westinghouse Bettis Atomic Laboratory
P.O. Box 79
West Mifflin, PA 15122
ATT: J. W. Wolfe, ZAP 34N

ABB/CE
1000 Prospect Mill Road
Winsor, CT 06095
CEP 9612-2207
ATT: R. Schneider

G. E. Knolls Atomic Power Lab.
Box 1072
Schenectady, NY 12501
ATT: John Conine, D2-221

Japan Atomic Energy Research Institute
Tokai-mura, Naka-gun, Ibaraki-ken
319-11
Japan
ATT: J. Sugimoto

Korea Advanced Energy Research Institute
P.O. Box 7
Daeduk-Danji
Taejeon 305-353
Korea
ATT: Hee-Dong Kim

Nuclear Power Engineering Center
Fujitakanko Building
17-1, 3-Chrome, Toranomon, Minato-Ku
Japan, Tokyo 105
ATT: Kenji Takumi

Institute of Nuclear Energy Research
P.O. Box 3
Lungtan
Taiwan 325
Republic of China
ATT: S. I. Chang

Consejo de Seguridad Nuckan
SOR Angela de 1a Cruz No 3
Madrid 28056
Spain
ATT: J. Bagues

E. T. S. Ingenieros Industriales
Jost Gutierrez Abascal, 2
28006 Madrid
Spain
ATT: A. Alonso

General Atomics
P.O. Box 85608
San Diego, CA 92138-5608
ATT: S. Inamati

Massachusetts Institute of Technology
Nuclear Engineerlng Department
77 Massachusetts Avenue
Cambridge, MA 02139
ATT: M. Kazimi
N. Todreas

Belgonucleaire
Department of LWR Fuel
Rue de Champde Mars. 25
B-1050 Brussels
Belgium
ATT: E. Stubbe

Whiteshell Laboratories
AECL Research
Reactor Safety Research Division
Pinawa, Manitoba
Canada ROE lLO
ATT: L. A. Simpson

Kernforschungszentrum Karlsruhe
Postfach 3640
75 Karlsruhe
Germany
ATT: B. Kuczera
P. Hofmann

Nucleare e della Protezione Sanitaria
(DISP)
Ente Nazionnle Energie Alternative
(ENEA)
Viale Regina Margherita, 125
Casella Postale M. 2358
I-00100 Roma A. D.
Italy
ATT: G. Petrangeli

UKAEA
Winfrith, Dorchester DT2-8DH
Dorset, England
United Kingdom
ATT: S. Kinnersly, 203/A32
D. Williams

Statens Karnkraftinspektion
P.0. Box 27106
S-10252 Stockholm
Sweden
ATT: W. Frid

Reactor Centrum Nederland
1755 ZG Petten
The Netherlands
ATT: K. J. Brinkman

Thermodynamics and Radiation Physics
CEC Joint Research Center, Ispra
I-201020 Ispra (Varese)
Italy
ATT: Paola Fasoli-Stella

VATESI
Gediminis Prospect 36
Vilnius, Lithuania
ATT: P. Vaisnys

Hungarian Atomic Energy Commission
H-1374 Budapest, P.O. Box 565
Budapest, Hungary
ATT: S. Elo

State Office for Nuclear Safety
Slezska 9, 120 00 Prague 2
Czech Republic
ATT: J. Stuller

Cadarache Center for Nuclear Studies
F-13108 Saint Paul-Lez-Durance
Cedex France
ATT: A. Meyer-Heinc
J. Leveque
B. Andre

Swiss Federal Nuclear Safety Inspectorate
CH-5232 Villigen - HSK
Switzerland
ATT: S. Chakraborty

N.V. Kema
P.O. Box 9035
6800 ET ARNHEM
The Netherlands
ATT: P. Kloeg

Consijo De Seguridad Nuclear
Justo Dorado 11
28040 Madrid
Spain
ATT: J. A. Martlnez

I. V. Kurchatov Institute of Atomic Energy
Nuclear Safety Department
Moscow, 123182
Russia
ATT: V. Asmolov

Institut de Protection et de Surete Nucleaire
CEN/FAR - B. P. No6
F-92265
Fontenay-aux-Roses
Cedex, France
ATT: M. LiVolant

Paul Scherrer Institut
Programm LWR-Sicherheit
CH-5232 Villigen, PSI
Switzerland
ATT: P. Hosemann

Committee on the Use of Atomic Energy for Peaceful Purposes
69 Shipchenski
prokhod Blvd, 1574, Sofia Bulgaria
ATT: Y. Yanev

Nuclear Regulatory Authority
Slovak Republic
Bajkalska 27, 827 21 Bratislave
Slovak Republic
ATT: J. Misak

Netherlands Energy Research Foundation
P.O. Box 1 1755 ZG Petten
The Netherlands
ATT: E. Cordfunke

Jozef Stefan Institute
Jamova 39 61111 Ljubljana
Slovenia
ATT: B. Mavko

Russian Academy of Sciences
Nuclear Safety Institute
52, B. Tulskaya
Moscow, 113191
Russia
ATT: L. Bolshov

Netherlands Energy Research Foundation
P.O. Box 1
1755 ZG Petten
The Netherlands
ATT: P. Stoop

NRC FORM 335 (2-89) NRCM 1102, 3201, 3202

U.S. NUCLEAR REGULATORY COMMISSION

BIBLIOGRAPHIC DATA SHEET

(See instructions on the reverse)

1. REPORT NUMBER (Assigned by NRC, Add Vol., Supp., Rev., and Addendum Numbers, if any.)

NUREG/CR-6160
NEA-CSNI-R(94)3
EGG-2721

2. TITLE AND SUBTITLE

Summary of Important Results and SCDAP/RELAP5 Analysis for OECD LOFT Experiment LP-FP-2

3. DATE REPORT PUBLISHED

MONTH: April
YEAR: 1994

4. FIN OR GRANT NUMBER

L1367

5. AUTHOR(S)

E. W. Coryell

Contributing Authors
D. W. Akers, C. M. Allison, M. L. Carboneau, R. R. Hobbins, J. K. Hohorst, S. M. Jensen, S. M. Modro

6. TYPE OF REPORT

Technical

7. PERIOD COVERED (Inclusive Dates)

8. PERFORMING ORGANIZATION – NAME AND ADDRESS (If NRC, provide Division, Office or Region, U.S. Nuclear Regulatory Commission, and mailing address; if contractor, provide name and mailing address.)

EG&G Idaho, Inc.
Idaho Falls, ID 83415

9. SPONSORING ORGANIZATION – NAME AND ADDRESS (If NRC, type "Same as above"; if contractor, provide NRC Division, Office or Region, U.S. Nuclear Regulatory Commission, and mailing address.)

Division of Systems Research
Office of Nuclear Regulatory Research
U.S. Nuclear Regulatory Commission
Washington, D.C. 20555-0001

10. SUPPLEMENTARY NOTES

11. ABSTRACT (200 words or less)

This report summarizes significant technical findings from the LP-FP-2 Experiment sponsored by the Organization of Economic Cooperation and Development (OECD). It was the second, and final, fission product experiment conducted in the Loss-of-Fluid Test (LOFT) facility at the Idaho National Engineering Laboratory. The overall technical objective of the test was to contribute to the understanding of fuel rod behavior, hydrogen generation, and fission product release, transport, and deposition during a V-sequence accident scenario that resulted in severe core damage. An 11 by 11 test bundle, comprised of 100 prepressurized fuel rods, 11 control rods, and 10 instrumented guide tubes, was surrounded by an insulating shroud and contained in a specially designed central fuel module, that was inserted into the LOFT reactor. The simulated transient was a V-sequence loss-of-coolant accident scenario featuring a pipe break in the low pressure injection system line attached to the hot leg of the LOFT broken loop piping. The transient was terminated by reflood of the reactor vessel when the outer wall shroud temperature reached 1517 K. With sustained fission power and heat from oxidation and metal-water reactions, elevated temperatures resulted in zircaloy melting, fuel liquefaction, material relocation, and the release of hydrogen, aerosols, and fission products. A description and evaluation of the major phenomena, based upon the response of on-line instrumentation, analysis of fission product data, postirradiation examination of the fuel bundle, and calculations using the SCDAP/RELAP5 computer code, are presented.

12. KEY WORDS/DESCRIPTORS (List words or phrases that will assist researchers in locating the report.)

SCDAP/RELAP5, LOFT, Experiment LP-FP-2

13. AVAILABILITY STATEMENT

Unlimited

14. SECURITY CLASSIFICATION

(This Page)
Unclassified

(This Report)
Unclassified

15. NUMBER OF PAGES

16. PRICE

NRC FORM 335 (2-89)

Federal Recycling Program

UNITED STATES
NUCLEAR REGULATORY COMMISSION
WASHINGTON, D.C. 20555-0001

OFFICIAL BUSINESS
PENALTY FOR PRIVATE USE, $300

120555139531 1 1AN
US NRC-OADM
DIV FOIA & PUBLICATIONS SVCS
TPS-PDR-NUREG
2WFN-6F7 DC 20555
WASHINGTON

SPECIAL FOURTH-CLASS RATE
POSTAGE AND FEES PAID
USNRC
PERMIT NO. G-67